



# Soft hybrid materials for cell growth and proliferation

Federica Fiorini

## ► To cite this version:

Federica Fiorini. Soft hybrid materials for cell growth and proliferation. Other. Université de Strasbourg, 2016. English. NNT : 2016STRAF027 . tel-01599250

**HAL Id: tel-01599250**

**<https://theses.hal.science/tel-01599250>**

Submitted on 2 Oct 2017

**HAL** is a multi-disciplinary open access archive for the deposit and dissemination of scientific research documents, whether they are published or not. The documents may come from teaching and research institutions in France or abroad, or from public or private research centers.

L'archive ouverte pluridisciplinaire **HAL**, est destinée au dépôt et à la diffusion de documents scientifiques de niveau recherche, publiés ou non, émanant des établissements d'enseignement et de recherche français ou étrangers, des laboratoires publics ou privés.

**ÉCOLE DOCTORALE DES SCIENCES CHIMIQUES**  
**Institut de Science et d'Ingénierie Supramoléculaires**

# THÈSE présentée par :

**Federica FIORINI**

soutenue le : **28 Septembre 2016**

pour obtenir le grade de : **Docteur de l'université de Strasbourg**

Discipline/ Spécialité : Chimie

## **Soft hybrid materials for cell growth and proliferation**

**THÈSE dirigée par :**

**Mme DE COLA Luisa**

Professeur, Université de Strasbourg

**RAPPORTEURS :**

**M. FARINOLA Gianluca**

**M. MORDINI Alessandro**

Professeur, Università degli Studi di Bari (Italie)

CNR Senior Researcher, Istituto di Chimica dei Composti Organometallici – Sesto Fiorentino (Italie)

---

**AUTRES MEMBRES DU JURY :**

**Mme BOULMEDAIS Fouzia**

**M. SEEBERGER Peter**

Directrice de Recherche, Université de Strasbourg

Professeur et Directeur de l'Institut Max-Planck for Colloids and Surfaces –Potsdam (Allemagne)



To my colleagues (who are also dear friends),  
because most of this work would have not been possible without your help and support.  
It was a pleasure to meet you and share these years of “Strasbourg life” and work with you!



# Table of contents

<b>Résumé de thèse .....</b>	<b>1</b>
<b>1. Hydrogels for tissue engineering and biomedical applications .....</b>	<b>24</b>
1.1 Hydrogels, an overview.....	25
1.1.1 Network characteristics: physical and chemical hydrogels .....	26
1.2 Engineering hydrogels as extracellular matrix mimics for 3D cell culture.....	28
1.2.1 Design criteria.....	28
1.2.2 Natural and synthetic hydrogels.....	30
1.3 Hydrogels in tissue engineering .....	33
1.3.1 Tissue engineering .....	33
1.3.2 Areas of application .....	34
1.4 Nanocomposite hydrogels .....	36
1.5 Injectable hydrogels .....	39
1.6 Biodegradable hydrogels.....	41
1.7 Polyamidoamine hydrogels .....	43
1.8 Aim of the thesis .....	44
1.9 References .....	46
<b>2. Making the tools: polyamidoamines-based hydrogels .....</b>	<b>52</b>
2.1 Polyamidoamine-based hydrogels general characteristics.....	53
2.2 Equilibrium swelling degree .....	55
2.3 Optimization of the hydrogel structure design.....	57
2.4 Stability at different pH.....	61
2.5 Oscillatory rheology.....	63
2.6 Conclusions .....	65
2.7 Experimental part .....	66
2.7.1 Synthesis of hydrogels .....	66
2.7.2 Sample lyophilization .....	66
2.7.3 Scanning electron microscopy analysis .....	67
2.7.4 Swelling measurements .....	67
2.7.5 Oscillatory shear rheology .....	67
2.8 References .....	68

<b>3.</b>	<b>Monitoring <i>in vitro</i> cell proliferation in a hybrid, emission switchable hydrogel....</b>	<b>70</b>
3.1	From 2D to 3D: imaging the cell .....	71
3.2	Synthesis and characterization of the cyclometalated iridium(III) complex.....	74
3.3	Design and photophysical behavior of the novel Ir-PAA .....	77
3.4	<i>In vitro</i> investigation of Ir-PAA .....	81
3.5	Conclusions .....	89
3.6	Experimental part .....	90
3.6.1	Synthesis of the ancillary ligand .....	90
3.6.2	Synthesis of the Ir(III) complex .....	91
3.6.3	Synthesis of Ir-PAA .....	91
3.6.4	Photophysical experiments .....	92
3.6.5	<i>In vitro</i> cell culture .....	92
3.6.6	<i>In vitro</i> cell culture onto the hydrogels .....	92
3.6.7	Organelle staining .....	92
3.6.8	Cell viability.....	93
3.6.9	Ir(III) complexes incubation (2D measurements).....	93
3.6.10	Live-Cell fluorescence confocal microscopy.....	94
3.6.11	Statistic methods .....	94
3.7	References .....	94
<b>4.</b>	<b>Nanocomposite hydrogels for cells growth and chemotaxis .....</b>	<b>98</b>
4.1	Tissue engineering: challenging and promises for novel nanocomposites implants	99
4.2	Design and synthesis of the nanocomposite scaffold.....	101
4.2.1	Study design.....	101
4.2.2	Mesoporous silica nanoparticles: the nanostructured components.....	101
4.2.3	Synthesis and characterization of the scaffolds .....	105
4.3	Rheological study .....	109
4.4	<i>In vitro</i> cells adherence and proliferation.....	111
4.5	Concentric cylinder hydrogel and homing of stem cells <i>in vitro</i> .....	114
4.6	<i>In vivo</i> response to the nanocomposite hydrogels.....	117
4.6.1	Importance of <i>in vivo</i> evaluation for novel implantable biomaterials.....	117
4.6.2	<i>In vivo</i> study .....	117
4.7	Conclusions .....	120

4.8	Experimental section .....	121
4.8.1	Synthesis and amino-functionalization of mesoporous silica nanoparticles...	121
4.8.2	Calculation of the average number of amino groups on the particle surface..	121
4.8.3	Loading of SDF-1 $\alpha$ .....	122
4.8.4	Synthesis of MSN-hydrogel and pristine hydrogel.....	124
4.8.5	Synthesis of concentric cylinder hydrogel (CCH) .....	124
4.8.6	Hydrogels mechanical characterization .....	125
4.8.7	Cell culture in 2D and onto the hydrogels .....	126
4.8.8	Cell staining and viability studies .....	127
4.8.9	Surgical model and scaffolds implantation.....	127
4.8.10	Histological evaluation .....	127
4.8.11	Statistic methods .....	128
4.9	References .....	128
<b>5.</b>	<b>Biodegradable hydrogels for submucosal fluid cushion .....</b>	<b>131</b>
5.1	Endoscopic submucosal dissection .....	132
5.2	Design and synthesis of an injectable biodegradable nanocomposite.....	135
5.2.1	Study design.....	135
5.2.2	Synthesis of breakable nanocapsules .....	136
5.2.3	Synthesis of the nanocomposite hydrogel, dPAA.....	138
5.2.4	Degradation in presence of GSH .....	139
5.2.5	Tunability of the degradation kinetic .....	141
5.2.6	Release of the model protein.....	142
5.3	In vitro and ex vivo analyses.....	144
5.3.1	Cell-mediated degradation .....	144
5.3.2	dPAA injectability and formation of SFC .....	147
5.4	<i>In vivo</i> ESD procedure .....	150
5.5	Conclusions .....	153
5.6	Experimental part .....	154
5.6.1	Synthesis and functionalization of BNCs .....	154
5.6.2	Synthesis of dPAA .....	154
5.6.3	Degradation kinetic in presence of GSH .....	155
5.6.4	In vitro cell culture.....	156



5.6.5	In vitro cell culture onto the nanocomposite hydrogels .....	156
5.6.6	Cell staining and viability studies .....	156
5.6.7	Cell-mediated degradation of dPAA.....	157
5.6.8	Evaluation of the gelation and formation of SFC ex vivo .....	157
5.6.9	Creating submucosal cushion and performing ESD in a living pig.....	157
5.7	References .....	158
<b>6.</b>	<b>Instrumental techniques.....</b>	<b>160</b>
6.1	Scanning electron microscopy (SEM).....	161
6.2	Confocal laser scanning microscopy (CLSM) .....	163
6.3	Dynamic light scattering (DLS) .....	166
6.4	Zeta potential.....	168
6.5	Fluorescence spectroscopy .....	170
6.6	Luminescence quantum yield.....	171
6.7	Lifetime measurements .....	172
6.8	References .....	173
	<b>Curriculum Vitae .....</b>	<b>175</b>
	<b>Acknowledgements .....</b>	<b>178</b>





## Résumé de thèse

L'ingénierie tissulaire (IT) est un domaine interdisciplinaire en pleine expansion, qui porte sur le comportement et les interactions entre les cellules, les biomatériaux et les facteurs de croissance.<sup>[1]</sup> L'IT vise à remplacer des tissus malades ou améliorer leur fonction avec des « scaffolds » qui permettent l'encapsulation de cellules, par la mise en œuvre de matériaux présentant des facteurs biochimiques et physico-chimiques appropriés.<sup>[2]</sup>

Ainsi, il est souhaitable d'avoir des scaffolds artificiels<sup>[3]</sup> permettant de répliquer les fonctions des tissus pour des études *in vitro*. Ceux-ci doivent fournir un milieu de culture cellulaire qui ressemble étroitement au tissu corporel, qui se compose de la matrice extracellulaire (MEC) et des molécules bioactives solubles.<sup>[4]</sup> Ces cadres artificiels doivent être synthétisés dans des conditions douces et biocompatibles ; ainsi que posséder une stabilité mécanique. Ils devraient imiter le plus fidèlement possible la MEC connue dans les tissus naturels, en termes d'architecture, de composition, des signaux mécaniques, pour permettre la migration des cellules, l'organisation, la prolifération et la différenciation, non seulement d'un point de vue intercellulaire mais également pour les interactions cellules-matériaux.<sup>[5]</sup> De plus, un objectif ambitieux de l'IT est d'améliorer les l'infiltration et la prolifération des cellules *in vivo*, dans le but final régénérer des tissus.<sup>[6]</sup>

Au cours des dernières années, des progrès importants ont été réalisés dans la conception des scaffolds naturels et artificiels, allant de simples matrices de supports à des bio-matériaux plus complexes. Une des exigences importantes pour tous les systèmes développés est leur capacité à contenir de l'eau et ainsi les hydrogels sont des candidats idéaux.

Les hydrogels sont des réseaux tri-dimensionnels (3D) composés de chaînes polymères hydrophiles réticulés, avec la capacité à gonfler, sans dissolution, en absorbant jusqu'à des milliers de fois leur poids sec dans l'eau.<sup>[7]</sup>

Depuis leur introduction à la fin des années 1960,<sup>[8]</sup> ils ont été employés avec succès comme MEC synthétiques pour différentes applications.<sup>[4, 9]</sup>

Cette classe de matériaux a reçu une attention considérable en raison de leur biocompatibilité, leur teneur élevée en eau,<sup>[10]</sup> leurs propriétés élastiques ressemblant à celles des tissus et leur structure poreuse 3D<sup>[11]</sup> qui permet la pénétration de l'oxygène, de nutriments et éventuellement la vascularisation.<sup>[12]</sup>

Les scaffolds de l'IT doivent présenter des propriétés mécaniques et chimiques qui permettent l'activité des cellules de façon naturelle. Pour cela, les hydrogels présentent de nombreux avantages, car leurs propriétés mécaniques, physico-chimiques (par exemple, la taille des pores<sup>[13]</sup>) et la rigidité (par exemple la dureté<sup>[14]</sup>) peut être ajustée pour l'application souhaitée. Les hydrogels peuvent être constitués de polymères naturels ou synthétiques. En raison de mauvaises propriétés mécaniques des hydrogels naturels, leur reproductibilité pas toujours évidente, leur coût élevé et leur disponibilité limitée, les polymères synthétiques ont émergé comme des alternatives intéressantes.<sup>[15]</sup>

En comparaison à leurs homologues naturels, les hydrogels synthétiques peuvent être obtenus avec un contrôle plus élevé sur leur composition, leurs caractéristiques de surface et d'autres paramètres clés tels que l'absorption de l'eau et des propriétés mécaniques.<sup>[16]</sup> En outre, leur synthèse et leurs propriétés sont hautement reproductibles et donc permettent l'incorporation de fonctionnalités adaptées,<sup>[17]</sup> molécules biologiques<sup>[18]</sup> ou inorganiques à l'échelle nanométrique qui peuvent être liés de manière covalente aux structures polymères.<sup>[19]</sup>

Le but de cette thèse était d'explorer de nouveaux hydrogels biocompatibles possédant une certaine activité biologique ainsi que des applications spécifiques en biomédecine et IT. L'objectif du travail portait sur le développement des hydrogels composés de chaînes polymériques hydrophiles chimiquement réticulés, comme des polyamidoamines, avec de nouvelles caractéristiques intéressantes et à les utiliser comme scaffolds en 3D pour la croissance cellulaire ainsi que pour étudier les réponses *in vitro* et *in vivo*.

Les polyamidoamines sont une classe prometteuse de polymères synthétiques pour l'application en IT.<sup>[20]</sup> Ils ont été choisis en raison de leur biocompatibilité renommée et en particulier en raison de leur polyvalence chimique.

Les hydrogels faits à partir de ces polymères peuvent être préparés par une synthèse « one-pot » à partir de molécules disponibles dans le commerce, dans des conditions douces.

De plus, la capacité d'adaptation de la chimie impliquée permet le choix des monomères de départ afin d'obtenir des matériaux facilement modifiables en introduisant les fonctionnalités chimiques nécessaires ou des groupements bioactifs.<sup>[21]</sup> Ils sont notamment intéressants dans la mesure où potentiellement toute amine primaire ou secondaire peut être choisie pour obtenir la polyaddition de bis-acrylamides.

Au début de la thèse, la synthèse des hydrogels appropriés de type polyamidoamines a été étudiée. Des résultats intéressants ont été obtenus à l'aide d'une polyaddition de type Michael de N,N'-méthylène bisacrylamide (MBA) avec des diamines telles que l'éthylène diamine (EDA) primaires, pour des connexions inter-canaux.<sup>[22]</sup> En particulier, la synthèse a été effectuée dans l'eau, à température ambiante, sans ajout base ou de catalyseur étant donné que les amines présentes dans le mélange réactionnel peuvent agir à la fois comme agents nucléophiles et bases.

Dans un mode opératoire typique de synthèse, la MBA a été solubilisé dans de l'eau distillée. Après la dissolution complète, l'agent de réticulation de type diamine, a été ajouté pour induire la polymérisation du système. On laisse le mélange réagir à la température ambiante dans des conditions statiques pendant 3 à 4 heures, en obtenant ainsi l'échafaudage d'hydrogel. Cependant, l'hydrogel obtenu était très dur et fragile, avec pas ou peu de capacité à gonfler dans l'eau. Le comportement désiré et réversible dégonflé/gonflé d'hydrogels n'est pas observé, ceci étant probablement dû au degré de réticulation élevé dans le réseau. Ainsi, pour réduire le degré de réticulation, un autre monomère a été ajouté, le N, N-diméthyléthylènediamine (DED), comme représenté sur la Figure 1.

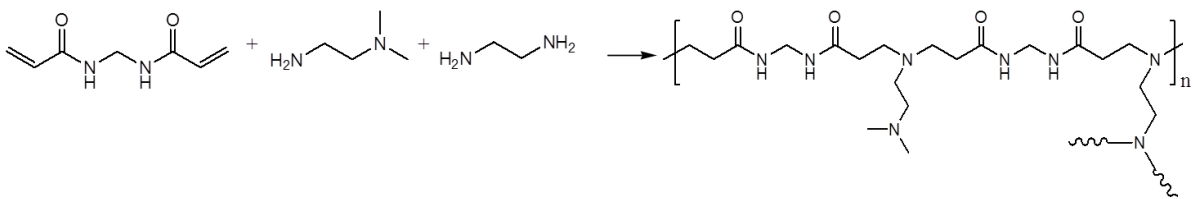


**Figure 1.** Schéma réactionnel de la polyaddition de type Michael.

L'hydrogel obtenu était transparent, et la méthode dite "Inverted test tube method" (retournement de tube à essai avec conservation de forme) a été utilisée comme un moyen simple et direct pour confirmer la gélification. L'hydrogel obtenu n'est pas tombé après le retournement de l'échantillon, montrant une résistance à la gravitation sans tomber quand le pilulier a été inversé. Un paramètre intéressant pour la caractérisation des hydrogels, en particulier pour des applications biomédicales, est l'équilibre de degré de gonflement (EDG). En raison du gonflement des hydrogels dans l'eau et les solutions physiologiques qui affecte le transport de l'oxygène, les nutriments et les facteurs de croissance, qui sont essentiels pour la survie des cellules et la croissance,<sup>[23]</sup> nous nous sommes intéressés à cet aspect.

L'EDG donne des indications sur la stabilité de l'échafaudage d'hydrogel dans l'eau ou à un pH spécifique et la quantité de la teneur en eau maximale, qui est liée à l'élasticité du matériau. Pour les hydrogels synthétisés, l'EDG a été calculée au moyen de mesures gravimétriques, suivant l'équation 1 :

$$EDG (\%) = \frac{W_s - W_d}{W_d} \times 100 \quad (1)$$

Où  $W_s$  est la masse de l'hydrogel à l'état de gonflement, et  $W_d$  est la masse à l'état sec.

La prise d'eau maximale calculée en utilisant la N,N-diméthylethylenediamine est de 61%, avec un EDG de 156%.

Diverses procédures ont ensuite été développées pour augmenter l'hydrophilie et la biocompatibilité de ces matériaux.

L'utilisation d'acide amino-butyrique  $\gamma$  qui fournit des groupes carboxyliques dans le réseau, a permis d'augmenter la quantité d'eau dans l'hydrogel par liaison hydrogène supplémentaire.<sup>[24]</sup>

De plus, cela a permis d'obtenir une structure amphotère, avec une augmentation potentielle de de cyto-compatibilité. Il a été montré qu'une augmentation de la biocompatibilité a été obtenue en utilisant des polyamidoamines linéaires amphotères,<sup>[25]</sup> et des travaux antérieurs étudiant les réponses de cytotoxicité<sup>[26]</sup> ont démontré que tous les hydrogels à base de polyamidoamine amphotères considérés étaient cyto- et biocompatibles.

Le rapport entre les monomères et les conditions de réaction ont été optimisées afin d'obtenir un hydrogel souple capable de gonfler, qui conserve cependant sa forme, comme représenté sur la Figure 2. De plus, il a été possible d'augmenter la quantité de teneur en eau jusqu'à 72%, EDG = 260 % et plus intéressant, la capacité de gonflement du matériau, à la fois dans l'eau et dans le milieu de culture, était réversible : il a été en mesure de subir des cycles mouillage-séchage, impliquant un comportement de type gonflement / dégonflement, même après 20 jours à partir de la synthèse. Vu les propriétés mécaniques intéressantes et un gonflement de la matière synthétique, des tests de prolifération des cellules préliminaires ont été réalisées avec des cellules HeLa qui ont été semés sur un échantillon hydrogel de forme carrée (1 ~ 1 cm) et cultivées pendant 48 heures.



**Figure 2.** Hydrogel contenant de l'acide aminobutyrique en tant que co-monomère ; pilulier retourné et SEM.

Pour améliorer encore la capacité de gonflement et de l'élasticité, l'EDA a été remplacée par la pentaéthylènehexamine (PEHA) comme agent de réticulation de la structure. La caractérisation rhéologique effectuée par nos collaborateurs à Universidad Complutense de Madrid nous a permis de mesurer une différence de valeurs de déformation lorsque les hydrogels sont réticulés avec le PEHA à la place de l'EDA. En effet, la rigidité et les propriétés mécaniques des matrices d'hydrogel peuvent être ajustées en modifiant les molécules de réticulation et le degré de réticulation, comme indiqué ailleurs pour d'autres systèmes.<sup>[25, 27]</sup>

Les tests de prolifération cellulaire ont montré que les cellules HeLa ont été capables de croître et de proliférer dans toute l'épaisseur du matériau, ce qui confirme la cyto-compatibilité de l'hydrogel conçu et son efficacité en tant que plate-forme 3D pour la culture de cellules.

Ces études nous ont permis d'individualiser et d'optimiser le rapport correct entre les monomères afin d'obtenir de souples hydrogels gonflants, adaptés à l'adhésion cellulaire 3D, pour l'IT spécifique et applications biomédicales.

Les hydrogels ont été utilisés dans divers domaines biomédicaux. Cependant, à notre connaissance, l'application des hydrogels comme un outil pour visualiser les cellules et suivre leur prolifération dans les scaffolds n'a pas encore été étudiée.

La mise en œuvre ce type des scaffolds avec des sondes luminescentes capables de révéler la présence de cellules pourrait en faire des plateformes d'imagerie avec un grand potentiel pour la détection luminescente et la visualisation des cellules en 3D.



En particulier, l'imagerie par microscopie à fluorescence est devenu un outil puissant pour les études biomédicales, en raison de la grande quantité d'informations qu'elle peut donner et surtout parce qu'il s'agit d'une méthode non-invasive.<sup>[28]</sup>

Ainsi, l'incorporation d'une sonde fluorescente pour la visualisation des cellules dans les hydrogels 3D, qui peut donc combiner les avantages de la détection par fluorescence et l'hydrogel pour la prolifération cellulaire en 3D, est hautement souhaitable pour des applications biomédicales et pourrait ouvrir de nouvelles voies pour les techniques d'imagerie *in vitro*.

Cependant, la présence de colorants pour les cellules est considérée comme une modification du cycle cellulaire naturel ; nous avons par conséquent conçu une plateforme d'hydrogel pour la visualisation des cellules en l'absence de colorants internalisés.

Dans le chapitre 3, nous avons introduit un nouvel hydrogel pour études de cellules *in vitro*, avec incorporation de manière covalente de complexes cyclométallés d'Ir (III) comme sondes fluorescentes.

Le complexe neutre d'Ir (III) cyclométallé, contenant des ligands à base de 6-phenylphenanthridine, a été synthétisé suivant des procédures modifiées déjà décrites dans la littérature.<sup>[29]</sup>

Il a été conçu avec une émission "off / on", en réponse à différents environnements.

En particulier, il affiche un maximum d'émission ( $\lambda_{em}$ ) à 638 nm dans le dichlorométhane, légèrement décalée vers le rouge dans l'eau, ce qui indique une stabilisation plus forte de l'état excité dans les solvants polaires, comme prévu pour la nature du transfert de charge de métal à ligand de l'état excité.

En outre, la diminution de la durée de vie à l'état excité et du PLQY (rendement quantique de photoluminescence) dans l'air a montré que la nature de l'état d'émission triplet est susceptible d'extinction par le dioxygène.

Le complexe d'Ir (III) a ensuite été greffé covalamment<sup>[29a]</sup> au réseau d'un hydrogel à base polyamidoamines, via une simple addition 1,4 dans l'eau.<sup>[30]</sup>

La figure 3 montre une structure schématique du matériau, nommé Ir-PAA, ainsi que ses propriétés morphologiques et de gonflement.

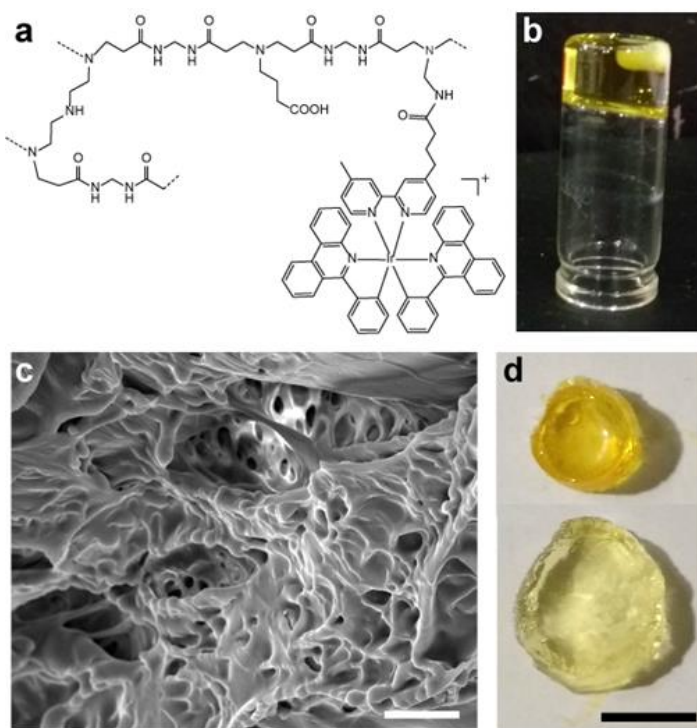


**Figure 3.** Schéma de la structure chimique de l'Ir-PAA (a); test de confirmation de la gélification et montrant la transparence optique du matériau obtenu (b); image SEM de la structure morphologique (c), barre d'échelle de 100  $\mu\text{m}$ ; photographie de l'Ir-PAA sec et regonflé en eau (d), barre d'échelle de 1 cm.

Le comportement photoluminescence (PL) de l'hydrogel obtenu sec et en état de gonflement dans l'eau a été analysée. Il expose deux bandes d'émission, liées à l'émission du complexe Ir (III) embarqué (avec un pic à environ 640 nm) et au réseau polymère (à plus haute énergie).

L'Ir-PAA contrôlé à 640 nm présentait une durée de vie bi-exponentielle de l'ordre de la microseconde ( $\mu\text{s}$ ) lorsqu'il été sec. Cette durée de vie est plus que deux fois plus courte à l'état gonflement dans l'eau. Cela indique une extinction de phosphorescence de l'état de triplet en raison de molécules d'oxygène dans la solution.

Ce phénomène d'extinction de l'émission de fluorescence du complexe d'Ir (III) dû à l'oxygène pour l'hydrogel gonflé dans un milieu aqueux est confirmée lors de la mesure du PLQY à l'état sec (14%) et dans l'eau (5%).

L'efficacité de l'hydrogel Ir-PAA pour soutenir la prolifération des cellules en 3D a été évaluée pendant une période de 7 jours et une augmentation substantielle de 20% de l'activité métabolique cellulaire a été montrée, indiquant sa cyto-compatibilité et ainsi suggérant que l'Ir-PAA est une excellente plate-forme pour la croissance cellulaire 3D

Le potentiel du nouveau matériau Ir-PAA avec une sonde d'imagerie intégrée a ensuite été étudiée pour l'imagerie 3D sur cellules vivantes en temps réel.

En particulier, la présence de cellules, en interaction avec les complexes Ir (III) greffés sur le réseau a induite l'émission de fluorescence, qui a été détectée au niveau des membranes plasmatiques des cellules (Figure 4), sans coloration cellulaire supplémentaire et sans fluorescence de fond.

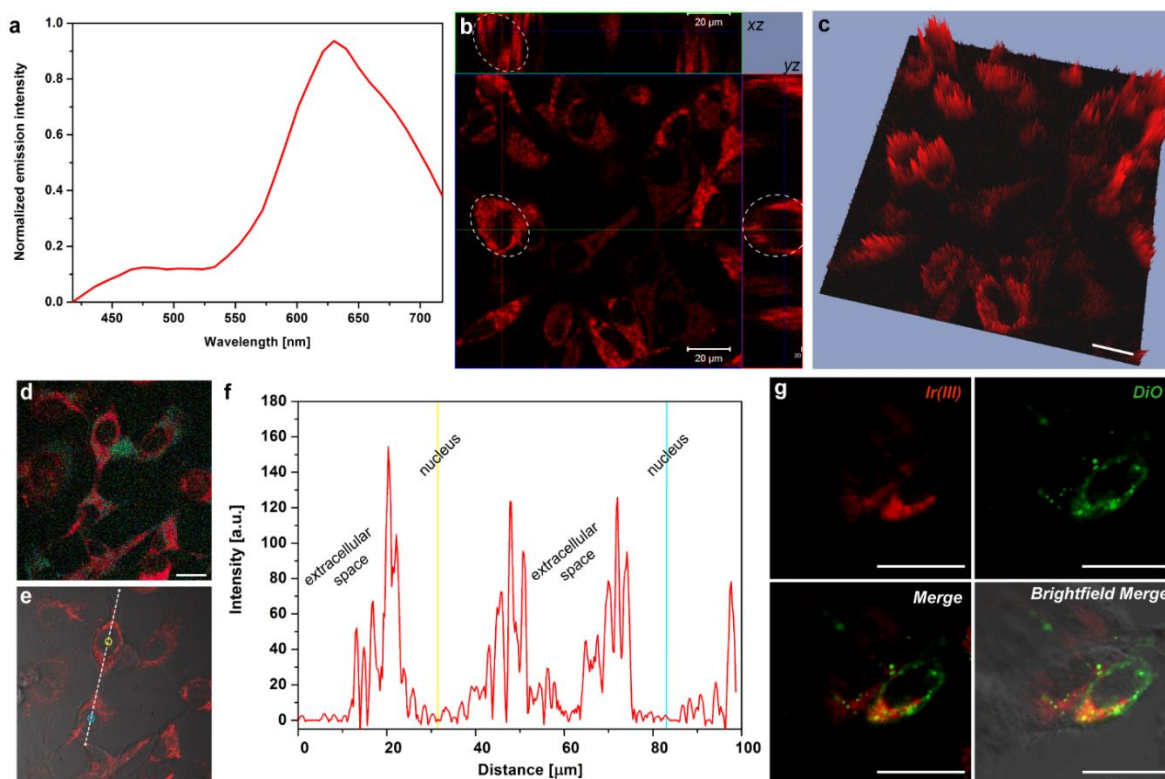


**Figure 4.** Spectre d'émission de la membrane plasmique des cellules cultivées sur Ir-PAA (a); Z stack d'images à augmentation du profondeur sur l'axe z (b) et profil 2.5D (c); couleur vraie des HeLa sur Ir-PAA après 96 h (d); superposition des canaux rouge et fond clair (e); profil d'intensité de luminescence à travers la ligne représentée sur la figure (e) et correspondant à la région extracellulaire, à la membrane et la région nucléaire (cercles jaune et bleu) de deux cellules (f); canal séparé et superposer de la visualisation de la colocalisation du signal Ir (III) et DiO plasma tache verte (g). La barre d'échelle est de 20 μm et la magnification est de 60x dans toutes les images.

Cela a permis la visualisation claire et facile en temps réel des cellules proliférantes sur l'hydrogel jusqu'à 7 jours. Le mécanisme de type « off / on » de l'eau à l'environnement lipophile des membranes plasmatiques des cellules a été étudié.

Nous avons supposé que l'interaction hydrophobique entre la membrane cellulaire et l'Ir (III) conduit à une insertion du Ir (III) dans la membrane, comme illustré sur la figure 5, et rapporté ailleurs pour d'autres systèmes.<sup>[31]</sup> La lipophilie des complexes d'Ir (III), donnée par l'aromaticité des ligands, est supposée faciliter cette interaction.<sup>[32]</sup>

Nous avons pensé que l'insertion du complexe d'Ir (III) dans la membrane plasmique protège les complexes par l'oxygène présent dans l'environnement aqueux extracellulaire, permettant ainsi une luminescence sensible à l'environnement, qui se traduit par une commutation "off / on" d'émissions.

L'émission rouge observé de la région de la membrane cellulaire soutient l'hypothèse que les complexes d'Ir (III) insérés dans la bicouche lipidique pourraient agir en tant que sondes fluorescents lipophiles de l'environnement local.

Ce comportement porte à la protection du Ir (III) de l'environnement aqueux (et donc par le dioxygène), induisant une augmentation de la luminescence.

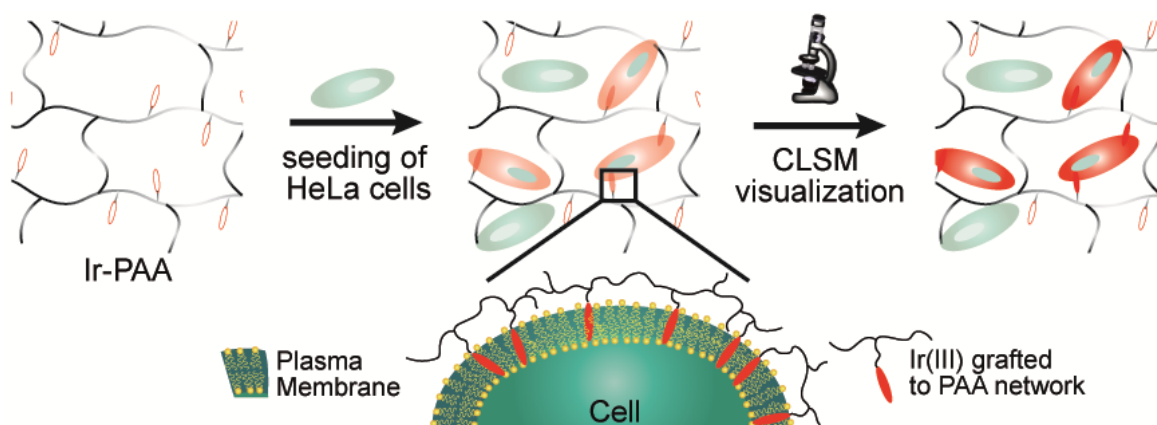


**Figure 5.** Schéma du mécanisme de la "off / on" des émissions. Le complexe est trempé dans l'eau, mais lorsque les cellules sontensemencées sur l'Ir-PAA, certaines cellules peuvent interagir avec les complexes d'Ir (III) greffés sur le réseau polymère. Le complexe métallique hydrophobe est insérée dans la membrane plasmique, provoquant « l'allumage » de l'émission dans le rouge vif.

Le principal résultat de la présente recherche est la divulgation d'une stratégie innovatrice pour le développement de plates-formes luminescent-sonde-3D, ce qui, pour nous, peut être bénéfique pour les études des cellules *in vitro*.

L'introduction de nanoparticules inorganiques en tant que composants des hydrogels peut en modulée l'élasticité et l'adhérence des cellules.<sup>[33]</sup> Les hydrogels nano-composites obtenus sont

des matériaux hybrides souples, dont le réseau polymère est réticulé à des nanoparticules ou des nanostructures.<sup>[34]</sup>

Dans ces systèmes, les nanoparticules interagissent de manière physique ou covalente avec les chaînes polymériques, ce qui entraîne de nouvelles propriétés intéressantes du réseau d'hydrogel.<sup>[35]</sup> Cependant, malgré les progrès considérables qui ont été accomplis dans la synthèse et la fonctionnalisation de nano-composites, ces biomatériaux ont rarement trouvé une traduction clinique réussie dans les implants de l'ingénierie tissulaire, principalement en raison des réponses inflammatoires qu'ils génèrent.<sup>[36]</sup>

Dans le chapitre 4 de cette thèse, un hydrogel nano-composite a été préparé et étudié *in vitro* et *in vivo*. Cet hydrogel est composé de chaînes polymériques biocompatibles réticulés chimiquement et des nanoparticules de silice mésoporeuse incorporés, MSNs.<sup>[36]</sup> Les MSNs ont été sélectionnées en tant que composants nanostructurés en raison de leurs nombreuses caractéristiques telles que la possibilité de charger et de libérer des composants actifs, des cadres stables et rigides, une chimie de surface polyvalente,<sup>[37]</sup> et des pores ayant un volume modifiable.<sup>[38]</sup> En particulier, la surface des particules a été fonctionnalisée avec des groupements amine, afin de fournir un point d'ancrage au squelette polymérique de l'échafaudage (NH<sub>2</sub>-MSNs, Figure 6).

L'avantage d'utiliser des pores est liée à la possibilité de libérer des substances chimiques qui peuvent être chargées dans la structure de canaux du matériaux mésoporeux.<sup>[39]</sup> De plus, il a été démontré que les nanomatériaux à base de silice peuvent améliorer la stabilité mécanique et l'élasticité des hydrogels,<sup>[40]</sup> et ils suscitent un grand intérêt dans des applications biomédicales en raison de leur stabilité chimique et une faible cytotoxicité.<sup>[41]</sup>

Après avoir prouvé que des petites molécules peuvent être chargées et libérées dans l'hydrogel, nous avons démontré que les cellules présentes dans celui-ci peuvent absorber du colorant libéré, Hoechst a été utilisé comme exemple, et leurs noyaux sont colorés à partir du colorant libéré.

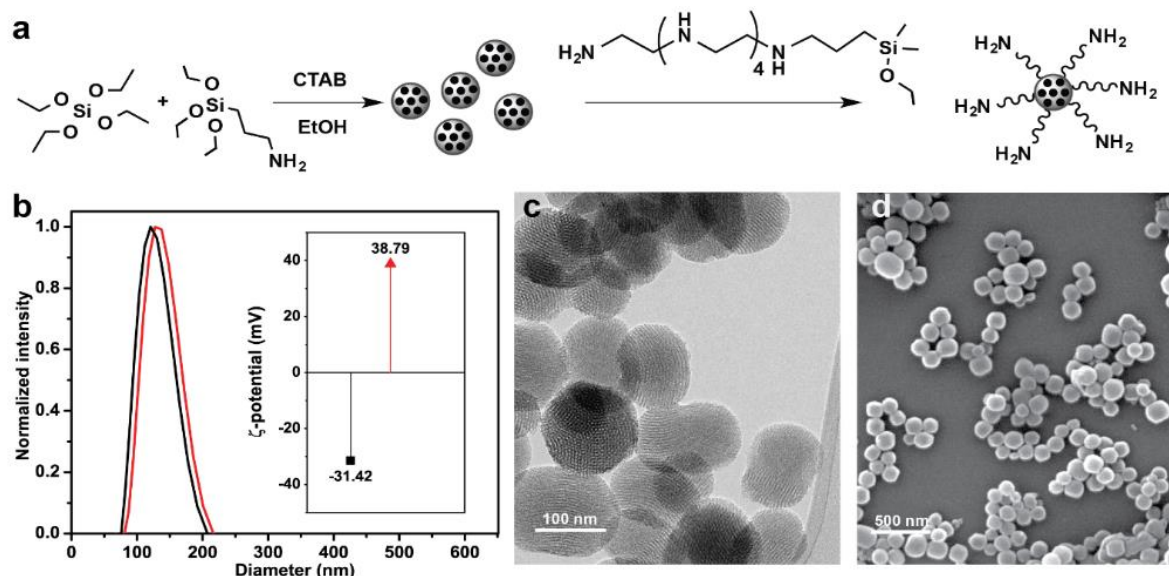


**Figure 6.** Schéma réactionnel de la synthèse et de l'amino-fonctionalisation des MSNs (a), Diffusion dynamique de la lumière, DLS (b) des MSNs (noir) et des NH<sub>2</sub>-MSNs (rouge) ; valeurs de potentiel- $\zeta$  pour les MSNs (noir), et les NH<sub>2</sub>-MSNs (rouge) à l'intérieur. Images TEM (c) des MSNs et SEM (d) des NH<sub>2</sub>-MSNs.

Ce résultat a été étendu aux protéines et afin d'améliorer le potentiel thérapeutique de l'hydrogel, le cytokine « Stromal cell-Derived Factor 1 $\alpha$  » (SDF-1 $\alpha$ ) a été chargé dans les MSNs embarqués dans l'échafaudage. SDF-1 $\alpha$  est un candidat intéressant pour cette étude en raison de son activité chimiotactique envers les cellules souches mésenchymateuses (MSC), ainsi il peut être utilisé pour guider les cellules souches vers l'échafaudage implanté.<sup>[42]</sup> Plus précisément, pour assurer la migration des MSC à travers l'échafaudage MEC, la matrice d'hydrogel mécanique biomimétique a été conçue pour avoir une rigidité suffisante dans le but de soutenir la résilience structurelle lors de la prolifération des cellules et une viscosité suffisamment faible, ceci facilitant la migration des cellules dans l'échafaudage de support.<sup>[42]</sup> Le nano-composite hydrogel développé (MSN-hydrogel) a montré être un échafaudage souple et déformable, idéal pour la prolifération des cellules et la migration (Figure 7).

Les propriétés mécaniques et de cyto-compatibilité du MSN-hydrogel ont été étudiées et ont montré d'excellentes propriétés élastiques, ce qui a entraîné une plus grande quantité de cellules adhérentes et proliférées (cellules souches osseuses mésenchymateuses de la moelle de la souris, mBM-MSC) après 7 jours de culture, comparés au même hydrogel sans nanoparticules (hydrogel seul).



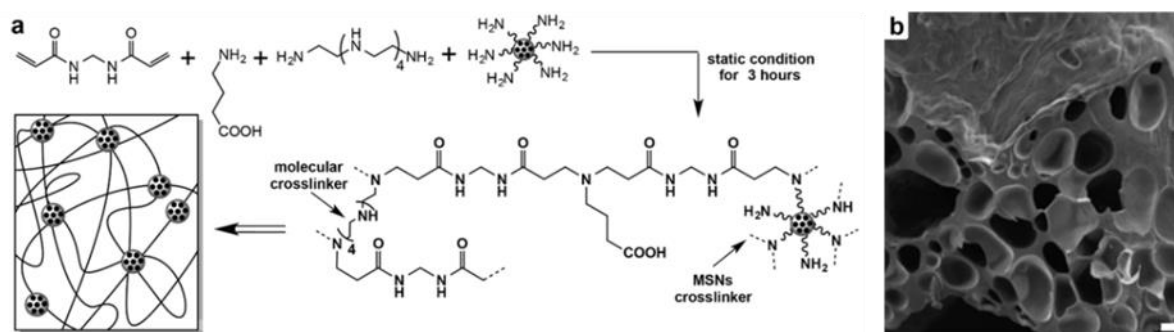


**Figure 7.** Schéma de synthèse (a) et image SEM (b) du MSN-hydrogel, l'échelle est 20  $\mu\text{m}$ .

En particulier, nous avons détecté une augmentation de 25 % de l'activité cellulaire après 7 jours de culture (72 % au jour 7 comparés à 47% au jour 1) pour le MSN-hydrogel. Ces résultats indiquent qu'il n'y avait pas d'effet cytotoxique sur la viabilité des mBM- MSC; leur porosité élevée (Figure 7b, les pores ont une taille de 20 à 80  $\mu\text{m}$ ) a permis aux cellules de migrer à travers les échafaudages, tout en maintenant leur viabilité.

Nous avons ensuite étudié l'efficacité de cet hydrogel ainsi que SDF-1 $\alpha$  en promouvant la migration des mBM-MSK *in vitro*. Nous avons formulé un système d'hydrogel double, à savoir SDF@CCH, qui a été conçu pour simuler le « homing (hématopoïétique) » des cellules souches endogènes. En bref, ce système est constitué d'un noyau interne de MSN-hydrogel cylindrique, où MSNs ont été préalablement chargées avec le SDF-1 $\alpha$  ; et un cylindre extérieur, résultant en un matériau structuré double. La représentation schématique du dispositif est représentée sur la Figure 8.

L'approche était de séparer spatialement l'hydrogel contenant le système de distribution SDF-1 $\alpha$  de la partie où les cellules ont été initialementensemencées, et observer la migration des cellules lors de la libération de la chimiokine.

Ainsi, les mBM-MSK ont étéensemencées sur les bords externes du SDF@CCH et leur migration à partir des bords de l'échafaudage jusqu'à l'intérieur, libérant l' SDF-1 $\alpha$ , a été surveillée pendant 7 jours. Fait intéressant, déjà au jour 3 nous avons observé une migration des cellules dans le coeur du système. En outre, les cellules affichent un alignement vers la source de SDF-1 $\alpha$ , ce qui indique un mouvement qui suit le gradient du facteur libéré.

Après 7 jours, le noyau central du système a montré la présence abondante de cellules, alors qu'au jour 0 cette partie de l'échafaudage était complètement vide.

La migration des cellules vers l' SDF-1 $\alpha$  libéré a été étudié par microscopie optique, par microscopie électronique à balayage et microscopie de fluorescence en mode z-stack, ce qui nous a permis d'observer la migration en 3D (les cellules ont été colorées en rouge avec un colorant fluorescent Vybrant DiD), comme représenté sur la Figure 9.

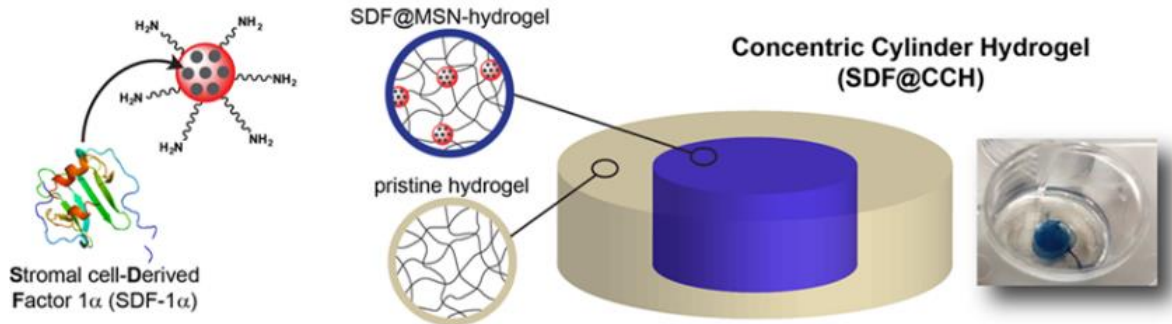


**Figure 8.** Schematic representations of SDF-1 $\alpha$  loading into MSNs, of concentric cylinder hydrogel, SDF@CCH, and photograph of the obtained SDF@CCH.

Enfin, en utilisant la détection par fluorescence et un logiciel de suivi, nous avons pu confirmer la migration vers le gradient de SDF-1 $\alpha$ . Nos résultats, obtenus à partir de 5 heures d'expérience, indiquent encore une fois que le mouvement de la mBM-MSC est dirigé vers le noyau interne de l'échafaud.

Nous avons étudié la réponse *in vivo* à ces nouveaux échafauds dans la fenêtre inflammatoire aiguë (3-7 jours). Les hydrogels ont été implantés dans des poches dorsales sous-cutanées dans des souris de type BALB / c.<sup>[43]</sup> Les hydrogels sont restés en place sans important changement de volume et de poids et aucun signe macroscopique d'inflammation ou d'infection a été détecté au moment de l'explantation. L'analyse histologique des hydrogels explantées et les tissus environnants ont montré qu'aucun processus inflammatoire chronique défavorable évident n'avait eu lieu ; l'hydrogel relâchant SDF a montré une densité cellulaire réduite et une capsule moins organisée autour d'elle. Cela est probablement dû à la présence du SDF-1 $\alpha$  libérée de l'échafaudage, ce qui a provoqué une modulation de la phase inflammatoire affectant le dépôt de tissu fibreux, comme indiqué ailleurs pour d'autres systèmes.<sup>[42b]</sup>

Ces résultats démontrent que les hydrogels conçus ont généré une réaction inflammatoire minimale quand ils sont implantés *in vivo*, et sont responsables de la modulation de la réponse



tissulaire ; ce qui suggère la possibilité de nouveaux hydrogels nano-composites comme implants pour le futur.

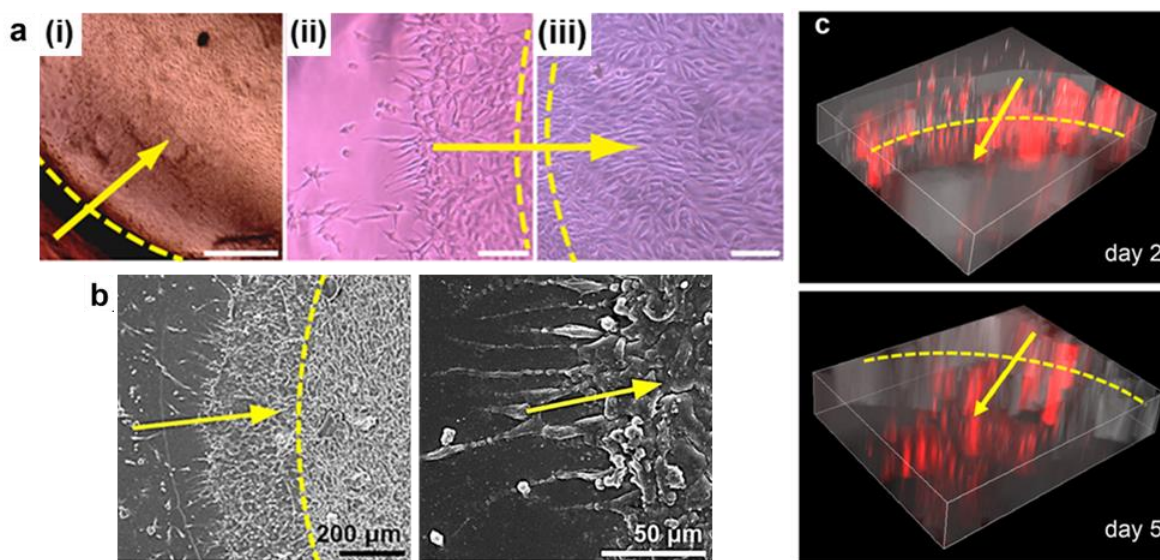


**Figure 9.** Images de « fond clair (brightfield) » de cellules en croissance sur SDF@CCH et migration vers le noyau après 7 jours (a) ; l'image (i) montre l'interface entre la partie extérieure et le noyau interne de la plate-forme, l'échelle est de 500 µm ; les images (ii) montrent la partie extérieure de l'échafaudage, composé d'hydrogel seul, l'échelle est de 50 µm ; l'image (iii) représente le noyau interne de l'échafaudage, libérant l' SDF-1α, l'échelle est de 50 µm. Les images SEM de cellules qui migrent vers le noyau après 7 jours (b) et la migration 3D (c).

L'implant des scaffolds préformés nécessite des procédures invasives chirurgicales qui peuvent limiter les applications biomédicales réussies des implants pré-synthétisés classiques.<sup>[44]</sup>

Au lieu de cela, les thérapies IT bénéficieraient d'interventions chirurgicales minimales pour diminuer la morbidité des patients. Par conséquent, au cours des dernières années, les efforts se sont portés davantage sur la conception et la synthèse de biomatériaux « injectables » ou « gélifié *in situ* », et en particulier les hydrogels. Ces matériaux peuvent être livrés *in vivo* par injection, puis gélifier rapidement à l'intérieur du corps.<sup>[45]</sup>

Notamment pour l'ingénierie des tissus mous ou souples, l'utilisation des scaffolds injectables offrent plusieurs avantages par rapport aux scaffolds préfabriqués. Les précurseurs d'hydrogels, ou leur forme liquide non visqueuse, peuvent être introduits dans le corps de l'hôte d'une manière peu invasive, ce qui réduit considérablement l'inconfort et les coûts de traitement des patients. En outre, l'injection peut être effectuée dans des endroits qui ne sont guère

accessibles en chirurgie classique, en introduisant ainsi de nouvelles possibilités pour l'utilisation potentielle des scaffolds d'hydrogel dans des zones qui sont généralement défavorisées pour des interventions chirurgicales de routine.<sup>43a,44</sup> Des perforations gastro-intestinales telles que les fistules et les blessures causées par le diabète ou d'autres maladies, ne sont que deux exemples pour lesquels hydrogels injectables pourraient représenter une solution intéressante.

Grâce à une collaboration avec Prof. Silvana Perretta de IRCAD et IHU, nous avons étudié la capacité d'injection et de gélification *in situ* des scaffolds d'hydrogel développés et nous avons également étudié leur aptitude à la dissection sous-muqueuse endoscopique (ESD). Il s'agit d'une procédure clinique appliquée pour les lésions néoplasiques à un stade précoce dans le tractus gastro-intestinal, ce qui permet une résection en bloc de grandes lésions.

La formation de l'hydrogel a été optimisée pour permettre cette procédure.

La réaction d'addition de Michael, qui est à la base de nos systèmes, affiche des taux de réaction rapides de nos systèmes dans des conditions douces, à température ambiante et sans catalyseur, et ne présente aucun sous-produit.<sup>[46]</sup> À la différence des matériaux précédents obtenus par photo-réticulation ou gélification thermique, qui ont montré un blocage des systèmes de relargage à la température normale de l'intérieur de du corps, ces hydrogels sont formés *in situ*<sup>[47]</sup> par réaction d'addition de type Michael, dans des conditions physiologiques.

Ainsi, dans le chapitre 5, nous avons optimisé les conditions pour obtenir des pré-gels qui pourraient être utilisés par des techniques d'injection. En effet, en profitant de la fenêtre de temps de gélification, il serait possible d'injecter les solutions liquides d'hydrogel par une aiguille (23G). Les expériences *in vivo* ont été effectués sur des porcs en raison de la similitude de leur estomac et de leur intestin à l'humain.

Fait intéressant, quand ils ont été injectés *in vivo* dans la sous-muqueuse de l'estomac d'un cochon, nous avons pu observer une gélification plus rapide, qui a eu lieu dans les 3 min suivantes à 37 °C et à un pH de 7,4, probablement dû à l'interaction avec des protéines du tissu. Par exemple, la formation de liaisons hydrogène entre les unités d'hydrogel et le collagène, ainsi que l'interpénétration des chaînes de polymère dans le mucus pourraient favoriser le processus de gélification (Figure 10).<sup>[48]</sup>

Encouragé par les résultats positifs obtenus, nous avons développé un système polyamidoamines-hydrogel injectable et biodégradable, ces travaux présentant le chapitre 5.

En particulier, nous nous sommes intéressés à la conception d'un échafaudage qui pourrait être introduit *in vivo* grâce à la technique invasive minimale, comme l'injection, et pourrait donc être dégradé par des stimuli externes ou par la prolifération des cellules sur l'échafaudage sur une période de plusieurs jours.

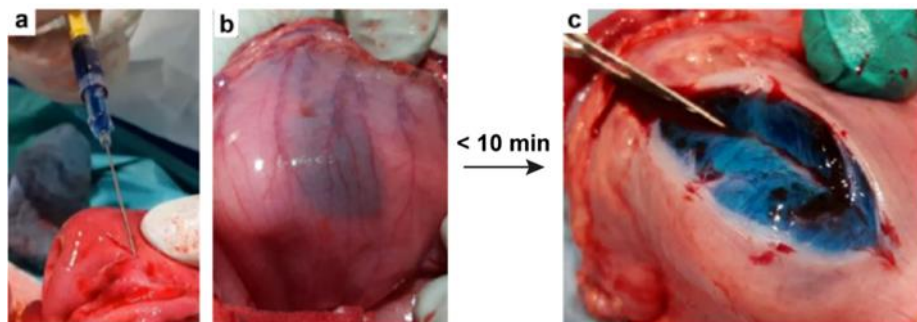


**Figure 10.** Injection de la solution d'hydrogel marquée par du bleu de méthylène pour une vue plus claire (a) ; détail du tissu montrant que l'hydrogel reste là où il a été injecté et n'est pas absorbé par le tissu (b) ; formation de l'hydrogel *in situ* (c).

Ainsi, nous avons synthétisés un hydrogel réticulé avec une cystamine, une disulfure diamine redox-sensible, dont le but était d'obtenir un réseau dégradé par l'échange de thiol réductrice par le glutathion (GSH), comme montré dans la Figure 11. L'énergie de liaison disulfure d'environ 60 kcal / mol rend cet échange très labile pour les thiols et les agents réducteurs. Le GSH est un produit du métabolisme cellulaire, ainsi couramment présents dans le corps, où il peut être trouvé dans des concentrations différentes dans l'environnement intra et extracellulaires (2-10 mM et 5 à 10  $\mu$ M respectivement).<sup>[49]</sup>

Par conséquent, nous avons examiné l'ampleur et la durée de la dégradation d'hydrogel en présence de GSH à différentes concentrations, lorsque différentes quantités de cystamine (10 % en masse, 20 % en masse, 40 % en masse) ont été incorporés comme agents de réticulation du réseau polymère. Bien que plusieurs études antérieures ont mis l'accent sur la dégradation de la réduction déclenchée par des différents systèmes à haut niveau GSH, la dégradation par GSH dans des conditions extracellulaires a rarement été mentionné auparavant.<sup>[50]</sup> Cette observation a soulevé des questions intéressantes quant à la possibilité d'obtenir un hydrogel dégradé par l'action des cellules.

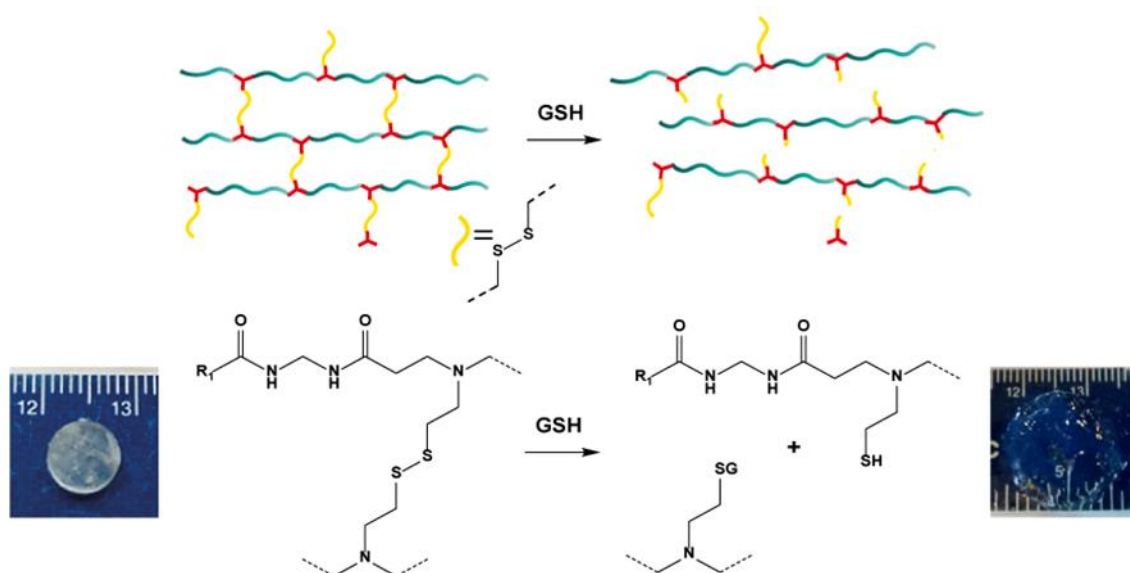


**Figure 11.** Mécanisme de la dégradation du réseau lors de l'exposition au GSH, avec la représentation schématique des images et du réseau d'hydrogel avant et après la dégradation. Les lignes jaunes représentent les unités de disulfure; la dégradation de l'échafaudage d'hydrogel se produit au niveau du site de clivage du disulfure par échange thiol-disulfure.

Nos résultats ont montré que la dégradation réductrice de ces matières peut être modifiée dans le temps de 1 heure à 6 jours en fonction du contenu de la cystamine dans l'échafaudage et de la concentration de GSH dans la solution dégradante. De même, des résultats préliminaires *in vitro* ont montré la faisabilité d'une dégradation par les cellules, alors que des fibroblastes dermiques humain adulte ont été cultivés et (HDFa) amenés à proliférer sur les hydrogels (Figure 8b). L'hypothèse selon laquelle les hydrogels ont présenté une dégradation en présence de cellules sans avoir besoin d'aucun stimulus externe a été confirmée. En particulier, l'hydrogel avec 20 % en masse de cystamine, contenant  $2.5 \times 10^5$  HDFa a subi une désintégration complète en moins de 72 heures, comme observé dans l'étude de la dégradation de la concentration en GSH de 10  $\mu$ M.

De plus, en tirant parti de notre expérience dans la synthèse de nanoparticules,<sup>[37, 51]</sup> nous avons pensé à incorporer des nanocapsules de silice cassables dans l'hydrogel. Ces nanocapsule sont conçues comme nano-conteneurs pour la molécule active choisie, avec la possibilité de la libérer par une dégradation par médiation cellulaire de l'hydrogel. Par conséquent, nous avons synthétisé des nanocapsules de silice (BNCs) portant une coquille cassable qui pourrait être rompue par le même mécanisme de clivage de ponts disulfures par stimulus redox utilisé pour

l'hydrogel et contenant du cytochrome C (Cyt-C) en tant que protéine modèle, car il est facilement détectable grâce à sa forte absorption à 405 nm. Ces nanocapsules cassables pourraient alors libérer le composant actif choisi en fonction de l'application, par exemple pour favoriser la guérison des tissus pendant le processus de dégradation de l'hydrogel.<sup>[52]</sup>

Les études de dégradation effectuées sur ces matériaux ont confirmé la libération de la protéine. Les résultats prometteurs obtenus nous ont encouragés à tester les hydrogels dégradables pour l'ESD.

Il s'agit d'une procédure endoscopique mini-invasive maintenant acceptée dans le monde entier comme modalité de traitement préférée pour l'élimination du cancer gastrique.<sup>[53]</sup>

Elle permet une résection *en bloc* des lésions ulcéreuses grandes<sup>[54]</sup> grâce à la résection directe de la couche sous-muqueuse. Elle est réalisée par électrocoagulation, ce qui implique un risque élevé de perforation.<sup>[55]</sup> Pour améliorer l'efficacité et l'innocuité de la technique ESD, l'injection d'une solution dans l'espace sous-muqueux est nécessaire. De cette façon, un coussin de fluide sous-muqueux (FSM) est créé entre la lésion et la couche musculaire proprement dit,<sup>[56]</sup> qui est responsable de l'élévation de la sous-muqueuse et au maintien de la hauteur d'élévation souhaitée lors de la procédure, ce qui est essentiel pour une dissection efficace.<sup>[57]</sup>

Même si plusieurs solutions et matériaux d'injection ont été proposées et testées, une solution saline normale est le plus couramment utilisé comme FSM, en raison de son faible coût et la facilité d'utilisation. Cependant, l'utilisation de ce fluide est entravée par de faibles élévations de la muqueuse, ce qui rend la procédure difficile et entraîne souvent des dommages par électrocoagulation de la musculature, et une absorption rapide dans les tissus environnants, donc nécessitant des injections répétées de résection étendue.<sup>[58]</sup> Par conséquent, le matériel adéquat est encore une question de débat.<sup>[56a, 59]</sup>

Cela nous invite à poursuivre la recherche sur des nouveaux hydrogels injectables et biodégradable comme un nouveau matériel d'injection ESD.

De plus, étant donné que l'échafaudage d'hydrogel développé est composé de nanocapsules de silice cassables greffées sur des chaînes polyamidoamines, il a le potentiel de fournir des molécules actives thérapeutiques ou pendant la phase de dégradation, d'aider la cicatrisation du tissu après la procédure.



Dans les procédures d'ESD, la capacité de la muqueuse de levage et son entretien sont indispensables pour éviter la perforation et la réalisation en toute sécurité de la résection en bloc de la lésion.

Des résultats *ex vivo* ont montré que l'hydrogel été facilement injectable et capable de fournir un coussin prolongé et épais fluide muqueux pour permettre à la procédure de l'ESD en toute sécurité.<sup>[59]</sup>

En particulier, les FSM sont apparues sur le site d'injection et les changements de hauteur dans l'élévation de la muqueuse ont été enregistrées au bout de 10 secondes, 10 minutes et 1 heure, pour couvrir toute la durée de la procédure d'ESD, qui est d'environ 40 minutes (Figure 12).

Bien que la solution saline normale examinée et l'hydrogel aient conduit à l'élévation des muqueuses juste après l'injection, l'hydrogel nanocomposite affiche une FSM plus haut et de plus longue durée avec la même quantité de solution injectée.

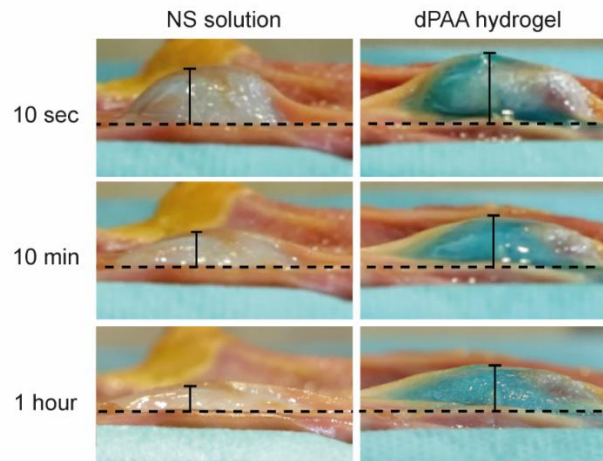


**Figure 12.** Variation d'élévation de la muqueuse en fonction du temps après l'injection de solution saline ou d'hydrogel dans un estomac de porc réséqué. Le bleu de méthylène a été mélangé à titre d'agent colorant. Les valeurs de hauteur (barre noire) obtenus pour la solution (NS) étaient de 6,7 mm, 4,2 mm et 2,9 mm après 10 sec, 10 min et 1 h respectivement ; pour (dPAA) étaient de 8,3 mm, 6,4 mm, 5,8 mm après 10 sec, 10 min et 1 h respectivement.

Enfin, une étude de faisabilité pour évaluer l'efficacité *in vivo* de l'hydrogel développé pour l'ESD a été réalisée sur un porc vivant.

Nous avons observé que les solutions d'hydrogel injectées ont conduit à la gélification de la matière en 3 minutes, avec une élévation claire et stable de la muqueuse. En outre, la levée de la muqueuse obtenue a permis au chirurgien d'effectuer la procédure ESD entière (40 min),

sans nécessiter une deuxième injection, par conséquent simplifie considérablement la procédure et en évitant une forte injection de liquides.

Aucune complication ni perforation importantes ont eu lieu au cours de la procédure, grâce à la levée de la muqueuse fiable et de longue durée atteinte.

On peut aussi observer la partie de l'hydrogel resté sous la muqueuse réséquée, en formant une couche protectrice sur la cavité nouvellement formée.

De plus, la possibilité de libérer un composant actif par la dégradation de l'hydrogel formé pourrait être très bénéfique à la fin de cette procédure délicate. Des biomolécules, telles que l'adrénaline, des inhibiteurs de la pompe à protons ou des antibiotiques pourraient être efficacement délivrées pour faciliter la cautérisation du tissu réséqué ou la prévention des inflammations.

En conclusion, nous avons démontré comment les hydrogels et les nano-composites à base de polyamidoamines peuvent être obtenus avec des caractéristiques différentes (élasticité mécanique, injectabilité, biodégradabilité). Les travaux résumés ici ont conduit au développement de nouveaux matériaux fonctionnels ayant des propriétés améliorées qui ont une excellente biocompatibilité et ont déjà été appliqués *in vivo* pour tester la réponse immunitaire, ainsi que pour permettre une intervention chirurgicale délicate où un espaceur est nécessaire. De tels matériaux sont certainement une plateforme intéressante pour différentes applications médicales.

- [1] J. M. Knipe, N. A. Peppas, *Regenerative Biomaterials* **2014**, 1, 57.
- [2] M. P. Lutolf, J. A. Hubbell, *Nat Biotech* **2005**, 23, 47.
- [3] I. M. El-Sherbiny, M. H. Yacoub, *Global Cardiology Science & Practice* **2013**, 2013, 316.
- [4] H. Geckil, F. Xu, X. Zhang, S. Moon, U. Demirci, *Nanomedicine* **2010**, 5, 469.
- [5] T. G. Kim, H. Shin, D. W. Lim, *Adv. Funct. Mater.* **2012**, 22, 2446.
- [6] M. J. Webber, O. F. Khan, S. A. Sydlík, B. C. Tang, R. Langer, *Ann. Biomed. Eng.* **2015**, 43, 641.
- [7] D. Buenger, F. Topuz, J. Groll, *Prog. Polym. Sci.* **2012**, 37, 1678.
- [8] O. Wichterle, D. Lím, *Nature* **1960**, 185, 117.
- [9] a) J. A. Rowley, G. Madlambayan, D. J. Mooney, *Biomaterials* **1999**, 20, 45; b) M. W. Tibbitt, K. S. Anseth, *Biotechnol. Bioeng.* **2009**, 103, 655.
- [10] Q. Wang, J. L. Mynar, M. Yoshida, E. Lee, M. Lee, K. Okuro, K. Kinbara, T. Aida, *Nature* **2010**, 463, 339.

- [11] I. Lynch, K. A. Dawson, *Macromol. Chem. Phys.* **2003**, 204, 443.
- [12] Q. L. Loh, C. Choong, D. Oxon, M. Hons, C. Mimmm, *Tissue Eng.: Part B* **2013**, 19, 485.
- [13] M. Dadsetan, T. E. Hefferan, J. P. Szatkowski, P. K. Mishra, S. I. Macura, L. Lu, M. J. Yaszemski, *Biomaterials* **2008**, 29, 2193.
- [14] M. P. E. Wenger, L. Bozec, M. A. Horton, P. Mesquida, *Biophys. J.* **2007**, 93, 1255.
- [15] a) D. Seliktar, *Science* **2012**, 336, 1124; b) M. P. Lutolf, J. A. Hubbell, *Nat. Biotechnol.* **2005**, 23, 47.
- [16] A. C. Fonseca, M. H. Gil, P. N. Simões, *Prog. Polym. Sci.* **2014**, 39, 1291.
- [17] M. Malkoch, R. Vestberg, N. Gupta, L. Mespouille, P. Dubois, A. F. Mason, J. L. Hedrick, Q. Liao, C. W. Frank, K. Kingsbury, C. J. Hawker, *Chem. Commun.* **2006**, 2774.
- [18] S. B. Lowe, V. T. G. Tan, A. H. Soeriyadi, T. P. Davis, J. J. Gooding, *Bioconjugate Chem.* **2014**, 25, 1581.
- [19] E. S. Place, J. H. George, C. K. Williams, M. M. Stevens, *Chem. Soc. Rev.* **2009**, 38, 1139.
- [20] P. Ferruti, M. A. Marchisio, R. Duncan, *Macromol. Rapid Commun.* **2002**, 23, 332.
- [21] P. Ferruti, S. Bianchi, E. Ranucci, F. Chiellini, A. M. Piras, **2005**, 2229.
- [22] E. Emilitri, F. Guizzardi, C. Lenardi, M. Suardi, E. Ranucci, P. Ferruti, *Macromol. Symp.* **2008**, 266, 41.
- [23] O. Jeon, D. S. Alt, S. M. Ahmed, E. Alsberg, *Biomaterials* **2012**, 33, 3503.
- [24] C. Lin, Z. Zhong, M. C. Lok, X. Jiang, W. E. Hennink, J. Feijen, J. F. J. Engbersen, *Bioconjugate Chem.* **2007**, 18, 138.
- [25] E. Karpushkin, M. Dušková-Smrčková, M. Šlouf, K. Dušek, *Polymer* **2013**, 54, 661.
- [26] P. Ferruti, S. Bianchi, E. Ranucci, F. Chiellini, V. Caruso, *Macromol. Biosci.* **2005**, 5, 613.
- [27] a) K. Baek, N. E. Clay, E. C. Qin, K. M. Sullivan, D. H. Kim, H. Kong, *Eur. Polym. J.* **2015**, 72, 413; b) A. A. M. Shimojo, A. M. B. Pires, R. Lichy, A. A. Rodrigues, M. H. A. Santana, *Journal of Biomedical Materials Research Part A* **2015**, 103, 730.
- [28] a) V. R. Kondepoti, H. M. Heise, J. Backhaus, *Anal. Bioanal. Chem.* **2007**, 390, 125; b) H. Wang, J. Liu, A. Han, N. Xiao, Z. Xue, G. Wang, J. Long, D. Kong, B. Liu, Z. Yang, D. Ding, *ACS Nano* **2014**, 8, 1475.
- [29] a) S. Lamansky, P. Djurovich, D. Murphy, F. Abdel-Razzaq, R. Kwong, I. Tsyba, M. Bortz, B. Mui, R. Bau, M. E. Thompson, *Inorg. Chem.* **2001**, 40, 1704; b) I.-S. Shin, J. I. Kim, T.-H. Kwon, J.-I. Hong, J.-K. Lee, H. Kim, *The Journal of Physical Chemistry C* **2007**, 111, 2280.
- [30] a) V. Magnaghi, V. Conte, P. Procacci, G. Pivato, P. Cortese, E. Cavalli, G. Pajardi, E. Ranucci, F. Fenili, A. Manfredi, P. Ferruti, *Journal of biomedical materials research. Part A* **2011**, 98, 19; b) N. Segovia, M. Pont, N. Oliva, V. Ramos, S. Borros, N. Artzi, *Advanced Healthcare Materials* **2015**, 4, 271.
- [31] a) R. Schops, E. Amado, S. S. Muller, H. Frey, J. Kressler, *Faraday Discuss.* **2013**, 166, 303; b) B. Gruber, B. König, *Chemistry – A European Journal* **2013**, 19, 438.
- [32] a) R. Cao, J. Jia, X. Ma, M. Zhou, H. Fei, *J. Med. Chem.* **2013**, 56, 3636; b) K. K.-W. Lo, A. W.-T. Choi, W. H.-T. Law, *Dalton Transactions* **2012**, 41, 6021.
- [33] F. Song, X. Li, Q. Wang, L. Liao, C. Zhang, *J. Biomed. Nanotechnol.* **2015**, 11, 40.
- [34] A. K. Gaharwar, N. a. Peppas, A. Khademhosseini, *Biotechnol. Bioeng.* **2014**, 111, 441.
- [35] N. S. Kehr, E. A. Prasetyanto, K. Benson, B. Ergün, A. Galstyan, H.-J. Galla, *Angew. Chem. Int. Ed.* **2012**, 125, 1194.



- [36] a) S. C. Mendes, R. L. Reis, Y. P. Bovell, A. M. Cunha, C. A. van Blitterswijk, J. D. de Bruijn, *Biomaterials* **2001**, 22, 2057; b) U. B. Yoshinori Onuki, Fotios Papadimitrakopoulos, Diane J. Burgess, *J. Diabetes Sci. Technol.* **2008**, 2, 1003.
- [37] K. Benson, E. A. Prasetyanto, H.-J. Galla, N. S. Kehr, *Soft Matter* **2012**, 8, 10845.
- [38] C. Bharti, U. Nagaich, A. K. Pal, N. Gulati, *Int. J. Pharm. Investig.* **2015**, 5, 124.
- [39] D. Tarn, C. E. Ashley, M. Xue, E. C. Carnes, J. I. Zink, C. J. Brinker, *Acc. Chem. Res.* **2013**, 46, 792.
- [40] a) M. Supová, G. Martynková, K. Barabaszová, *Sci. Adv. Mater.* **2011**, 3, 1; b) J. Zaragoza, N. Babhadiashar, V. O'Brien, A. Chang, M. Blanco, A. Zabalegui, H. Lee, P. Asuri, *PLoS One* **2015**, 10, e0136293; c) J. Yang, C.-R. Han, J.-F. Duan, F. Xu, R.-C. Sun, *Nanoscale* **2013**, 5, 10858.
- [41] a) Y. Piao, A. Burns, J. Kim, U. Wiesner, T. Hyeon, *Adv. Funct. Mater.* **2008**, 18, 3745; b) A. Bertucci, E. A. Prasetyanto, D. Septiadi, A. Manicardi, E. Brognara, R. Gambari, R. Corradini, L. De Cola, *Small* **2015**, DOI: 10.1002/sml.201500540.
- [42] a) M. B. Murphy, D. Blashki, R. M. Buchanan, I. K. Yazdi, M. Ferrari, P. J. Simmons, E. Tasciotti, *Biomaterials* **2012**, 33, 5308; b) P. Thevenot, A. Nair, J. Shen, P. Lotfi, C. Y. Ko, L. Tang, *Biomaterials* **2010**, 31, 3997.
- [43] S. Dong, H. Guo, Y. Zhang, Z. Li, F. Kang, B. Yang, X. Kang, C. Wen, Y. Yan, B. Jiang, Y. Fan, *Tissue Eng. Part A* **2013**, 19, 2464.
- [44] M. Patenaude, N. M. B. Smeets, T. Hoare, *Macromol. Rapid Commun.* **2014**, 35, 598.
- [45] a) E. Bakaic, N. M. B. Smeets, T. Hoare, *RSC Advances* **2015**, 5, 35469; b) Y. Li, J. Rodrigues, H. Tomas, *Chem. Soc. Rev.* **2012**, 41, 2193.
- [46] a) Y. Fu, W. J. Kao, *Journal of Biomedical Materials Research Part A* **2011**, 98A, 201; b) J. W. Chan, C. E. Hoyle, A. B. Lowe, M. Bowman, *Macromolecules* **2010**, 43, 6381.
- [47] J. L. Ifkovits, J. A. Burdick, *Tissue Eng.* **2007**, 13, 2369.
- [48] a) S. J. Buwalda, P. J. Dijkstra, J. Feijen, *Macromol. Chem. Phys.* **2012**, 213, 766; b) T. Betancourt, J. Pardo, K. Soo, N. A. Peppas, *Journal of biomedical materials research. Part A* **2010**, 93, 175; c) L. Serra, J. Doménech, N. A. Peppas, *Eur. J. Pharm. Biopharm.* **2006**, 63, 11.
- [49] a) S. Mura, J. Nicolas, P. Couvreur, *Nat Mater* **2013**, 12, 991; b) P. M. Kharkar, A. M. Kloxin, K. L. Kiick, *Journal of Materials Chemistry B* **2014**, 2, 5511.
- [50] a) F. Yang, J. Wang, G. Peng, S. Fu, S. Zhang, C. Liu, *J. Mater. Sci. Mater. Med.* **2012**, 23, 697; b) M. Kar, Y.-R. Vernon Shih, D. O. Velez, P. Cabrales, S. Varghese, *Biomaterials* **2016**, 77, 186.
- [51] A. Bertucci, H. Lülff, D. Septiadi, A. Manicardi, R. Corradini, **2014**, 1.
- [52] E. A. Prasetyanto, A. Bertucci, D. Septiadi, R. Corradini, P. Castro-Hartmann, L. De Cola, *Angew. Chem. Int. Ed.* **2016**, 55, 3323.
- [53] S. Coda, S.-Y. Lee, T. Gotoda, *Gut and Liver* **2007**, 1, 12.
- [54] a) S. Oka, S. Tanaka, I. Kaneko, R. Mouri, M. Hirata, T. Kawamura, M. Yoshihara, K. Chayama, *Gastrointest. Endosc.* **2006**, 64, 877; b) T. Gotoda, H. Yamamoto, M. R. Soetikno, *J. Gastroenterol.* **2006**, 41, 929.
- [55] a) M. Fujishiro, N. Yahagi, K. Kashimura, T. Matsuura, M. Nakamura, N. Kakushima, S. Kodashima, S. Ono, K. Kobayashi, T. Hashimoto, N. Yamamichi, A. Tateishi, Y. Shimizu, M.

- Oka, M. Ichinose, M. Omata, *Gastrointest. Endosc.* **2005**, 62, 933; b) K. B. Cho, W. J. Jeon, J. J. Kim, *World Journal of Gastroenterology : WJG* **2011**, 17, 2611.
- [56] a) L. Yu, W. Xu, W. Shen, L. Cao, Y. Liu, Z. Li, J. Ding, *Acta Biomater.* **2014**, 10, 1251; b) M. Fujishiro, N. Yahagi, K. Kashimura, Y. Mizushima, M. Oka, S. Enomoto, N. Kakushima, K. Kobayashi, T. Hashimoto, M. Iguchi, Y. Shimizu, M. Ichinose, M. Omata, *Endoscopy* **2004**, 36, 579.
- [57] K. J. Kang, B.-H. Min, J. H. Lee, E. R. Kim, C. O. Sung, J. Y. Cho, S. W. Seo, J. J. Kim, *Dig. Dis. Sci.* **2013**, 58, 1491.
- [58] R. T. Tran, M. Palmer, S.-J. Tang, T. L. Abell, J. Yang, *Gastrointest. Endosc.* **2012**, 75, 1092.
- [59] A. O. Ferreira, J. Moleiro, J. Torres, M. Dinis-Ribeiro, *Endoscopy International Open* **2016**, 4, E1.

# **1. Hydrogels for tissue engineering and biomedical applications**

## **Abstract**

This chapter introduces general concepts in order to provide the background and state for the research work presented throughout this thesis.

First, an overview on hydrogels is given, to present their properties in terms of structure and possible types of networks.

Then, their attractive features as scaffolds for 3D cells growth are underlined, with a special focus on the design criteria that must be met by hydrogels developed for this purpose.

A brief summary on natural and synthetic hydrogels, developed and investigated as a platform for the adhesion and proliferation of cells, is then presented.

The various applications of hydrogels in tissue engineering are examined, after a brief prospect on this highly interdisciplinary field.

Nanocomposite hydrogels, whose polymer network is cross-linked to nanoparticles, are presented, as well as the advantages that this combination offers in biomedical applications, especially for the release of bio-active molecules.

Then, a short overview on injectable and biodegradable hydrogels is given, highlighting the several benefits that they provide, particularly for soft tissue engineering.

Finally, the family of polymers employed for this thesis work, polyamidoamines, is described, with a particular focus on the unique characteristics that make polyamidoamine-based hydrogels ideal candidates for biomedical applications.

## 1.1 Hydrogels, an overview

Hydrogels are three-dimensional (3D) networks composed of cross-linked hydrophilic polymer chains, with the ability to swell, without dissolution, by absorption of up to thousands of times their dry weight in water.<sup>[1]</sup>

Since their introduction in 1960,<sup>[2]</sup> hydrogels have attracted a great deal of attention, and significant progress has been made in their design and synthesis.

They can assume virtually any shape and size (Figure 1.1). Thanks to their hydrophilic character and potential biocompatibility, they have been of great interest to biomaterial scientists for many years<sup>[3]</sup> and have found numerous applications in the biomedical<sup>[4]</sup> and tissue engineering sectors.<sup>[5]</sup>

The pioneering work of Lim and Sun in 1980 demonstrated the successful encapsulation of cells in cross-linked alginate microcapsules, permeable to small molecules.<sup>[6]</sup> Later on, Yannas and coworkers synthesized highly porous, cross-linked collagen-glycosaminoglycan copolymers for use as artificial burn dressings.<sup>[7]</sup>



Figure 1.1 Example of transparent high-water-content hydrogel of different molded shapes. Left: adapted from Q. Wang et al., *Nature*, **2010**, 463, 339-343; right: adapted from M. C. Straccia et al., *Carbohydrate Polymers*, **2015**, 125, 103-112.

Hydrogels resemble natural living tissue more than any other class of synthetic biomaterials, thanks to their biocompatibility, high water content,<sup>[8]</sup> tissue-like elastic properties and 3D porous structure<sup>[9]</sup> that allows for the permeation of oxygen, nutrients and eventually vascularization.<sup>[10]</sup>

Many hydrogel scaffolds with different chemical and physical properties have been developed over the last decades, using a wide variety of building blocks and various techniques. This has increased the knowledge on the topic, to a point that it is now possible to tailor the scaffold properties, such as biocompatibility, cellular attachment, structural integrity,<sup>[11]</sup> biodegradability and solute transport,<sup>[12]</sup> to meet the target application.<sup>[13]</sup>

### 1.1.1 Network characteristics: physical and chemical hydrogels

The gelation process is defined as the progressive cross-linking of macromolecular chains together, which results in the formation of a polymeric network with limited or no solubility.<sup>[14]</sup> It can take place either by “physical” or by “chemical gelation”, with the type of cross-linking greatly modifying the properties of the material. Thus, hydrogels can be classified into physical and chemical hydrogels based on their cross-linking mechanism (Figure 1.2).<sup>[15]</sup>

Physical hydrogels are cross-linked with transient junctions that include polymer chain entanglements, hydrogen bonding, hydrophobic and ionic interactions. These are not permanent bonds, but they are sufficiently strong to create a network and to make hydrogels insoluble in an aqueous media.

Physical cross-linking, due to the non-covalent nature of the bonds, produces reversible hydrogels. However these hydrogels can present network defects due to free chain ends or chain loops and are mechanically unstable.<sup>[16]</sup>

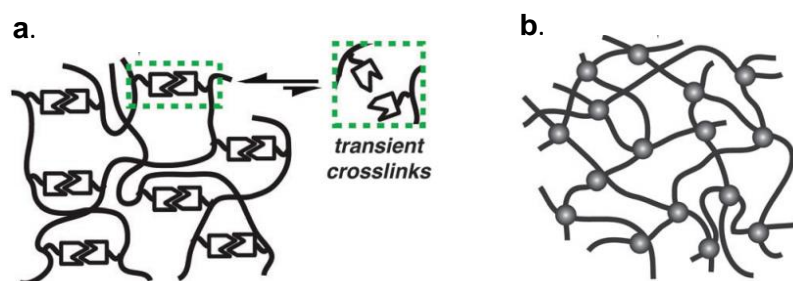


Figure 1.2 Schematic representation of a physical hydrogel (a), characterized by transient cross-links and of a chemical hydrogel (b), characterized by a covalent network. Image adapted from *Chem. Soc. Rev.*, **2012**, *41*, 6195–6214.

Physical hydrogels can be obtained for example by thermal-induced cross-linking of temperature-responsive polymers. Poly(N-isopropylacrylamide), pNIPAAm, is one of the most studied, thanks to the ease of the network formation process. It undergoes a coil-to-globule transition on warming above its lower critical solution temperature of 32 °C, through the release of water molecules bound to the polymers isopropyl side groups, which results in increasing intra- and inter- molecular hydrophobic interactions between these groups.<sup>[17]</sup>

Agarose is a different type of temperature-responsive hydrogel; its cross-linking is driven by the formation and aggregation of double helical structures, with the decrease of temperature from the melting point (~85 °C).<sup>[18]</sup>

Another strategy to form physical hydrogels is based on the weak and non-covalent interactions that are formed between short peptides chains. By adjusting the amino acid sequences, it is possible to form physical hydrogels with highly order structures via self-assembly, these structures further spontaneously organize into nanofibres that aggregate to form 3D hydrogels.<sup>[19]</sup>

On the other hand, chemical hydrogels are formed by covalent cross-links; as a result, they are stable materials that do not dissolve in water without breakage of the covalent polymer network; they are also called “irreversible” hydrogels.<sup>[20]</sup>

Chemical hydrogels are usually obtained by cross-linking of polymeric chains in fairly concentrated aqueous solutions.<sup>[21]</sup> Numerous covalent reactions can be used for the synthesis, including photo-initiated radical polymerization,<sup>[22]</sup> Michael-type polyaddition,<sup>[23]</sup> Schiff base formation,<sup>[24]</sup> and enzyme-catalysed reactions<sup>[25]</sup> (Figure 1.3).

Radical polymerization for hydrogel synthesis is often initiated by free radicals produced via the decomposition of a photoinitiator upon visible or UV light exposure. Then, the free radicals react with the monomers, such as acrylate moieties, to form the network structure of the hydrogel.<sup>[5b]</sup>

Michael-type addition between thiols or amines and acrylates, unlike other addition reactions, can be carried out in aqueous medium, at room temperature, and at physiological pH. Thus, hydrogels synthesized using this technique have been widely developed for biomedicine.<sup>[26]</sup>

Schiff base reactions, between amines and aldehyde groups to form carbon–nitrogen double bonds, can be used as well to achieve synthetic hydrogel networks. Moreover, aldehyde groups,

present in polymer chains, can react with amino groups of natural tissues, promoting integration of the hydrogel to surrounding environment.<sup>[27]</sup>

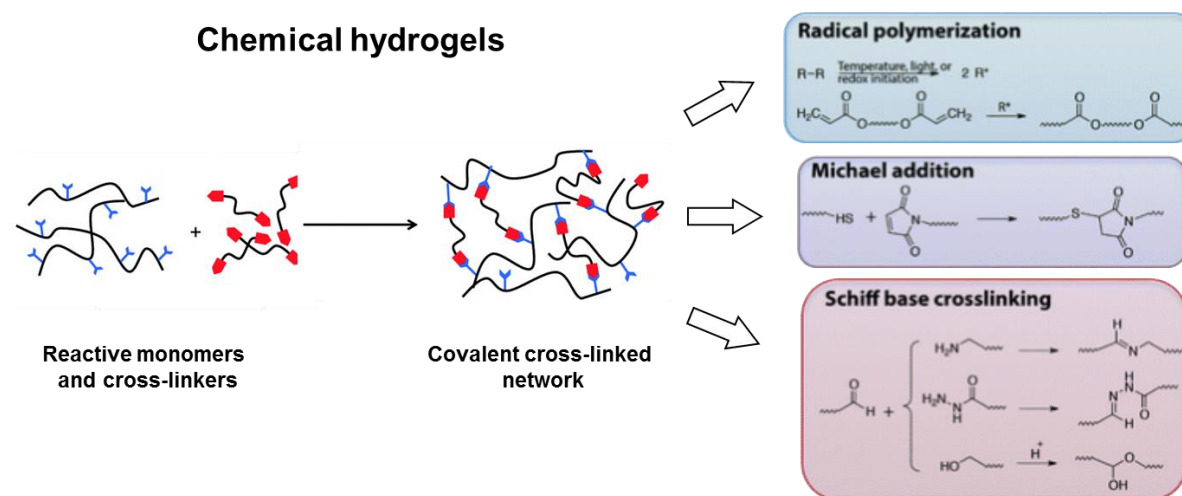


Figure 1.3 Pictorial representations of chemical hydrogels; a wide range of covalent reactions are available for this kind of hydrogel formation. Adapted from C. Ghobril, M. W. Grinstaff, *Chem. Soc. Rev.*, **2015**, *44*, 1820-1835 and P. M. Kharkar et al., *Chem. Soc. Rev.*, **2013**, *42*, 7335-7372.

The permanent non-reversible bonds which interconnect the polymer chains of synthetic hydrogels, however, can make the hydrogel rather fragile and unable to self-heal once the network is broken.<sup>[28]</sup>

Therefore, chemical hydrogels that include as well transient junctions, such as polymer chain entanglements or hydrogen bonds, present more advantages.

Finally, the adequately tuning of the cross-linker allow to obtain chemical hydrogels with different mechanical properties.<sup>[29]</sup>

## 1.2 Engineering hydrogels as extracellular matrix mimics for 3D cell culture

### 1.2.1 Design criteria

The physical properties of hydrogels make them attractive for a variety of bionanotechnology and biomedical applications. Their biocompatibility, when using non toxic components leading

to biocompatible products, and structural integrity allow them to be used as scaffolds for cells growth and tissue regeneration, whereas their hydrophilicity can be exploited for drug release. The design of hydrogels as artificial 3D environments for cells must meet a number of design criteria to function appropriately (Figure 1.4).

In native tissues, the extracellular matrix (ECM) provides structural integrity and binding support to the cells;<sup>[5a]</sup> therefore, it is one of the most important guides for scaffolds design. The ECM itself is a hydrophilic 3D matrix formed of collagen fibers, which provide durability and tensile strength, and of interstitial fluid.<sup>[30]</sup>

Hydrogels developed as platforms for cells growth should mimic the ECM, thus provide an optimal 3D network for cells adhesion, proliferation and migration.

Their fundamental requirement is to maintain cellular proliferation and desired cellular distribution throughout their expected service life.<sup>[13]</sup> Thus, they should be cyto- and biocompatible, both for *in vitro* culture and during *in vivo* implantation.

The hydrogel network needs to be compatible with cellular components and not induce harmful immunological, toxic, or foreign body responses when used for *in vivo* applications.<sup>[31]</sup>

In this respect, one of the main challenges is represented by toxic chemicals that may be used during the synthesis of the hydrogel network, such as stabilizers, radical initiators and organic solvents. These may be harmful if they come into contact with the seeded cells or if they leak to the tissues. For example, Irgacure, a free radical photo-initiator commonly used for scaffolds synthesis, has been found to decrease cell viability, even when used in limited concentrations.<sup>[32]</sup>

Hence, hydrogels for bionanotechnology and biomedical applications, especially if developed as implantable materials, necessitate *in vitro* and *in vivo* investigation to test their local and systemic effects on the cells and on the host.

The design criteria should also include other physicochemical parameters according to the application, such as porosity, mechanical stability and biodegradation.

Hydrogels should provide void volume, i.e. a porous structure, to encourage cell ingrowth, uniform cell distribution and to allow efficient nutrients and metabolites transport, without compromising the mechanical stability of the scaffold.<sup>[33]</sup>



As 3D cells scaffolds, they should provide structural and shape stability; therefore, their elastic and mechanical characteristics can have a significant effect on cells proliferating onto the network.<sup>[34]</sup>

Moreover, certain applications require degradable biomaterials, therefore the rate and extent of biodegradation are critical design considerations. Degradable hydrogel are generally achieved through the incorporation of cleavable cross-links or moieties into the polymer backbone.<sup>[35]</sup>

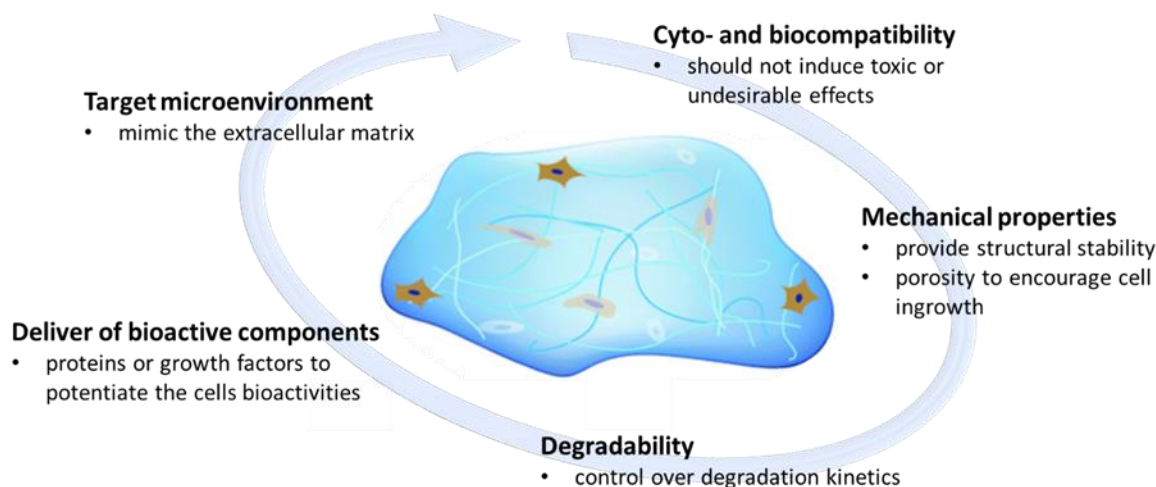


Figure 1.4 Example of design considerations for hydrogels developed as scaffolds for cell growth; adapted from P. M. Kharkar et al., *Chem. Soc. Rev.*, **2013**, 42, 7335-7372.

Finally, hydrogels scaffolds may be synthesized to actively deliver bioactive cues to the residing cells and act as reservoir of proteins or growth factors to potentiate their bioactivity.<sup>[36]</sup> The release mechanism can be controlled by the hydrogel swelling ability<sup>[37]</sup> or through its degradation.

### 1.2.2 Natural and synthetic hydrogels

The suitability of hydrogels as scaffold for cells growth and their performances in the target biomedical applications are largely related to their structure.

Based on their derivation and composition, hydrogels can be classified as natural or synthetic. Hydrogels obtained from natural polymers have been used in biomedical applications because of their inherent biocompatibility, low toxicity and susceptibility to enzymatic degradation.<sup>[38]</sup>

There are two major classes of natural polymers used in hydrogel preparation: fibrous proteins and polysaccharides, which are both components of the ECM.<sup>[39]</sup>

The main proteins used to prepare hydrogels are collagen,<sup>[40]</sup> the most abundant protein in mammals; gelatin,<sup>[41]</sup> formed by partial hydrolysis of collagen; fibrin;<sup>[42]</sup> silk<sup>[43]</sup> and Matrigel™,<sup>[44]</sup> a gelatinous protein mixture resembling the complex extracellular environment found in many tissues.

They have been investigated for bio-applications due to their excellent biocompatibility and biodegradability. Collagen in particular can be degraded naturally by metallo-matrix proteinases (MMPs), thus allowing for local degradation controlled by cells present in the hydrogel.

Among polysaccharides, the most applied are hyaluronic acid (HA),<sup>[45]</sup> widely distributed throughout the ECM of connective tissues; agarose;<sup>[46]</sup> dextran<sup>[47]</sup> and chitosan,<sup>[48]</sup> a copolymer of glucosamine and N-acetylglucosamine.

Nevertheless, the use of natural component-based hydrogels has shown some drawbacks, such as complexity of purification, batch-to-batch variability,<sup>[49]</sup> immunogenicity and possibility of pathogen transmission, as well as poor mechanical stability.<sup>[50]</sup>

In the last years, synthetic hydrogels have gained attention because of their interesting features.<sup>[51]</sup> In comparison to their natural counterparts, they can be prepared with greater control over the hydrogel composition, surface characteristics and other key parameters such as water absorption and mechanical properties, which are important for biomedical applications.<sup>[52]</sup>

Currently, synthetic hydrogels have emerged as an attractive alternative for fabricating scaffolds, particularly because their syntheses are highly reproducible and allow the incorporation of tailored functionalities,<sup>[53]</sup> biological molecules<sup>[54]</sup> or inorganic nanometer-scale objects, which can be covalently bonded to the polymer structure.<sup>[55]</sup>

Synthetic hydrogels can be obtained for example from derivatives of poly(ethylene glycol) (PEG), poly(vinyl alcohol) (PVA) and poly(hydroxyethyl methacrylate) (PHEMA); Figure 1.5 shows the structures of their repeating unit.

PEG hydrogels are probably the most widely studied and used because they are nontoxic, non-immunogenic, and already approved by FDA for various clinical uses.<sup>[56]</sup> PEG chains can be

covalently cross-linked using a variety of methods that include the photopolymerization using acrylate-terminated PEG oligomers.<sup>[57]</sup>

Similar to PEG, PVA is another synthetic hydrophilic polymer used for hydrogels. PVA scaffolds are stable and elastic; they can be formed both by physical method, through repeated freezing/thawing cycles<sup>[58]</sup> or chemically, with glutaraldehyde or epichlorohydrin as cross-linkers.<sup>[59]</sup>

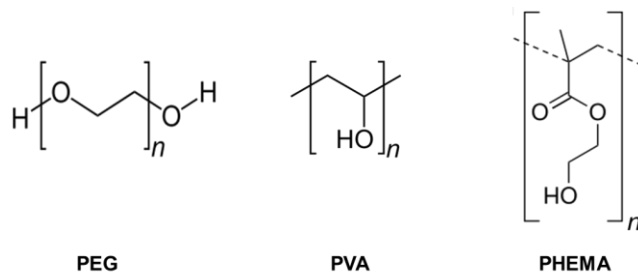


Figure 1.5 Repeating units of the polymers PEG, PVA, PHEMA that can be used to form cross-linked synthetic hydrogels.

PHEMA is one of the most widely applied hydrogel; it is used in several bio-applications, for example to produce contact lenses.<sup>[60]</sup> It can be modified to enhance its properties<sup>[61]</sup> and in recent years it has also been prepared as photocross-linked hydrogels by using polyethylene glycol dimethacrylate as a cross-linking agent.<sup>[62]</sup>

The limitation of these synthetic hydrogels is related to the lack of cell-specific bioactivities, such as cell adhesion, migration and cell-mediated biodegradation.

To overcome this limitation, specific functionalities or bioactive molecules can be covalently incorporated into synthetic hydrogels.<sup>[39, 63]</sup> Enzymes or amino acid sequences derived from natural proteins, such as RGD, have been immobilized within the synthetic polymer network to enhance cells adhesion.<sup>[64]</sup>

Another form of biological modification of synthetic hydrogels is the incorporation of bioactive molecules and growth factors, which can be subsequently released to the cells proliferating onto the scaffolds.<sup>[65]</sup>

Finally, the integration of degradable linkers within the synthetic network has been exploited to tune the degradation properties of the hydrogels.<sup>[66]</sup>

Compared to natural hydrogels, biocompatible synthetic hydrogels modified with bioactive components provide an optimal biomimetic platform for cell growth, while offering an improved control over the matrix architecture and chemical composition.

### **1.3 Hydrogels in tissue engineering**

#### *1.3.1 Tissue engineering*

Hydrogels are interesting biomedical tools because of their characteristics of broad cytocompatibility and 3D structure tunability to mimic native tissues. Therefore, they are the subject of huge research interest, especially in tissue engineering (TE).<sup>[67]</sup>

TE is a highly interdisciplinary field, which involves bio-chemical science, cell biology, cell-material interactions and material characterization.

It investigates the behavior of cells, biomaterials and growth factors to enhance tissue functions where possible.<sup>[68]</sup> More importantly, it aims to replace diseased or damaged tissues with scaffolds that allow the encapsulation of cells, and which may induce the regeneration of new tissue via the migration of existing cells.<sup>[69]</sup>

The term “tissue engineering” was first proposed in 1988 at the National Science Foundation (NSF) meeting.<sup>[70]</sup> Later on it has been defined by Langer and Vacanti as “an interdisciplinary field that applies the principles of engineering and life sciences toward the development of biological substitutes that restore, maintain or improve tissue or organ function”.<sup>[71]</sup>

As such, it involves the contribution of different key constituents: the biomaterial scaffold, to provide a platform for cell adhesion, growing and migration; cells (often stem cells) and signaling molecules, such as proteins and growth factors, in order to activate different physiological responses depending of the final application (Figure 1.6).

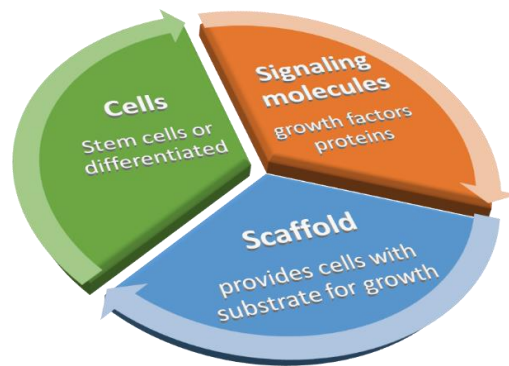


Figure 1.6 A schematic illustration of the key components of tissue engineering.

### 1.3.2 Areas of application

From a TE perspective, it is desirable to have hydrogel scaffolds that replicate tissue functions, thus providing a cell culture environment that resembles the body tissues.<sup>[72]</sup>

They should mimic as closely as possible the ECM experienced in natural tissues, in terms of architecture, composition and biological cues.<sup>[72]</sup>

Moreover, they should improve cells infiltration and proliferation *in vivo*<sup>[73]</sup> and once implanted they should avoid or reduce the host immunoresponse to achieve the final tissue healing.<sup>[74]</sup>

However, obtaining an artificial scaffold, which possesses the above-mentioned characteristics and allows cell activity in a native manner is still one of the major challenges in TE.

In the last years, significant progress has been made in the design of scaffolds and has led to an advance from simple supporting matrices to more complex biomaterials.

For instance, hydrogels are exploited to encapsulate cells *in vivo* and for the delivery of bioactive moieties that encourage the natural tissue reparative process.

The list of TE applications that hydrogels have been suggested for includes many different areas, such as bones<sup>[75]</sup> and blood vessels<sup>[76]</sup> reconstruction and neural<sup>[77]</sup> or muscular<sup>[78]</sup> repair, which highlights the versatility of this class of materials (Figure 1.7).

While the physio-mechanical properties of hydrogels may not seem suitable for bone reconstruction, considerable research efforts are devoted to hydrogel-mediated bone augmentation.

This is often achieved by incorporating calcium phosphate or hydroxyapatite into hydrogel scaffolds, thus providing cells with a calcified matrix while also conferring suitable cell sustain

through the hydrogel network components. Several studies reported that the presence of these components induced an increase of proliferation of fetal osteoblast cells onto the scaffold and better supported the osteogenic phenotype maintenance, compared to naked hydrogels.<sup>[79]</sup> These methods could lead to higher bone volume and excellent bone remodeling after 20 weeks.<sup>[80]</sup>

Another prolific area of research is centered on TE approaches for neural repair. Central nervous tissues have a limited endogenous repair capacity, thus damages in this area can have debilitating consequences.<sup>[81]</sup> The ability to induce and sustain this regeneration with artificial material would present a crucial advance in healthcare technology.

For example, recently Broguiere and coworkers reported an enzymatically cross-linked hyaluronan hydrogel that enabled the formation of 3D neuronal cultures, showing fast neurite outgrowth and strong synaptic connectivity, with long-lasting coordinated electrical activity.<sup>[82]</sup>

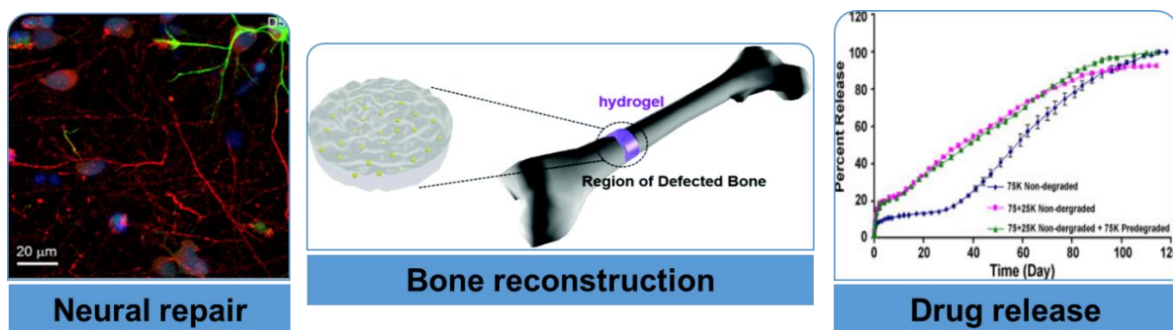


Figure 1.7 Examples of hydrogels used in different TE applications. Adapted from N. Broguiere et al., *Biomaterials*, **2016**, 99, 47-55 (left); D. N. Heo et al., *J. Mater. Chem. B*, **2014**, 2, 1584-1593 (center) and U. Bhardwaj et al., *Int. J. Pharm.* **2010**, 384, 78-86 (right).

The loading of growth factors into the hydrogel scaffolds was also investigated, for acute spinal cord repair. The release of a factor to promote oligodendrocytic differentiation from implanted methylcellulose hydrogels has shown improved graft survival, suggesting the potential of the developed scaffold as vehicle to deliver cells to the injured spinal cord.<sup>[77]</sup>

In general, the delivery of active bio-molecules from the scaffolds might have effects onto the cells proliferation and migration, as well as on the implant integration with the host tissues.

Often the clinical application of the hydrogel scaffold is hindered by the body response to the foreign material, which can compromise its functionality and durability.

Therefore, the localized and sustained delivery of anti-inflammatory molecules or specific growth factors and proteins has been investigated to overcome this limitation.

For instance, the release of neurotrophic factors from poly(lactic-co-glycolic acid) microparticles entrapped within a PEG-based-hydrogel has shown to reduce the localized inflammatory response in different regions of the brain upon scaffold implantation.<sup>[83]</sup>

Sustained delivery of anti-inflammatory drugs, such as dexamethasone from PVA hydrogels, has been used to modulate for a 1-month time the endogenous immune response to implanted hydrogels.<sup>[84]</sup>

## **1.4 Nanocomposite hydrogels**

Nanocomposite hydrogels are soft materials, whose polymer network is cross-linked to nanoparticles or nanostructures.<sup>[85]</sup> In these systems, the nano-sized objects interact in a physical or covalent manner with the polymeric chains, resulting in novel appealing properties of the hydrogel network.<sup>[86]</sup>

The nanofillers and the polymer network are two entirely different types of materials, whose combination generates not only structural diversity, but also a plurality of property enhancements.<sup>[87]</sup>

Traditionally, the nanocomposite strategy has been employed to design hydrogels with enhanced mechanical properties, and reinforcing materials have been typically limited to organic/polymeric nanoparticles.

The first attempt to reinforce materials with inorganic nanoparticles was made by Usuki et al., who introduced montmorillonite clay nanofillers into a nylon-6 matrix, obtaining a significant improvement of tensile strength.<sup>[88]</sup>

Since then, various nanoparticles have been used to obtain nanocomposite hydrogels. These include carbon-based nano-materials (carbon nanotubes, nano-diamonds), inorganic/ceramic nanoparticles (hydroxyapatite, silica, calcium phosphate), metal/metal-oxide nanoparticles (gold, silver, iron-oxide) as well as polymer nanoparticles (Figure 1.8).



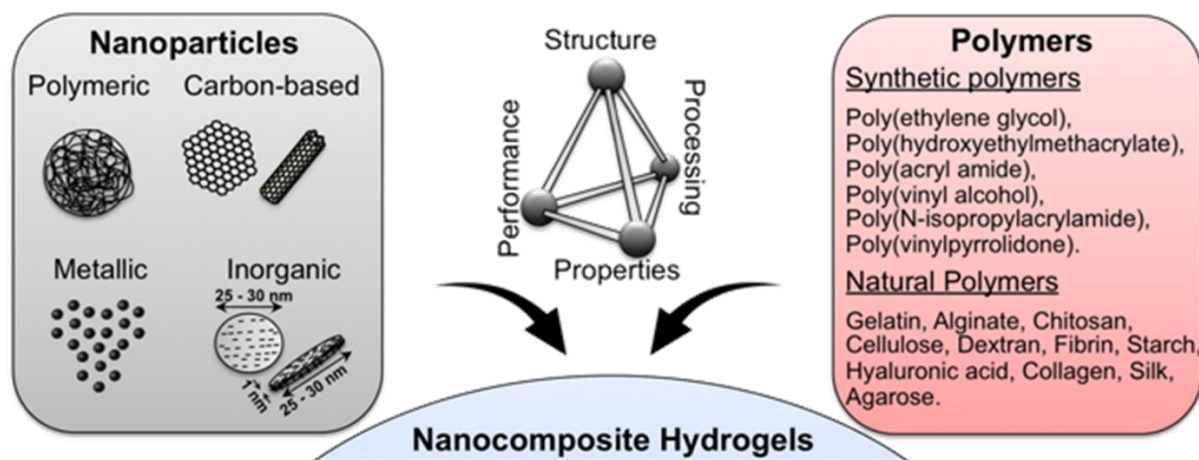


Figure 1.8 A range of nanoparticles can be cross-linked to synthetic or natural polymer networks to obtain nanocomposite hydrogels with desired properties; adapted from A. K. Gaharwar et al., *Biotechnol. Bioeng.*, **2014**, *111*, 441–453.

One of the main reasons for using nanoparticles is the large surface-to-volume ratio, which increases the particles–matrix interactions, thus improving the nanoparticles effect on the overall material. Indeed, the interfacial region between the dispersed nanoparticles and the matrix is responsible for the ‘communication’ between these two.

Although much research has been done on nanocomposites preparation, often achieving homogeneous dispersion of the nanoparticles in polymeric matrices can be problematic.<sup>[89]</sup> The aggregation of the nanofillers or the limited interfacial adhesion with the network can result in early failure of the material.

This is why inorganic nanoparticles are often surface modified to increase the interaction with the polymer network,<sup>[90]</sup> which has been proved to be a widely applicable technique and shown to enhance particle/matrix interactions.<sup>[91]</sup>

In general, the surface modification of inorganic fillers is achieved with the organic functionalization of the nanoparticles, which can be carried out by physical or chemical interactions between the particles and the modifiers.

The most used physical treatment is based on coverage of the nanoparticles surface with a polymer by electrostatic interaction.<sup>[92]</sup>

In comparison with physical methods, chemical functionalization is more effective in many applications, because the covalent bonds between the nanoparticles and the modifier avoids



the desorption of the latter.<sup>[93]</sup> Moreover, reactive groups of interest can be introduced as part of the functionalization to allow the formation of chemical bonds between the fillers and the nanocomposite polymer network.

Developing nanocomposite hydrogels with tailored functionalities has opened new possibilities,<sup>[94]</sup> thanks to the fact that nanomaterials often possess specialized and advantageous functions that are not found in the polymers matrices.

Research efforts are being made to create nanocomposite hydrogels with properties such as mechanical strength and swelling,<sup>[8, 95]</sup> stimuli-responsive behavior induced via magnetic<sup>[96]</sup>, optical,<sup>[97]</sup> or thermal changes.<sup>[98]</sup>

Recent trends indicate a significant and growing interest in developing nanocomposite hydrogels for different applications, especially in the biomedical field ( Figure 1.9).

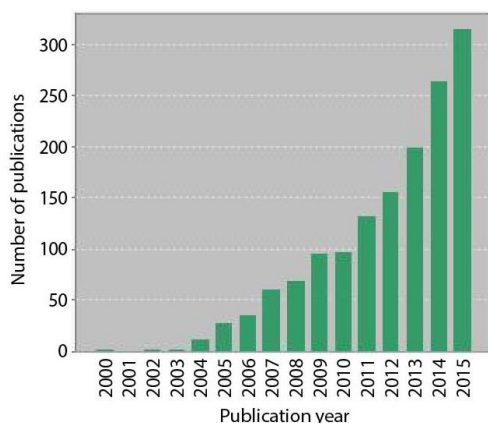


Figure 1.9 Number of publications on nanocomposite hydrogels according to Web of Science from January 2000 to December 2015. A steady increase in the number of publication indicates growing interest in the development of nanocomposite hydrogels.

Nanocomposite hydrogels with high biocompatibility have been exploited indeed in 3D cell culture,<sup>[99]</sup> tissue engineering,<sup>[100]</sup> bone reconstruction,<sup>[101]</sup> wound healing<sup>[102]</sup> and for drug release.<sup>[103]</sup>

In particular for drug release, nanocomposite hydrogels represent interesting platforms that combine the possibility of incorporating the drug into the (porous) nanoparticles with the control over the release kinetic, which can be achieved due to changes in the hydrogel network

(i.e. swelling, dissolution or degradation). Moreover, these systems could enable new routes of drug administration while providing clinically useful formulations.<sup>[104]</sup>

## 1.5 Injectable hydrogels

Tissue engineering and regenerative medicine are exciting and rapidly growing fields focused on finding concrete solutions to some of the world's most detrimental diseases and medical conditions.<sup>[105]</sup>

Implanted scaffolds are essential for TE development and for modern medical practice; however, the transplant of preformed scaffolds requires surgical invasive procedures that can limit successful biomedical applications of conventional pre-synthesized implants.<sup>[106]</sup> Instead, TE therapies would benefit from minimal surgical procedures to decrease patient morbidity. As a result, in the past few years, significant focus was shifted to the design and synthesis of “injectable” or “*in situ* gelling” scaffolds.

These are biomaterials that can be delivered *in vivo* via injection, and then rapidly solidify inside the body.<sup>[107]</sup>

Particularly for soft tissues engineering, the use of injectable hydrogels provide several advantages over preformed ones, which are shaped into their final form before implantation. The hydrogels precursors, or their viscous liquid form, can be introduced in the host body in a minimally invasive manner, significantly reducing patient discomfort and treatment costs.

In this way it is possible to avoid the need for surgery to implant the scaffold, thus reducing the risk connected with invasive procedures, pain and minimizing healing time and scarring.<sup>[106]</sup> Moreover, the injection can be performed at sites that are otherwise scarcely accessible through conventional surgery.

This approach introduces new possibilities for potential use of hydrogel scaffolds in areas that are generally disfavored for routine surgical procedures.

Injectability allows the delivery of the hydrogel directly in the area of interest, enabling effective molding of the implant shape from the adjacent tissue *in situ*, and a higher potential in applications requiring the filling of cavities or tissue defects.<sup>[107a, 108]</sup>

Finally, hydrogels that can be formed *in situ* under physiological conditions might also contain bioactive compounds, which can be mixed homogeneously with the polymer solutions prior to gelation.<sup>[109]</sup>

In general, the development of injectable hydrogels is very attractive, mostly in light of their high potential in clinical translation, thanks to the easy combination with the existing clinical procedures.

Three common methods are generally used to develop injectable hydrogels that can be formed *in situ*, these are photo-gelation, thermal-gelation and chemical-gelation (Figure 1.10).

Photo-gelation methods are based on the exposure of water soluble polymers or monomers with photolabile groups to visible or near ultra violet radiation, in the presence of photo initiators.

Thermal-gelation instead takes advantage of phase transition properties of certain polymers near physiological temperature, as previously described (paragraph 1.1.1), thus obtaining hydrogels through small changes in temperature after the injection.<sup>[110]</sup>

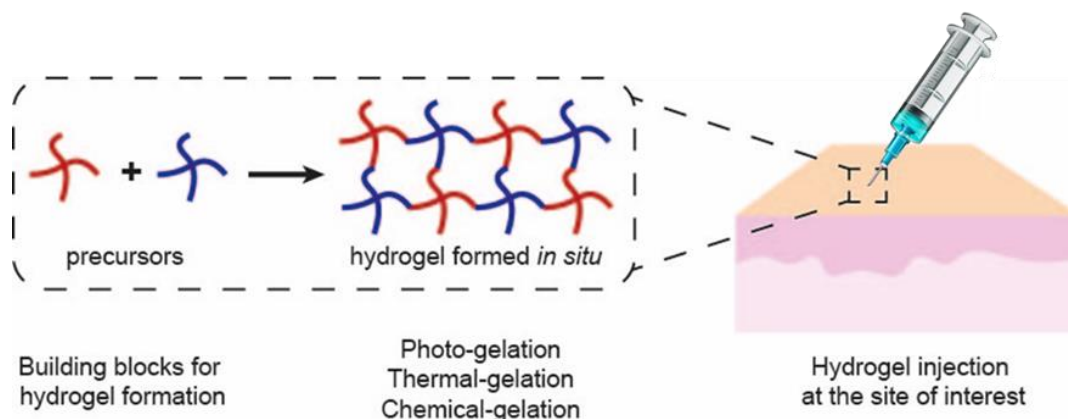


Figure 1.10 Injectable hydrogels can be prepared using different building blocks and can be delivered in their liquid form, using minimal surgical procedures. They form *in situ* via photo-gelation, thermal-gelation or chemical-gelation.

Adapted from [www.sigmaaldrich.com/technical-documents/articles/materials-science/injectable-hydrogels.html](http://www.sigmaaldrich.com/technical-documents/articles/materials-science/injectable-hydrogels.html)

However, these methods may present some inconveniences. The use of UV light for photoinitiated polymerization of the injected hydrogels, for example, may be challenging in areas difficult to reach; while thermo-responsive materials can form clogs inside long delivery surgical tools at normal body temperature.<sup>[111]</sup> Moreover, the diluting environment of the body can lead to local reduction of polymer concentration over time. This affects weakly cross-

linked materials, such as the thermal-gelated ones, and can result in a loss of mechanical integrity.<sup>[106]</sup>

To overcome these challenges, growing interest is focused on the design of injectable hydrogels via chemical-gelation. Typically, these hydrogels are formed by mixing monomers and cross-linker with complementary reactive functional groups that can lead to covalent bond formation.

A variety of chemistries has been explored in the last years for the development of injectable hydrogels cross-linked via covalent bond formation. These include Schiff base, and disulfide bond formation as well as Michael addition reactions.<sup>[112]</sup>

In particular, the 1,4-addition, also called Michael addition, of a nucleophile to the  $\beta$  position of an  $\alpha,\beta$ -unsaturated carbonyl compound, is an interesting approach to obtain injectable hydrogels. This reaction occurs in very mild reaction settings and can be carried on under physiological conditions.

Nucleophiles that have been proposed for the formation of injectable hydrogels via Michael addition include thiols, alcohols, and amines.<sup>[113]</sup>

Moreover, Michael addition chemistry can be combined with physical cross-linking strategies to create hydrogel systems that display an even faster gelation *in situ*.<sup>[114]</sup>

## 1.6 Biodegradable hydrogels

Many TE and drug delivery applications require hydrogels that can be easily degraded in physiological conditions, in order to be eliminated from the organism after the required amount of time.

Degradation provides space for proliferating cells and can favor infiltration of blood vessels,<sup>[115]</sup> it permits control of the release of cargo molecules<sup>[116]</sup> and can significantly enhance patient compliance because there is no need to perform surgical procedures to recover the implant.<sup>[108]</sup>

The desired degradation rate is closely related to the *in vivo* residential time, and thus should be designed to match the entire duration of the clinical application.<sup>[117]</sup> Therefore it is necessary to optimize the degradation rate of the hydrogels to maximize their performance.

While this can be difficult to control when natural hydrogels, such as collagen, fibrin or alginate, are used,<sup>[66]</sup> the degradation rate of synthetic hydrogel matrices can be tuned by tailoring the polymer architecture, the cross-linking density, and the amount of incorporated degradable moieties.

Different approaches have been exploited in the last few years to achieve biodegradable hydrogels.<sup>[107b]</sup>

In particular, the most effective strategy is the intercalation in the hydrogel network of linkers that are degraded by specific agents, for example via ester hydrolysis, enzymatic degradation, photolytic cleavage or reversible click reactions. The degradable linkers may be introduced during the synthesis of the hydrogel by the formation of degradable bonds between polymerizable moieties or by using cross-linkers already containing suitable cleavable bonds. The initially insoluble 3D network goes through a degradation process where the degradable bonds are dissolved and the whole structure is thus disintegrated (Figure 1.11).

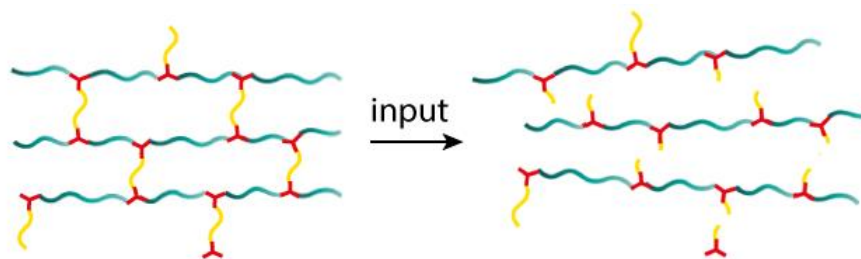


Figure 1.11 Schematic degradation of hydrogels containing degradable cross-linkers.

Particularly interesting for TE applications are hydrogel scaffolds containing cell-cleavable bonds, which are degraded upon the effect of cell-secreted molecules.

Native ECM undergoes dynamic remodeling through matrix assembly and degradation, where degradation occurs via proteolytic enzymes (e.g. matrix metalloproteinases, MMPs), produced by the cells.<sup>[118]</sup>

This has led many researchers to incorporating protease-cleavable moieties as cross-links into the hydrogel network, to locally support cell mediated degradation.<sup>[119]</sup>

For instance, Patterson and Hubbell prepared PEG hydrogels containing protease-sensitive peptides, which could be degraded via enzymatic hydrolysis when incubated with MMP1 and MMP2.<sup>[120]</sup>

However, MMP-mediated degradation of hydrogels is dependent upon the level of MMPs, which can vary significantly from tissue to tissue and their health states.<sup>[121]</sup>

Increasing interest has been directed to preparing hydrogels incorporating disulfide bonds, since the cleavage of this moiety is controllable under physiological conditions by altering the concentration of a reductant such as glutathione, which is a cell metabolite.<sup>[122]</sup>

Recently, Kar and coworkers proposed a PEG hydrogel incorporating disulfide moieties for cell transplantation. The release of human mesenchymal stem cells encapsulated into the scaffold was triggered by the degradation of the hydrogel, which was responsive to cell-secreted reductants.

They confirmed that the differentiation potential of the cells released from the hydrogels was maintained *in vitro*.<sup>[123]</sup>

In general, this degradation strategy, triggered by thiols omnipresent in the organism (e.g. glutathione, serum albumin, cysteine, homocysteine, glycylcysteine) with a rate adjustable by the hydrogel composition, is very promising for site-specific controlled drug delivery.

## 1.7 Polyamidoamine hydrogels

Polyamidoamines are a family of synthetic hydrophilic polymers obtained by Michael-type polyaddition of primary or secondary diamines to bisacrylamides (Figure 1.12).

The first study on linear chain polyamidoamines was published in 1970 by Danusso and Ferruti;<sup>[124]</sup> afterwards the chemistry and properties of these polymers have been investigated in several works.<sup>[125]</sup>

In the early eighties of the nineteenth century the self-polyaddition of 1-acrylamido-2-aminoethane hydro-chloride was exploited to develop hyperbranched dendrimers polyamidoamine, commonly known as PAMAM,<sup>[126]</sup> which were then studied for a number of biotechnological and biomedical applications.<sup>[127]</sup>

Polyamidoamines are characterized by a structure that contains amides and tertiary amine groups regularly arranged along the polymer chain. They are extremely versatile and their polymerization reaction can be tailored to introduce many additional functional groups as side substituents, such as hydroxy, allyl, amide, carboxyl and ether groups, by using the suitably

functionalized monomers. Peptides and proteins can also participate in the polyaddition reaction through their terminal amino groups.<sup>[128]</sup>

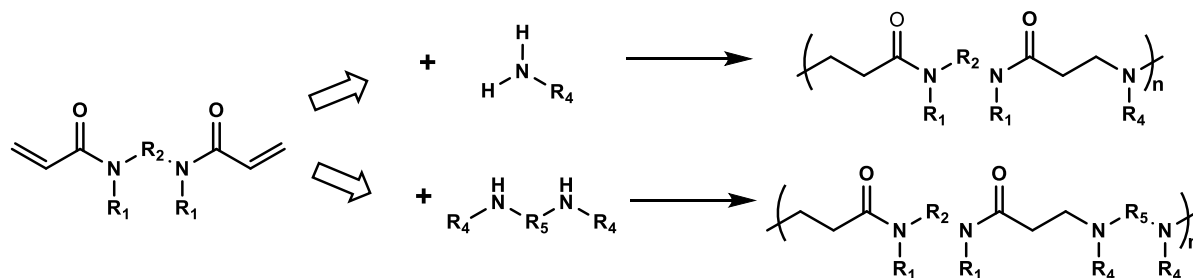


Figure 1.12 Common routes for the synthesis of linear PAAs, using primary amines or secondary diamines.

The potential of such hydrogels as scaffolds for 3D cell cultures and TE emerged only recently, when Emilietri et al. reported a polyamidoamine hydrogels containing an RGD-mimicking structure for the adhesion of Madin-Darby canine kidney cells.<sup>[130]</sup>

## 1.8 Aim of the thesis

The focus of this work is on the development of hydrogels composed of chemically cross-linked hydrophilic polymer chains, such as polyamidoamines, with novel attractive

characteristics, to be used as three-dimensional scaffolds for cell growth and for investigating the *in vitro* and *in vivo* response of cells to the material.

Polyamidoamines are a promising class of synthetic polymers for TE application. They were chosen because of their ability to form chemically cross-linked networks at room temperature, without any catalyst, and for their well-known biocompatibility. In addition, the chemical versatility allows the choice of the initial monomers, and of any other component, in order to obtain materials with tailor-made functionalities or bioactive groups.

After an introduction of the topic (Chapter 1), Chapter 2 explores the synthesis of suitable polyamidoamines-based hydrogels and their main physicochemical and mechanical characteristics. It describes the optimization of the hydrogel structure developed and used with some modifications in the following chapters, for specific applications.

Chapter 3 explores the possibility of using a polyamidoamines-based hydrogel, decorated with switchable chromophores, as a 3D bioimaging platform, which enables the clear and easy real-time visualization of cells proliferating onto the scaffold, without additional cell staining.

Chapter 4 reports the design of a novel nanocomposite hydrogel, cross-linked with porous nanomaterials (i.e. mesoporous silica nanoparticles). Its ability to provide optimal structural support for stem cells infiltration and proliferation was confirmed, demonstrating also its potentiality in stimulating chemotactic recruitment of cells *in vitro* and *in vivo*.

Chapter 5 then moves to a direct therapeutic application based on the use of an injectable *in situ*-gelling nanocomposite hydrogel, containing cell-cleavable bonds along its network, for endoscopic submucosal dissection of early stage neoplastic lesions.

Chapter 6 describes the principles of the main instrumental techniques used throughout this thesis.

This work has been carried out in the Laboratoire de Chimie et des Biomatériaux Supramoléculaires (Institut de Science et d'Ingénierie Supramoléculaires, Université de Strasbourg) under the supervision of Prof. Luisa De Cola.

Part of the work described in Chapter 4 has been carried out while visiting Dr Ennio Tasciotti's group, at the Department of Regenerative Medicine (Houston Methodist Research Institute, Houston, Texas).



The *in vivo* experiments described in Chapter 5 have been performed at Strasbourg's Image-Guided Surgery Institute (IHU/IRCAD), under the supervision of Prof. Silvana Perretta.

## 1.9 References

- [1] a) D. Seliktar, *Science (New York, N.Y.)* **2012**, 336, 1124; b) D. Buenger, F. Topuz, J. Groll, *Prog. Polym. Sci.* **2012**, 37, 1678.
- [2] O. Wichterle, D. Lím, *Nature* **1960**, 185, 117.
- [3] A. S. Hoffman, *Adv. Drug Del. Rev.* **2012**, 64, 18.
- [4] a) J. A. Rowley, G. Madlambayan, D. J. Mooney, *Biomaterials* **1999**, 20, 45; b) M. W. Tibbitt, K. S. Anseth, *Biotechnol. Bioeng.* **2009**, 103, 655.
- [5] a) H. Geckil, F. Xu, X. Zhang, S. Moon, U. Demirci, *Nanomedicine* **2010**, 5, 469; b) J. A. Hunt, R. Chen, T. van Veen, N. Bryan, *Journal of Materials Chemistry B* **2014**, 2, 5319.
- [6] F. Lim, A. M. Sun, *Science* **1980**, 210, 908.
- [7] I. V. Yannas, E. Lee, D. P. Orgill, E. M. Skrabut, G. F. Murphy, *Proc. Natl. Acad. Sci. U. S. A.* **1989**, 86, 933.
- [8] Q. Wang, J. L. Mynar, M. Yoshida, E. Lee, M. Lee, K. Okuro, K. Kinbara, T. Aida, *Nature* **2010**, 463, 339.
- [9] I. Lynch, K. A. Dawson, *Macromol. Chem. Phys.* **2003**, 204, 443.
- [10] Q. L. Loh, C. Choong, D. Oxon, M. Hons, C. Mimm, *Tissue Eng.: Part B* **2013**, 19, 485.
- [11] M. P. E. Wenger, L. Bozec, M. A. Horton, P. Mesquida, *Biophys. J.* **2007**, 93, 1255.
- [12] M. Dadsetan, T. E. Hefferan, J. P. Szatkowski, P. K. Mishra, S. I. Macura, L. Lu, M. J. Yaszemski, *Biomaterials* **2008**, 29, 2193.
- [13] B. V. Slaughter, S. S. Khurshid, O. Z. Fisher, A. Khademhosseini, N. a. Peppas, *Advanced materials (Deerfield Beach, Fla.)* **2009**, 21, 3307.
- [14] S. K. H. Gulrez, S. Al-Assaf, G. O. Phillips, *Progress in Molecular and Environmental Bioengineering* **2003**, 51, 117.
- [15] a) H. J. Chung, T. G. Park, *Nano Today* **2009**, 4, 429; b) J. K. Oh, *Can. J. Chem.* **2009**, 88, 173; c) J. Lee, M. J. Cuddihy, N. A. Kotov, *Tissue Eng Part B Rev* **2008**, 14, 61.
- [16] K. T. Nguyen, J. L. West, *Biomaterials* **2002**, 23, 4307.
- [17] X.-Z. Zhang, C.-C. Chu, *Chem. Commun.* **2004**, 350.
- [18] N. Fatin-Rouge, A. Milon, J. Buffle, R. R. Goulet, A. Tessier, *The Journal of Physical Chemistry B* **2003**, 107, 12126.
- [19] a) Y. Loo, S. Zhang, C. A. E. Hauser, *Biotechnol. Adv.* **2012**, 30, 593; b) C. Xu, J. Kopeček, *Polym. Bull.* **2007**, 58, 53.
- [20] a) F. Topuz, O. Okay, *Biomacromolecules* **2009**, 10, 2652; b) K. Trabbic-Carlson, L. A. Setton, A. Chilkoti, *Biomacromolecules* **2003**, 4, 572; c) D. A. Ossipov, J. Hilborn, *Macromolecules* **2006**, 39, 1709.
- [21] J. Jagur-Grodzinski, *Polym. Adv. Technol.* **2010**, 21, 27.
- [22] K. T. Nguyen, J. L. West, *Biomaterials* **2002**, 23, 4307.

- [23] a) C. D. Pritchard, T. M. O'Shea, D. J. Siegwart, E. Calo, D. G. Anderson, F. M. Reynolds, J. A. Thomas, J. R. Slotkin, E. J. Woodard, R. Langer, *Biomaterials* **2011**, 32, 587; b) F. Fiorini, E. A. Prasetyanto, F. Taraballi, L. Pandolfi, F. Monroy, I. López-Montero, E. Tasciotti, L. De Cola, *Small* **2016**, 12, 4881.
- [24] K. P. Koutroumanis, K. Avgoustakis, D. Bikiaris, *Carbohydr. Polym.* **2010**, 82, 181.
- [25] a) R. Jin, C. Hiemstra, Z. Zhong, J. Feijen, *Biomaterials* **2007**, 28, 2791; b) J. W. Bae, J. H. Choi, Y. Lee, K. D. Park, *J. Tissue Eng. Regen. Med.* **2015**, 9, 1225.
- [26] a) P. Ferruti, S. Bianchi, E. Ranucci, F. Chiellini, V. Caruso, *Macromol. Biosci.* **2005**, 613; b) M. P. Lutolf, N. Tirelli, S. Cerritelli, L. Cavalli, J. A. Hubbell, *Bioconjugate Chem.* **2001**, 12, 1051.
- [27] F. Yu, X. Cao, J. Du, G. Wang, X. Chen, *ACS Applied Materials & Interfaces* **2015**, 7, 24023.
- [28] E. a. Appel, O. a. Scherman, J. del Barrio, X. J. Loh, *Chem. Soc. Rev.* **2012**, 41, 6195.
- [29] R. Suriano, G. Griffini, M. Chiari, M. Levi, S. Turri, *Journal of the mechanical behavior of biomedical materials* **2014**, 30, 339.
- [30] J. E. Hall, Guyton, A. C., *Textbook of medical physiology*, 10th ed., Philadelphia, PA, **2000**.
- [31] Liverpool University Press, **1999**.
- [32] S. J. Bryant, C. R. Nuttelman, K. S. Anseth, *J. Biomater. Sci. Polym. Ed.* **2000**, 11, 439.
- [33] a) S. Yang, K. F. Leong, Z. Du, C. K. Chua, *Tissue Eng.* **2001**, 7, 679; b) A. Al-Abboudi, J. Fu, P. M. Doran, T. T. Y. Tan, P. P. Y. Chan, *Advanced healthcare materials* **2014**, 3, 725; c) A. Reisch, P. Tirado, E. Roger, F. Boulmedais, D. Collin, J.-C. Voegel, B. Frisch, P. Schaaf, J. B. Schlenoff, *Adv. Funct. Mater.* **2013**, 23, 673.
- [34] a) N. V. Gupta, H. G. Shivakumar, *Iranian Journal of Pharmaceutical Research : IJPR* **2012**, 11, 481; b) D. Feng, B. Bai, H. Wang, Y. Suo, *New J. Chem.* **2016**, 40, 3350.
- [35] K. S. Anseth, A. T. Metters, S. J. Bryant, P. J. Martens, J. H. Elisseeff, C. N. Bowman, *J. Controlled Release* **2002**, 78, 199.
- [36] E. Schonherr, H. J. Hausser, *Dev. Immunol.* **2000**, 7, 89.
- [37] S. Swaminathan, R. Cavalli, F. Trotta, P. Ferruti, E. Ranucci, I. Gerges, A. Manfredi, D. Marinotto, P. R. Vavia, *J. Incl. Phenom. Macrocycl. Chem.* **2010**, 68, 183.
- [38] I. M. El-Sherbiny, M. H. Yacoub, *Global Cardiology Science & Practice* **2013**, 2013, 316.
- [39] J. Zhu, R. E. Marchant, *Expert Rev. Med. Devices* **2011**, 8, 607.
- [40] J. Glowacki, S. Mizuno, *Biopolymers* **2008**, 89, 338.
- [41] S. Sakai, K. Hirose, K. Taguchi, Y. Ogushi, K. Kawakami, *Biomaterials* **2009**, 30, 3371.
- [42] a) M. Ehrbar, S. C. Rizzi, R. G. Schoenmakers, B. S. Miguel, J. A. Hubbell, F. E. Weber, M. P. Lutolf, *Biomacromolecules* **2007**, 8, 3000; b) J. J. Sperinde, L. G. Griffith, *Macromolecules* **2000**, 33, 5476.
- [43] a) M. A. de Moraes, C. R. Albrecht Mahl, M. Ferreira Silva, M. M. Beppu, *J. Appl. Polym. Sci.* **2015**, 132, n/a; b) K. Schacht, T. Scheibel, *Biomacromolecules* **2011**, 12, 2488.
- [44] a) H. K. Kleinman, G. R. Martin, *Semin. Cancer Biol.* **2005**, 15, 378; b) B. J. Kang, H. H. Ryu, S. S. Park, Y. Kim, H. M. Woo, W. H. Kim, O. K. Kweon, *J. Vet. Med. Sci.* **2012**, 74, 827.
- [45] J. Baier Leach, K. A. Bivens, C. W. Patrick, Jr., C. E. Schmidt, *Biotechnol. Bioeng.* **2003**, 82, 578.
- [46] N. Jin, E. A. Morin, D. M. Henn, Y. Cao, J. W. Woodcock, S. Tang, W. He, B. Zhao, *Biomacromolecules* **2013**, 14, 2713.

- [47] a) W. E. Hennink, O. Franssen, W. N. E. van Dijk-Wolthuis, H. Talsma, *J. Controlled Release* **1997**, 48, 107; b) G. Sun, X. Zhang, Y.-I. Shen, R. Sebastian, L. E. Dickinson, K. Fox-Talbot, M. Reinblatt, C. Steenbergen, J. W. Harmon, S. Gerecht, *Proceedings of the National Academy of Sciences* **2011**, 108, 20976.
- [48] a) I. Y. Kim, S. J. Seo, H. S. Moon, M. K. Yoo, I. Y. Park, B. C. Kim, C. S. Cho, *Biotechnol. Adv.* **2008**, 26, 1; b) K. E. Crompton, J. D. Goud, R. V. Bellamkonda, T. R. Gengenbach, D. I. Finkelstein, M. K. Horne, J. S. Forsythe, *Biomaterials* **2007**, 28, 441.
- [49] Y. Aizawa, S. C. Owen, M. S. Shoichet, *Prog. Polym. Sci.* **2012**, 37, 645.
- [50] C. R. Nuttelman, M. A. Rice, A. E. Rydholm, C. N. Salinas, D. N. Shah, K. S. Anseth, *Prog. Polym. Sci.* **2008**, 33, 167.
- [51] a) D. Seliktar, *Science* **2012**, 336, 1124; b) M. P. Lutolf, J. A. Hubbell, *Nat. Biotechnol.* **2005**, 23, 47.
- [52] A. C. Fonseca, M. H. Gil, P. N. Simões, *Prog. Polym. Sci.* **2014**, 39, 1291.
- [53] M. Malkoch, R. Vestberg, N. Gupta, L. Mespouille, P. Dubois, A. F. Mason, J. L. Hedrick, Q. Liao, C. W. Frank, K. Kingsbury, C. J. Hawker, *Chem. Commun.* **2006**, 2774.
- [54] S. B. Lowe, V. T. G. Tan, A. H. Soeriyadi, T. P. Davis, J. J. Gooding, *Bioconjugate Chem.* **2014**, 25, 1581.
- [55] E. S. Place, J. H. George, C. K. Williams, M. M. Stevens, *Chem. Soc. Rev.* **2009**, 38, 1139.
- [56] a) S. N. S. Alconcel, A. S. Baas, H. D. Maynard, *Polymer Chemistry* **2011**, 2, 1442; b) S. Brocchini, A. Godwin, S. Balan, J.-w. Choi, M. Zloh, S. Shaunak, *Adv. Drug Del. Rev.* **2008**, 60, 3.
- [57] a) A. K. Gaharwar, C. Rivera, C.-J. Wu, B. K. Chan, G. Schmidt, *Materials science & engineering. C, Materials for biological applications* **2013**, 33, 1800; b) L. He, E. S. Read, S. P. Armes, D. J. Adams, *Macromolecules* **2007**, 40, 4429.
- [58] B. E. B. Jensen, I. Dávila, A. N. Zelikin, *The Journal of Physical Chemistry B* **2016**, 120, 5916.
- [59] E. A. Kamoun, X. Chen, M. S. Mohy Eldin, E.-R. S. Kenawy, *Arabian Journal of Chemistry* **2015**, 8, 1.
- [60] A. Kidane, J. M. Szabocsik, K. Park, *Biomaterials* **1998**, 19, 2051.
- [61] S. Kubinova, D. Horak, N. Kozubenko, V. Vanecek, V. Proks, J. Price, G. Cocks, E. Sykova, *Biomaterials* **2010**, 31, 5966.
- [62] F. Ayhan, S. Ozkan, *Drug Deliv.* **2007**, 14, 433.
- [63] a) U. Freudenberg, A. Hermann, P. B. Welzel, K. Stirl, S. C. Schwarz, M. Grimmer, A. Zieris, W. Panyanuwat, S. Zschoche, D. Meinhold, A. Storch, C. Werner, *Biomaterials* **2009**, 30, 5049; b) M. P. Lutolf, *Nat Mater* **2009**, 8, 451; c) R. H. Schmedlen, K. S. Masters, J. L. West, *Biomaterials* **2002**, 23, 4325; d) E. Cambria, K. Renggli, C. C. Ahrens, C. D. Cook, C. Kroll, A. T. Krueger, B. Imperiali, L. G. Griffith, *Biomacromolecules* **2015**, 16, 2316.
- [64] a) F. Yang, C. G. Williams, D. A. Wang, H. Lee, P. N. Manson, J. Elisseeff, *Biomaterials* **2005**, 26, 5991; b) S. Q. Liu, Q. Tian, L. Wang, J. L. Hedrick, J. H. Hui, Y. Y. Yang, P. L. Ee, *Macromol. Rapid Commun.* **2010**, 31, 1148.
- [65] a) R. M. Eman, F. C. Öner, M. C. Kruyt, W. J. A. Dhert, J. Alblas, *Tissue Eng. Part A* **2014**, 20, 466; b) A. Nair, P. Thevenot, J. Dey, J. Shen, M.-W. Sun, J. Yang, L. Tang, *Tissue engineering. Part C, Methods* **2010**, 16, 23; c) N. Segovia, M. Pont, N. Oliva, V. Ramos, S. Borrós, N. Artzi, *Advanced healthcare materials* **2014**, 1.
- [66] G. D. Nicodemus, S. J. Bryant, *Tissue Engineering. Part B, Reviews* **2008**, 14, 149.

- [67] a) N. Annabi, A. Tamayol, J. A. Uquillas, M. Akbari, L. E. Bertassoni, C. Cha, G. Camci-Unal, M. R. Dokmeci, N. a. Peppas, A. Khademhosseini, *Advanced materials research* **2014**, 26, 85; b) Q. L. Loh, C. Choong, D. Oxon, M. Hons, C. Mimmm, *Tissue Eng. Part B* **2013**, 19, 485.
- [68] J. M. Knipe, N. A. Peppas, *Regenerative Biomaterials* **2014**, 1, 57.
- [69] M. P. Lutolf, J. A. Hubbell, *Nat Biotech* **2005**, 23, 47.
- [70] a) M. B. Eslaminejad, H. Mirzadeh, Y. Mohamadi, A. Nickmahzar, *J. Tissue Eng. Regen. Med.* **2007**, 1, 417; b) M. S. Chapekar, *J. Biomed. Mater. Res.* **2000**, 53, 617.
- [71] R. Langer, J. P. Vacanti, *Science* **1993**, 260, 920.
- [72] T. G. Kim, H. Shin, D. W. Lim, *Adv. Funct. Mater.* **2012**, 22, 2446.
- [73] M. J. Webber, O. F. Khan, S. A. Sydlík, B. C. Tang, R. Langer, *Ann. Biomed. Eng.* **2015**, 43, 641.
- [74] V. Barron, A. Pandit, in *Topics in Tissue Engineering* (Eds.: N. A. Eds, P. Ferretti), **2003**.
- [75] A. R. Amini, C. T. Laurencin, S. P. Nukavarapu, *Crit. Rev. Biomed. Eng.* **2012**, 40, 363.
- [76] a) J. E. Saik, D. J. Gould, E. M. Watkins, M. E. Dickinson, J. L. West, *Acta Biomater.* **2011**, 7, 133; b) R. B. Michael, G. Sharon, *Biomedical Materials* **2015**, 10, 034001.
- [77] A. J. Mothe, R. Y. Tam, T. Zahir, C. H. Tator, M. S. Shoichet, *Biomaterials* **2013**, 34, 3775.
- [78] S. L. Hume, S. M. Hoyt, J. S. Walker, B. V. Sridhar, J. F. Ashley, C. N. Bowman, S. J. Bryant, *Acta Biomater.* **2012**, 8, 2193.
- [79] a) K.-W. Park, Y.-P. Yun, S. E. Kim, H.-R. Song, *International Journal of Molecular Sciences* **2015**, 16, 26738; b) J. P. Chen, M. J. Tsai, H. T. Liao, *Colloids Surf. B. Biointerfaces* **2013**, 110, 120.
- [80] a) S. Fu, P. Ni, B. Wang, B. Chu, L. Zheng, F. Luo, J. Luo, Z. Qian, *Biomaterials* **2012**, 33, 4801; b) S. Minardi, B. Corradetti, F. Taraballi, M. Sandri, J. Van Eps, F. J. Cabrera, B. K. Weiner, A. Tampieri, E. Tasciotti, *Biomaterials* **2015**, 62, 128.
- [81] X. Li, E. Katsanevakis, X. Liu, N. Zhang, X. Wen, *Prog. Polym. Sci.* **2012**, 37, 1105.
- [82] N. Broguiere, L. Isenmann, M. Zenobi-Wong, *Biomaterials* **2016**, 99, 47.
- [83] K. J. Lampe, D. S. Kern, M. J. Mahoney, K. B. Bjugstad, *Journal of Biomedical Materials Research Part A* **2011**, 96A, 595.
- [84] a) U. Bhardwaj, R. Sura, F. Papadimitrakopoulos, D. J. Burgess, *Int. J. Pharm.* **2010**, 384, 78; b) I. Galeska, T.-K. Kim, S. D. Patil, U. Bhardwaj, D. Chattopadhyay, F. Papadimitrakopoulos, D. J. Burgess, *The AAPS Journal* **2005**, 7, E231.
- [85] A. K. Gaharwar, N. a. Peppas, A. Khademhosseini, *Biotechnol. Bioeng.* **2014**, 111, 441.
- [86] N. S. Kehr, E. A. Prasetyanto, K. Benson, B. Ergün, A. Galstyan, H.-J. Galla, *Angew. Chem. Int. Ed.* **2012**, 125, 1194.
- [87] F. Song, X. Li, Q. Wang, L. Liao, C. Zhang, *J. Biomed. Nanotechnol.* **2015**, 11, 40.
- [88] H. Sato, H. Ohtani, R. Harada, S. Tsuge, M. Kato, A. Usuki, *Polym. J* **2006**, 38, 171.
- [89] M. Oliveira, A. V. Machado, in *Nanocomposites: Synthesis, Characterization and Applications* (Ed.: N. Publishers), **2013**.
- [90] M. Supová, G. Martynková, K. Barabaszová, *Sci. Adv. Mater.* **2011**, 3, 1.
- [91] M. Z. Rong, M. Q. Zhang, W. H. Ruan, *Mater. Sci. Technol.* **2006**, 22, 787.
- [92] H. Lülfi, A. Bertucci, D. Septiadi, R. Corradini, L. De Cola, *Chemistry – A European Journal* **2014**, 20, 10900.
- [93] S. Niedermayer, V. Weiss, A. Herrmann, A. Schmidt, S. Datz, K. Muller, E. Wagner, T. Bein, C. Brauchle, *Nanoscale* **2015**, 7, 7953.

- [94] P. N.A., H. J.Z., T. J.B., Horizon Bioscience, **2007**.
- [95] C. M. Paranhos, B. G. Soares, R. N. Oliveira, L. A. Pessan, *Macromolecular Materials and Engineering* **2007**, 292, 620.
- [96] N. S. Satarkar, J. Z. Hilt, *Journal of controlled release : official journal of the Controlled Release Society* **2008**, 130, 246.
- [97] I. Tokarev, I. Tokareva, S. Minko, *Adv. Mater.* **2008**, 20, 2730.
- [98] C. Wang, N. T. Flynn, R. Langer, *Adv. Mater.* **2004**, 16, 1074.
- [99] a) K. Haraguchi, T. Takehisa, M. Ebato, *Biomacromolecules* **2006**, 7, 3267; b) T. Wang, W. Sun, X. Liu, C. Wang, S. Fu, Z. Tong, *React. Funct. Polym.* **2013**, 73, 683; c) Y. S. Pek, C. A. WanAndrew, A. Shekaran, L. Zhuo, J. Y. Ying, *Nat Nano* **2008**, 3, 671.
- [100] C.-W. Chang, A. van Spreeuwel, C. Zhang, S. Varghese, *Soft Matter* **2010**, 6, 5157.
- [101] a) J. R. Xavier, T. Thakur, P. Desai, M. K. Jaiswal, N. Sears, E. Cosgriff-Hernandez, R. Kaunas, A. K. Gaharwar, *ACS Nano* **2015**, 9, 3109; b) S. Pina, J. M. Oliveira, R. L. Reis, *Adv. Mater.* **2015**, 27, 1143.
- [102] a) K.-T. Huang, C.-J. Huang, in *1st Global Conference on Biomedical Engineering & 9th Asian-Pacific Conference on Medical and Biological Engineering: October 9-12, 2014, Tainan, Taiwan* (Eds.: F.-C. Su, S.-H. Wang, M.-L. Yeh), Springer International Publishing, Cham, **2015**, pp. 35; b) X. Li, S. Chen, B. Zhang, M. Li, K. Diao, Z. Zhang, J. Li, Y. Xu, X. Wang, H. Chen, *Int. J. Pharm.* **2012**, 437, 110.
- [103] S. Merino, C. Martin, K. Kostarelos, M. Prato, E. Vázquez, *ACS Nano* **2015**, 150504170626008.
- [104] C. J. Wu, A. K. Gaharwar, P. J. Schexnailder, G. Schmidt, *Materials* **2010**, 3, 2986.
- [105] B. T. Corona, C. L. Ward, B. S. Harrison, G. J. Christ, *J. Investig. Med.* **2010**, 58, 849.
- [106] M. Patenaude, N. M. B. Smeets, T. Hoare, *Macromol. Rapid Commun.* **2014**, 35, 598.
- [107] a) E. Bakaic, N. M. B. Smeets, T. Hoare, *RSC Advances* **2015**, 5, 35469; b) Y. Li, J. Rodrigues, H. Tomas, *Chem. Soc. Rev.* **2012**, 41, 2193.
- [108] K. H. Bae, L.-S. Wang, M. Kurisawa, *Journal of Materials Chemistry B* **2013**, 1, 5371.
- [109] B. Choi, X. J. Loh, A. Tan, C. K. Loh, E. Ye, M. K. Joo, B. Jeong, in *In-Situ Gelling Polymers: For Biomedical Applications* (Ed.: J. X. Loh), Springer Singapore, Singapore, **2015**, pp. 5.
- [110] H. Singh, L. S. Nair, in *Integrated Biomaterials for Biomedical Technology*, John Wiley & Sons, Inc., **2012**, pp. 359.
- [111] J. L. Ifkovits, J. A. Burdick, *Tissue Eng.* **2007**, 13, 2369.
- [112] M. K. Nguyen, D. S. Lee, *Macromol. Biosci.* **2010**, 10, 563.
- [113] a) M. K. Nguyen, D. K. Park, D. S. Lee, *Biomacromolecules* **2009**, 10, 728; b) C. D. Pritchard, T. M. O'Shea, D. J. Siegwart, E. Calo, D. G. Anderson, F. M. Reynolds, J. A. Thomas, J. R. Slotkin, E. J. Woodard, R. Langer, *Biomaterials* **2011**, 32, 587.
- [114] R. Censi, P. J. Fieten, P. di Martino, W. E. Hennink, T. Vermonden, *Macromolecules* **2010**, 43, 5771.
- [115] a) J. D. Kretlow, A. G. Mikos, *AIChE J.* **2008**, 54, 3048; b) E. C. Novosel, C. Kleinhans, P. J. Kluger, *Adv Drug Deliv Rev* **2011**, 63, 300.
- [116] C. C. Lin, K. S. Anseth, *Pharm. Res.* **2009**, 26, 631.
- [117] D. Y. Ko, U. P. Shinde, B. Yeon, B. Jeong, *Prog. Polym. Sci.* **2013**, 38, 672.
- [118] W. P. Daley, S. B. Peters, M. Larsen, *J. Cell Sci.* **2008**, 121, 255.

- [119] M. P. Lutolf, J. L. Lauer-Fields, H. G. Schmoekel, A. T. Metters, F. E. Weber, G. B. Fields, J. A. Hubbell, *Proc. Natl. Acad. Sci. U. S. A.* **2003**, *100*, 5413.
- [120] J. Patterson, J. A. Hubbell, *Biomaterials* **2010**, *31*, 7836.
- [121] K. Komosinska-Vassev, P. Olczyk, K. Winsz-Szczotka, K. Kuznik-Trocha, K. Klimek, K. Olczyk, *Gerontology* **2011**, *57*, 44.
- [122] a) L. Bromberg, M. Temchenko, V. Alakhov, T. A. Hatton, *Langmuir* **2005**, *21*, 1590; b) J. Zhang, A. Skardal, G. D. Prestwich, *Biomaterials* **2008**, *29*, 4521.
- [123] M. Kar, Y.-R. Vernon Shih, D. O. Velez, P. Cabrales, S. Varghese, *Biomaterials* **2016**, *77*, 186.
- [124] F. Danusso, P. Ferruti, *Polymer* **1970**, *11*, 88.
- [125] P. Ferruti, *J. Polym. Sci., Part A: Polym. Chem.* **2013**, *51*, 2319.
- [126] D. A. Tomalia, J. R. Dewald, U.S. Patent 4, 507, 466, **1985**.
- [127] a) M. Labieniec-Watala, C. Watala, *J. Pharm. Sci.* **2015**, *104*, 2; b) R. Esfand, D. A. Tomalia, *Drug Discov. Today* **2001**, *6*, 427.
- [128] P. Ferruti, M. A. Marchisio, R. Duncan, *Macromol. Rapid Commun.* **2002**, *23*, 332.
- [129] E. Ranucci, G. Spagnoli, P. Ferruti, D. Sgouras, R. Duncan, *J. Biomater. Sci. Polym. Ed.* **1991**, *2*, 303.
- [130] E. Emilietri, F. Guizzardi, C. Lenardi, M. Suardi, E. Ranucci, P. Ferruti, *Macromol. Symp.* **2008**, *266*, 41.
- [131] N. Mauro, A. Manfredi, E. Ranucci, P. Procacci, M. Laus, D. Antonioli, C. Mantovani, V. Magnaghi, P. Ferruti, *Macromol. Biosci.* **2013**, *13*, 332.
- [132] Y. Sun, Z. Deng, Y. Tian, C. Lin, *J. Appl. Polym. Sci.* **2013**, *127*, 40.

## **2. Making the tools: polyamidoamines-based hydrogels**

### Abstract

This chapter describes the synthesis and optimization of the polyamidoamines-based scaffold developed and used with some modifications in the following chapters, for specific applications.

Herein we analyzed the synthesis, morphology, swelling ability and mechanical properties of the hydrogels, leading to the improvement of the material.

The scaffolds were obtained by Michael-type polyaddition of primary or secondary aliphatic amines to bis-acrylamides in water, offering great flexibility to incorporate specific functionalities within the hydrogel architectures.

The introduction of polar functional groups, such as carboxylic and amino groups, resulted in an improved swelling ability of the network. This is a major parameter, since it can affect solute diffusion, surface properties and mechanical behavior.

The viability of cells encapsulated in the hydrogel can also be influenced by the hydrogel swelling.

Finally, studies on stability at different pH and mechanical properties of the scaffolds are reported.

## 2.1 Polyamidoamine-based hydrogels general characteristics

Polyamidoamines are a family of synthetic functional polymers that in recent years have been studied for biomedical uses and have been developed especially in form of linear polymers and dendrimers, thus as soluble bioactive structures.<sup>[1]</sup>

Our interest was to exploit them as polymeric hydrogels for cell culturing and tissue engineering applications.

Their synthetic network is obtained via stepwise aza-Michael polyaddition of primary or secondary aliphatic amines to bis-acrylamides, with the addition of a cross-linker, i.e. a multifunctional monomer such as a primary diamine containing four different mobile hydrogens that can react in a tetrafunctional manner (Figure 2.1).<sup>[2]</sup>

Their structure is therefore characterized by the presence of tert-amino groups along the polymeric chain.<sup>[3]</sup>

To form a cross-linked network the average functionality of the combined precursors must be greater than two; a number of hydrogel architectures are possible by using different precursor monomers.

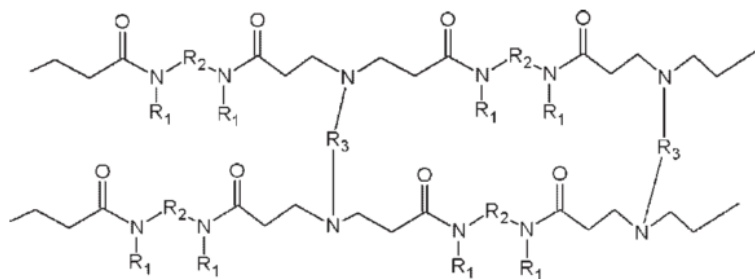


Figure 2.1 Polyamidoamine general structure, adapted from P. Ferruti, S. Bianchi, E. Ranucci, F. Chiellini, V. Caruso, *Macromol. Biosci.* **2005**, 5, 613–622

The synthesis is generally performed in aqueous media to achieve a better yield thanks to the formation of hydrogen bonds between the oxygen atom of the  $\alpha,\beta$ -unsaturated carbonyl and the water molecules, which increases the electrophilic character of the  $\beta$ -carbon.



Moreover, hydrogen bond formation involving the water oxygen and the amine hydrogen favors the nucleophilic character of the nitrogen. Water has thus been suggested to activate the amine as well as the conjugated alkene and facilitate the addition reaction.<sup>[4]</sup>

Alternatively, the reaction has been shown to work in protic organic solvents, such as methanol whereas aprotic solvents are unsuitable as reaction media, since a source of protons is necessary to promote rapid proton transfer and to stabilize charged intermediates.<sup>[5]</sup>

The use of amines that can act as both nucleophiles and bases allows avoiding the addition of a base, which is otherwise typically needed in these reactions.

For the systems presented in this thesis, the Michael acceptor is N,N'-methylene bisacrylamide, which was chosen to obtain mechanical strength that is expected to increase in the presence of amide hydrogen bonds along the polymer chain.<sup>[6]</sup> The terminal acrylates react with the amine monomers and cross-linker to form the hydrogel network.

Typically, hydrogels present unique tissue-like properties for interactions with living cells, such as water content and permeability to oxygen and metabolites.<sup>[7]</sup> Polyamidoamine-based hydrogels couple these mentioned features with the possibility of control over the scaffold composition and swelling.<sup>[8]</sup>

The conjugate-addition reaction between amines and vinyl groups offers great synthetic flexibility and can be easily tuned to incorporate specific functionalities within the hydrogel architectures.

Suitably functionalized monomers can be used to achieve the formation of hydrogel networks containing desired chemical groups as side-substituents. In principle, nearly every aliphatic amine and bis-acrylamide can be used as a monomer, provided they do not undergo addition reactions with activated double bonds, thus interfering with the polymerization reaction. The presence of hydroxy-, tert-amino-, allyl-, amido- and ether groups do not interfere with the polymerization process.

For example, in an early work phenolic groups were introduced as side substituents by using tyramine as a comonomer in linear polyamidoamines.<sup>[9]</sup> Amino-carbohydrate derivatives, peptides and proteins have also been shown to participate in the poly-addition reaction through their terminal amino groups.<sup>[3, 10]</sup>

Structures with hydrophobic moieties as side groups can be obtained as well; however, when water-insoluble monomers are used, the polymerization has to be carried out in organic

solvents.<sup>[11]</sup> In chapter 3 will be presented a polyamidoamines-based hydrogel with a water-insoluble Ir(III) complex as side substituent, designed as bio-probe for cell imaging; the reaction in this case was carried out in methanol.

The swelling characteristics of a polymer network are important in various applications as they can affect solute diffusion, surface properties and mechanical behavior. Viability of cells encapsulated in the hydrogel can also be affected by the hydrogel swelling, which can lead to poor nutrient and gas exchange if it is too low.<sup>[12]</sup>

The degree of hydrogel swelling is determined mainly by the interaction between the polymer chains and the solvent: the hydrophilic/hydrophobic balance of the network, the degree of cross-linking, the ionization and the porosity are the important parameters for the equilibrium swelling.<sup>[13]</sup>

In the biomedical field hydrogel scaffold for drug delivery and tissue engineering are designed with specific structures and characteristics in view of the desired performance. For example, variations of swelling can influence the uptake of a drug within the network and its subsequent release.<sup>[14]</sup> The network structure and porosity can favor the diffusion of nutrients and active molecules, which are fundamental for the growth of cells onto the scaffolds.<sup>[15]</sup>

These features and network structure variations are treated in relation to the different aims of the hydrogel scaffolds in the next chapters of this thesis.

Herein, we report preliminary studies carried on polyamidoamines-based hydrogels, with respect to different functionalization, swelling ability, stability at different pH and mechanical properties.

## **2.2 Equilibrium swelling degree**

The equilibrium swelling degree (EDS) is an essential parameter for hydrogels characterization, especially when they are designed for biomedical applications. The water uptake ability can determine the overall permeation of nutrients and oxygen into the network, and of cellular products out of it.<sup>[16]</sup> The amount of water uptaken by a hydrogel regulates the absorption and diffusion of solutes throughout the scaffold.

When a dry hydrogel begins to absorb water, water molecules will initially hydrate the most polar hydrophilic groups present in the polymer chains, such as amino or carbonyl groups present in the polyamidoamines-based structure. As a result of polar groups hydration, the network swells while exposing hydrophobic groups, leading to hydrophobically-bound water. Finally, the network imbibe additional water (Figure 2.2), due to the osmotic driving force of the network chains towards infinite dilution.<sup>[17]</sup> Hydrogels reach their EDS when a balance occurs between osmotic driving forces and the cohesive forces exerted by the cross-linked network. The latter contrast the hydrogel expansion to an extent that depends mainly on the hydrogel cross-linking characteristics and density.<sup>[18]</sup>

Hydrophilic structures, such as polyamidoamines-based hydrogel, usually absorb water ranging from 100 to 1000% of their own dry weight, or even more.<sup>[19]</sup>

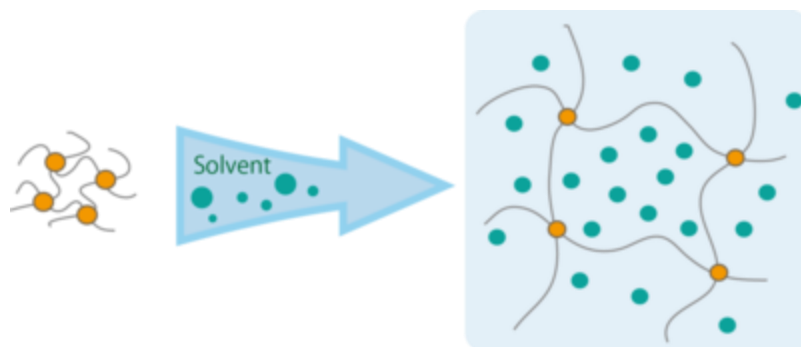


Figure 2.2 Schematic diagram of the network structure of a hydrogel, swelling when immersed into a solvent (i.e. water). Adapted from [http://www.aip.nagoya-u.ac.jp/en/public/nu\\_research/highlights](http://www.aip.nagoya-u.ac.jp/en/public/nu_research/highlights)

The equilibrium swelling degree gives information on the stability of the hydrogel scaffold in water or at a specific pH, it indicates the amount of the maximum water content and it is related to the elasticity of the material.

For the hydrogels synthesized in this thesis, EDS was calculated through gravimetric measurements, following equation 1:

$$EDS (\%) = \frac{W_s - W_d}{W_d} \times 100 \quad (1)$$

where  $W_s$  is the weight of the hydrogel in the swollen state and  $W_d$  is the dry weight.

### 2.3 Optimization of the hydrogel structure design

Initially, the synthesis of polyamidoamines-based hydrogels was investigated exploiting different monomers to obtain a self-standing material, with optimal structure and cytocompatibility for cell proliferation in 3D.

First results were achieved via Michael-type polyaddition of N,N'-methylene bisacrylamide to ethylenediamine (EDA) as cross-linker, following the work of Emilietri et al.<sup>[20]</sup> A precise stoichiometric equivalence between double bonds and amine hydrogens was used.

The synthesis was conducted in water, at room temperature, without any additional base or catalyst.

In a typical synthetic procedure, N,N'-methylene bisacrylamide (MBA) was solubilized in distilled water, with initial heating to facilitate its solubility, which is low in water at room temperature (20g/l at 20 °C). Following complete dissolution, EDA was added, to induce the polymerization and cross-linking of the system. The mixture was allowed to react at room temperature in static conditions for 3-4 hours, thus obtaining the hydrogel scaffold.

Under nonselective conditions, a monomer bearing two primary amino groups as EDA is expected to react tetrafunctionally, because the secondary amino groups generated in the first addition step are prone to further addition.<sup>[21]</sup> This is what was observed, achieving the formation of the hydrogel scaffold. However, the obtained material was very brittle, with no to little ability to swell in water. The observed non reversible collapsed/swollen behavior of this first hydrogel was an undesired effect due to the high degree of cross-linking in the network.

It has indeed been reported that highly cross-linked products obtained from reaction consisting of stoichiometrically-balanced mixtures of bisacrylamides and multifunctional amines with minor, if any, amount of difunctional amines, result in very hard and rigid materials with limited swelling in aqueous media.<sup>[22]</sup>

For this reason, the use of mixtures containing a third component, to reduce the degree of cross-linking was necessary to obtain scaffold with increased swelling ability. Thus, N,N-dimethylethylenediamine (DED) was added to the polymerization. The reaction mechanism is shown in Figure 2.3. The stoichiometric equivalence between double bonds and amine hydrogens was maintained, but the presence of a third component allowed to “dilute” the cross-

linker amount. The choice of the cross-linking degree was based upon preliminary experiments that recognized 10 mol% as the minimum amount needed to obtain the hydrogel.

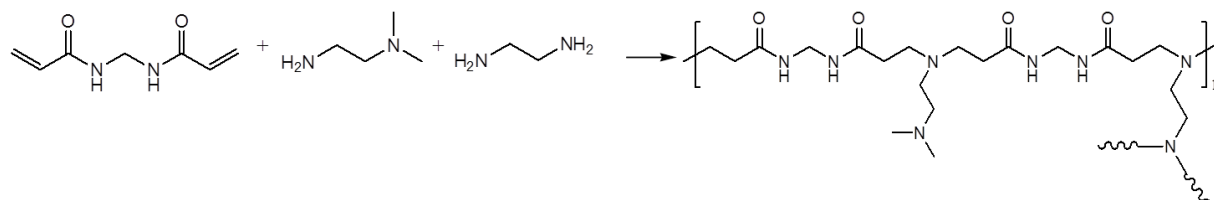


Figure 2.3 Reaction scheme of the Michael-type polyaddition between MBA, DED and DEA with formation of the hydrogel network.

The hydrogel obtained was transparent and homogeneous, with no sign of phase separation, which can be sometimes observed due to the formation of crystalline domains inside the polymer network in the initial stages of the reaction, leading to partial precipitation.<sup>[6]</sup> “Inverted test tube method” was used as a simple and direct way to confirm gelation. The synthesized hydrogel was self-standing, showing that the matter withstood gravitation without falling out when the test tubes was inverted. It was elastic and flexible and showed to retain its integrity in the swollen state. The calculated EDS in water was however only 156%, with a maximum water content of 61 wt%.

Thus, various procedures were taken into account to increase the hydrophilicity of the hydrogel. Different co-monomers were tested, such as L-lysine (i.e. a synthetic positively charged  $\gamma$ -amino acid, usually used in the polymeric form as coating substrate to enhance cell adhesion to plastic surfaces) and the tripeptide RGD (L-arginine, glycine, and L-aspartic acid). However, the products obtained with varying the co-monomers and their ratio with the cross-linker did not lead to an improvement in the obtained product. In some cases, they did not form a hydrogel, but instead viscous oil was produced, showing the difficulty of making a cross-linked structure in the presence of such complex systems.

Finally, interesting results were achieved using  $\gamma$ -aminobutyric acid (GABA) as co-monomer, which was added in the same ratio as DED in the previous synthesis. GABA is a common neurotransmitter in neuronal cells, thus potentially more beneficial in terms of cytocompatibility. It was chosen especially because it could provide carboxylic functionalities

as side-chain groups, thus allowing to increase the hydrophilicity and the water uptake ability of the scaffold through additional hydrogen bonding.<sup>[1b]</sup>

Copolymerizing monomers containing a carboxylate functional group in the network is known to enhance the hydrophilicity of the matrix.<sup>[23]</sup> It yields amphoteric structures containing amide, amine and carboxylate groups in regular sequence, which can be considered in a sense protein-like synthetic materials. It was shown indeed that an increase of biocompatibility was obtained using amphoteric linear polyamidoamines, probably thanks to their low net positive charge at physiological pH values.<sup>[24]</sup> Previous work studying cytotoxicity responses,<sup>[25]</sup> demonstrated that the amphoteric polyamidoamine-based hydrogels considered were approximately as cyto-biocompatible as dextran.<sup>[26]</sup>

Therefore we obtained a soft, swellable hydrogel, namely EDA-hydrogel (Figure 2.4).

It was possible to increase the amount of water content up to 72 wt%, with an EDS of 260%, reached after 12 h of swelling.

Moreover, the swelling ability of the material in water was reversible: it was able to undergo wetting-drying cycles, which involved a swell/collapse behavior, even after 20 days from the synthesis.



Figure 2.4 Hydrogel containing  $\gamma$ -aminobutyric acid as co-monomer; inverted vial test and SEM morphological characterizations.

Finally, improved results were obtained by using pentaethylenhexamine (PEHA) as cross-linking agent of the polymeric structure, instead of EDA.

PEHA was selected to further improve the swelling ability and elasticity of the hydrogel, bearing several hydrophilic moieties along the aliphatic chain, such as amino groups, that could give additional hydrogen bonds.<sup>[27]</sup>

Indeed, the chemical nature and length of the bridging units of cross-linker have been previously shown to influence water uptake and swelling.<sup>[28]</sup>

The hydrogel synthesis proceeded in water at room temperature and various trials allowed us to optimize the ratio between the monomers, which resulted in MBA:GABA:PEHA = 4:2:1 equivalents (Figure 2.5).

The hydrogel obtained, namely PEHA-hydrogel, displayed an enhanced EDS of 345% and allowed to reach the swelling equilibrium faster, after 6 h, instead of 12 h.

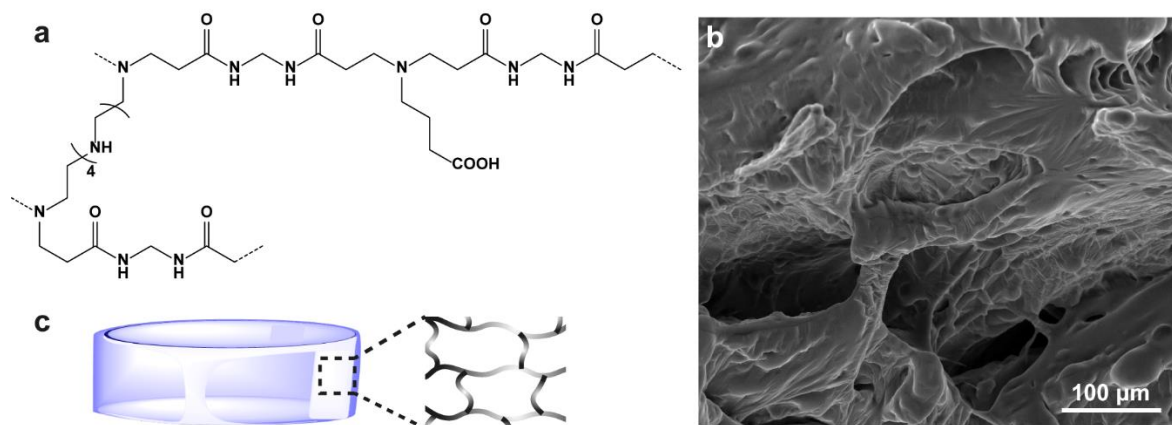


Figure 2.5 PEHA-hydrogel: polymeric structure (a), SEM image of the morphology (b), scheme of the hydrogel 3D network (c).

While covalent bonds are the main interactions that form the network, other more labile interactions cannot be excluded, in particular thanks to the addition of side functionalities such as amino and carboxylic groups. Interchain hydrogen bonds and hydrophobic interactions can indeed occur between carbonyls, amide, amino and carboxylic units within the hydrogel structure.<sup>[29]</sup>

We observed that after the synthesis fragments of the same scaffold weld rapidly to each other when brought into contact.



They exhibited self-adhesive properties without the need of an external stimuli. We were able to connect several blocks of hydrogel that were previously sliced to expose fresh surfaces, by pushing the pieces together so that these surfaces came into contact (Figure 2.6).

The polar functional groups mediated hydrogen bonding across two separate hydrogel pieces of the hydrogel, thus allowing a good adhesion.

This ability to restore partially reforming broken bonds is an interesting feature, since the material displays both the structural integrity of a covalently cross-linked hydrogel and self-adhesion ability via functionalized side-groups that could potentially be tuned to response to various environmental conditions.<sup>[30]</sup>

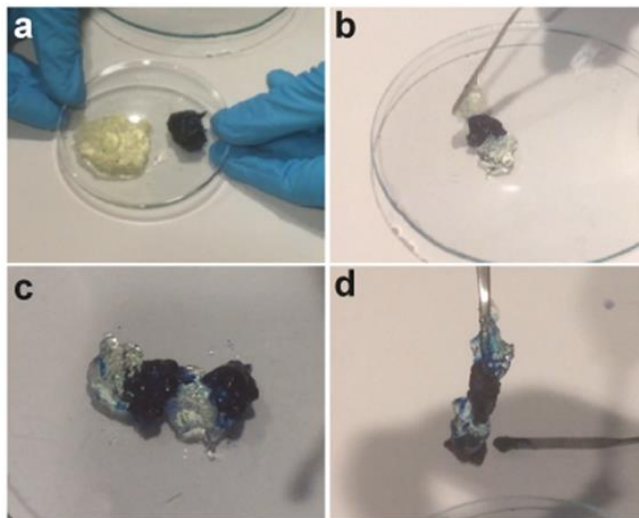


Figure 2.6 Transparent and Methylene Blue-stained PEHA-hydrogel (a); pieces of PEHA-hydrogel are brought into contact (b); several pieces are connected together (c) and hold from one side with tweezers (d).

## 2.4 Stability at different pH

To determine the stability of PEHA-hydrogel at different pH values, lyophilized samples were incubated in buffer solutions at 37 °C. The swelling behavior of the lyophilized samples was studied in biological-related intervals, at pH 2 (chloride buffer), pH 5 (acetate buffer) and pH 7.4 (phosphate buffer saline, PBS).



The analysis of swelling behavior and EDS was determined on dried hydrogels disks weighed and then placed in buffer solutions; after swelling, the samples were taken out of the solutions at specified time intervals, blotted free of surface water and weighed.

The results showed an EDS of 300% when the sample was immersed in PBS, while higher swelling values (i.e. up to 790%) were observed when the samples were placed in buffer at pH 2 and pH 5 (Figure 2.7a).

This is not unexpected, since at low pH the amines constituting the polymeric network are protonated and this accumulation of positive charges is responsible for strong inter-chain electrostatic repulsion of adjacent charged groups, which results in global repulsive forces within the network and enhances the swelling to its maximum.

In a similar manner, there is a higher attraction between the network chains and water molecules, caused by increase in the internal osmotic pressure, which also contributes to expand the equilibrium swelling capacity of the hydrogels in the acidic region. In basic pH regions (pH 7.4), the swelling ability was instead lower and steady over time.

Moreover, swelling behavior as function of time indicated that the swelling equilibrium of lyophilized hydrogels was reached within few hours both in PBS and in different pH environments (Figure 2.7b).

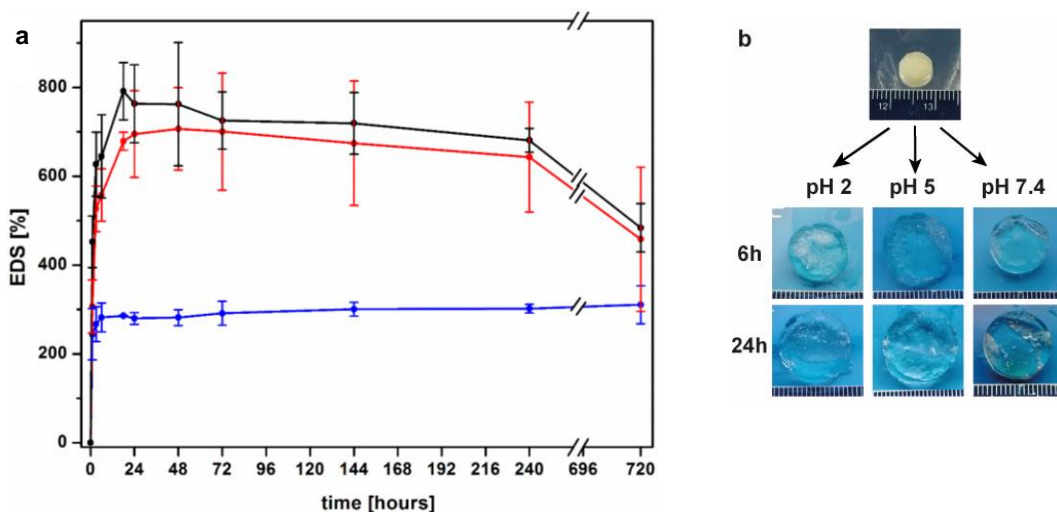


Figure 2.7 Stability of PEHA-hydrogel at different pH values (pH 7.4 blue curve; pH 2 red curve; pH 5 black curve) evaluated via EDS calculation over a period 30 days (a); images of the samples lyophilized and after the swelling at different pH, at 6 and 24 hours (b).

30-days swelling evaluation was performed to test the long-term stability of the hydrogels in the different pH conditions.

The samples exhibited good stability of the 3D network in physiological conditions, at pH 7.4. An inversion of swelling tendency was observed after 6-7 days in acidic environments (pH 2 and 5). We hypothesized that this behavior is caused by the dissociations of secondary interchain interactions, such as hydrogen bonds occurring between carbonyl/carboxyl and amino groups, which, while increasing the swelling ability of the scaffold to its maximum, destabilize the structure after this maximum is reached, as reported for other systems.<sup>[31]</sup>

Nevertheless, the degradation of the network, defined as the progressive rupture of covalent bonds, yielding a limpid solution without solid residues, was not observed during the 30-day study period.

The results confirmed that the hydrogels are chemically stable at different pH values, showing that the degree of cross-linking is adequate to preserve the integrity of the 3D structure in absence of a reductive stimulus.

## **2.5 Oscillatory rheology**

Rheological characterization and data treatment were performed by Dr. Iván López-Montero and Prof. Francisco Monroy at the Universidad Complutense of Madrid.

The rheological characteristics of hydrogels are key parameters to understand their structure and consequently their application fields.

The mechanical properties of polyamidoamine-based hydrogels were examined by oscillatory rheology of water-equilibrated samples.

Measurements were performed at saturated swelling conditions to mimic the physical conditions that the hydrogel would have in the biological environment.

By using oscillatory rheology, it is possible to quantify both the elastic-like and viscous-like properties of the materials; it is thus a valuable tool for understanding the structural and dynamical properties of the systems.

The effects of oscillatory stresses on the viscoelastic properties are measured and two dynamic moduli are obtained: the storage modulus,  $G'$ , which describes the elastic response, and the

loss modulus,  $G''$ , which is related to the viscous behavior. A hydrogel should exhibit a solid-like mechanical spectrum, that is,  $G' > G''$  throughout the experimentally accessible frequency range.

When oscillatory shear measurements are performed in the linear viscoelastic regime,  $G'$  and  $G''$  are independent of the strain amplitude. Thus, to define the linear viscoelastic zone, the PEHA-hydrogel and EDA-hydrogel were subjected to a strain-sweep analysis, in which they were deformed at different shear strains ( $\gamma$ ) at 1 Hz frequency.

The typical obtained strain sweep analysis plot is shown in Figure 2.8.

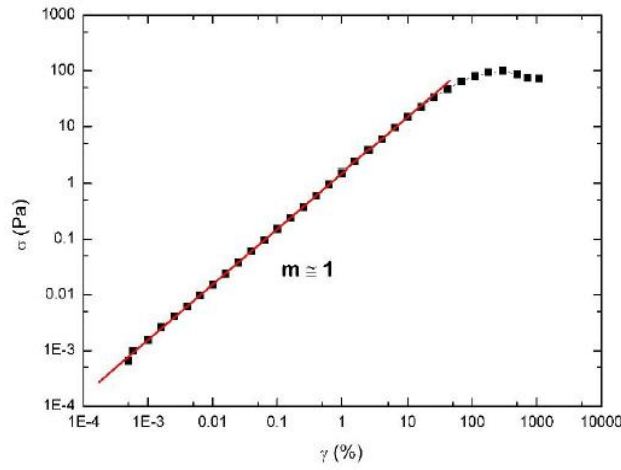


Figure 2.8 Stress-strain curve of sample PEHA-hydrogel.

The response of the samples displayed a large viscoelastic window of linearity; the rheological experiments were then performed at  $\gamma=10\%$  to ensure that the measurements were done in the linear viscoelastic region.

The samples were analyzed with a frequency sweep over the range of frequencies ( $\omega$ ) from 0.01 to 100 rad/s. A qualitative similarity was found between the viscoelastic behavior of the investigated samples, in particular, the  $G'$  values were larger than that of  $G''$  over the range of frequencies tested for both the samples, indicating a solid-like viscoelastic behavior ( $G' \gg G''$ ).<sup>[32]</sup> The storage and loss moduli values were found to be respectively  $2 \times 10^3$  Pa and  $2 \times 10^2$  Pa for PEHA-hydrogel and  $6 \times 10^3$  Pa and  $3 \times 10^2$  Pa for EDA-hydrogel (Figure 2.9).

The significant separation between the two moduli values showed that the obtained hydrogels were mechanically strong hydrogels, even in their swollen form.<sup>[33]</sup>

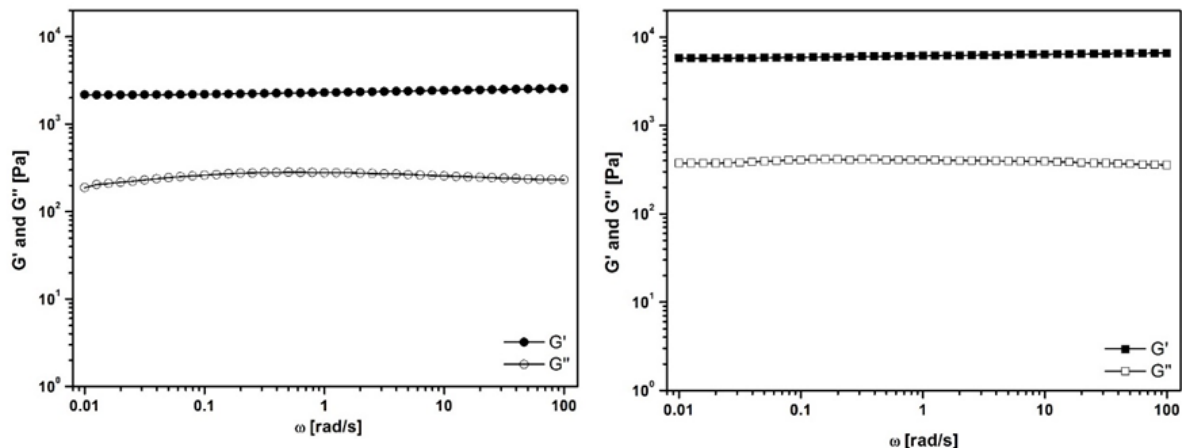


Figure 2.9  $G'$  and  $G''$  as function of the frequency of oscillation for the PEHA-hydrogel sample (left) and the EDA-hydrogel sample (right).

In addition, the frequency-independent behavior of  $G'$  and  $G''$  displayed by both the samples, indicated the formation of a well-developed, cross-linked, and robust network.<sup>[34]</sup>

Finally, the elastic moduli obtained for the two hydrogels, differing only from the cross-linker used, EDA or PEHA, confirmed that the length of the cross-linker and the presence of polar groups, can modify the elasticity of the scaffold.

This behavior showed a close correlation with the swelling degree. In particular, we found that a lower elastic modulus (PEHA-hydrogel) corresponded to an increased swelling ability (i.e. EDS=345% and 260% for the PEHA-hydrogel and EDA-hydrogel respectively), as observed previously for other systems.<sup>[18, 35]</sup>

## 2.6 Conclusions

The results of these preliminary investigations on polyamidoamines-based hydrogels, point to the conclusion that PEHA-hydrogels, combining amphoteric characteristics, enhanced swelling ability and self-adhesive properties, have the potential to be further developed as platform for 3D cell proliferation.

Moreover, it showed to be stable in different pH environments for a month.

With regards to the physico-mechanical properties, rheological measurements provided evidence of well-developed cross-linked network.

The combination of favorable properties exhibited by the fully synthetic PEHA-hydrogel, prompted us to adopt it for further investigation in relation to specific targets, which are described in the next chapters.

## 2.7 Experimental part

### 2.7.1 *Synthesis of hydrogels*

General synthetic procedure: in a 10 ml round bottom flask N,N'-methylene bisacrylamide (MBA; 3.24 mmol) was dissolved in 2.5 ml of distilled water, while heating the solution at 70 °C for few minutes to favor complete dissolution. Then, the co-monomer was added and stirred vigorously for approximately 10 minutes; finally the cross-linker was added to the mixture. The mixture was stirred for additional 20 minutes at room temperature, then it was transferred into a glass vial and allowed to react in static conditions at r.t for 3 hours, thus obtaining the hydrogel scaffold, which was subsequently washed with water. Several washings with water were performed, and the extracted washing solutions were freeze-dried and analyzed by H-NMR spectroscopy, which confirmed that no unreacted monomers was present. We therefore concluded that the final hydrogel composition was not significantly different from the starting monomer mixture, as elsewhere observed.<sup>[25]</sup>

The other reagents added for the different hydrogel synthesis were as following. MBA-EDA hydrogel: EDA (1.62 mmol); MBA-EDA-DED hydrogel: EDA (0.81 mmol) and DED (1.62 mmol); EDA-hydrogel: EDA (0.81 mmol) and GABA (1.62 mmol); PEHA-hydrogel: PEHA (0.81 mmol) and GABA (1.62 mmol).

### 2.7.2 *Sample lyophilization*

Lyophilization, also known as freeze-drying, uses rapid cooling to allow solvent removal by sublimation under vacuum.<sup>[36]</sup>

The scaffolds were swollen in water and frozen at -80 °C overnight. Then, they were transferred to a lyophilizing jar and lyophilized for 12 hours at a pressure of 150 mT.

Lyophilized samples were used right away for SEM analysis or swelling measurements.

### 2.7.3 *Scanning electron microscopy analysis*

The lyophilized samples were mounted on aluminum stubs using adhesive carbon tape. Samples were then sputtered with gold to form a layer of approximately 20 nm on the surface. SEM images were captured at 10-20 kV accelerating voltage using a SEM FEI Quanta FEG 250 instrument.

### 2.7.4 *Swelling measurements*

EDS were measured by gravimetric method after lyophilization of the hydrogels.

Disc-shape samples (diameter of 7 mm and height of 1 mm) were immersed in distilled water and were removed at set time points (after 1h, 3h, 6h, 18h, 24h, then every day up to one week, then after 10 days and 30 days). Their surface was blotted free of water using filter paper and their swollen weights were measured on an analytical balance.

To determine the stability of the hydrogels at different pH conditions, the scaffolds were incubated in buffer solutions: pH 2 (chloride buffer), pH 5 (acetate buffer 50 mM), pH 7.4 (PBS 50 mM).

Thus, lyophilized hydrogels were incubated at 37 °C in 2 ml of buffer solution; their stability was then evaluated via swelling ratio measurements in time.

### 2.7.5 *Oscillatory shear rheology*

All tests were carried out by our collaborators at Universidad Complutense de Madrid, using a Discovery HR-2 rheometer (TA instruments), with a parallel plate geometry (40 mm diameter). The linear viscoelastic zone was determined by applying a shear strain ramp from  $10^{-4}$  up to 10000%. The  $\sigma$ - $\gamma$  plot was measured at a constant oscillation frequency of 1 Hz, corresponding to an angular velocity,  $\omega = 2\pi$  rad/s.

Then, the working strain of  $\gamma=10\%$  was chosen, well above the yield point but high enough to require stresses above the experimental accuracy in the linear regime.

The rheological response of the sample was measured at this constant strain amplitude, varying the oscillation frequency in the range  $10^{-2} < \omega/s^{-1} < 10^2$ .

Prior to start any measurement, the sample was subjected to pre-shearing at constant strain in the linear regime and constant frequency (1 Hz). The rheological experiment was started only when the shear response remained constant for minutes within the experimental accuracy. Temperature ( $\pm 1$  °C) was controlled with a Peltier chamber connected to an external water thermostat. To prevent dehydration during rheological measurements, both the sample and the plate tool were covered with a Solvent Trap (TA instruments). Each measurement was performed at least twice on different disc-shaped hydrogel samples of the same composition.

## 2.8 References

- [1] a) M. Donalizio, E. Ranucci, V. Cagno, A. Civra, A. Manfredi, R. Cavalli, P. Ferruti, D. Lembo, **2014**, 58, 6315; b) C. Lin, Z. Zhong, M. C. Lok, X. Jiang, W. E. Hennink, J. Feijen, J. F. J. Engbersen, *Bioconjugate Chem.* **2007**, 18, 138; c) W. Yang, C.-Y. Pan, *Macromol. Rapid Commun.* **2009**, 30, 2096.
- [2] P. Ferruti, S. Bianchi, E. Ranucci, F. Chiellini, V. Caruso, *Macromol. Biosci.* **2005**, 613.
- [3] P. Ferruti, M. A. Marchisio, R. Duncan, *Macromol. Rapid Commun.* **2002**, 23, 332.
- [4] A. Manfredi, E. Ranucci, M. Suardi, P. Ferruti, *J. Bioact. Compatible Polym.* **2007**, 22, 219.
- [5] B. D. Mather, K. Viswanathan, K. M. Miller, T. E. Long, *Progress in Polymer Science (Oxford)* **2006**, 31, 487.
- [6] N. Mauro, A. Manfredi, E. Ranucci, P. Procacci, M. Laus, D. Antonioli, C. Mantovani, V. Magnaghi, P. Ferruti, *Macromol. Biosci.* **2013**, 13, 332.
- [7] M. P. Lutolf, J. A. Hubbell, *Nat Biotech* **2005**, 23, 47.
- [8] C. Alexander, K. M. Shakesheff, *Adv. Mater.* **2006**, 18, 3321.
- [9] S. Richardson, P. Ferruti, R. Duncan, *J. Drug Targeting* **1999**, 6, 391.
- [10] S. Swaminathan, R. Cavalli, F. Trotta, P. Ferruti, E. Ranucci, I. Gerges, A. Manfredi, D. Marinotto, P. R. Vavia, *J. Incl. Phenom. Macrocycl. Chem.* **2010**, 68, 183.
- [11] B. Malgesini, I. Verpilio, R. Duncan, P. Ferruti, *Macromol. Biosci.* **2003**, 3, 59.
- [12] J. A. Burdick, C. Chung, X. Jia, M. A. Randolph, R. Langer, *Biomacromolecules* **2005**, 6, 386.
- [13] Y. Yin, Y. Yang, H. Xu, *J. Appl. Polym. Sci.* **2002**, 83, 2835.
- [14] K. S. Anseth, A. T. Metters, S. J. Bryant, P. J. Martens, J. H. Elisseeff, C. N. Bowman, *J. Controlled Release* **2002**, 78, 199.
- [15] M. K. Nguyen, E. Alsberg, *Prog. Polym. Sci.* **2014**, 39, 1235.
- [16] O. Jeon, D. S. Alt, S. M. Ahmed, E. Alsberg, *Biomaterials* **2012**, 33, 3503.
- [17] A. S. Hoffman, *Adv. Drug Del. Rev.* **2012**, 64, 18.
- [18] A. A. M. Shimojo, A. M. B. Pires, R. Lichy, A. A. Rodrigues, M. H. A. Santana, *Journal of Biomedical Materials Research Part A* **2015**, 103, 730.
- [19] D. Buenger, F. Topuz, J. Groll, *Prog. Polym. Sci.* **2012**, 37, 1678.

- [20] E. Emilritri, F. Guizzardi, C. Lenardi, M. Suardi, E. Ranucci, P. Ferruti, *Macromol. Symp.* **2008**, 266, 41.
- [21] G. Caldwell, E. W. Neuse, A. Stephanou, *J. Appl. Polym. Sci.* **1993**, 50, 393.
- [22] P. Ferruti, *J. Polym. Sci., Part A: Polym. Chem.* **2013**, 51, 2319.
- [23] C.-W. Chang, Y. Hwang, D. Brafman, T. Hagan, C. Phung, S. Varghese, *Biomaterials* **2013**, 34, 912.
- [24] E. Ranucci, P. Ferruti, E. Lattanzio, A. Manfredi, M. Rossi, P. R. Mussini, F. Chiellini, C. Bartoli, *J. Polym. Sci., Part A: Polym. Chem.* **2009**, 47, 6977.
- [25] P. Ferruti, S. Bianchi, E. Ranucci, F. Chiellini, V. Caruso, *Macromol. Biosci.* **2005**, 5, 613.
- [26] E. Jacchetti, E. Emilritri, S. Rodighiero, M. Indrieri, A. Gianfelice, C. Lenardi, A. Podestà, E. Ranucci, P. Ferruti, P. Milani, *Journal of Nanobiotechnology* **2008**, 6, 14.
- [27] M. V. Risbud, S. V. Bhat, *J. Mater. Sci. Mater. Med.* **2001**, 12, 75.
- [28] A. Dal Pozzo, L. Vanini, M. Fagnoni, M. Guerrini, A. De Benedittis, R. A. A. Muzzarelli, *Carbohydr. Polym.* **2000**, 42, 201.
- [29] A. Phadke, C. Zhang, B. Arman, C.-C. Hsu, R. A. Mashelkar, A. K. Lele, M. J. Tauber, G. Arya, S. Varghese, *Proceedings of the National Academy of Sciences* **2012**, 109, 4383.
- [30] Y. Yang, M. W. Urban, *Chem. Soc. Rev.* **2013**, 42, 7446.
- [31] J. Berger, M. Reist, J. M. Mayer, O. Felt, N. A. Peppas, R. Gurny, *Eur. J. Pharm. Biopharm.* **2004**, 57, 19.
- [32] a) J. M. Zuidema, C. J. Rivet, R. J. Gilbert, F. A. Morrison, *Journal of Biomedical Materials Research Part B: Applied Biomaterials* **2014**, 102, 1063; b) Y. Wang, Q. Zhao, H. Zhang, S. Yang, X. Jia, *Adv. Mater.* **2014**, 26, 4163.
- [33] A. Ström, E. Schuster, S. M. Goh, *Carbohydr. Polym.* **2014**, 113, 336.
- [34] a) G. Dumortier, J. L. Grossiord, M. Zuber, G. Couarraze, J. C. Chaumeil, *Drug Dev. Ind. Pharm.* **1991**, 17, 1255; b) A. S. Sarvestani, X. He, E. Jabbari, *Biopolymers* **2007**, 85, 370.
- [35] E. Karpushkin, M. Dušková-Smrčková, M. Šlouf, K. Dušek, *Polymer* **2013**, 54, 661.
- [36] R. C. Thomson, M. C. Wake, M. J. Yaszemski, A. G. Mikos, in *Biopolymers II* (Eds.: N. A. Peppas, R. S. Langer), Springer Berlin Heidelberg, Berlin, Heidelberg, **1995**, pp. 245.



### 3. Monitoring *in vitro* cell proliferation in a hybrid, emission switchable hydrogel

#### Abstract

Nowadays studying the interaction of healthy and/or cancer cells with materials and molecules is a hot topic in research, especially in the fields of nanomedicine and tissue engineering. Traditionally, these interactions have been investigated in the context of two-dimensional (2D) environments. However, many findings suggest that 2D substrates force cells to adopt non-natural behaviors. Therefore, there is a strong need for three-dimensional (3D) cell culture platforms for *in vitro* cell analyses that instead can mimic their natural niche and allow cells to proliferate in a more realistic manner. In this context, the direct visualization of living cells growing onto 3D platforms in real-time promises to be a powerful tool to reveal information for *in vitro* biomedical investigation. However, the presence of dyes to stain the cells is considered as an alteration of the natural cell cycle. Our effort to visualize living organisms in the absence of internalized dyes is therefore a step towards imaging without staining.

We introduce herein, a novel hybrid hydrogel for *in vitro* cell study, with covalently incorporated cyclometalated Ir(III)-fluorescent probes. The Ir(III) complex was designed with a “off/on” emission, in response to the different environments.

In our hydrogel, the cells presence induces fluorescence emission, enabling the clear and easy real-time visualization of the cells proliferating onto the hydrogel up to 7 days, without additional cell staining and with no fluorescence background.

The mechanism for the off/on switching from water to the lipophilic environment of the cells plasma membranes is studied in details, demonstrating such novel luminescent probe-incorporated scaffold, namely Ir-PAA, to be a very interesting 3D platform for *in vitro* real-time investigation of cells.

### 3.1 From 2D to 3D: imaging the cell

Two-dimensional (2D) cell culture is conventionally used to study cell growth and behavior, providing a common and useful tool to elucidate cellular mechanisms, differentiation, cytotoxicity and eventually therapeutic efficacy, in an easy and economical way.

However, several findings suggest that cells cultured on traditional flat substrates adapt to this synthetic 2D environment, often becoming flattened and showing a non-natural behavior.<sup>[1]</sup> As an approach to overcome these limitations, the development of three dimensional (3D) substrates for *in vitro* cell growth has received much interest. Considerable effort has recently been made to design materials for 3D *in vitro* cell culture. It is now recognized that 3D platforms, able to mimic extracellular matrices, allow cells to grow and organize in a manner similar to the one experienced in natural tissues.

Hydrogels are common materials that have been successfully employed to support cell growth in various systems. They are 3D networks composed of cross-linked hydrophilic polymer networks, able to swell in water without dissolution.<sup>[2]</sup>

Since their introduction in late 1950s,<sup>[3]</sup> hydrogels have been investigated for several biomedical applications such as sensing, drug delivery and tissue regeneration<sup>[4]</sup> due to their ability to resemble the environment of natural tissues (*i.e.* high water content,<sup>[5]</sup> presence of interconnecting pores facilitating the diffusion of oxygen, nutrients and growth factors, etc).

To the best of our knowledge, the application of hydrogels as a tool to visualize cells and track their proliferation has not been investigated yet. Implementing such kind of scaffolds with luminescent probes able to reveal the presence of a cell, could turn them into imaging probes with the great potential of luminescent detection and visualization of cells in 3D, without the need of staining the cells.

Nowadays an increasing need of understanding biological processes is pushing the development of instruments and techniques that give the possibility to visualize cells and cell-related events in real-time. Imaging by fluorescence microscopy has become therefore a powerful tool for biomedical studies, because of the great deal of information that it can give and especially because it is non-invasive.<sup>[6]</sup>

Thus, the incorporation of a fluorescent probe for cells visualization within 3D hydrogels, which combines the advantages of fluorescence detection and hydrogel for 3D *in vitro* cell

proliferation, is highly desirable for biomedical applications and could open new paths for *in vitro* imaging techniques.

Currently, organic fluorescence dyes are the most used commercial imaging agents.<sup>[7]</sup> This is due to their high photoluminescence quantum yields and the easiness of manipulation. However, they suffer from photobleaching issues over time, short excited state lifetimes, that prevent the use of time gate techniques for detection, and often small shift of the emission from the absorption, causing overlap of excitation light with the emitted light.<sup>[8]</sup>

For these reasons, the research of better imaging labels is still a hot topic in cell biology.

An alternative to organic molecules is represented nowadays by the use of phosphorescent complexes.<sup>[9]</sup> They exhibit advantageous photophysical properties, such as (1) high luminescence quantum yield; (2) relatively long lifetime ranging from hundreds of nanoseconds to tens of microseconds, due to their strong spin-orbit coupling, which facilitates the spin-forbidden character of the phosphorescent transition promoting efficient intersystem crossing;<sup>[10]</sup> (3) enhanced photostability;<sup>[11]</sup> (4) large Stock shift, mainly due to the energy gap between the absorbing singlet state and the luminescent triplet state.<sup>[9c, 12]</sup> This enables a clear separation between excitation and emission maxima, which allows to prevent self-quenching and avoid interferences with emissive bio-molecules.<sup>[13]</sup> Moreover, recently the use of different ligands coordinated to the same metal showed that it is possible to selectively stain different part of the cell.

Amongst the most studied ones, cyclometalated Ir(III) complexes are very appealing as bio-imaging reagents for cellular visualization.<sup>[14]</sup> Beside their outstanding photophysical properties, they exhibit the possibility of easily tune the excited state energy over the whole visible electromagnetic spectrum, from the ultraviolet to the near infrared region by ligand modification.<sup>[15]</sup> These characteristics result in increased sensitivity and possibility of implementation of time-gated techniques with elimination of short-lived fluorescence background ( $\sim$ ns),<sup>[16]</sup> rendering cyclometalated Iridium(III) complexes optimal candidates as luminescent bio-probes.<sup>[12, 17]</sup>

Among their features is the intrinsic ability of sensing oxygen in the surrounding environment due to the oxygen-sensitivity of their triplet-state originated luminescence.<sup>[18]</sup>

Herein, we report a new hybrid system that benefits of both the 3D structure of a hydrogel able to act as extracellular matrix, and a luminescent iridium complex, able to change its emission

properties depending on the surrounding environment. The novelty of this combination relies on the possibility of an *in vitro* culture combined with the localization and real-time visualization of cells, without requiring additional staining with dyes.

In particular, we have developed a new strategy that relies on the interaction of an Ir(III) complex covalently anchored to the hydrogel, with the cells plasma membranes. Such a change in the environment, from aqueous solution to lipid layer, causes the turn on of the emission of the iridium complex.

The cyclometallated Ir (III) complex was grafted via co-polymerization reaction to the backbone of a hydrogel scaffold based on polyamidoamines, PAA.<sup>[19]</sup> The obtained material was named Ir-PAA.

The concept of the work is schematized in Figure 3.1.

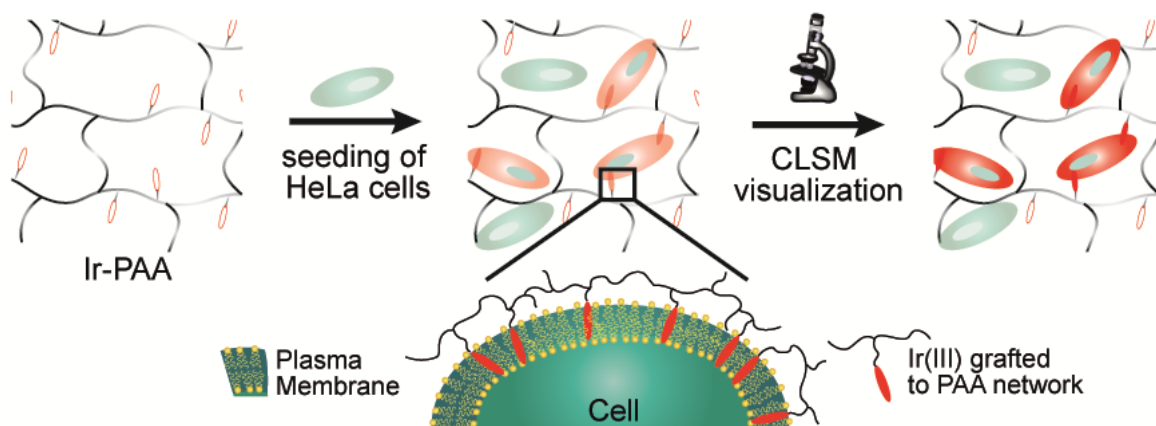


Figure 3.1 Scheme of the mechanism of the “off/on” emission. The complex is quenched in water but when cells are seeded onto the Ir-PAA, some of the cells can interact with the Ir(III) complex grafted to the polymeric network. The hydrophobic metal compound is inserted into the plasma membrane causing the turning on of the bright red emission.

The design of the complex, able to change its emission, is related to the use of rigid and highly conjugated ligands, phenylphenanthridines and a substituted bipyridine as ancillary chelate (see next section).

The complex exhibits a bright red emission ( $\lambda_{\text{max}} = 638 \text{ nm}$ ) and, due to its long lived excited state lifetime, is very sensitive to the presence of dioxygen.

We observed a “turn-on” of the red luminescence of the complex, which is almost non-emissive when the Ir-PAA is equilibrated in culture medium, when cells are seeded onto the hydrogel and can interact with the complex.

This cell-induced emission enhancement is a powerful tool in live cell imaging, since it enables the visualization of the cells proliferating in 3D onto the hydrogel scaffold, without interfering with the cell viability and, most importantly, with no need of additional cell staining procedures.

Finally, we demonstrated that the so constructed hydrogel has an excellent cyto-compatibility. Our novel hybrid Ir-PAA scaffold sustained the proliferation of HeLa cells onto the scaffold, enabling the visualizations of living cells in real time up to 7 days.

Such platform permits a precise and real-time localization and imaging of the living cells proliferating on it at any moment, without any background signal, making the 3D *in vitro* study very easy and fast.

### 3.2 Synthesis and characterization of the cyclometalated iridium(III) complex

The synthesis and photophysical characterization of the cyclometalated iridium(III) complex were performed by Dr. Elena Longhi (Laboratoire de Chimie et des Biomatériaux Supramoléculaires).

The neutral cyclometalated Ir(III) complex **3**, containing 6-phenylphenanthridine-based ligands (

Figure 3.2) was synthesized following modified procedures already described in literature.<sup>[10,</sup>

<sup>20]</sup> The Ir-dimer used as precursor for the preparation of the final complex was prepared by the well-established Nonoyama reaction<sup>[21]</sup> and used in the next step without further purification.

The complex  $[\text{Ir}(\text{C}^{\wedge}\text{N})_2(\text{N}^{\wedge}\text{N})]^+$  was prepared by reaction of the Ir-dimer with an opportunely synthesized ancillary ligand bearing a protected amino group (see paragraph 3.6.1). The product obtained as chloride salt after HPLC purification was then precipitated as hexafluorophosphate salt by addition of  $\text{NH}_4\text{PF}_6$  in a mixture water/MeOH.

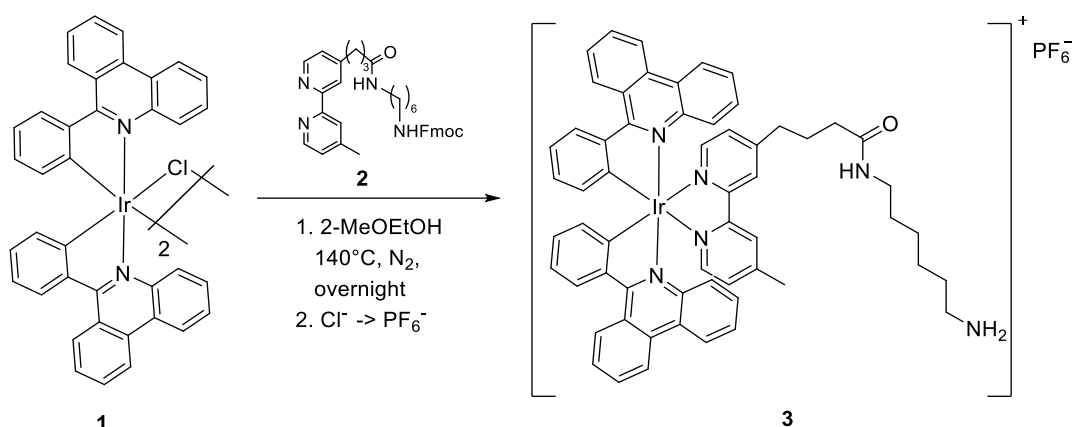


Figure 3.2 Scheme of the synthesis of the Iridium complex **3**.

The complex obtained was characterized by NMR, mass spectroscopy and elemental analysis. The UV-vis absorption spectra of the complex in water and dichloromethane, DCM, at room temperature showed, in the range of 250-400 nm, intense bands with molar extinction coefficients ( $\epsilon$ ) c.ca  $10^4 \text{ M}^{-1} \text{ cm}^{-1}$  assigned to  $\pi$ - $\pi^*$  transitions localized on the cyclometalated ligands (Figure 3.3). The bands at lower energies (above 420 nm) are instead assigned to spin-allowed and spin-forbidden singlet and triplet metal-to-ligand charge transfer (MLCT) transitions. They involved the iridium unit and the pyridine of the phenylphenanthrene ligand, as described in the literature for analogous complexes.<sup>[10, 20, 22]</sup>

The emission curves of compound **3** in air-equilibrated water and DCM are reported in Figure 3.3; the emissive properties of the compounds in degassed and air-equilibrated water and DCM solutions are summarized in Table 3.1.

In bis-cyclometalated Ir(III) complexes as  $[\text{Ir}(\text{C}^{\wedge}\text{N})_2(\text{N}^{\wedge}\text{N})]^+$  the room-temperature phosphorescence is mainly controlled by the  $\text{Ir}(\text{C}^{\wedge}\text{N})_2$  fragment<sup>[10, 23]</sup> when the singlet and triplet energies of the ancillary ligand are sufficiently high compared to the  $\text{C}^{\wedge}\text{N}$  ligand.<sup>[10]</sup>

Compound **3** displayed an emission maximum ( $\lambda_{\text{em}}$ ) at 638 nm in DCM, slightly red-shifted in water  $\lambda_{\text{em}} = 650 \text{ nm}$ . Such positive solvatochromism points towards a stronger stabilization of the excited state in polar solvents as expected for the metal to ligand charge transfer nature of the luminescent state. The complex exhibited monoexponential lifetimes of the emissive excited states both in degassed and air-equilibrated DCM solution (2.63 and 0.68  $\mu\text{s}$  respectively) and emission quantum yields (PLQY) of 24% (degassed) and 7% (air-equilibrated).

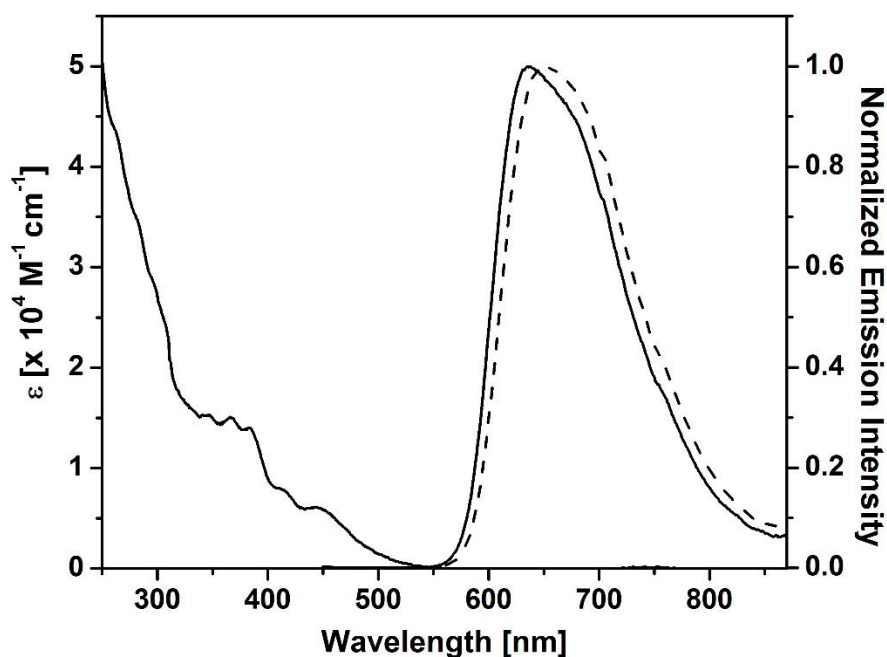


Figure 3.3 Absorption and emission traces of the Iridium complex **3** in water (dash line) and DCM (solid line).

On the contrary, it showed a biexponential lifetime in water, with values of 0.99 and 0.34  $\mu\text{s}$  in air-equilibrated conditions and 1.45 and 0.32  $\mu\text{s}$  in degassed. PLQY was measured to be 4 and 7% respectively. The biexponential lifetime measured in water is possibly due to the partial aggregation of the complex, due to its poor solubility in water.

However, the decrease of both lifetime and PLQYs in air-equilibrated media (Table 3.1) is ascribed to the triplet nature of the emitting state that is susceptible to dioxygen quenching.

Table 3.1 Photophysical data of the complex **3** in DCM and in water, air-equilibrated and degassed.

	<i>DCM</i>		<i>water</i>	
	<i>air-equilibrated</i>	<i>degassed</i>	<i>air-equilibrated</i>	<i>degassed</i>
$\lambda_{\text{em}}$ [nm]	638	638	650	647
PLQY [%]	7	24	4	7
$\tau^a$ [ $\mu\text{s}$ ]	0.68	2.63	0.34(41.7%)	1.45(70.8%)
			0.99(55.1%)	0.32(29.2%)

<sup>a</sup> recorded at emission maxima

### 3.3 Design and photophysical behavior of the novel Ir-PAA

Generally, there are two main approaches through which it is possible to obtain luminescent hydrogels: covalent and non-covalent.<sup>[24]</sup> The first requires direct application of luminescent molecules as starting materials. The non-covalent strategy exploits the incorporation of luminescent probes in the hydrogel matrix through labile bonds, such as electrostatic interaction,<sup>[25]</sup> coordination<sup>[26]</sup> and physical encapsulation.<sup>[27]</sup>

This latter offers several advantages, among which the easiness of the fabrication process, with only minor impairment to the structure of the luminescent molecules, thereby maximizing the luminescent properties, and the possibility to combine different hydrogel matrices with the selected luminescent probe.

However, as major drawback, this method shows stability issues: the scaffolds obtained suffer from leaking of the luminescent molecule over time, causing the diminishing of the emission intensity and possible cytotoxicity for the cells upon uptake.

For this reason, our approach was based on the covalent grafting<sup>[10]</sup> of the Ir(III) complex to the polymeric backbone of the hydrogel, via simple 1,4-addition in water.<sup>[28]</sup>

The hybrid hydrogel presented in this work is indeed composed of an amphoteric PAA network, obtained by Michael-type polyaddition of  $\gamma$ -aminobutyric acid (GABA) to N,N'-methylene bisacrylamide (MBA) and cross-linked with pentaethylenhexamine. In particular, the Ir(III) complex was equipped with an amino terminal group, to be introduced into the polymeric structure via poly-addition to MBA. Figure 3.4a displays a schematic chemical structure of the Ir-PAA.

Specifically, we decided to perform the polyaddition of amines to MBA in presence of compound **3** to obtain an homogeneous grafting throughout the hydrogel network. Thus, a methanol suspension of the iridium complex was added to a mixture of MBA and GABA. The synthesis proceeded in methanol, at room temperature, after an initial phase at 60 °C (10 min) to favor the dissolution of the reagents. No addition of base or catalyst was necessary since amines present in the reaction mixture could act as both nucleophiles and bases.

Further reaction of this mixture in static conditions led to the formation of an optically transparent and porous Ir-PAA, which was observed after 3 hours and confirmed by “inverted test tube method” (Figure 3.4b). The morphology of the hydrogel was investigated by scanning



electron microscopy (SEM, Figure 3.4c) and revealed a high porosity, with pores diameter ranging between 20-80  $\mu\text{m}$ .

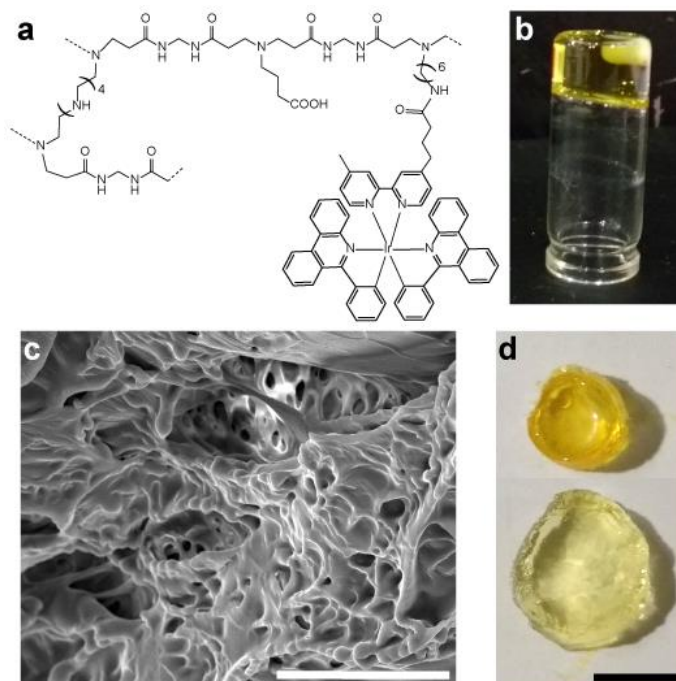


Figure 3.4 Scheme of the chemical structure of the Ir-PAA (a); inverted vial test confirming gelation and showing the optical transparency of the obtained material (b); SEM image of the morphological structure (c), scale bar is 100  $\mu\text{m}$ ; photograph of the Ir-PAA in dry and water swollen state (d), scale bar is 1 cm.

Swelling studies on Ir-PAA showed that the equilibrium swelling of the hydrogel was reached after being immersed in water overnight. The equilibrium swelling degree (EDS) was found to be 1150% and remained constant for the 7-day-study period.

As introduced before, the swelling ability of a hydrogel in water and physiological solutions is a fundamental parameter that can affect the transport of oxygen, nutrients and growth factors, and thus the ability of cells survival and growth in the 3D environment.<sup>[29]</sup>

Figure 3.4d shows a photograph of the dry (up) and swollen Ir-PAA (down).

After the synthesis, the scaffold was washed with methanol and then with water. The washing solutions were checked at NMR confirmed the absence of complex **3** traces and therefore its successful and stable grafting to the polymeric network.

Moreover, a complete photophysical characterization of the hybrid Ir-PAA was carried out. We first visually checked the color of the hydrogel, which was dark yellow in the dry state and pale yellow-transparent in swelling-state, after equilibration in deionized water (Figure 3.4d). However, when excited with a portable UV lamp at 365 nm, only the Ir-PAA in the dry state showed a bright red emission (Figure 3.5a); instead no red emission was observed for the water-equilibrated sample (Figure 3.5b), as effect of the turn on/turn off behavior of the embedded Ir(III) in response to the different environment.

Next, we studied the photoluminescence (PL) behavior of the Ir-PAA in dry and water swelling-state.

Additional PL spectra of the sample equilibrated in DCM and in Dulbecco's Modified Eagle Medium (DMEM) were also recorded. Nevertheless, when incubated in DCM the Ir-PAA did not show any swelling, as expected, due to hydrophilicity of the network that did not imbibe the solvent. Thus, the polymeric chains composing the hydrogel were not solvated by DCM, indeed the PL behavior observed for the sample treated with DCM was essentially the same as what displayed by the dry Ir-PAA.

Figure 3.5c shows the PL spectra of the hydrogels in the dry state and in the different solvents, upon excitation at 405 nm.

The luminescent hydrogel exhibited two emission bands. One at lower energy peaking at around 640 nm, which remained almost unvaried upon changing the solvent. A second emission showed a maximum at 524 and 530 nm, for the dry and DCM equilibrated sample respectively and at 456 and 480 nm for the DMEM and water swollen ones, dramatically changing according the polarity of the solvent.

The overlap of the emission spectra of complex **3** with the emission band at lower energy of the Ir-PAA in the dry state suggests the absence of aggregation phenomena due to inter- or intra-polymer Ir(III) complexes interactions.

The high energy band recorded in the spectra, with maxima in the range 520-530 nm, has been attributed to the emission of the polyamidoamine network composing the hydrogel. Indeed polyamidoamines-structured materials are known to have weak fluorescence emission<sup>[30]</sup> presumably produced by the lone pair electrons on the tertiary nitrogen,<sup>[30a, 31]</sup> which are present in the structure.

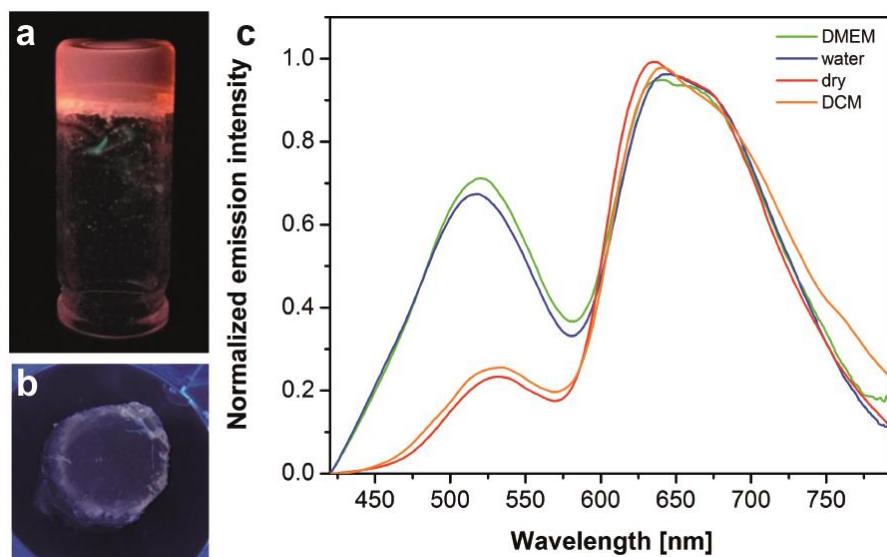


Figure 3.5 Dry (a) and water-equilibrated (b) Ir-PAA excited by a portable UV lamp; PL spectra of the Ir-PAA in the dry state and in the different solvents, upon excitation at 405 nm.

The photophysical parameters obtained are summarized in Table 3.2.

Ir-PAA monitored at 640 nm exhibited a monoexponential lifetime of 1.98  $\mu\text{s}$  for the dry and 1.87  $\mu\text{s}$  for the DCM equilibrated samples. These lifetimes were found to be much longer, more than the double, than those measured for the Ir-PAA scaffolds swollen in water or in DMEM, which were 0.89  $\mu\text{s}$  and 0.73  $\mu\text{s}$  for the water and DMEM equilibrated samples respectively. The DMEM equilibrated sample showed a secondary component of 6 ns.

Once again, the trend showed by the complex **3** in solution was observed as well when the complex was linked to the hydrogel network, indicating a phosphorescence quenching of the excited triplet state due to oxygen molecules in solution.

Instead, the phosphorescence decay curves of the scaffolds monitored at 530 nm showed lifetimes in the order of ns, with a tri-exponential decay and similar values in the range 8-0.5 ns for all the conditions.

Table 3.2 Photophysical data of the hydrogel Ir-PAA, in dry conditions, in DCM, swollen in water and swollen in DMEM.

	<i>dry</i>	<i>DCM</i>	<i>water</i>	<i>DMEM</i>
$\lambda_{em}$ [nm]	530, 640	531, 640	518, 643	520, 645
PLQY [%]	14	11	5	4
$\tau^a$ [ $\mu$ s]	1.98	1.87	0.89	0.73 (85.7%) 0.006(14.3%)
$\tau^b$ [ns]	7.86(48.0%)	7.40(48.0%)	7.90(41.7%)	7.32(42.6%)
	3.33(37.6%)	3.03(35.3%)	2.75(41.7%)	2.46(39.4%)
	0.64(14.4%)	0.66(16.7%)	0.59(16.6%)	0.53(18.0%)

<sup>a</sup> recorded at  $\lambda_{em} = 640$  nm

<sup>b</sup> recorded at  $\lambda_{em} = 530$  nm

The fluorescence quantum yields of the Ir-PAA in the four conditions (dry, DCM, water and DMEM equilibrated) were also measured.

We could confirm the oxygen-quenching of the Ir(III) complexes fluorescent emission in aqueous media; indeed, the PLQY in the dry state and in DCM were significantly larger (14% and 11%, respectively) than those found for the sample equilibrated in water and DMEM (5% and 4% respectively).

The photophysical data of the DCM-incubated sample, showing a strong similarity particularly in emission maxima and lifetime to the dry hydrogel, should be interpreted keeping into account what already mentioned, that the Ir-PAA did not show any swelling in DCM. Being the bulk polymeric chains not solvated by DCM, the observed PL behavior is thus identifiable with the behavior of the sample in dry conditions. The photophysical data of the Ir-PAA in DCM were reported for the sake of completeness.

### 3.4 *In vitro* investigation of Ir-PAA

A challenge with 3D platforms compared to 2D surfaces is to ensure that the scaffolds are cyto-compatible, to allow cell proliferation, oxygen and nutrient supply.<sup>[32]</sup>

The efficacy of the novel Ir-PAA hydrogel to support cell proliferation in 3D was evaluated using cervical cancer cells, HeLa. Particular attention was put on the influence of the covalently embedded Ir(III) complexes on the material cytotoxicity.

The viability of HeLa cells seeded onto the hybrid scaffold was studied for a period of 7 days, using quantitative alamarBlue assay and qualitative live/dead staining.

A substantial increase of 20% in cellular metabolic activity was observed after 7 days in culture (68% at day 7 compare to 48% at day 1). The cell proliferation rate data were confirmed by qualitative live/dead assay (i.e. Sytox green staining of dead cells). These results clearly indicated that the novel Ir-PAA is cyto-compatible, that the embedded compound **3** did not adversely affect cell growth and viability (Figure 3.6a) and that cells proliferated on Ir-PAA were normal healthy cells (Figure 3.6b).

Overall, our results suggested that Ir-PAA is an excellent platform for 3D cell growth.

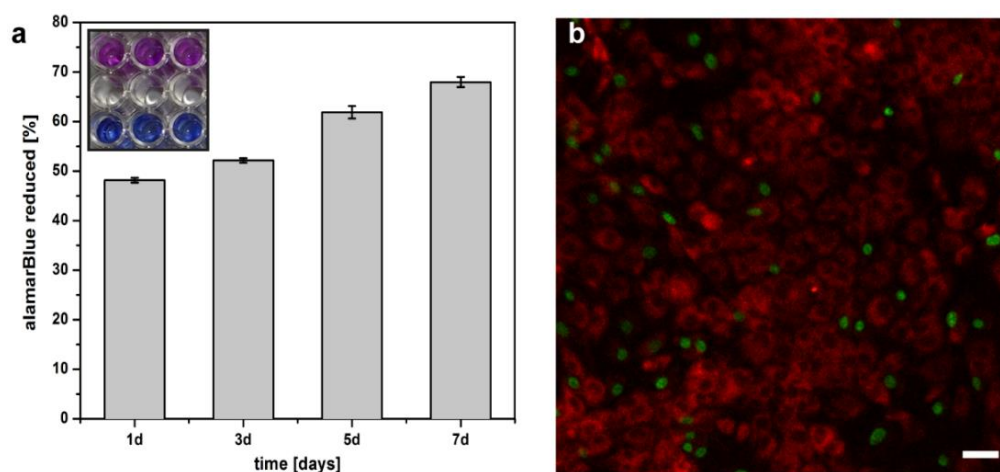


Figure 3.6 AlamarBlue graph showing HeLa cell proliferation rate onto Ir-PAA (a); in the inset: alamarBlue plate showing the metabolic activity of the sample and of the control (Ir-PAA without cells). Overlay of Sytox Green fluorescence stain for dead cells (green) and embedded Ir(III) complexes emission (red), indicating that the majority of cells are alive after 7 days (b). Scale bar is 10  $\mu$ m.

The potentiality of the new Ir-PAA scaffold with a built-in imaging probe was then investigated as platform for real-time, 3D live-cell imaging applications.

First, the behavior of the acellular scaffold in the dry and DMEM-equilibrated state was assessed via confocal laser scanning microscopy, CLSM.

Figure 3.7a depicts the luminescence of the Ir-PAA in dry and DMEM-swollen conditions. A quenching of the emission is observable when the sample was swollen, where only the low

emission at around 460 nm was observed. Very interestingly, the luminescence was restored when HeLa cells started to grow and interact with the material.

HeLa cells were easily detected, thanks to the bright red emission centered at around 640 nm, across and into the hydrogel over the 7-day culture period (Figure 3.7b, c).

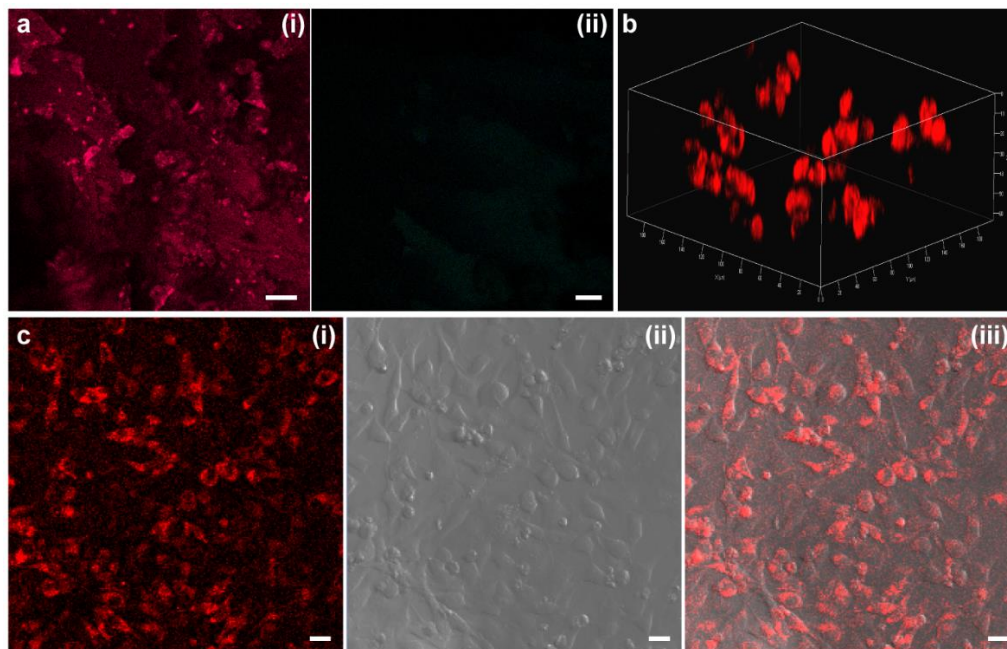


Figure 3.7 CLSM images of acellular Ir-PAA (a) dry(i) and swollen in DMEM(ii), scale bar is 50 μm; CLSM z-stack image of living HeLa cells growing in 3D onto the Ir-PAA (b); 3-channel visualization of HeLa growing onto the scaffold after 72 h, red channel (i), brightfield (ii) and overlay (iii), scale bar is 20 μm.

The emission was detected throughout the cells plasma membrane (Figure 3.8a), without the addition of any dye, while no nuclear staining was observed.

The localization of the luminescence was also confirmed by CLSM Z-stack images at increasing depths along the z-axis (Figure 3.8b,c), as shown as well in the xy, in the xz and yz cross-sectional images, Figure 3.8b.

Moreover, as can be observed from Figure 3.8f, the luminescence intensity profile of HeLa growing onto the Ir-PAA revealed a high signal ratio between the detected emission coming from the lipophilic membrane and the emission coming from the other regions, such as cytoplasm, nuclei and extra-cellular region.



The staining of the plasma membrane can appear very differently from sample to sample (i.e. 3D vs 2D; different cell lines,...), often it is visualized as a rim around the cell or as a uniform and very flat staining across the entire cell, because the plasma membrane beneath the cell is stained. To confirm the localization of the Ir(III) complex into the plasma membrane, HeLa cells growing onto the scaffold were incubated with Vybrant DiO membrane staining (green). The overlaid confocal microscopy images in Figure 3.8g showed substantial colocalization of the Ir(III) complex emission and the DiO plasma stain (colocalization coefficient: 0.78), further indicating that the complexes were interacting with the plasma membranes.

This confirmed that the linker bridging the complex to the PAA scaffold was long enough to allow insertion of the complex in the plasma membrane, when the cell is in its adjacencies.

The majority of commercially available organic dyes for cell-labelling require plasma membrane permeation. Many exhibit fluorescence enhancement only when they are uptaken from the nuclei, thus intercalated between the stacked base pairs of nucleic acids.<sup>[33]</sup>

Only few fluorescent membrane dyes are available for membrane staining purposes.<sup>[34]</sup> However, they suffer from rapid internalization and diffusion throughout the whole cell<sup>[35]</sup> or fast detachment from the plasma membrane.<sup>[36]</sup> Thus they allow only a short-time imaging window, i.e. from 90 min for the commercially available CellMask stain, up to 8 hours for the two-step modification and labeling strategy recently reported by Jia et al.<sup>[37]</sup>

With our system instead, we were able to visualize and image the cell membrane of HeLa proliferating into the Ir-PAA scaffold up to 7 days.

We hypothesize that the Ir(III) complexes were only partially incorporated into the plasma membrane, without the possibility of permeate the interior of the cell, because of the covalent link with the polymeric backbone of the hydrogel. We supposed that the hydrophobic interaction between the membrane and the Ir(III) pendants led to an insertion of the Ir(III) complexes into the membranes, such as illustrated in Figure 3.1, and as reported elsewhere for other systems.<sup>[38]</sup> The lipophilicity of the Ir(III) pendants, given by the aromaticity of the ligands, is anticipated to facilitate this interaction.<sup>[12, 39]</sup>

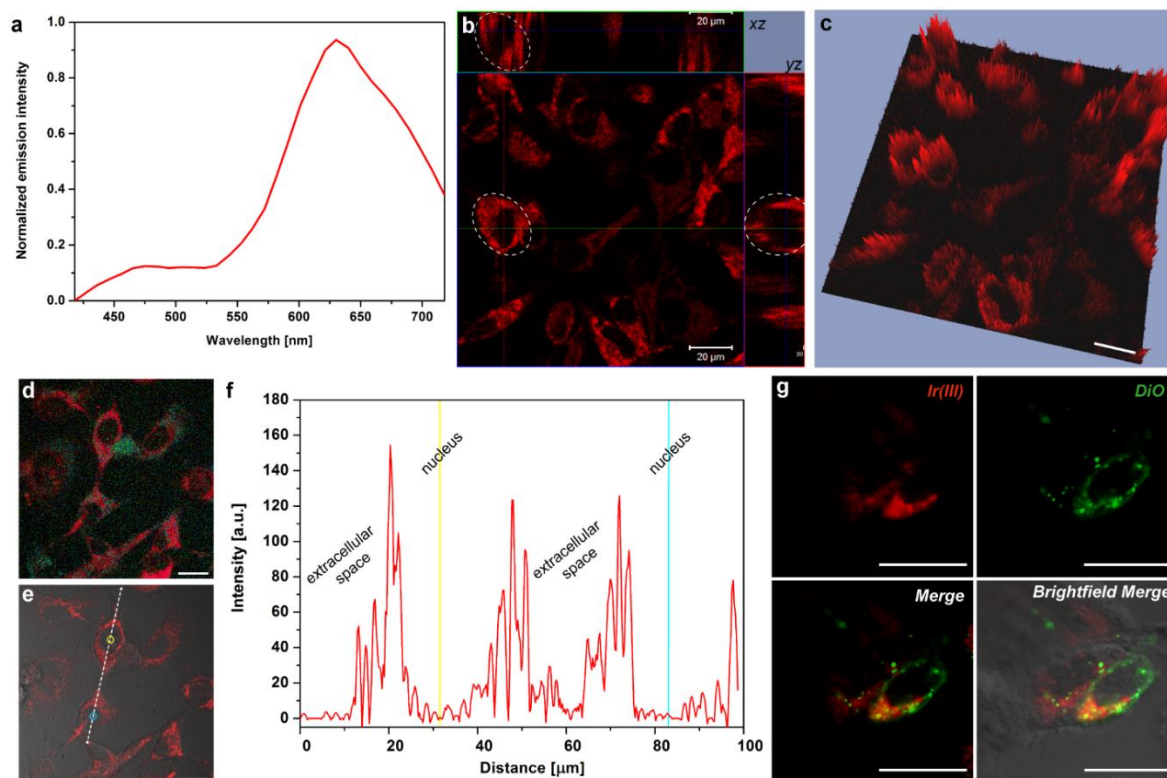


Figure 3.8 CLSM emission spectrum from the plasma membrane of cells grown onto Ir-PAA(a); Z-stack images at increasing depths along the z-axis (b) and 2.5D profile (c); true color of living HeLa on Ir-PAA after 96 h (d); overlay of red channel and brightfield (e); luminescence intensity profile across the line shown in figure e, corresponding to extracellular region, membrane and nuclear region (yellow and blue circles and lines) of two cells (f); separate channel and overlay visualization of the colocalization of the Ir(III) complex signal and the DiO green plasma membrane stain (g). Scale bar is 20  $\mu\text{m}$  and CLSM 60x magnification in all the images.

We reasoned that the insertion of the Ir(III) pendants into the plasma membranes protects the complexes from the oxygen present in the extracellular aqueous environment, thus enabling its environment-sensitive luminescence, which resulted in a switched “off/on” emission.

The observed red emission coming from the cellular membrane region supported the hypothesis that the Ir(III) complexes inserted into the lipid bilayer could act as fluorescent reporter of the local lipophilic environment.

Presumably, when the complexes grafted to the Ir-PAA network are in close proximity to the cells and can sense the hydrophobic environment of the plasma membrane, their interaction with the cell membrane causes their intercalation within the lyophilic bilayer of the plasma membrane. A similar observation indeed has been reported for luminophore-labelled protein



systems.<sup>[40]</sup> This behavior results in the shielding of the Ir(III) pendants from the the aqueous environment (and therefore from the dioxygen), inducing a turn on of the luminescence.

It is known that the oxygen permeability coefficient for the plasma membrane is two times lower than for a water layer of the same thickness as the membrane.<sup>[41]</sup> Different oxygen concentrations measured between extracellular and intracellular compartment in normal physiologic conditions, were reported indeed to show a higher oxygen level in the extracellular compartment.<sup>[42]</sup>

Several studies have been discussed metal complexes as lipophilic biological probes,<sup>[17c, 43]</sup> however, in all of them the complexes are completely uptaken from the cells, mainly by endocytosis.

Endocytosis is an energy-requiring process that can be inhibited by lowering the temperature thus blocking active membrane transport mechanisms.

To prove that no uptake of the complex and in particular no endocytotic processes were occurring in our system, we cultured the HeLa cells onto the Ir-PAA at 4 °C for 1 hour.

As expected, after the treatment, a bright red emission was still visible from the cells membrane, confirming that there were not endocytic processes taking place.<sup>[44]</sup>

In the presented Ir-PAA platform, the Ir(III) complex is covalently bound to the hydrogel polymer network, as previously discussed. The absence of uptake of the Ir(III) complexes by the cells was confirmed by removing the cells from the hydrogel scaffold after 7 days of culture, and seeding them in 2D on a new clean surface. Cells were trypsinised from the Ir-PAA and re-seeded on glass bottom petri dishes without any washing, to avoid the possible removal of eventual residues of complex **3**. The HeLa cells detached from the hydrogel were imaged after 24 hours. CLSM visualization of live cells clearly showed no residues of Ir(III) complexes. Figure 3.9 shows the absence of luminescence emission signal in the region between 600-700 nm (Ir(III) complex channel).

To enable a clearer visualization, the cells nuclei were stained with Hoechst 33342 in a second time.

Quantification of the luminescence intensity profile of HeLa cells confirmed that only the signal coming from the Hoechst-stained nuclei was visible, with a high signal ratio between the nucleus (>70) and the surrounding region (i.e. cytoplasm and extracellular compartment)

and a clear emission maxima at  $\sim 460$  nm (Figure 3.9d,e). The viability of the cells was found to be 98.2% after 24h.

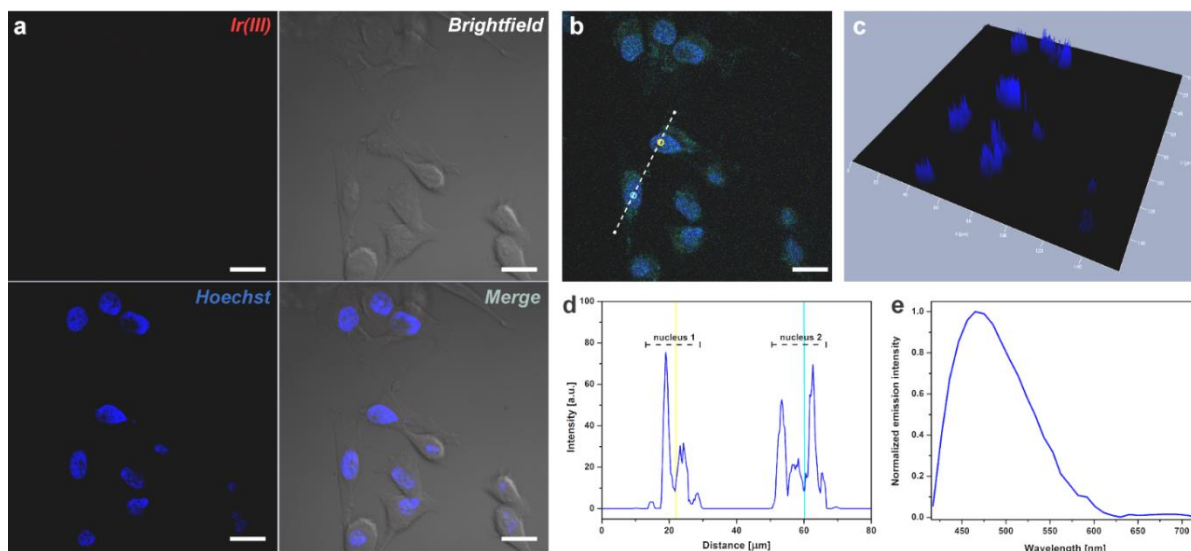


Figure 3.9 Color channels and brightfield visualization of HeLa extracted for the hydrogel; scale bar is 20  $\mu\text{m}$  (a);  $\lambda$  mode visualization in true colors (b), scale bar is 20  $\mu\text{m}$ ; profile visualization (c); profile intensity (d) and emission intensity (e) of points shown in (b).

Finally, a comparison of cytotoxicity and internalization mechanism was carried out with the free complex **3**. HeLa cells were cultured in 2D and incubated with **3**, in the same concentration used for the hydrogel, keeping into account the different number of cells seeded (i.e. 30  $\mu\text{M}$  for Ir-PAA, where 40,000 cells were seeded and 15  $\mu\text{M}$  for the 2D study, considering that 20,000 cells were seeded).

After 30 min of incubation, the cells were imaged and an intense red luminescence was detected in the cytoplasm region upon excitation at 405 nm, while there was no emission coming from the nuclei (Figure 3.10a). Already after 1 hour of incubation, many cells started to exhibit a clear uptake of **3** diffusing also in the nuclear region, which instead was never observed in the 3D Ir-PAA investigation.

Interestingly, the cells started to manifest shrinkage, membrane blebbing,<sup>[45]</sup> and plasma membrane vesiculation, indicating an unhealthy (apoptotic) state.<sup>[46]</sup> When the incubation with **3** was protracted for 4 hours, this behavior was more obviously exhibited. The viability of the

HeLa was found to be of 11% after 4 hours of treatment with the complex, whereas the viability of the non treated HeLa cells was 100%.

2D experiments were performed as well with a lower concentration of **3**, in particular 20,000 cells were incubated with a 1.5 nM solution of **3** in DMEM. Even in these conditions, the uptake was evident and led to cell apoptosis after 4 h (Figure 3.10b).

The cells were also incubated at 4 °C for 1 hour with **3**, in this case no interiorization was observed (Figure 3.10c), confirming that the uptake of the complex and its subsequent localization are due to energy-requiring processes such as endocytosis.

These results imply that when the complex **3** is not covalently linked to the polymeric network it is fully internalized into the cells.

Moreover, we could observed a direct correlation between cellular uptake of **3** and their cytotoxicity, indicating that when the complex is free in solution it can be easily and rapidly internalized in all the cell compartments, causing the apoptosis of the HeLa cells.

The association between cellular uptake efficiency and cytotoxicity of the bio-imaging reagents derived from iridium(III) complexes has been already reported in various studies.<sup>[39, 43a, 47]</sup>

Colocalization studies performed on the cells incubated with **3**, by adding the ER-Tracker dye revealed that complex **3** was uptaken also in the endoplasmic reticulum (ER), as displayed in Figure 3.10d. The accumulation of complex **3** in the ER regions might have induced ER stress and calcium release into cytoplasm, which further triggered the onset of apoptotic cell death mechanism, as already reported by Cao et al. for similar structures.<sup>[39]</sup> Even though the investigation of the apoptosis mechanism induced by the internalization of the Ir(III) complexes could be very interesting, it is beyond the scope of the present study, and it was not investigated further. Here the observation of the HeLa apoptosis after treatment with complex **3** is reported as an additional evidence of the different interaction between the cells and the iridium probe, when the latter is free in solution (cell apoptosis induced) or when it is grafted to the hydrogel network (excellent cyto-compatibility).

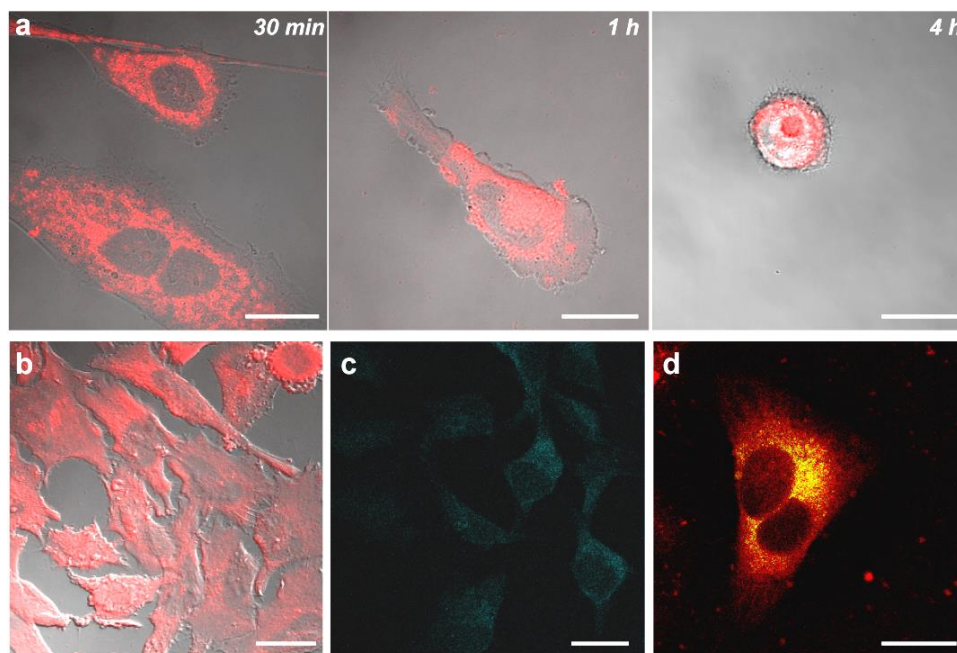


Figure 3.10 2D experiments of cells uptake of the free compound **3** at a concentration 15  $\mu\text{M}$ , after 30 min, 1 h and 4 h of incubation (a); at a concentration of 1.5  $\mu\text{M}$  after 4 h of incubation (b); at a concentration of 15  $\mu\text{M}$ , after 1 h of incubation at 4  $^{\circ}\text{C}$  showing no internalization of **3** (c); colocalization of the uptaken **3** and the ER-Tracker (yellow). Scale bar is 20  $\mu\text{m}$  and magnification is 60x in every image.

### 3.5 Conclusions

We have successfully designed and synthesized a novel hybrid hydrogel platform for the *in vitro* culture of HeLa cells, which allows their localization and imaging through “off/on” luminescent emission, without additional cell staining required. Since the polymerization reaction used is very versatile, it is also possible to vary the structure of the obtained scaffold by introducing biomolecules or other components for future different applications.

To the best of our knowledge, the Ir-PAA scaffold presented here is the first 3D platform with embedded phosphorescence-enhanced cell imaging agent.

We demonstrated that HeLa cells proliferated onto the scaffold with a high viability up to 7 days and that our strategy enabled clear identification and imaging of the cells in real time for the whole study time.

We have explained the design approach of the “off/on” emission by hypothesizing a hydrophobic interaction between the Ir(III) complex pendants and the cell membranes, which protect Ir(III) complexes from the dioxygen-quenching, giving rise to a bright red emission. This was followed by a thorough experimental demonstration of the concept through studies conducted in 3D and in 2D with different amounts of Ir(III) complexes and at different temperatures (37 °C and 4 °C).

The major outcome of the present investigation is the disclosure of an innovative strategy for the development of luminescent-probe-3D platforms, which we believe will be beneficial for *in vitro* living cell-related studies. We hope this will lead to the development of novel approaches for luminescent *in vitro* models that could have significant impact on the success of biomedical research in the future.

## 3.6 Experimental part

### 3.6.1 *Synthesis of the ancillary ligand*

A suspension of 4-(4-methyl-2,2-bipyridine-4'-yl)butyric acid (200 mg, 0.78 mmol) and N-hydroxysuccinimide, NHS (90 mg, 0.79 mmol) was stirred at 0 °C for 10 minutes then N,N'-dicyclohexylcarbodiimide, DCC (174 mg, 0.84 mmol) was added. The reaction was allowed to warm to room temperature and stirred for 24 hours. Then water was added to the mixture and the product was extracted with dichloromethane, DCM. A white solid formed and was filtered off. The organic fraction was concentrated to dryness and used without further purification for the next reaction. 320 mg of pale yellow oil were obtained.

The thus obtained product (320 mg, 0.9 mmol) was reacted under nitrogen in dimethylformamide, DMF, solution with Fmoc-protected hexamethyldiamine (339 mg, 1.09 mmol), at room temperature for 2 hours. Then 0.15 ml of triethanolamine, TEA, were added and the mixture was left to react overnight. The day after, the mixture was concentrated to dryness and the residue was resuspended in DCM and washed with sodium bicarbonate. The organic fraction was concentrated to dryness and the obtained 4-(4-methyl-2,2-bipyridine-4'-yl)(N-Fmoc-hexamethyldiamine-butyric acid) **2** was used without further purification for the next reaction.

### 3.6.2 Synthesis of the Ir(III) complex

A solution of tetrakis[2-(6'-phenantridine)benzene- $C^2,N'$ ]( $\mu$ -dichloro)diiridium **1** (200 mg, 0.135 mmol) and **2** (152 mg, 0.28 mmol) was refluxed overnight in 2-methoxyethanol, 2-MeOEtOH, (18 ml), under nitrogen. The day after the mixture was concentrated to dryness and the residue was purified by preparative HPLC Acetonitrile/water/TFA (6:4:0.1). During the purification the Fmoc deprotection occurred. The residue was dissolved in methanol, MeOH, and 20 ml of a mixture of MeOH and saturated solution of  $NH_4PF_6$  (8:1) was added. The product **3** precipitate as a red solid (50 mg).

$^1H$  NMR (400 MHz, Methylene Chloride- $d_2$ )  $\delta$  9.14 (t,  $J$  = 6.9 Hz, 2H), 8.64 – 8.31 (m, 8H), 8.01 – 7.85 (m, 4H), 7.68-7.62 (m, 4H), 7.44 (t,  $J$  = 7.6 Hz, 2H), 7.32 – 7.21 (m, 2H), 7.13 – 6.99 (m, 4H), 6.92-6.81 (m, 4H), 3.04 (q,  $J$  = 6.6 Hz, 4H), 2.53 (t,  $J$  = 7.9 Hz, 2H), 2.25 (s, 3H), 1.97 (t,  $J$  = 7.4 Hz, 2H), 1.73 – 1.56 (m, 2H), 1.44-1.16 (m, 10H).

$^{13}C$  NMR (400 MHz,  $CDCl_3$ )  $\delta$  = 173.38; 173.36; 171.49; 155.53; 155.09; 154.86; 152.44; 151.71; 147.57; 147.49; 147.46; 142.65; 142.63; 136.41; 136.38; 133.47; 132.64; 132.57; 130.11; 130.09; 129.13; 129.04; 128.85; 128.50; 127.79; 127.72; 127.67; 126.12; 124.77; 124.74; 123.87; 123.54; 123.51; 123.28; 122.68; 34.79; 34.17; 29.59; 26.6; 25.93; 20.87.

Anal. Calc. for  $C_{59}H_{54}F_6IrN_6OP \cdot CH_2Cl_2$ : C, 56.07; H, 4.39; N, 6.54.

Found: C, 56.05; H, 4.16; N, 5.70.

### 3.6.3 Synthesis of Ir-PAA

In a 10 ml round bottom flask, **3** (20  $\mu$ l of a 3 mM dimethyl sulfoxide, DMSO, solution) was dissolved in 2 ml of MeOH. Then, N,N'-methylene bisacrylamide (MBA; 200 mg) and  $\gamma$ -aminobutyric acid (66 mg) were added and stirred vigorously stirring, while heating the solution to favor complete dissolution to 70  $^{\circ}C$  for 5-10 minutes. After that, pentaethylenhexamine, PEHA, (70  $\mu$ l) was added to the mixture as the cross-linker. The mixture was stirred for additional 20 minutes at room temperature, then it was transferred to a glass vial and allowed to react in static conditions at r.t for 3 hours, thus obtaining the hydrogel scaffold, which was subsequently washed with MeOH and water.

#### 3.6.4 *Photophysical experiments*

The instrumental description can be found in chapter 6. Complex **3** was measured with a concentration of  $1 \times 10^{-5}$  M in DCM and water. Degassed samples were prepared by the freeze-pump-thaw technique.

#### 3.6.5 *In vitro cell culture*

Human cervical carcinoma, HeLa cells were cultured in Dulbecco's Modified Eagle Medium (DMEM) 10% Fetal Bovine Serum (FBS), 1% Penicillin-Streptomycin and 1% L-Glutamine 200 mM. Cells were kept in 75 cm<sup>2</sup> culture flasks (Corning Inc., NY, USA) at 37 °C with a controlled atmosphere of 5% CO<sub>2</sub> and were grown until reaching 80 to 85% of confluence. Then, they were washed twice with Phosphate Buffer Solution (PBS) and treated with trypsin to detach them from the flask surface. Cells were split every 2-3 days; the medium was changed every other day.

#### 3.6.6 *In vitro cell culture onto the hydrogels*

Hydrogel samples were immersed into 4 ml of 70% (v/v) ethanol in nanopure water for 20 min; then the ethanol-water mixture was discarded and 5 ml nanopure water was added. The hydrogels were left in water for 10 min and the procedure was repeated 5 times, to completely remove ethanol. After sterilization, they were equilibrated in culture media at 37°C. HeLa cells were detached from the culture flask by trypsination and approximately 40,000 cells were re-seeded onto the hydrogel scaffolds. Fresh culture media (2-3 mL) was added gently. The number of cells was counted using a TC20™ Automated Cell Counter (Bio-Rad).

#### 3.6.7 *Organelle staining*

Cells grown onto the hydrogel were detached from the material by trypsination (ca.8-10 min). Then they were re-seeded on glass bottom petri dishes without any washing, to avoid the possible removal of eventual Ir(III) residues, and imaged after 24 hours. Once established that no residues were present, for a better visualization cells nuclei was stained with 4',6-diamidino-2-phenylindole carboxamide (DAPI) and washed twice with PBS.



Where needed, cells grown onto the hydrogel were stained with Vybrant DiO (Life Technologies, Thermo Fisher Scientific) that was added to the culture medium following the manufacturer's protocol, to obtain membrane labeling.

Cells grown in 2D were stained where needed with ER-Tracker™ Red (Thermo Fisher Scientific) that was added to the culture medium following the manufacturer's protocol, to obtain endoplasmic reticulum staining for colocalization purposes. In the reported figures the ER-Tracker is reported in green (false color), to distinguish it from the Ir(III) emission. The ER-Tracker dye and Ir(III) do no overlay in their absorbance and are excited at two different wavelength (587 and 405 nm respectively).

### 3.6.8 *Cell viability*

Cell viability was assessed using alamarBlue assay (Thermo Fischer Scientific). Briefly, the alamarBlue solution was added to the culture medium (1:10 dilution) of unstained cells growing onto hydrogel scaffolds. After 4 h of incubation, 200 µL of the media were transferred to a 96-well plate and absorbance signals generated from the dye resazurin (dark blue) being reduced to resorufin (pink) by metabolically active cells were recorded using a VICTOR X5 Multilabel Plate Reader (PerkinElmer). Each sample was tested in three replicates and the results were expressed as percentage of reduced alamarBlue.

SYTOX green from LIVE/DEAD Cell Vitality Assay Kit (Molecular Probes, USA), was used to visually confirm the alamarBlue results. SYTOX green is impermeant to live cells; it can permeate compromised cell membrane (dead cells) and become strongly fluorescent upon binding to nucleic acid. Cells displaying green emission were classified as dead.

Cell viability for 2D experiments was measured with a TC20™ Automated Cell Counter (Bio-Rad) and positive control of cells grown without complex was also performed.

All experiments were repeated at least three times.

### 3.6.9 *Ir(III) complexes incubation (2D measurements)*

Approximately 20,000 HeLa cells were seeded onto a glass bottom petri dish and grown for 24 h in DMEM. Then, the culture media was removed and 2 ml of DMEM solution containing the Ir(III) complexes (10 or 1 µl of a 3 µM DMSO solution) were gently added onto the cells.



The samples were incubated at 37°C and 5% of CO<sub>2</sub> for 30 min, 1 h or 4 h. After the selected incubation time, the staining medium was removed and replaced by fresh medium.

For the 4 °C experiment, cells were incubated for 1 hour at 4 °C after treating them with 2 ml of DMEM solution containing Ir(III) complex (10 µl of a 3 µM DMSO solution); then they were recovered at room temperature and visualized immediately with CLSM without washing.

#### 3.6.10 *Live-Cell fluorescence confocal microscopy*

HeLa cells, both grown onto Ir-PAA in glass bottom petri dishes or in 2D directly onto glass bottom dishes, were visualized as they were. Imaging was performed using Zeiss LSM 710 confocal microscope set up with 63× magnification, numerical aperture, NA, 1.3 of Zeiss LCI Plan-NEOFLUAR water immersion objective lens (Zeiss GmbH, Germany). The samples were excited by continuous wave (cw) laser at 405 nm. The emission was collected in the range from 420 to 720 nm. For co-localization and viability experiments, the samples priory co-stained with different dyes, DAPI (excitation/emission wavelength: 358 nm/461 nm), SYTOX Green (excitation/emission wavelength: 504 nm/523 nm), Vybrant DiO (excitation/emission wavelength: 488 nm/510 nm) and ER-tracker (excitation/emission wavelength: 587 nm/615 nm) were excited independently at 405, 514, 488 and 594 nm, respectively. All image processing was performed by using ZEN software (Zeiss GmbH, Germany). False colour images were reported to better distinguish different emission coming from the Ir(III) complex or from cellular organelles.

#### 3.6.11 *Statistic methods*

Three replicates for each *in vitro* experiment (cells viability onto hydrogels and in 2D) were performed and the results are reported as mean ± standard deviation.

### 3.7 References

- [1] a) Daniel J. Maltman, Stefan A. Przyborski, *Biochem. Soc. Trans.* **2010**, 38, 1072; b) E. Cukierman, D. E. Bassi, *Semin. Cancer Biol.* **2010**, 20, 139; c) E. Santos, R. M. Hernández, J. L. Pedraz, G. Orive, *Trends Biotechnol.* **2012**, 30, 331.
- [2] D. Seliktar, *Science (New York, N.Y.)* **2012**, 336, 1124.

- [3] O. Wichterle, D. Lím, *Nature* **1960**, *185*, 117.
- [4] N. Annabi, A. Tamayol, J. A. Uquillas, M. Akbari, L. E. Bertassoni, C. Cha, G. Camci-Unal, M. R. Dokmeci, N. a. Peppas, A. Khademhosseini, *Advanced materials research* **2014**, *26*, 85.
- [5] Q. Wang, J. L. Mynar, M. Yoshida, E. Lee, M. Lee, K. Okuro, K. Kinbara, T. Aida, *Nature* **2010**, *463*, 339.
- [6] a) V. R. Kondepoti, H. M. Heise, J. Backhaus, *Anal. Bioanal. Chem.* **2007**, *390*, 125; b) H. Wang, J. Liu, A. Han, N. Xiao, Z. Xue, G. Wang, J. Long, D. Kong, B. Liu, Z. Yang, D. Ding, *ACS Nano* **2014**, *8*, 1475.
- [7] A. Waggoner, *Curr. Opin. Chem. Biol.* **2006**, *10*, 62.
- [8] a) Y. Goto, R. Matsuno, T. Konno, M. Takai, K. Ishihara, *Biomacromolecules* **2008**, *9*, 3252; b) X. Gao, Y. Cui, R. M. Levenson, L. W. K. Chung, S. Nie, *Nat Biotech* **2004**, *22*, 969.
- [9] a) M. Mauro, A. Aliprandi, D. Septiadi, N. S. Kehr, L. De Cola, *Chem. Soc. Rev.* **2014**, *43*, 4144; b) H.-Y. Shiu, H.-C. Chong, Y.-C. Leung, T. Zou, C.-M. Che, *Chem. Commun.* **2014**, *50*, 4375; c) E. Baggailey, J. A. Weinstein, J. A. G. Williams, *Coord. Chem. Rev.* **2012**, *256*, 1762; d) A. Colombo, F. Fiorini, D. Septiadi, C. Dragonetti, F. Nisic, A. Valore, D. Roberto, M. Mauro, L. De Cola, *Dalton Trans.* **2014**, *44*, 8478.
- [10] S. Lamansky, P. Djurovich, D. Murphy, F. Abdel-Razzaq, R. Kwong, I. Tsyba, M. Bortz, B. Mui, R. Bau, M. E. Thompson, *Inorg. Chem.* **2001**, *40*, 1704.
- [11] E. Baggailey, S. W. Botchway, J. W. Haycock, H. Morris, I. V. Sazanovich, J. A. G. Williams, J. A. Weinstein, *Chemical Science* **2014**, *5*, 879.
- [12] K. K.-W. Lo, A. W.-T. Choi, W. H.-T. Law, *Dalton Transactions* **2012**, *41*, 6021.
- [13] Y. Chi, P.-T. Chou, *Chem. Soc. Rev.* **2010**, *39*, 638.
- [14] G. Zhang, H. Zhang, Y. Gao, R. Tao, L. Xin, J. Yi, F. Li, W. Liu, J. Qiao, *Organometallics* **2014**, *33*, 61.
- [15] C. Ulbricht, B. Beyer, C. Friebe, A. Winter, U. S. Schubert, *Adv. Mater.* **2009**, *21*, 4418.
- [16] L. Murphy, A. Congreve, L.-O. Palsson, J. A. G. Williams, *Chem. Commun.* **2010**, *46*, 8743.
- [17] a) K. K.-W. Lo, K. Y. Zhang, *RSC Advances* **2012**, *2*, 12069; b) G. Li, Q. Lin, L. Ji, H. Chao, *Journal of Materials Chemistry B* **2014**, *2*, 7918; c) K. K.-W. Lo, K. K.-S. Tso, *Inorganic Chemistry Frontiers* **2015**, *2*, 510; d) D. Maggioni, M. Galli, L. D'Alfonso, D. Inverso, M. V. Dozzi, L. Sironi, M. Iannaccone, M. Collini, P. Ferruti, E. Ranucci, G. D'Alfonso, *Inorg. Chem.* **2015**, *54*, 544; e) M. Yu, Q. Zhao, L. Shi, F. Li, Z. Zhou, H. Yang, T. Yi, C. Huang, *Chem. Commun.* **2008**, 2115.
- [18] X.-d. Wang, O. S. Wolfbeis, *Chemical Society Reviews* **2014**, *43*, 3666.
- [19] P. Ferruti, *J. Polym. Sci., Part A: Polym. Chem.* **2013**, *51*, 2319.
- [20] I.-S. Shin, J. I. Kim, T.-H. Kwon, J.-I. Hong, J.-K. Lee, H. Kim, *The Journal of Physical Chemistry C* **2007**, *111*, 2280.
- [21] M. Nonoyama, *Bulletin of the Chemical Society of Japan* **1974**, *47*, 767.
- [22] J. M. Fernandez-Hernandez, E. Longhi, R. Cysewski, F. Polo, H.-P. Josel, L. De Cola, *Analytical Chemistry* **2016**, *88*, 4174.
- [23] a) S. Lamansky, P. Djurovich, D. Murphy, F. Abdel-Razzaq, H.-E. Lee, C. Adachi, P. E. Burrows, S. R. Forrest, M. E. Thompson, *Journal of the American Chemical Society* **2001**, *123*, 4304; b) D. H. Kim, N. S. Cho, H.-Y. Oh, J. H. Yang, W. S. Jeon, J. S. Park, M. C. Suh, J. H. Kwon, *Advanced Materials* **2011**, *23*, 2721.

- [24] Z. Li, Z. Wei, F. Xu, Y. H. Li, T. J. Lu, Y. M. Chen, G. J. Zhou, *Macromol. Rapid Commun.* **2012**, *33*, 1191.
- [25] S. Marpu, Z. Hu, M. A. Omary, *Langmuir* **2010**, *26*, 15523.
- [26] M. X. Wang, C. H. Yang, Z. Q. Liu, J. Zhou, F. Xu, Z. Suo, J. H. Yang, Y. M. Chen, *Macromol. Rapid Commun.* **2015**, *36*, 465.
- [27] C. Chang, J. Peng, L. Zhang, D.-W. Pang, *J. Mater. Chem.* **2009**, *19*, 7771.
- [28] a) V. Magnaghi, V. Conte, P. Procacci, G. Pivato, P. Cortese, E. Cavalli, G. Pajardi, E. Ranucci, F. Fenili, A. Manfredi, P. Ferruti, *Journal of biomedical materials research. Part A* **2011**, *98*, 19; b) N. Segovia, M. Pont, N. Oliva, V. Ramos, S. Borros, N. Artzi, *Advanced Healthcare Materials* **2015**, *4*, 271.
- [29] a) O. Jeon, D. S. Alt, S. M. Ahmed, E. Alsberg, *Biomaterials* **2012**, *33*, 3503; b) H. Park, X. Guo, J. S. Temenoff, Y. Tabata, A. I. Caplan, F. K. Kasper, A. G. Mikos, *Biomacromolecules* **2009**, *10*, 541.
- [30] a) W. Yang, C.-Y. Pan, *Macromol. Rapid Commun.* **2009**, *30*, 2096; b) W. Yang, X. Wu, F. Liu, Y. Dou, Z. Hu, W. Hao, *RSC Advances* **2016**, *6*, 34254.
- [31] C.-C. Chu, T. Imae, *Macromol. Rapid Commun.* **2009**, *30*, 89.
- [32] E. Knight, S. Przyborski, *J. Anat.* **2015**, *227*, 746.
- [33] a) M. Collot, R. Kreder, A. L. Tatarets, L. D. Patsenker, Y. Mely, A. S. Klymchenko, *Chem. Commun.* **2015**, *51*, 17136; b) C. Li, M. Yu, Y. Sun, Y. Wu, C. Huang, F. Li, *J. Am. Chem. Soc.* **2011**, *133*, 11231; c) J. F. Keij, C. Bell-Prince, J. A. Steinkamp, *Cytometry* **2000**, *39*, 203.
- [34] a) C. Zhang, S. Jin, K. Yang, X. Xue, Z. Li, Y. Jiang, W.-Q. Chen, L. Dai, G. Zou, X.-J. Liang, *ACS Applied Materials & Interfaces* **2014**, *6*, 8971; b) R. Kreder, S. Oncul, O. A. Kucherak, K. A. Pyrshev, E. Real, Y. Mely, A. S. Klymchenko, *RSC Advances* **2015**, *5*, 22899; c) C.-K. Koo, K.-L. Wong, C. W.-Y. Man, H.-L. Tam, S.-W. Tsao, K.-W. Cheah, M. H.-W. Lam, *Inorg. Chem.* **2009**, *48*, 7501.
- [35] a) P. Yan, A. Xie, M. Wei, L. M. Loew, *The Journal of organic chemistry* **2008**, *73*, 6587; b) R. Kamitani, K. Niikura, T. Okajima, Y. Matsuo, K. Ijio, *ChemBioChem* **2009**, *10*, 230.
- [36] Y. Teramura, Y. Kaneda, T. Totani, H. Iwata, *Biomaterials* **2008**, *29*, 1345.
- [37] H.-R. Jia, H.-Y. Wang, Z.-W. Yu, Z. Chen, F.-G. Wu, *Bioconjugate Chem.* **2016**, *27*, 782.
- [38] a) R. Schops, E. Amado, S. S. Muller, H. Frey, J. Kressler, *Faraday Discuss.* **2013**, *166*, 303; b) B. Gruber, B. König, *Chemistry – A European Journal* **2013**, *19*, 438.
- [39] R. Cao, J. Jia, X. Ma, M. Zhou, H. Fei, *J. Med. Chem.* **2013**, *56*, 3636.
- [40] J. D. Dattelbaum, O. O. Abugo, J. R. Lakowicz, *Bioconjugate Chem.* **2000**, *11*, 533.
- [41] W. K. Subczynski, L. E. Hopwood, J. S. Hyde, *J. Gen. Physiol.* **1992**, *100*, 69.
- [42] R. I. Dmitriev, A. V. Zhdanov, G. Jasione, D. B. Papkovsky, *Anal. Chem.* **2012**, *84*, 2930.
- [43] a) K. K.-W. Lo, P.-K. Lee, J. S.-Y. Lau, *Organometallics* **2008**, *27*, 2998; b) V. Fernandez-Moreira, F. L. Thorp-Greenwood, A. J. Amoroso, J. Cable, J. B. Court, V. Gray, A. J. Hayes, R. L. Jenkins, B. M. Kariuki, D. Lloyd, C. O. Millet, C. F. Williams, M. P. Coogan, *Org. Biomol. Chem.* **2010**, *8*, 3888; c) S. G. König, S. Oz, R. Kramer, *Molecular BioSystems* **2016**, *12*, 1114; d) S. Bakthavatsalam, A. Sarkar, A. Rakshit, S. Jain, A. Kumar, A. Datta, *Chem. Commun.* **2015**, *51*, 2605; e) C. A. Puckett, J. K. Barton, *J. Am. Chem. Soc.* **2007**, *129*, 46.
- [44] E. Reaven, L. Tsai, S. Azhar, *J. Biol. Chem.* **1996**, *271*, 16208.
- [45] D. V. Krysko, T. Vanden Berghe, K. D'Herde, P. Vandenabeele, *Methods* **2008**, *44*, 205.
- [46] B. J. Hoerl, R. E. Scott, *Virchows Arch. B Cell Pathol.* **1978**, *27*, 335.

- [47] K. Y. Zhang, K. K.-W. Lo, *Inorg. Chem.* **2009**, *48*, 6011.

## 4. Nanocomposite hydrogels for cells growth and chemotaxis

### Abstract

The challenge of mimicking extracellular matrix (ECM) with artificial scaffolds that are able to reduce immunoresponse is still unmet. Recent findings have shown that mesenchymal stem cells (MSC) infiltrating into the implant have effects on the scaffold integration by improving the healing process.

Towards this aim, we synthesized a novel polyamidoamines-based nanocomposite hydrogel, cross-linked with porous nanomaterials (i.e. mesoporous silica nanoparticles). A comprehensive viscoelasticity study confirmed that the hydrogel provided optimal structural support for MSC infiltration and proliferation.

Chemotaxis of MSC *in vitro* was investigated with a dual hydrogel system (concentric cylinder hydrogel, CCH), engineered to deliver the chemoattractant Stromal cell-Derived Factor-1 $\alpha$  (SDF-1 $\alpha$ ) from the filled nanocomposite core. We demonstrated the ability of this platform to stimulate chemotactic recruitment of MSC *in vitro* by following the migration of the seeded cells from the edges of the scaffold towards the core, over 7 days. Finally, subcutaneous implantation of SDF-1 $\alpha$ -releasing hydrogels in mice resulted in a modulation of the inflammatory and fibrotic reaction.

Overall, the proposed SDF-1 $\alpha$ -nanocomposite hydrogel proved to be a promising biomaterial for applications in tissue engineering.

F. Fiorini, E.A. Prasetyanto, F. Taraballi, L. Pandolfi, F. Monroy, I. López-Montero, E. Tasciotti, L. De Cola, “Nanocomposite Hydrogels as Platform for Cells Growth, Proliferation and Chemotaxis”, *Small*, **2016**, 12, 4881

#### **4.1 Tissue engineering: challenging and promises for novel nanocomposites implants**

Tissue engineering (TE) is a fast expanding field, whose primary aim is the replacement of diseased or damaged tissues with scaffolds that allow the encapsulation of cells, and which may elicit the regeneration of new tissue.<sup>[1]</sup>

A promising class of synthetic polymers for tissue engineering application are polyamidoamine,<sup>[2]</sup> as discussed in the previous chapters. The hydrogels based on these polymers are very versatile and can be prepared via one-pot synthesis from commercially available molecules in mild conditions. The adaptability of the involved chemistry allows choosing the initial monomers in order to obtain biocompatible materials easily modifiable by introducing the required chemical functionalities or bioactive groups.<sup>[3]</sup>

Moreover, in recent years the fast evolving field of nanotechnology has placed much interest in developing nanoparticles (NPs) for various biomedical applications.<sup>[4]</sup>

NPs can be obtained from many different sources (i.e. organic and inorganic) and with a variety of synthetic routes; they can be engineered to possess almost any shape and surface/bulk properties through chemical modification.<sup>[5]</sup>

Thus, due to this diverse selection of NPs with different physical and chemical properties, the search for better properties in the development of materials for biomedical applications has led to the incorporation of NPs into hydrogel systems.<sup>[6]</sup>

In particular, silica-based nanoparticles (MSNs),<sup>[7]</sup> have attracted a great interest as inorganic fillers, thanks to their easily controllable size, uniform structure on the nanoscale, and stable function in aqueous solutions.<sup>[8]</sup>

They have been investigated as fillers in hydrogel nanocomposites because of their large surface area, which promotes strong physical contact and efficient stress transfer between the silica-based nanomaterials and the hydrophilic polymer network, thus improving the mechanical stability and elasticity of the scaffold.<sup>[9]</sup>

Moreover, they have been extensively studied and attracted great interest in biomedical applications due to their chemical stability and low cytotoxicity.<sup>[10]</sup> Regarding biocompatibility, silica is “Generally Recognized As Safe” (GRAS) by the United States Food and Drug Administration (FDA).

Nanocomposite hydrogels, as discussed in chapter 1, are soft materials, whose polymer network is cross-linked to nanoparticles,<sup>[11]</sup> which interact in a physical or covalent manner with the polymeric chains, resulting in novel interesting properties of the hydrogel network.<sup>[12]</sup>

Despite the substantial progress that has been made in nanocomposites synthesis and functionalization, these biomaterials rarely have found a successful clinical translation in tissue-engineered implants, mainly because of the inflammatory responses that they generate.<sup>[13]</sup> This not only limits their efficiency, but can also be detrimental to their safety and biocompatibility, subsequently leading to clinical device failure.<sup>[14]</sup>

Recent findings have shown that Mesenchymal Stem cells (MSC) infiltrating into the implant have effects on the scaffold integration by improving the healing process, thanks to their regenerative and immunosuppressive potential.<sup>[15]</sup>

Several studies<sup>[16]</sup> based on MSC therapy have been published promising results regarding the ability of these cells to accelerate the wound healing process, which is suggested to take place through the release of signaling factors<sup>[17]</sup> and/or the differentiation into resident cells.<sup>[16b]</sup> However, even though there are some promising results, direct transplantation of cells still presents some disadvantages such as limit availability of the source of cells, cells culturing before implantation, invasive surgery procedures and low viability of cells.<sup>[18]</sup>

To overcome these issues, the ideal scaffold should be able to recruit endogenous Mesenchymal Stem cells towards the implant site, allow their infiltration and support their proliferation and differentiation; moreover, this kind of approach focuses on stimulating the body's own response and regenerative capacities.<sup>[19]</sup>

A substantial recruitment of MSC may be achieved with a local release of chemokines.<sup>[20]</sup> These are chemotactic signaling molecules, which play an important role in the initial phase of cells homing and engraftment within the implanted scaffold. In particular, Stromal cell-Derived Factor-1 $\alpha$  (SDF-1 $\alpha$ ), which has been shown to be chemotactic for MSC, is an interesting candidate and could be used to guide Stem cells towards the implanted scaffold.<sup>[19b, 21]</sup>

Herein we report the design, synthesis and mechanical characterization of a biocompatible nanocomposite hydrogel by introducing mesoporous silica nanoparticles able to release SDF-1 $\alpha$ , to study the recruitment of stem cells towards the releasing site.

The polyamidoamines-based hydrogel network is covalently cross-linked with mesoporous silica nanoparticles (MSNs) which also function as nanocontainers<sup>[22]</sup> for the release of SDF-1 $\alpha$ .

## 4.2 Design and synthesis of the nanocomposite scaffold

### 4.2.1 Study design

MSNs (i.e. nanostructured components of the nanocomposite hydrogel) were synthesized and their surface was functionalized with pentaethylenhexamine, in order to obtain amino functionalized mesoporous silica nanoparticles, NH<sub>2</sub>-MSNs, bearing reactive primary amine as terminal groups.

Then, the nanocomposite scaffold, namely MSN-hydrogel, was synthesized by covalent cross-linking of the obtained NH<sub>2</sub>-MSNs to the polymeric backbone of the hydrogel. Pristine hydrogel (i.e. without embedded MSNs), with the same chemical composition of the MSN-hydrogel, was also synthesized for comparison purposes.

The viscoelasticity properties of both the scaffolds were evaluated to assess their mechanical suitability for cells proliferation and migration. Once this was proved, we checked the ability of both the hydrogels to support adhesion and proliferation of mouse bone marrow mesenchymal stem cells (mBM-MSC) for 7 days.

Given the promising results obtained, we designed a dual hydrogel system to induce chemotaxis *in vitro* through the release of SDF-1 $\alpha$  from the embedded MSNs, referred to as SDF@CCH. An additional platform was synthesized also in this case for comparison purposes, using NH<sub>2</sub>-MSNs not loaded with SDF-1 $\alpha$  (CCH).

Finally, we tested the scaffolds *in vivo* as subcutaneous implants in mice to evaluate the tissue response in the acute inflammatory window (3-7 days).

### 4.2.2 Mesoporous silica nanoparticles: the nanostructured components

MSNs were selected as nanostructured components of the nanocomposite hydrogel because of their many distinctive features such as stable and rigid frameworks, high surface areas, versatile surface chemistry,<sup>[23]</sup> which allows for different kinds of functionalization, and



tunable pores volume.<sup>[24]</sup> In addition, the nanoparticles incorporated into the scaffolds had to perform as reservoirs of SDF-1 $\alpha$ . Thus, the choice of MSNs was dictated also by their ability to load, even with high capacity, various types of cargos.<sup>[10c, 25]</sup>

MSNs were synthesized following a modified reported procedure.<sup>[26]</sup> In particular, the synthesis was based on a co-condensation of 3-aminopropyltriethoxysilane (APTES) and the silicon alkoxide precursor, tetraethyl orthosilicate (TEOS), in the presence of hexadecyltrimethyl-ammonium bromide (CTAB), which is a cationic surfactant acting as template for the mesoporous structure, as shown in Figure 4.1.

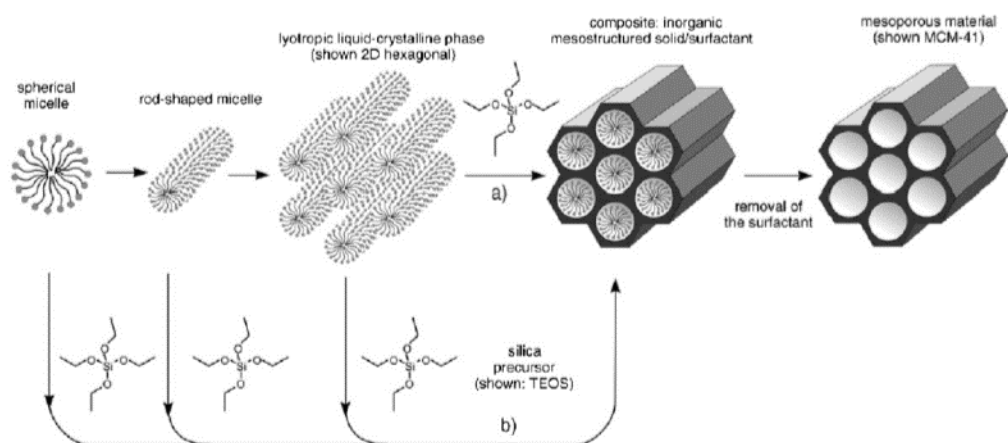


Figure 4.1 Scheme of the synthesis of MSNs with CTAB surfactant micelles as template, adapted from F. Tang, L. Li, and D. Chen, *Adv. Mater.*, **2012**, 24, 1504–1534

The hydrolysis of TEOS, followed by the surfactant-templated polycondensation of the monomers, afforded the desired meso-structured spherical nanoparticles, with a diameter of around 130 nm, as confirmed by dynamic light scattering, DLS, measurements (Figure 4.2a). The ordered porous inner structure was visualised by transmission electron microscopy (TEM, Figure 4.2b). Additionally, Small-Angle X-ray Scattering (SAXS) was performed to gain information on the characteristic distances of partially ordered structures and pore sizes.<sup>[27]</sup> Indeed, it was possible to identify the porous-structured hexagonal lattice of the obtained MSNs from the SAXS trace, by comparing it with patterns belonging to specific geometries. In particular, the presence of the typical 2D hexagonal lattice of the channels of the MSNs was confirmed by the occurrence of the three diffraction peaks tabulated for such porous geometry.

SAXS technique, as well as N<sub>2</sub> adsorption analysis (Figure 4.3c) were used to gain information on the pores size, which were determined to be 3 nm in diameter.

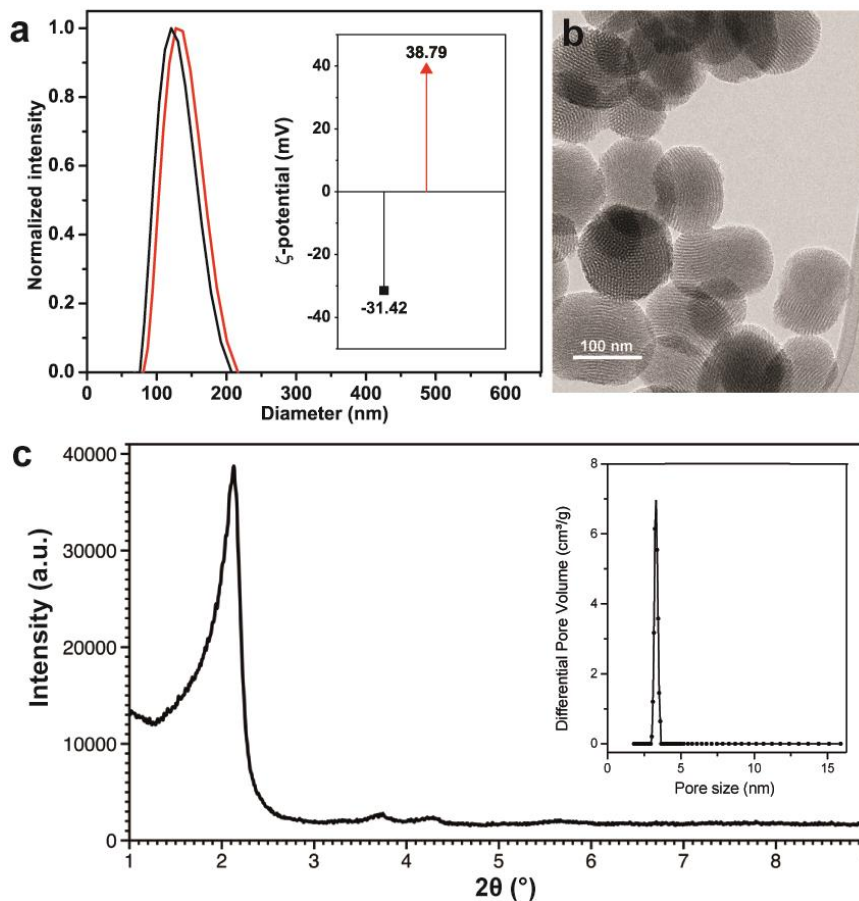


Figure 4.2 DLS of MSNs (black), and NH<sub>2</sub>-MSNs (red), and in the insert:  $\zeta$ -potential values for MSNs in black and NH<sub>2</sub>-MSNs in red (a); TEM (b) of MSNs, showing the porosity and shape of the silica particles; SAXS pattern (c) of the MSNs after removal of the templating surfactant. In the insert: N<sub>2</sub> adsorption analysis, showing a pores size distribution of the MSNs after removal of the templating surfactant.

Consequently, the obtained MSNs were treated with pentaethylenhexamine, previously coupled to chloropropyl dimethylmethoxysilane, in order to functionalize their surface with aliphatic chains bearing secondary amines along the chain and reactive primary amine groups as terminal. A schematic representation of the MSNs functionalization is shown in Figure 4.3

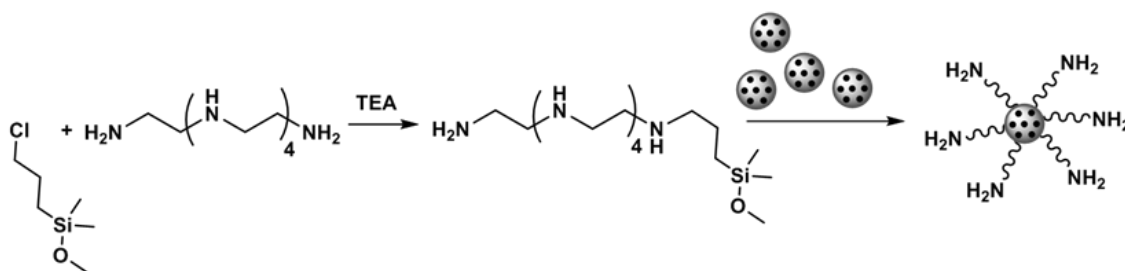


Figure 4.3 Reaction scheme of the amino-functionalization of MSNs, yielding  $\text{NH}_2$ -MSNs.

The surface functionalization was confirmed by the shift from negative (-31.42 mV) to positive (+38.79 mV) values of the  $\zeta$ -potential, Figure 4.2a (insert).

The obtained amino-functionalized nanometer-size particles ( $\text{NH}_2$ -MSNs) were then washed several times and their shape, morphology and size were confirmed by scanning electron microscopy (SEM, Figure 4.4a). The extent of the organic surface functionalization was determined by thermogravimetric analysis (TGA, Figure 4.4b) to be 25.25 wt%, corresponding to the weight loss between 200 and 550 °C.

The average number of amino groups on the surface of  $\text{NH}_2$ -MSNs was determined using a mathematical calculation based on thermogravimetry analysis data and  $\text{N}_2$  adsorption data (details in the experimental paragraph 4.8.2). Knowing that the weight loss observed by TGA is originated from the amino functionalization, we could estimate the average number of amino group per gram of sample and finally per particle, which was found to be  $4.98 \times 10^5$ . This number is consistent with other reported particle functionalization calculations.<sup>[28]</sup>

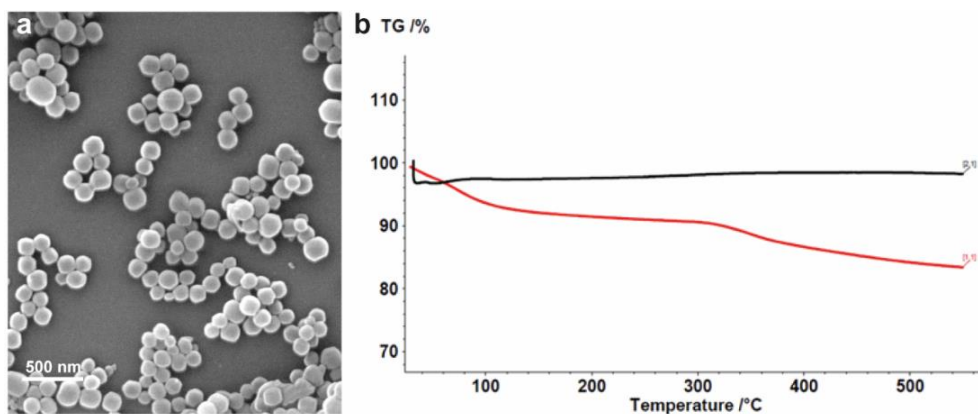


Figure 4.4 SEM image of  $\text{NH}_2$ -MSNs, showing the monodispersity particles (a) and TG traces of MSNs (black) and  $\text{NH}_2$ -MSNs (red); the used temperature program was dynamic heating from 25 °C to 550 °C (10.0 K/min) followed by an isothermal step of 30 min at 550 °C.

#### 4.2.3 Synthesis and characterization of the scaffolds

The synthesis of the nanocomposite hydrogel, MSN-hydrogel, was achieved by covalent cross-linking of  $\text{NH}_2$ -MSNs to the polymeric backbone of the hydrogel.<sup>[29]</sup> Specifically the scaffold was composed by N,N'-methylene bisacrylamide (MBA), which is the  $\alpha,\beta$ -unsaturated carbonyl,  $\gamma$ -aminobutyric acid, which is the amine co-monomer, and pentaerythritol hexamine (PEHA), that was added to further cross-link the network.

In the present study, we showed how we could obtain a soft and deformable scaffold, ideal for cells proliferation and migration, by using amino-functionalized mesoporous silica nanoparticles as cross-linkers of the hydrogel.

Thus, the synthesis of the MSN-hydrogel was designed to obtain a homogeneous nanocomposite, through surface-grafting of the poly amido-amine chains onto the aminated nanoparticles,  $\text{NH}_2$ -MSNs. To do so, we carried out the polyaddition of amines with MBA in the presence of the  $\text{NH}_2$ -MSNs. In particular, amino groups on MSNs were reacted with the unsaturated moiety of MBA through the aza-Michael addition, to form secondary or tertiary amines.

To prepare MSN-hydrogels a water suspension of  $\text{NH}_2$ -MSN was added to a solution of MBA and  $\gamma$ -aminobutyric acid, that was lastly further cross-linked with pentaerythritol hexamine (Figure 4.5). The ratio between the monomers was carefully evaluated to obtain a self-standing material, and the amount of cross-linker was the minimum possible, in addition to the cross-linking MSNs, to obtain a complete formation of the polymeric network.

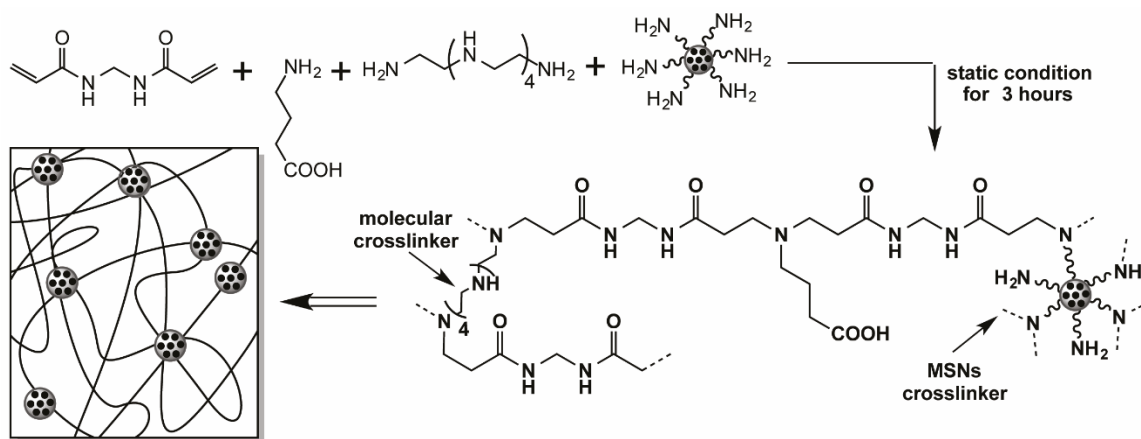


Figure 4.5 Scheme of the synthesis of MSN-hydrogel, obtained by covalent cross-linking of  $\text{NH}_2$ -MSNs to the polymeric network.

The synthesis proceeded without any additional base or catalyst and further reaction of this mixture in static conditions led to the formation of the transparent and self-standing MSN-hydrogel, which was observed after 3 hours. The mild reaction conditions, as well as the biocompatibility of the final product, enabled this hydrogel nanocomposite scaffold to be efficiently applied *in vivo*.

“Inverted test tube method” was used as a simple and direct way to confirm gelation (Figure 4.6a) and pores diameter were observed to be ranging between 20-70  $\mu\text{m}$  (Figure 4.6b,c).

The content of MSNs in MSN-hydrogel was calculated from thermogravimetric analysis to be 4 wt% of the total weight of the scaffold (Figure 4.6d), corresponding to an initial water suspension of 1 mg/ml of  $\text{NH}_2$ -MSNs. This resulted to be the optimal particles concentration to be effective on the mechanical properties of the scaffold. However, a higher concentration (e.g. more than 2 mg/ml) led to visible aggregates in the initial water dispersion and thus was discarded.

It is worth noting that in our approach, the  $\text{NH}_2$ -MSNs are covalently bound to the hydrogel backbone and they exert an important structural role, differently to what has been reported in other studies<sup>[30]</sup> where nanoparticles are simply dispersed into the polymer networks and used as physical fillers. The  $\text{NH}_2$ -MSNs act as cross-linker agent of the scaffold due to the amino-functionalization on their surface and thus of several amino-reacting groups on the same object.<sup>[31]</sup>

Moreover, the absence of functionalization and therefore the use of nanoparticles as simple fillers, could lead to a phase separation within the material (organic and inorganic phase separation), and therefore the structural improvement due to the nanoparticles is lost.<sup>[11, 32]</sup>

Indeed, the use of naked nanoparticles could provoke the lack of adhesion between the filler and polymer chains. This can cause the formation of nanoparticles aggregates, thus resulting in an early failure at the interface between the nanoparticles and the polymeric network and then in changes of the physical and mechanical properties of the final nanocomposite.

Instead, our approach enables the transfer of mechanical forces and physical properties within the cross-linked structure, because of the covalent cross-linking between the functionalized MSNs and the polymer network, as shown by rheological analysis (paragraph 4.3), where there is no indication of phase separation or loss of structural integrity

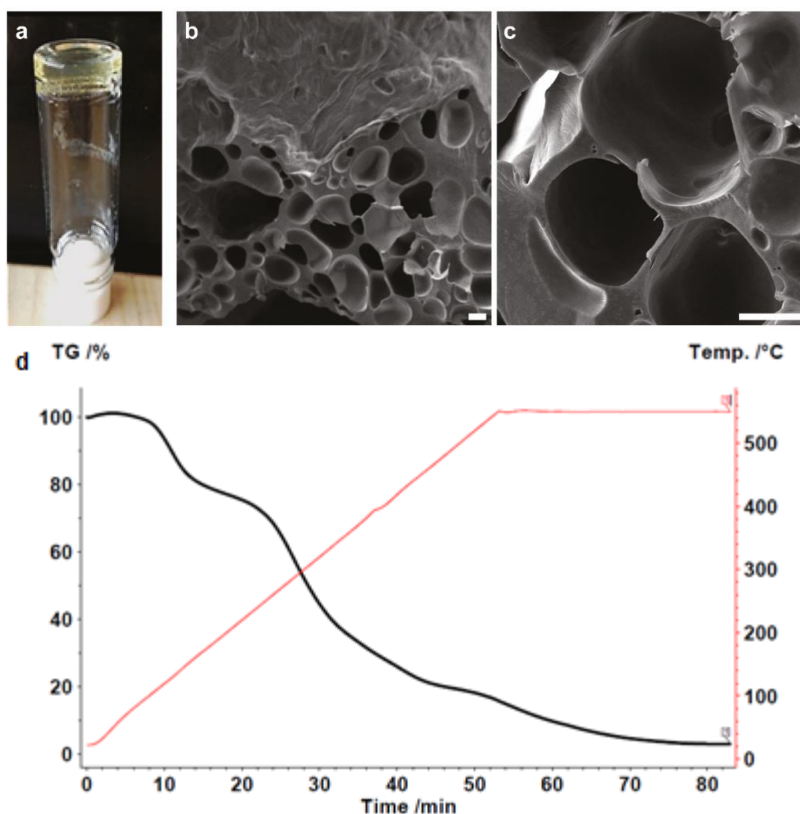


Figure 4.6 Inverted-vial test (a); SEM image of MSN-hydrogel (b) and its higher magnification (c), scale bar is 20  $\mu\text{m}$ ; TG pattern of MSN-hydrogel showing the weight loss corresponding to the organic part of the scaffold (d). The used temperature program was dynamic heating from 25  $^{\circ}\text{C}$  to 550  $^{\circ}\text{C}$  (10.0K/min) followed by an isothermal step of 30 min at 550  $^{\circ}\text{C}$ .

It has been reported that hydrogels prepared with inorganic nanoclays embedded into the polymeric structure, are very elastic and have much better mechanical properties than hydrogels cross-linked only chemically.<sup>[33]</sup>

For comparison purposes, we synthesized a pristine hydrogel, as described in chapter 2, without MSNs, the chemical composition of which being the same of the described MSN-hydrogel.

The nanoparticles loaded into the hydrogels did not affect the hydrogel properties such as gelation time and morphology, which remained essentially unchanged as compared to pristine hydrogel. Nonetheless, we could obtain better elastic and mechanical properties compared to hydrogels cross-linked only chemically.

Furthermore, we investigated the swelling degree at equilibrium (EDS) of the synthesized MSN-hydrogel and MSN-free hydrogel, since the swelling of hydrogel in water and

physiological solutions affects the transport of oxygen, nutrients and growth factors, which are essential for cells survival and growth.<sup>[34]</sup>

EDS of MSN-hydrogel was found to be 1330%, much higher than for MSN-free hydrogel (345%). The significant difference of swelling degree between the MSN-hydrogel and MSN-free hydrogel demonstrated that the embedding of MSNs in the polymeric matrix had a strong effect on the material's ability to adsorb and store water.

Moreover, we observed that both the hydrogels (pristine and MSN-hydrogel) exhibited self-adhesive properties, being able to adhere to each other without the need of additional external stimuli, after they were cut into pieces. Figure 4.7 shows that we were able to connect several blocks of pristine hydrogel (transparent) and MSN-hydrogel (blue stained), that were previously sliced to expose fresh surfaces, by pushing the pieces together so that these surfaces came into contact. The resulting worm-like structure was able to withstand its weight when suspended vertically from tweezers.

This behavior was attributed to the formation of new hydrogen bonds across separate hydrogel pieces, given especially from the side chains containing polar functional groups.

This property was exploited for the formation of a dual system hydrogel, namely concentric cylinder hydrogel, where the MSN-hydrogel was bound to the pristine hydrogel to obtain a single device, as is described in paragraph 4.5.

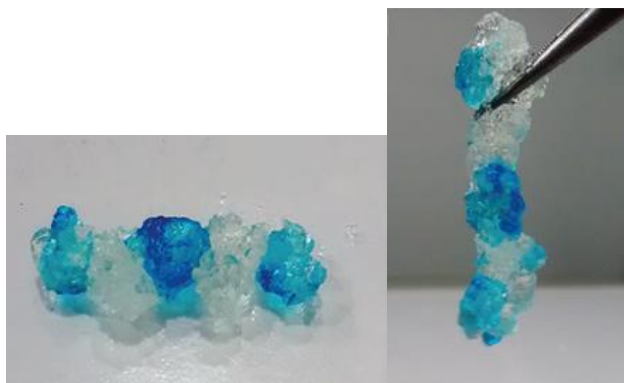


Figure 4.7 Example of adhesive behavior between pieces of pristine hydrogel (transparent) and MSN-hydrogel (blue, stained with Methylene blue).



### 4.3 Rheological study

Rheological tests were performed by our collaborators, Professor Francisco Monroy and Dr. Ivan Lopez-Montero, at Universidad Complutense de Madrid.

In order to study the viscoelasticity of the hydrogels developed, a comprehensive shear rheological characterization was performed. To mimic the physical conditions in the biological environment, the studied hydrogels were swollen in equilibrium with excess of water.

Figure 4.8a shows the stress–strain curves obtained for pristine hydrogel and MSN-hydrogel under oscillatory shear performed at constant frequency of 1 Hz. The stress responses are both characterized by an initial linear regime that reaches a plastic plateau above a yield strain,  $\gamma_Y \approx 0.2$  (20% strain). Nonlinear effects are detected at deformations above  $\gamma_C \approx 0.2$ , particularly a plastic yield is observed due to stress softening. Figure 4.8b represents the shear response as a function of the strain rate as obtained from Figure 4.8a. Both pristine hydrogel and MSN-hydrogel presented a prototypical plastic-like behavior.<sup>[35]</sup> In this case, the shear modulus,  $G'$ , remains constant up to shear rates  $d\gamma/dt \approx 0.1 \text{ s}^{-1}$  and then decreases monotonically as the strain rate increases above a critical rate that corresponds to the yield point,  $(d\gamma/dt)_C = \omega\gamma_Y$ . The loss modulus,  $G''$ , shows a distinctive dissipation peak before it decreases at strain rates higher than that corresponding to the yield point. The recorded absolute values of  $G'$  and  $G''$  are higher for pristine hydrogel than for MSN-hydrogel in the whole range of strain rates considered. In other words MSN-hydrogel is softer and less viscous, i.e. more deformable than pristine hydrogel, resulting in a better matrix for mechanically favored cell migration, at least at strain rates typical for cell growth applications.

To discuss the viscoelasticity of swollen hydrogels in a regime of shear deformations comparable to the small strain developed by the growing cells, we have performed a rheological characterization in the linear regime at strain amplitude  $\gamma = 1\%$  and  $\omega = 0.01 \text{ s}^{-1}$ , corresponding to a strain rate of  $10^{-4} \text{ s}^{-1}$ , well below the yield point (see Figure 4.8a). Being the value inside the linear regime, similar values of  $G'$  and  $G''$  would be obtained even at lower strain rates.

Moreover, since cells growth temperature is  $37^\circ \text{ C}$ , Figure 4.8c shows the  $G'$  and  $G''$  values as a function of temperature at a strain rate  $= 10^{-4} \text{ s}^{-1}$ , compatible with the very slow strain rate of growing cells (see below). Pristine hydrogel is observed to weakly stiffen upon heating,



whereas  $G''$  remains almost constant. However, in the case of MSN-hydrogels, an irreversible solid to fluid softening transition is observed upon heating. The hydrogel starts to melt at 60 °C ( $G' = 0$ ), and no shear rigidity is recovered under further cooling. Regarding dissipation, a slight decrease in  $G''$  is observed as temperature increases, which is compatible with the softening transition. At 37° C, MSN-hydrogel still preserves its structural integrity as a soft solid and behaves as a pasty material with a relative high structural rigidity rather than a viscous fluid ( $G' > G'' > 0$ ). At this temperature, the values of shear viscoelastic moduli are  $G' \approx 200$  Pa and  $G'' \approx 7$  Pa, one order of magnitude lower than the corresponding shear moduli of pristine hydrogel. In terms of energy dissipation, MSN-hydrogel is also more fluid than pristine hydrogel, as shown in Figure 4.8d. As derived from the  $G''$  data, the shear viscosity of MSN-hydrogel is two order of magnitude lower than viscosity of pristine hydrogel over the whole range of strain rates.

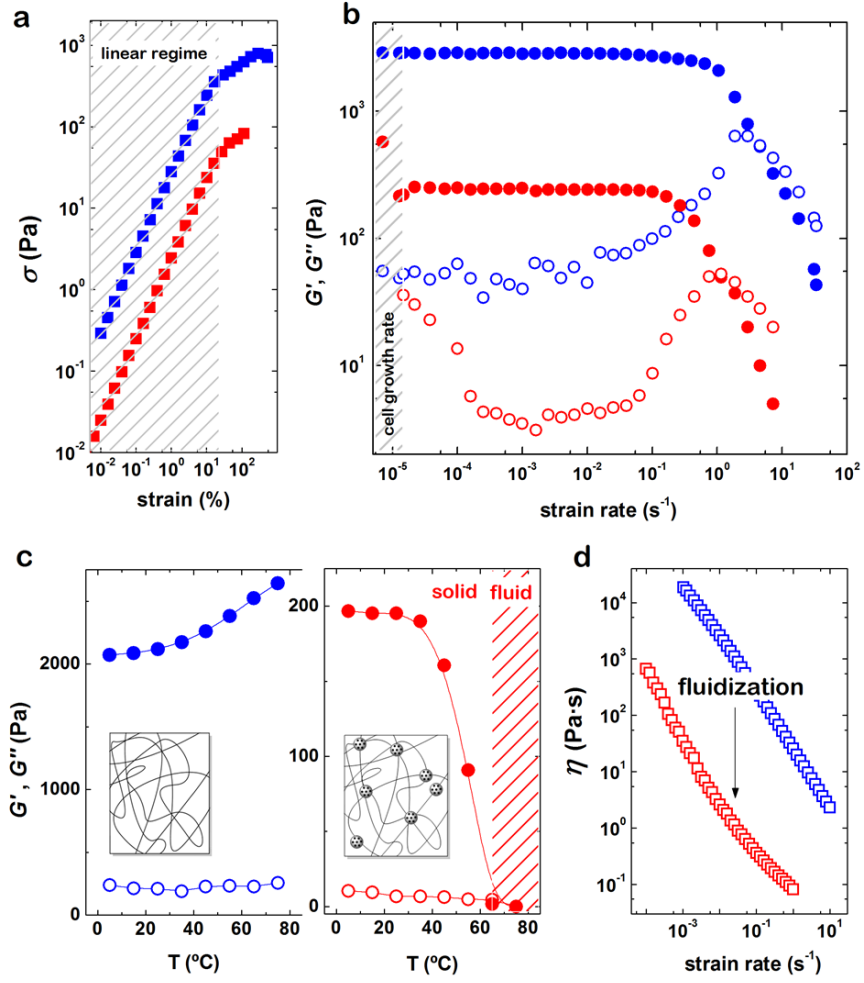


Figure 4.8 Stress-strain plot of pristine hydrogel (blue) and MSN-hydrogel (red) under oscillatory shear (a); shear modulus,  $G'$  (solid symbols) and loss modulus,  $G''$  (open symbols) as a function of strain rate for pristine hydrogel (blue) and MSN-hydrogel (red) (b). Typical shear rates slower than  $2 \cdot 10^{-5} s^{-1}$ , well within the linear viscoelastic regime, are involved in experiments with migrating cells (dashed region).  $G'$  and  $G''$  plotted as a function of temperature for pristine hydrogel (blue) and MSN-hydrogel (red) (c). Shear-thinning behavior of the viscosity of pristine hydrogel (blue) and MSN-hydrogel (red) as a function of strain rate (d).

#### 4.4 *In vitro* cells adherence and proliferation

In order to investigate the suitability of the developed hydrogel scaffolds for tissue engineering purposes, we checked their ability to support adhesion and proliferation of mBM-MSC, for 7 days.

We seeded and cultured the cells onto pristine hydrogel and onto MSN-hydrogel, to study the cells viability and understand the role of the nanoparticles. Figure 4.9a shows a representative example of mBM-MSC grown on the surface of MSN-hydrogel (i) and onto pristine hydrogel (ii). When compared with pristine hydrogel, MSN-hydrogel shows a higher amount of adhered and proliferated cells after 7 days of culture. Moreover, mBM-MSC grown onto MSN-hydrogel presented a typical elongated stem-cell-like phenotype. Figure 4.9b also shows that cells are present in the whole depth of the scaffold (800  $\mu\text{m}$  within 7 days), thus confirming a 3D proliferation over time.

These qualitative estimations on cells viability were further confirmed by the quantitative alamarBlue assay, that was performed to evaluate the metabolic activity and viability of mBM-MSC at each time point on both 3D cell culture systems, i.e. pristine and MSN-hydrogel, over a period of 7 days (Figure 4.9c).

Cells viability in pristine hydrogel grew only slightly after 7 days (53%) in comparison to day 1 (46%); however, in the case of MSN-hydrogel, we registered an increase in cellular activity of 25% after 7 days of culture (72% at day 7 compare to 47% at day 1). These results indicate that there is no cytotoxic effect on mBM-MSC viability from both hydrogel systems. Moreover, the assay showed a significantly increase in cell number after 7 days in the MSN-hydrogel compared to pristine hydrogel.

The introduction of MSNs in the polymeric structure of the scaffold can support and enhance the hydrogel cell attachment and proliferation.

To define the relevant time window of shear rheology data, a strain rate of mBM-MSC growth can be estimated from Figure 4.9b, as  $\Delta L \cdot \ln 2 / (L_0 \cdot t) = 10^{-5} \text{ s}^{-1}$ , being  $\Delta L$  the growth length (800  $\mu\text{m}$ ),  $L_0$  the size of a single mBM-MSC (around 50  $\mu\text{m}$  in length) and  $t$  the experimental growth time (7 days). This is in agreement with the strain rate calculated from the doubling time of cells,  $t = 28\text{-}30$  hours, which defines the time taken for a single cell to divide ( $\Delta L = L_0$ ).

Moreover, according to rheological studies, the displacement of an object (i.e. a cell) that is embedded within a hydrogel is optimized for softer scaffolds.<sup>[36]</sup> We observed that the shear-induced fluidization of MSN-hydrogel favors the movement of mBM-MSC during cell growth and migration.

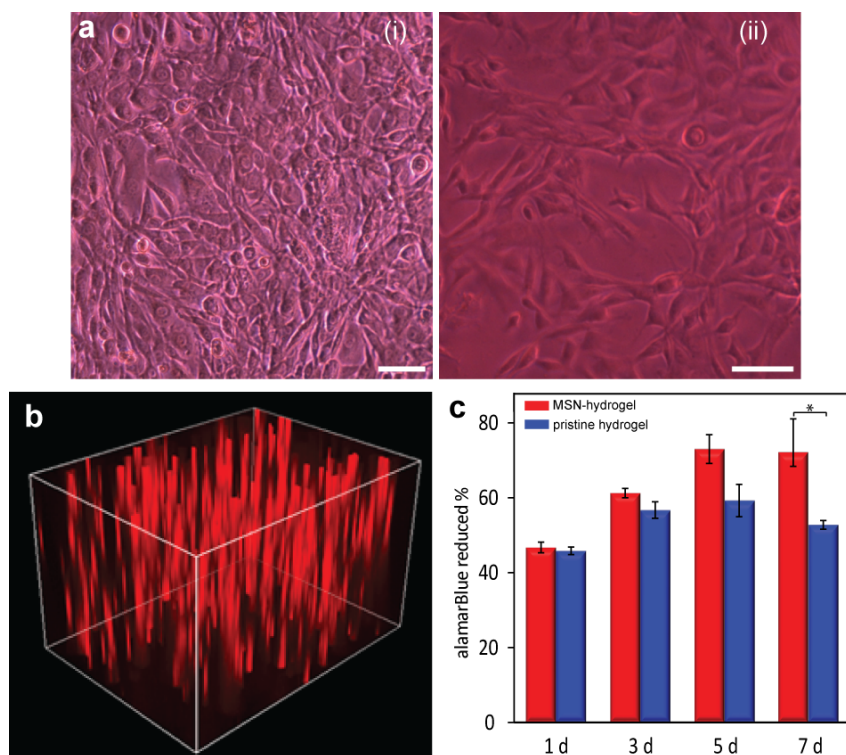


Figure 4.9 Brightfield images (10x) of mBM-MSC growing onto MSN-hydrogel (i) and pristine hydrogel (ii) after 7 days (a); scale bar is 50 μm. mBM-MSC growing in 3D after 7 days (b); scaffold imaged dimensions are width: 1.3 mm; height: 800 μm; depth: 860 μm. Viability assay (AlamarBlue test; mean ± standard deviation, n = 3; \*p<0.05) of mBM-MSC (c) onto the synthesized hydrogel scaffolds (MSN-hydrogel in red and pristine hydrogel in blue).

Thus, embedding MSNs into the hydrogel undertakes a double function. The nanoparticles act as a cross-linker that causes hydrogel softening without structural failure, therefore enabling cell infiltration into a solid matrix. Furthermore, MSNs act also as a lubricant, able to reduce viscous drag in the moving cells under slow shear flow. Therefore, we assume that MSN-hydrogels are mechanically improved for cell attachment and viability and provide a suitable substrate for cell growth. Their high porosity allowed cells to migrate throughout the scaffolds, while maintaining their viability.

#### 4.5 Concentric cylinder hydrogel and homing of stem cells *in vitro*

We developed a dual hydrogel system, named concentric cylinder hydrogel (CCH) in order to test the effect of SDF-1 $\alpha$  release from MSN-hydrogel and induce chemotaxis *in vitro*. The approach was to spatially separate the hydrogel containing the SDF-1 $\alpha$  delivery system from the part where the cells were initially seeded, and observe the cell migration upon the release of the chemokine. We have developed a simple device composed of an inner MSN-hydrogel cylindrical core (d = 0.8 cm; final desired volume of 200  $\mu$ l) and an outer cylinder made of pristine hydrogel resulting in a dual structured material. MSNs previously loaded with SDF-1 $\alpha$  (1.7  $\mu$ g of SDF-1 $\alpha$  effectively loaded into 1 mg/ml of nanoparticles), were used for the synthesis of MSN-hydrogel core, namely SDF@MSN-hydrogel. A schematic representation of the synthesis of this platform, SDF@CCH, and an image of it are depicted in Figure 4.10.

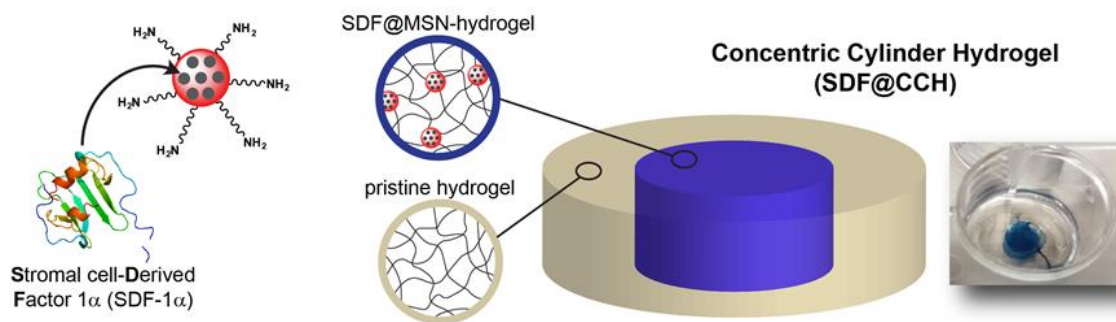


Figure 4.10 Schematic representations of SDF-1 $\alpha$  loading into MSNs, of concentric cylinder hydrogel, SDF@CCH, and photograph of the obtained SDF@CCH

Briefly, a pristine hydrogel was synthesized as previously described in a cylindrical shape mold. Once gelation took place, an inner cylindrical core of the desired diameter was removed with a sterile biopsy punch and the SDF@MSN-hydrogel mixture was gently placed in the inner cavity thus formed and let to gel (blue cylinder, Figure 4.10) and adhere to the outer pristine hydrogel ring (see paragraph 4.2.3).

When SDF@CCH was completely gelified, approx. 50,000 mBM-MSC stained with the red fluorescent dye Vybrant DiD, were seeded at the external edges of the platform.

The cells migration from the edges of the scaffold to the inner core was monitored for 7 days by means of optical microscopy (Figure 4.11a) and SEM (Figure 4.11b).



In particular, Figure 4.11a shows some indicative brightfield images of mBM-MSCs growing onto SDF@CCH and CCH, at day 3 and day 7. This additional CCH system was synthesized for comparison purposes, using empty  $\text{NH}_2$ -MSNs.

The first column, images (i), (iv) and (vii), collected with 4x magnification, displays the interface between the outer part and the inner core of the nanocomposite platforms; these two parts are then depicted with an higher magnification, 10x, in the second and third column, images (ii), (v) and (viii), and images (iii), (vi) and (ix).

Interestingly, already at day 3 it was possible to appreciate the directionality of cells movement, from the outer part of the scaffold towards the inner core of the scaffold (iii, vi). This indicates a movement which follows the gradient of the released SDF-1 $\alpha$ . After 7 days, the central core of SDF@CCH showed abundant presence of cells (vi), whereas at day 0 this part of the scaffold was completely empty.

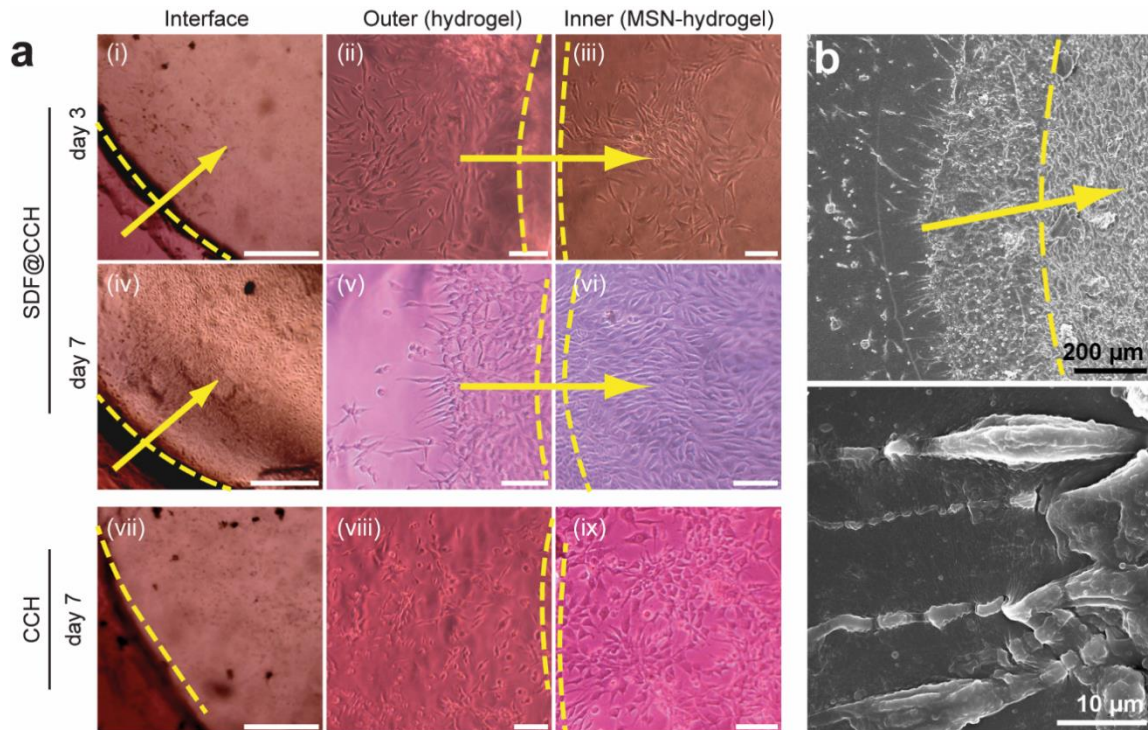


Figure 4.11 Brightfield images of mBM-MSCs growing onto SDF@CCH and CCH (a); left column scale bar is 500  $\mu\text{m}$ , central column and right column scale bars are 50  $\mu\text{m}$ . SEM images (b) of mBM-MSCs migration onto the SDF@CCH after 7 days from the seeding onto the scaffold.

Instead, cells growing onto CCH system (i.e. similar structured platform non-releasing SDF-1 $\alpha$ ) eventually reached the material's core after 7 days (ix), but don't show any migration process, as can be seen from the different disposition and cell density.

To visualize the movement in 3D of mBM-MSK towards the SDF@CCH inner core, fluorescence microscopy in z-stack mode was utilized, Figure 4.12a. Moreover, it was possible to track the cells movements over a period of 6 hours (Nikon NIS-Elements 4.3 software) and plotting their speed and directionality vectors onto a graph, confirming indeed the uniform migration (Figure 4.12b).

Thus, we could conclude that SDF-1 $\alpha$  released from MSN-hydrogel is able to induce mBM-MSK cell migration across the SDF@CCH system.

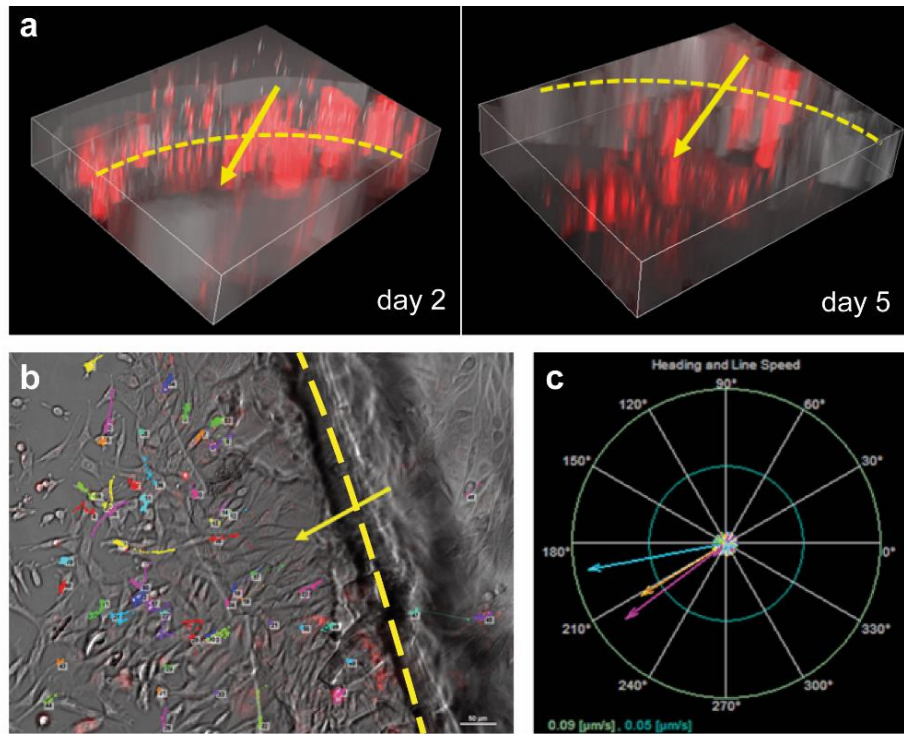


Figure 4.12 Migration of red-stained mBM-MSK in 3D onto SDF@CCH, after 2 days and 5 days from the seeding (a); size of scaffolds imaged: width=700  $\mu\text{m}$ , height=525  $\mu\text{m}$ , depth=102  $\mu\text{m}$ . Tracking of cells movements obtained with Nikon NIS-Elements 4.3 software, showing the directionality of the mBM-MSK migrating onto the SDF@CCH (b) and graph of their speed and direction vectors (c). Yellow dashed lines indicate the interface between the outer and inner parts of the SDF@CCH and yellow arrow indicating the directionality of the cells movement.

## 4.6 *In vivo* response to the nanocomposite hydrogels

### 4.6.1 *Importance of in vivo evaluation for novel implantable biomaterials*

A central requisite for a newly developed implantable biomaterial is its biocompatibility, i.e. its ability to perform in a specific situation with an appropriate host response.<sup>[37]</sup> This necessitates an *in vitro* and *in vivo* evaluation experiments to test their local and systemic effects on the host.<sup>[38]</sup>

Particularly, synthetic polymeric materials used for biomedical applications should be biocompatible and should not elicit acute immune-responses when implanted.<sup>[39]</sup>

Implanted medical devices are essential for tissue engineering development and for modern medical practice; however, it is important that they do not interact with the host body as foreign objects, i.e. encapsulated and walled off. Indeed, the host reactions at the injury site can include acute and chronic inflammation and foreign body reaction, which can lead to complications or even device failure.<sup>[40]</sup>

### 4.6.2 *In vivo* study

In this work, we have used *in vitro* cell culture tests to screen the cytotoxicity of the hydrogels developed to be used as implantable scaffolds. This allowed us to directly investigate the interaction between the cell and the hydrogels, to gain insights on the biological response of the tissue environment on which the hydrogels would have been implanted.

Mesenchymal stem cells adhesion and proliferation onto the synthesized scaffolds was already a good indication of the potential successful incorporation of the hydrogels into the body.<sup>[41]</sup>

By studying the effects of the release of SDF-1 $\alpha$  *in vitro* on mBM-MSc, we could acquire an understanding of the cellular reactions to the synthetic biomaterial and possibly predict, with the limitations of an *in vitro* system, the initial material–host interactions<sup>[42]</sup> that occurs upon implantation.

Seen the promising *in vitro* cellular responses to polyamidoamines-based hydrogels and SDF-releasing nanocomposites, which showed no cytotoxicity and excellent bioactivity, we next evaluated the biocompatibility *in vivo*.

*In vivo* tests allow the implanted biomaterial to come into contact with cells and also provide interactions with blood, proteins, enzymes,... Even though biomedical materials have been



developed and used as implants for many years, earlier ones proved to be failures because of infections and biological reactions occurring *in vivo*.<sup>[43]</sup>

Many different evaluation techniques can be exploited to determine the *in vivo* response of potential biomaterials, in relation to the final desired application.<sup>[44]</sup>

The goal of our *in vivo* study was to determine the response of the host tissue to the implanted scaffolds in the acute inflammatory window (3-7 days). Thus, we based our investigation on the analysis of the interface between the hydrogels and the tissues, after 7 days from the implantation.

SDF@MSN-hydrogel as well as MSN-hydrogel and pristine hydrogel were synthesized in order to obtain the same cylindrical shape of 0.8 cm in diameter and 0.2 cm in thickness for all samples (Figure 4.13a).

The three hydrogel scaffolds were implanted subcutaneously in BALB/c mice, Figure 4.13b, as previously established<sup>[45]</sup> and the inflammatory response to the implants was evaluated one week after implantation. The animals were monitored over a 7-day-period and no loss of body weight in any of the mice was witnessed. After the observation period, the mice were sacrificed and upon removal of the implanted hydrogels, we observed that the hydrogels remained in place without significant volume and weight change (Figure 4.13c,d). Moreover, there were not macroscopic signs of inflammation or infection at the time of explant, thus indicating the biocompatibility of such hydrogels *in vivo*.

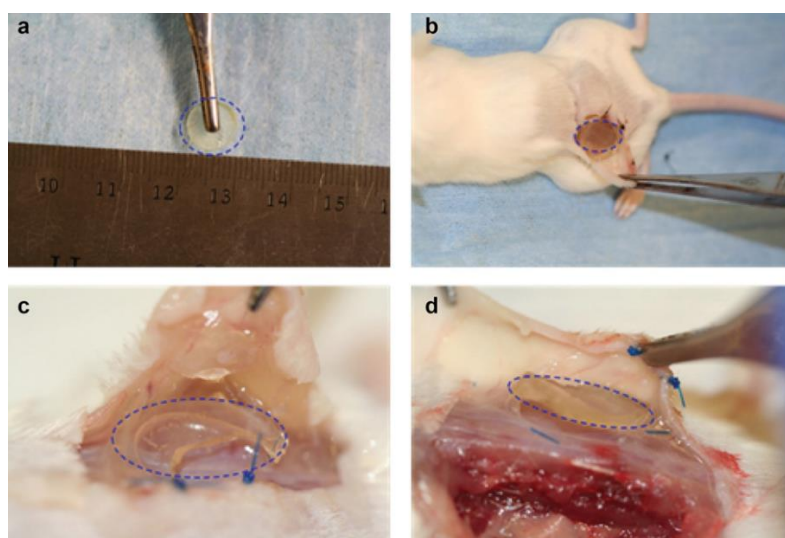


Figure 4.13 SDF@MSN-hydrogel implanted subcutaneously in BALB/c mice (a,b); the hydrogels remained in place (c), without significant change in volume and weight (d).

Since SDF-1 $\alpha$  has been previously reported as a powerful chemokine that enhances different regenerative processes,<sup>[46]</sup> we hypothesized that SDF-1 $\alpha$  released from hydrogels could affect the inflammatory phase after implantation. To evaluate tissue reactions to the artificial scaffolds in the acute inflammatory window, we performed histological analysis of the explanted hydrogels and surrounding tissues. This is one of the most common method used to evaluate the interface between the implant and the surrounding tissues.<sup>[44b]</sup> Only a good interaction between the material and the surrounding tissue can ensure its successful clinical translation and maximum patients' benefits.

Representative Haematoxylin and eosin (H&E)-stained images are reported in Figure 4.14 and show no obvious adverse chronic inflammatory process occurring, a part from the normal wound healing response to the materials.

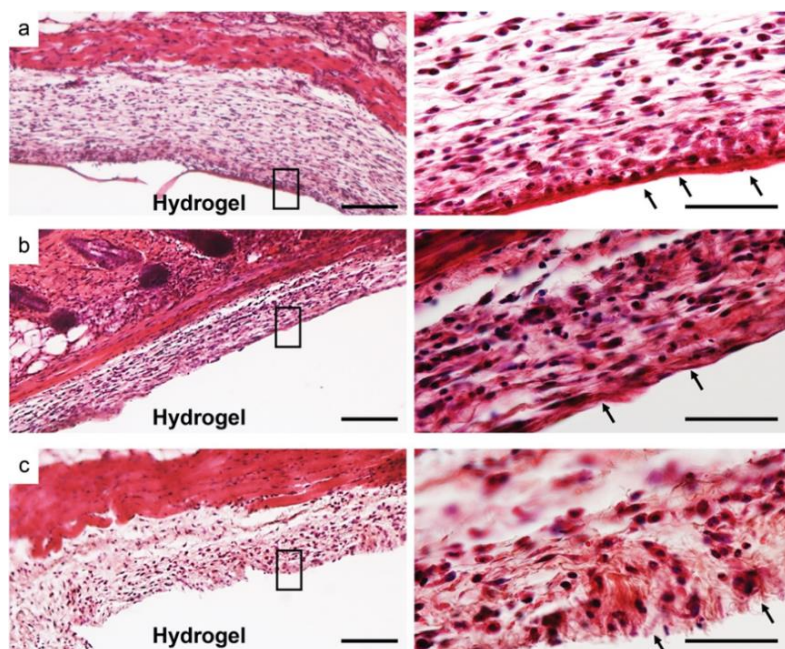


Figure 4.14 Histological staining of pristine hydrogel (a), MSN-hydrogel (b), and SDF@MSN-hydrogel (c) at 7 days after implantation. Black arrows indicate fibrotic capsule formation. SDF@MSN-hydrogel resulted the one with less thick and dense fibrotic capsule. Scale bar is 10  $\mu$ m.

In particular, explants analysis of pristine hydrogel and MSN-hydrogel at day 7 (Figure 4.14a,b) revealed the formation of a thin layer of fibrous capsule formed at the interface of the implants and the surrounding tissue, showing as a general trend a thicker layer for pristine hydrogel (ca. 25  $\mu$ m) than for MSN-hydrogel (ca. 12  $\mu$ m).

Interestingly, while presenting a thin layer of fibrotic deposition, comparable to the one generated by MSN-hydrogel implant, the SDF@MSN-hydrogel implant showed a less mature and less dense capsule around it (Figure 4.14c). These findings suggest that SDF@MSN-hydrogels did not elicit a substantial foreign-body reaction.

The lower inflammatory response of SDF@MSN-hydrogel is probably due to the presence of the SDF-1 $\alpha$  released from the scaffold, which caused a modulation of the inflammatory phase affecting the deposition of fibrous tissue, as reported elsewhere for other systems.<sup>[19b]</sup>

The outcome of our experiments showed a thin fibrous capsule formation for all three hydrogels, which was found particularly attenuated and less dense for SDF@MSN-hydrogels. SDF@MSN-hydrogel in particular generated a minimal inflammatory reaction when implanted *in vivo* and was responsible for modulating the tissue response to the scaffold.

## 4.7 Conclusions

We have successfully designed synthesized and characterized a nanocomposite hydrogel scaffold with the aim of recapitulate ECM features and be applied as implant for tissue engineering applications.

The hydrogel nanocomposite showed unique mechanical properties that enabled the scaffold to support the growth and migration of stem cell *in vitro*. The further functionalization of this versatile platform allowed induction of chemotaxis *in vitro* through the release of an active molecule, SDF-1 $\alpha$ .

Finally, we tested the scaffolds *in vivo* in the acute inflammatory window (3-7 days). Our results showed that all the hydrogels were biocompatible in the studied period and SDF@MSN-hydrogel was responsible for modulating the tissue response to the scaffold.

These findings suggest that the novel nanocomposites hydrogel scaffold has significant potential to improve the host tissue response towards the implant.

Furthermore, the platform could be potentially functionalized with active molecules for specific application, in order to activate different physiological responses.

## 4.8 Experimental section

### 4.8.1 *Synthesis and amino-functionalization of mesoporous silica nanoparticles*

The synthesis of mesoporous silica nanoparticles was performed as follows: in a 250 ml round bottom flask cetyl trimethylammonium bromide (CTAB; 0.5 g) was dissolved in 240 mL of sodium hydroxide solution (0.2 M) at 80 °C. Then, 2.5 mL of 0.88 M (1.833 g per 10 mL) ethanolic tetraethyl orthosilicate (TEOS) and 3-aminopropyltriethoxysilane (APTES; 50  $\mu$ l) were added to the solution under vigorous stirring. After 1 h, the mixture solution was aged for at least 12 h. Few drops of hydrochloric acid solution (6 M) were added to the as-synthesized colloid with stirring at room temperature for 5 h, to remove surfactant. The surfactant extraction step was repeated several times to ensure complete removal of CTAB. The MSNs were then washed with ethanol twice and resuspended in absolute ethanol.

Consequently, in order to functionalize the surface of the MSNs, the obtained nanoparticles were treated with pentaethylenehexamine. In particular, in a 100 ml round bottom flask pentaethylenehexamine (10  $\mu$ l) was dissolved in 3 ml of ethanol, in presence of 3-chloropropyltrimethylmethoxysilane (10  $\mu$ l) and a few drops of triethylamine. The solution was stirred for 30 min at room temperature and then a suspension of 60 mg of the previously synthesized MSNs in 30 ml of ethanol was added and stirred at reflux overnight. This procedure yielded MSNs with a surface functionalization of aliphatic chains bearing secondary amines along the chain and reactive primary amine groups as terminal. Finally, these amino-functionalized MSNs (NH<sub>2</sub>-MSNs) were washed with ethanol and recovered by centrifugation.

### 4.8.2 *Calculation of the average number of amino groups on the particle surface*

The average number of amino groups on the surface of NH<sub>2</sub>-MSNs was determined by using a mathematical calculation based on thermogravimetry analysis data and N<sub>2</sub> adsorption data. Knowing that the weight loss observed by TGA is originated from the amino functionalization, we can further calculate the average number of amino group per gram of sample and finally per particle.

From the TGA analysis we could detect a total weight loss of 33.62%, of which 25.25% due to the organic functionalization (weight loss between 200 and 550 °C). Indeed, the first weigh

loss of 8.37%, is detected between 100 and 200 °C and corresponds to the water loss, caused by the moisture.

Thus, from this value we can calculate the actual dry weight of 100 g of particles (i.e. after the water loss) as:  $100\text{ g} - 8.37\text{ g} = 91.63\text{ g}$

The organic functionalization of the sample corresponds to a contribute of 25.25%, as mentioned. Thus  $25.25\% * 91.63\text{ g} = 27.56\text{ g}$

Considering that the total molecular weight of the organic functionalization is 273 g/mol, we can calculate the total mols of organic part per 1 g of particles, being 1.01 mmol/g

Then it is necessary to consider one single particle.

For this geometric calculation the particles are understood to be spherical and monodisperse, with a diameter of 130 nm. Thus, the volume can be obtained by the formula for volumes of spheres:  $4/3\pi*r^3 = 1149763\text{ nm}^3$

In this special case mesoporous particles, the different densities of bulk SiO<sub>2</sub> and porous SiO<sub>2</sub> must be taken into account. The literature density value for bulk amorphous SiO<sub>2</sub> is 2.20 g/cm<sup>3</sup>.<sup>[47]</sup>

Considering the pores volume of the sample, as obtained from N<sub>2</sub> adsorption analysis equal to 0.95 cm<sup>3</sup>/g, we can easily calculate the density of porous SiO<sub>2</sub> as:  $(1\text{ g} / 2.20\text{ g/cm}^3 + 0.95\text{ cm}^3/\text{g}) / 1\text{ g} = 1.40\text{ cm}^3/\text{g}$ . Thus, the total mass per mesoporous SiO<sub>2</sub> particle is  $8.19*10^{-16}\text{ g}$ . Therefore, 1 g of particles powder contains  $1.22*10^{15}$  particles. Then, the organic functionalization in 1 g of mesoporous SiO<sub>2</sub> particles is  $8.26*10^{-19}\text{ mol/particles}$ . Finally, using the amount of organic functionalization calculated by this procedure, the average number of amino groups per particle is obtained as  $N_A * 8.26*10^{-19}\text{ mol/particles} = 4.98*10^5$ . This number is consistent with other reported particle functionalization calculations.<sup>[28]</sup>

#### 4.8.3 Loading of SDF-1 $\alpha$

SDF-1 $\alpha$  was reconstructed in MilliQ water to a concentration of 0.01 mg/ml. 0.25 ml of this solution were further diluted to 1 ml, then 1 mg of nanoparticles was added and the suspension was sonicated for 2h to disperse the nanoparticles and discourage the formation of aggregates. This suspension was mixed overnight at 20 °C with a thermomixer (Thermomixer Compact, Eppendorf, Hamburg, Germany).

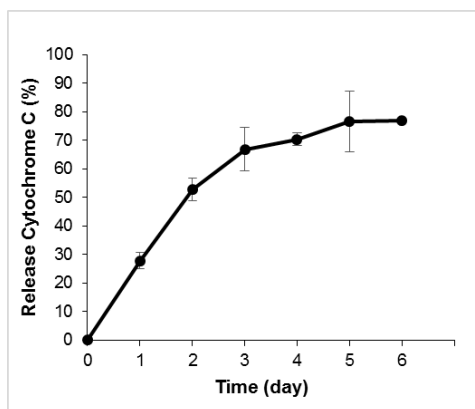
To evaluate the encapsulation efficiency of SDF-1 $\alpha$  in the nanoparticles, we measured the amount of the free chemokine in the supernatant by ELISA assay (Mouse CXCL12/SDF-1 alpha Quantikine ELISA Kit; R&D Systems, Minneapolis, MN, USA) and determined the efficiency by the following equation:

$$\text{Loading efficiency (\%)} = \frac{\text{Total amount of SDF added} - \text{free SDF}}{\text{Total amount of SDF added}} \times 100\%$$

The loading efficiency resulted to be 68%, which corresponds to 1.7  $\mu\text{g}$  of SDF-1 $\alpha$  loaded into 1 mg/ml of nanoparticles. The loaded NH<sub>2</sub>-MSN were used for the synthesis of the SDF@MSN-hydrogel.

The synthesis of the SDF@CCH core required an adjustment of the reagents amount to obtain a final volume of 0.2 ml, with a final amount of SDF-1 $\alpha$  of 0.34  $\mu\text{g}$  in the scaffold. The amount of SDF-1 $\alpha$  was planned on the basis of the release efficiency of the scaffold that were evaluated using Cytochrome C as model protein.

Briefly, 1.7  $\mu\text{g}$  of Cytochrome C was loaded into the scaffold during the preparation, as explained before for SDF-1  $\alpha$ , and the protein-loaded scaffold was put in PBS solution for the release test. At each time point (every 24h for 7 days) the solution was removed and the absorbance of Cytochrome C was quantified at 405 nm with a plate reader; the amount of released SDF-1 $\alpha$  was referred to the standard curve. PBS was refreshed at each time point. Our results indicated that approximately 50% of the loaded protein was released within 2 days, followed by a sustained release up to 6 days, for a total release of 77% of the initial loaded protein (see graph below).



Finally, it is possible to consider a cumulative release of SDF-1 $\alpha$  from the SDF@CCH corresponding to 77% of the effectively loaded amount, which results in a released level of



approx. 170 ng/ml over the studied period of 7 days. This amount was recently shown to be appropriate to induce chemotaxis *in vitro* and *in vivo* during the first week of implantation.<sup>[18a, 48]</sup>

#### 4.8.4 *Synthesis of MSN-hydrogel and pristine hydrogel.*

In a 25 ml round bottom flask N,N'-methylene bisacrylamide (MBA; 200 mg) was melted with vigorous stirring in distilled water, while heating the solution at 80 °C for 15 min. After complete dissolution,  $\gamma$ -aminobutyric acid (66 mg) was added and dissolved under stirring. Then, a water suspension (1 mg/ml) of NH<sub>2</sub>-MSN (1.5 ml) was added to the mixture and stirred for 15 min at r.t. Finally, the molecular cross-linker, pentaethylenehexamine (40  $\mu$ l) was added to the mixture. The mixture was stirred vigorously for other 5 min before transferring it into glass vials (or plastic well-plates) and allowed to react overnight at r.t. The obtained hydrogel scaffold was washed with water and Phosphate Buffer Solution and used for cell growing experiments.

The synthesis of the pristine hydrogel was achieved with a similar synthetic procedure to what already described, with minor variations. To summarize, in a 25 ml round bottom flask MBA (200 mg) was melted with vigorous stirring in distilled water, while heating the solution at 80 °C for 15 min. After complete dissolution,  $\gamma$ -aminobutyric acid (66mg) was added and dissolved under stirring. Then, the molecular cross-linker, pentaethylenehexamine (70  $\mu$ l), was added to the mixture. The mixture then was stirred vigorously for other 5 min before transferring it into glass vials (or plastic well-plates) and allowed to react overnight at r.t, thus obtaining the hydrogel scaffold, which was then washed with water and Phosphate Buffer Solution.

#### 4.8.5 *Synthesis of concentric cylinder hydrogel (CCH)*

Concentric cylinder hydrogel (CCH) is composed of an inner MSN-hydrogel cylindrical core and an outer cylinder made of pristine hydrogel. This dual structured system was designed and optimized to examine the release of SDF-1 $\alpha$  and the recruiting ability towards mBM-MS cells. The synthesis procedure for this scaffold was performed in a 12-well plate. Pristine hydrogel was synthesized as previously described; then, when the gelation process was completed, the

inner cylindrical core of the scaffold was removed with a sterile biopsy punch with a diameter of 8 mm.

After that, the inner cavity formed in this way was used as molecular vessel for the synthesis of SDF@MSN-hydrogel. In particular, the synthesis of SDF@MSN-hydrogel was performed as previously described and was initiated in a round bottom flask, adjusting the reagents quantity to the final desired volume of 200  $\mu$ l and using previously SDF-1 $\alpha$  loaded MSNs. Then, the obtained viscous SDF@MSN-hydrogel mixture was transferred in the inner cavity of the scaffold and let in static conditions to complete the gelation process, thus resulting in a dual structured material, CCH.

#### 4.8.6 *Hydrogels mechanical characterization*

A rheological protocol was designed to determine of the viscoelastic response of hydrogels under shear stress in a broad range of strain amplitudes and deformation rates. Such a protocol gave us access to the mechanical characterization of the considered hydrogels, both without and with embedded MSNs, at deformation conditions that are compatible with the shear deformations and stresses exerted by MSCs migrating in the supporting hydrogels. Briefly, we first measured the stress-strain curve in a range of shear deformations ranging from  $10^{-3}$  up to 1000 %. For a given sample, this  $\sigma$ - $\gamma$  plot determines the regime of the linear shear response, where the applied stress is linearly proportional to the produced strain, and beyond a yield point, when the linear relationship is lost and nonlinear regime is entered. For an aliquot of the sample, the  $\sigma$ - $\gamma$  plot is measured at a constant oscillation frequency, usually at 1 Hz, corresponding to an angular velocity,  $\omega = 2\pi$  rad/s. Once the strength of the linear regime has been determined, a working strain is chosen in the linear regime, well above the yield point but high enough to require stresses above the experimental accuracy. Then, the linear rheological response of the sample is measured for a second aliquot (non-stressed beyond yielding), which is measured, at constant strain amplitude, in terms of the oscillation frequency and temperature. The oscillation frequency is left to vary logarithmically in the range  $10^{-2} < \omega/s-1 < 102$ . The sample is subjected to thermal treatment, typically 15-20 sweeps at variable frequency, by first heating at increasing temperature from 5  $^{\circ}$ C up to 95  $^{\circ}$ C, every five degrees, and then cooling down room temperature. In this work, only rheological data at 37  $^{\circ}$ C are shown. Prior to starting any rheological measurement at the working temperature, the sample



is subjected to pre-shearing at constant strain in the linear regime and constant frequency (1 Hz). The rheological experiment is started only when the shear response remains constant for minutes within the experimental accuracy.

#### 4.8.7 *Cell culture in 2D and onto the hydrogels*

Mouse Bone Marrow Mesenchymal Stem Cells (mBM-MSC) were isolated from mice bone marrow, following a reported protocol.

In brief, bone marrow was obtained from 8–20-week-old mice, after sacrificing them by CO<sub>2</sub> inhalation and subsequent cervical dislocation; bone marrow was flushed out of tibias and femurs. After washing by centrifugation for 10 min cells were resuspended in culture media to a concentration of around  $5 \times 10^6$  viable cells per ml. To initiate the MSC culture, cells were plated in 75 cm<sup>2</sup> culture flasks (Corning Inc., NY, USA) and kept in an incubator at 37 °C with a controlled atmosphere of 5% CO<sub>2</sub>; after 72h non-adherent cells were removed by changing the medium.

Then, mBM-MSC were normally cultured in Dulbecco's Modified Eagle Medium (DMEM) additioned with Mesenchymal Stem Cell Medium Supplement Kit (M5566-Kit; Cell Biologics, Chicago, IL, USA). Cells were kept at 37 °C and 5% CO<sub>2</sub> and were grown until reaching 80 to 85% of confluence. Then, they were washed twice with Phosphate Buffer Solution (PBS) and treated with trypsin to detach them from the flask surface. Cells were splitted every 2-3 days; the medium was changed every other day.

Cells were cultured onto the hydrogels using the following procedure: the hydrogel scaffolds were sterilized under UV light (254 nm) for approximately 1h and then they were equilibrated by adding culture media at 37 °C.

mBM-MSC were detached from the culture flask by trypsination and approximately 50,000 cells were efficiently seeded onto the hydrogel scaffolds. The number of cells was counted using a hemocytometer. Then, the samples were placed in the incubator (37 °C, 5% CO<sub>2</sub>) for about 1h and fresh media (1 ml) was cautiously added on the top of the hydrogels to supply nurture for the cells and to prevent the drying of the hydrogel during incubation. Culture medium was added only after 1h from the seeding process, in order to allow anchorage of the cells where they were placed.

#### 4.8.8 *Cell staining and viability studies*

Where required (migration study), mBM-MSC were stained with Vybrant DiD (Life Technologies), following the reported protocol, prior to seed them. Cell viability was assessed using alamarBlue assay. Briefly, the alamarBlue solution was added to the culture medium (1:10 dilution) of cells growing onto hydrogel scaffolds. After 3h incubation, the absorbance signals from the dye resazurin (dark blue) being reduced to resorufin (pink) by metabolically active cells were recorded using a Synergy™ H4 Hybrid Multi-Mode Microplate Reader. Each sample was tested in three replicates and the results were expressed as a percentage of the absorbance.

#### 4.8.9 *Surgical model and scaffolds implantation*

6 BALB/c mice (8 to 12 weeks old; mice weighting 21–23 g) were housed and fed in the animal room at The Houston Methodist Research Institute (Houston, Texas) for 48 hours prior to the experiment. The study protocol number AUP-0115-0002 was approved by the Institutional Animal Care and Use Committee (IACUC) and performed following GMP standards. All efforts were made to minimize the number of animals used for experiments and their suffering. Animals were anaesthetized with 2–3 % isoflurane in 100 % oxygen at a flow rate of 1 l/min. A 3 × 3 cm<sup>2</sup> area of skin was shaved and sterilized. Following preparation of the dorsal area, a midline skin incision was made. Two animals per condition were used (time point 7 days; n = 4). Each animal was implanted with two scaffolds of the same type (biological duplicates), namely SDF@MSN-hydrogel, MSN-hydrogel and pristine hydrogel. Mice were euthanized at 7 days by CO<sub>2</sub> inhalation and subsequent cervical dislocation.

#### 4.8.10 *Histological evaluation*

At 7 days the implanted hydrogels were collected and fixed in Optimal Cutting Temperature compound for histology. Samples were cut 10 µm thick, and sections were washed twice in fresh xylene for 8-10 min and rehydrated with decreasing ethanol concentrations and DI water (8-10 min for each step).

Sections were stained with standard hematoxylin and eosin (H&E) for histological examination. Tissue analysis was performed from all animals. Stained sections were imaged on a Nikon Histological Microscope. Image analysis and stained area measurements were

calculated using the pixel calibration (both x and y) divided by the objective lens magnification.

#### 4.8.11 *Statistic methods*

Statistical analysis was performed using GraphPad Instat 3.00 for Windows. Three replicates for each *in vitro* experiment (cells proliferation, distribution, and migration) were performed and the results are reported as mean  $\pm$  standard deviation, with  $p \leq 0.05$  used as the threshold for significance.

## 4.9 References

- [1] M. P. Lutolf, J. A. Hubbell, *Nat Biotech* **2005**, 23, 47.
- [2] P. Ferruti, M. A. Marchisio, R. Duncan, *Macromol. Rapid Commun.* **2002**, 23, 332.
- [3] P. Ferruti, S. Bianchi, E. Ranucci, F. Chiellini, A. M. Piras, **2005**, 2229.
- [4] a) M. De, P. S. Ghosh, V. M. Rotello, *Adv. Mater.* **2008**, 20, 4225; b) S. Mignani, M. Bryszewska, B. Klajnert-Maculewicz, M. Zablocka, J.-P. Majoral, *Biomacromolecules* **2015**, 16, 1.
- [5] a) M. Z. Rong, M. Q. Zhang, W. H. Ruan, *Mater. Sci. Technol.* **2006**, 22, 787; b) V. Giglio, F. Fiorini, L. Maggini, L. D. Cola, *to be submitted*.
- [6] a) P. Thoniyot, M. J. Tan, A. A. Karim, D. J. Young, X. J. Loh, *Advanced Science* **2015**, 2, n/a; b) N. Annabi, A. Tamayol, J. A. Uquillas, M. Akbari, L. E. Bertassoni, C. Cha, G. Camci-Unal, M. R. Dokmeci, N. a. Peppas, A. Khademhosseini, *Advanced materials research* **2014**, 26, 85.
- [7] F. Hoffmann, M. Cornelius, J. Morell, M. Fröba, *Angew. Chem. Int. Ed.* **2006**, 45, 3216.
- [8] a) H. Zou, S. Wu, J. Shen, *Chem. Rev.* **2008**, 108, 3893; b) B. T. Cheesman, J. D. Willott, G. B. Webber, S. Edmondson, E. J. Wanless, *ACS Macro Letters* **2012**, 1, 1161.
- [9] a) M. Supová, G. Martynková, K. Barabaszová, *Sci. Adv. Mater.* **2011**, 3, 1; b) J. Zaragoza, N. Babhadiashar, V. O'Brien, A. Chang, M. Blanco, A. Zabalegui, H. Lee, P. Asuri, *PLoS One* **2015**, 10, e0136293; c) J. Yang, C.-R. Han, J.-F. Duan, F. Xu, R.-C. Sun, *Nanoscale* **2013**, 5, 10858.
- [10] a) Y. Piao, A. Burns, J. Kim, U. Wiesner, T. Hyeon, *Adv. Funct. Mater.* **2008**, 18, 3745; b) A. Bertucci, E. A. Prasetyanto, D. Septiadi, A. Manicardi, E. Brognara, R. Gambari, R. Corradini, L. De Cola, *Small* **2015**, DOI: 10.1002/sml.201500540; c) J. L. Vivero-Escoto, R. C. Huxford-Phillips, W. Lin, *Chem. Soc. Rev.* **2012**, 41, 2673.
- [11] A. K. Gaharwar, N. a. Peppas, A. Khademhosseini, *Biotechnol. Bioeng.* **2014**, 111, 441.
- [12] N. S. Kehr, E. A. Prasetyanto, K. Benson, B. Ergün, A. Galstyan, H.-J. Galla, *Angew. Chem. Int. Ed.* **2012**, 125, 1194.

- [13] a) S. C. Mendes, R. L. Reis, Y. P. Bovell, A. M. Cunha, C. A. van Blitterswijk, J. D. de Bruijn, *Biomaterials* **2001**, 22, 2057; b) U. B. Yoshinori Onuki, Fotios Papadimitrakopoulos, Diane J. Burgess, *J. Diabetes Sci. Technol.* **2008**, 2, 1003.
- [14] a) J. M. Anderson, A. Rodriguez, D. T. Chang, *Semin. Immunol.* **2008**, 20, 86; b) T. O. Socarrás, A. C. Vasconcelos, P. P. Campos, N. B. Pereira, J. P. C. Souza, S. P. Andrade, *PLoS One* **2014**, 9, e110945.
- [15] a) I. B. Copland, S. Lord-Dufour, J. Cuerquis, D. L. Coutu, B. Annabi, E. Wang, J. Galipeau, *Stem Cells* **2009**, 27, 467; b) H. Liu, M. Li, L. Du, P. Yang, S. Ge, *Mater. Sci. Eng. C Mater. Biol. Appl.* **2015**, 53, 83.
- [16] a) K. McFarlin, X. Gao, Y. B. Liu, D. S. Dulchavsky, D. Kwon, A. S. Arbab, M. Bansal, Y. Li, M. Chopp, S. A. Dulchavsky, S. C. Gautam, *Wound Repair Regen.* **2006**, 14, 471; b) Y. Wu, L. Chen, P. G. Scott, E. E. Tredget, *Stem Cells* **2007**, 25, 2648.
- [17] L. Chen, E. E. Tredget, P. Y. G. Wu, Y. Wu, *PLoS One* **2008**, 3, e1886.
- [18] a) R. M. Eman, F. C. Öner, M. C. Kruyt, W. J. A. Dhert, J. Alblas, *Tissue Eng. Part A* **2014**, 20, 466; b) K. E. A. van der Bogt, A. Y. Sheikh, S. Schrepfer, G. Hoyt, F. Cao, K. J. Ransohoff, R.-J. Swijnenburg, J. Pearl, A. Lee, M. Fischbein, C. H. Contag, R. C. Robbins, J. C. Wu, *Circulation* **2008**, 118, S121.
- [19] a) D. Kuraitis, C. Giordano, M. Ruel, A. Musarò, E. J. Suuronen, *Biomaterials* **2012**, 33, 428; b) P. Thevenot, A. Nair, J. Shen, P. Lotfi, C. Y. Ko, L. Tang, *Biomaterials* **2010**, 31, 3997; c) D. Isackson, K. J. Cook, L. D. McGill, K. N. Bachus, *Med. Eng. Phys.* **2013**, 35, 743.
- [20] a) A. M. Hocking, *Adv. Wound Care* **2015**, 4, 623; b) J. M. Karp, G. S. Leng Teo, *Cell Stem Cell* **2009**, 4, 206.
- [21] M. B. Murphy, D. Blashki, R. M. Buchanan, I. K. Yazdi, M. Ferrari, P. J. Simmons, E. Tasciotti, *Biomaterials* **2012**, 33, 5308.
- [22] C. de la Torre, I. Casanova, G. Acosta, C. Coll, M. J. Moreno, F. Albericio, E. Aznar, R. Mangues, M. Royo, F. Sancenón, R. Martínez-Máñez, *Adv. Funct. Mater.* **2015**, 25, 687.
- [23] K. Benson, E. A. Prasetyanto, H.-J. Galla, N. S. Kehr, *Soft Matter* **2012**, 8, 10845.
- [24] C. Bharti, U. Nagaich, A. K. Pal, N. Gulati, *Int. J. Pharm. Investig.* **2015**, 5, 124.
- [25] D. Tarn, C. E. Ashley, M. Xue, E. C. Carnes, J. I. Zink, C. J. Brinker, *Acc. Chem. Res.* **2013**, 46, 792.
- [26] W. Guo, J. Wang, S.-J. Lee, F. Dong, S. S. Park, C.-S. Ha, *Chemistry - A European Journal* **2010**, 16, 8641.
- [27] H. D. Bale, P. W. Schmidt, *Phys. Rev. Lett.* **1984**, 53, 596.
- [28] Y. Chen, Y. Zhang, *Anal. Bioanal. Chem.* **2011**, 399, 2503.
- [29] a) V. Magnaghi, V. Conte, P. Procacci, G. Pivato, P. Cortese, E. Cavalli, G. Pajardi, E. Ranucci, F. Fenili, A. Manfredi, P. Ferruti, *Journal of biomedical materials research. Part A* **2011**, 98, 19; b) P. N. Desai, Q. Yuan, H. Yang, *Biomacromolecules* **2010**, 11, 666; c) X. Xiao, L. Yu, Z. Dong, R. Mbelek, K. Xu, L. Cheng, W. Zhong, F. Lu, M. Xing, *J. Mater. Chem. B* **2015**.
- [30] Y. Murali Mohan, K. Lee, T. Premkumar, K. E. Geckeler, *Polymer* **2007**, 48, 158.
- [31] R. Fuhrer, E. K. Athanassiou, N. A. Luechinger, W. J. Stark, *Small* **2009**, 5, 383.
- [32] F. Mammeri, E. L. Bourhis, L. Rozes, C. Sanchez, *J. Mater. Chem.* **2005**, 15, 3787.
- [33] K. Haraguchi, T. Takada, *Macromolecules* **2010**, 43, 4294.
- [34] O. Jeon, D. S. Alt, S. M. Ahmed, E. Alsberg, *Biomaterials* **2012**, 33, 3503.
- [35] K. Miyazaki, H. M. Wyss, D. A. Weitz, D. R. Reichman, *Europhys. Lett.* **2006**, 75, 915.

- [36] a) J. Liu, Y. Tan, H. Zhang, Y. Zhang, P. Xu, J. Chen, Y.-C. Poh, K. Tang, N. Wang, B. Huang, *Nat Mater* **2012**, *11*, 734; b) M. P. Lutolf, P. M. Gilbert, H. M. Blau, *Nature* **2009**, *462*, 433.
- [37] D. W. Grainger, *Mater. Today* **1999**, *2*, 29.
- [38] in *Biomaterials Science (Third Edition)*, Academic Press, **2013**, pp. 587.
- [39] R. Langer, D. A. Tirrell, *Nature* **2004**, *428*, 487.
- [40] N. N. Le, M. B. Rose, H. Levinson, B. Klitzman, *Journal of Diabetes Science and Technology* **2011**, *5*, 605.
- [41] L. G. Griffith, *Acta Mater.* **2000**, *48*, 263.
- [42] J. M. Morais, F. Papadimitrakopoulos, D. J. Burgess, *The AAPS Journal* **2010**, *12*, 188.
- [43] B. D. Ratner, S. J. Bryant, *Annu. Rev. Biomed. Eng.* **2004**, *6*, 41.
- [44] a) J. M. Anderson, *Annual Review of Materials Research* **2001**, *31*, 81; b) J. Kim, M. Dadsedan, S. Ameenuddin, A. J. Windebank, M. J. Yaszemski, L. Lu, *Journal of biomedical materials research. Part A* **2010**, *95*, 191; c) J. L. Holloway, H. Ma, R. Rai, J. A. Burdick, *J. Controlled Release* **2014**, *191*, 63; d) D. Archana, B. K. Singh, J. Dutta, P. K. Dutta, *Carbohydr. Polym.* **2013**, *95*, 530.
- [45] S. Dong, H. Guo, Y. Zhang, Z. Li, F. Kang, B. Yang, X. Kang, C. Wen, Y. Yan, B. Jiang, Y. Fan, *Tissue Eng. Part A* **2013**, *19*, 2464.
- [46] a) W. Zhang, J. Chen, J. Tao, Y. Jiang, C. Hu, L. Huang, J. Ji, H. W. Ouyang, *Biomaterials* **2013**, *34*, 713; b) J. R. Krieger, M. E. Ogle, J. McFaline-Figueroa, C. E. Segar, J. S. Temenoff, E. A. Botchwey, *Biomaterials* **2016**, *77*, 280.
- [47] W. M. Haynes, *CRC handbook of chemistry and physics : a ready-reference book of chemical and physical data*, CRC Press, Boca Raton, FL., **2011**.
- [48] L. Baumann, S. Prokoph, C. Gabriel, U. Freudenberg, C. Werner, A. G. Beck-Sickinger, *J. Control. Release* **2012**, *162*, 68.

## 5. Biodegradable hydrogels for submucosal fluid cushion

This work was carried out in collaboration with Prof. Silvana Perretta and Pietro Riva (Strasbourg's Image-Guided Surgery Institute - IHU/IRCAD Strasbourg).

### Abstract

Biocompatible soft materials, and in particular hydrogels and liquids that can form interlayers between tissues, have been recently used in surgery to facilitate resection of tumors.

They find applications as submucosal fluid cushions (SFC), to avoid perforation and thus to facilitate endoscopic submucosal dissection (ESD). ESD is a clinical procedure applied for early stage neoplastic lesions in the gastrointestinal tract that allows *en bloc* resection of large lesions. During surgery it is necessary to lift the mucosa and to prevent the occurrence of damages to deeper tissues. The injection of materials, which can gel *in situ* forming a protective layer between the part to be removed and the healthy tissue, has been proposed as a way to avoid perforation and thus to facilitate ESD.

In this contest, we present an injectable biodegradable nanocomposite hydrogel as a novel SFC for ESD procedure. The nanocomposite hydrogel, namely dPAA, is composed of breakable silica nanocapsules covalently embedded into a polyamidoamine-based hydrogel network. The entire system undergoes degradation responding to cell-secreted molecules through reductive cleavage of disulfide moieties incorporated into the framework of the nanocapsules and in the hydrogel backbone. The possibility of loading a model protein into the nanocapsules and releasing it through degradation of the nanocomposite was also investigated.

The hydrogel solution, obtained at room temperature via a catalyst-free Michael poly-addition in water, showed rapid gelation when injected into the submucosa of a porcine stomach *in vivo*. The submucosal injection of the dPAA afforded a long-lasting high mucosal elevation and allowed the performance of ESD with a single injection of material.

Moreover, the adhesion of the dPAA to the muscularis layer provided protection during the procedure (i.e. no obvious bleeding or perforation were observed) and once it was completed. Its cell-mediated degradation and the possibility of releasing an active component that could assist the healing of the resected tissue is an additional feature of this novel nanocomposite. Therefore, dPAA provides an excellent submucosal injection system, and has great potential to improve the ESD technique.

## 5.1 Endoscopic submucosal dissection

Gastrointestinal (GI) tract cancer is one of the most aggressive tumors with an estimated worldwide mortality per year of over 1.75 million people.<sup>[1]</sup> Endoscopic early detection and surgical treatment could potentially lead to a reduction of mortality, especially for early gastrointestinal neoplasms or precancerous lesions.<sup>[2]</sup>

Endoscopic submucosal dissection (ESD) is a minimally invasive endoscopic procedure now accepted worldwide as the preferred treatment modality for the removal of early gastric cancer.<sup>[3]</sup>

ESD, developed in Japan in the mid-1990s, consents *en bloc* resection of large mucosal lesions in the stomach,<sup>[4]</sup> thanks to the direct resection from the submucosal layer. Additionally, this procedure allows an accurate histological assessment, therefore lowering the possibility of neoplastic recurrence. A scheme of the procedure is presented in Figure 5.1.

However, due to the use of electrocautery and the low thickness of the GI wall, there is a high risk of perforation;<sup>[5]</sup> to improve efficacy and safety, ESD technique requires the injection of a solution into the submucosal space. This creates a submucosal fluid cushion (SFC) between the lesion and the muscle layer,<sup>[6]</sup> which is responsible for the submucosal elevation. Maintenance of the desired elevation height during the procedure is essential for an efficient and safe dissection.<sup>[7]</sup>

Even though several injection solutions have been proposed and tested, normal saline solution (NS) is the most commonly used in the clinic because of its low cost and ease of use. However, it is hampered by low mucosal elevations, making the procedure difficult and often resulting in electrocautery damage of the muscularis (i.e. the thin layer of muscle of the GI tract, which is located underneath the submucosa). In addition, its rapid absorption in the surrounding tissues requires repeated injections for extensive resection.<sup>[8]</sup>

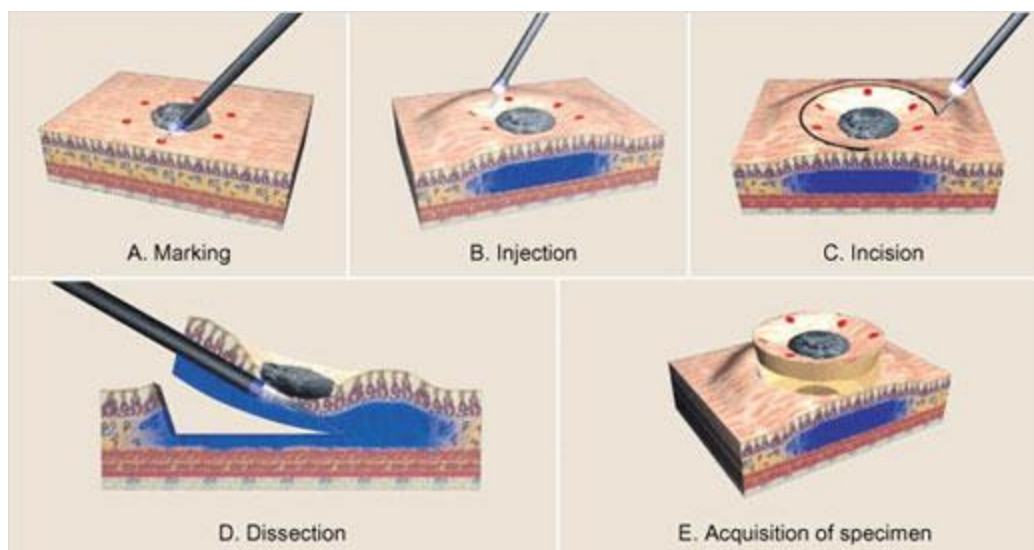


Figure 5.1 Scheme of ESD procedure with the injection of a normal saline solution and formation of SFC (B). Adapted from [www.ec21.com](http://www.ec21.com)

To be clinically applicable, the injection solution should be biocompatible, easily injectable, able to provide a prolonged and thick SFC to allow the ESD procedure safely, cost-effective, and finally it should preserve tissue specimens and allow for precise pathologic staging.<sup>[9]</sup> Additionally, significant features would be controlled and tunable biodegradability at the end of the procedure, and the possibility of releasing active components to assist the mucosal healing process after the resection.

Various substances, including glycerol,<sup>[10]</sup> hydroxypropyl methylcellulose<sup>[11]</sup> and hyaluronic acid<sup>[12]</sup> have been exploited to achieve sustained mucosal elevation and avoid injuries to the muscularis propria. Although hyaluronic acid solution is one of the best options,<sup>[12]</sup> it has been shown to stimulate the growth of residual tumors proliferation in animal models.<sup>[13]</sup> Moreover, a large amount of hyaluronic acid is necessary to create a SFC and its use is associated with high costs (US \$550.58/g) and a general lack of availability.<sup>[7]</sup>

Finally, the above mentioned materials maintain the same condensed state (liquid) before and after the injection, while an injectable biomaterial system with a liquid-to-gel translation, would be more promising in providing extended and thicker submucosal lift and easiness of handling.

In the last years, injectable hydrogels have brought a shift in the search for the optimal SFC material towards the development of solutions that rely on *in situ* gel formation. For example,



a photo-cross-linked chitosan<sup>[14]</sup> hydrogel has been recently reported as a submucosal injection agent:<sup>[15]</sup> mucosal elevation was created after the injection of the chitosan viscous solution, which was cross-linked *in situ* via UV irradiation, resulting in an insoluble hydrogel. However, the use of UV light for the photoinitiated radical polymerization may be difficult in hard-to-reach areas and resulted somehow inconvenient as performed by the authors: ...*was irradiated with UV light for a total of 5 min (30 s each at 10 different places by using an UV light-fiber through the endoscopic accessory channel and UV lamp system)*.<sup>[15]</sup> Moreover, the authors mentioned that UV irradiation may be associated with inflammation of the residual tissue.

Thermoresponsive polymers, or thermogels, have been investigated as well for ESD applications, such as the recently proposed water solution of a PEG/PLGA-based temperature-sensitive polymer.<sup>[6a]</sup> However, many of these materials have been shown to clog inside long delivery tools at normal body temperature.<sup>[16]</sup>

In conclusion, several of the *in situ* forming hydrogels so far proposed are hindered by administration difficulties, further complicating the EDS procedure. Therefore, the adequate material is still a matter of debate.<sup>[6a, 9]</sup>

In chapter 4 we have reported the development of polyamidoamines-based nanocomposite hydrogels, which have been designed to have excellent cyto- and biocompatibility *in vitro* and *in vivo* as well as drug-delivery potential.<sup>[17]</sup>

Herein we introduce an injectable nanocomposite hydrogel, namely dPAA, with the aim of meeting all the requirements of an ideal ESD material to address the limitations previously listed.

The hydrogel developed is composed of breakable<sup>[18]</sup> silica-shell nanocapsules, BNCs, grafted onto degradable disulfide polyamidoamines chains.

The ability of dPAA to be injected with a minimal invasive approach and to deliver active molecules or therapeutics during the degradation phase from the embedded BNCs, has encouraged us to pursue the investigation of this hydrogel as a new ESD injection material.

Unlike previous materials obtained by photo-cross-linking, or thermal gelation, the hydrogels of the present study are formed *in situ* via Michael-type addition reaction under physiological conditions from simple mixing of the monomers in aqueous solution through the formation of amine bonds.

Furthermore, in view of a clinical EDS application, we investigated the formation of a stable and long-lasting SFC, that could allow the procedure with a single injection of material.

Moreover, seen the potential of the *in vivo* application, we were interested in whether the hydrogel degradation could occur and be controlled by the proliferation of cells onto the scaffolds. Therefore, we examined the extent and time of hydrogel degradation in presence of reduced glutathione (GSH) *in vitro*, to mimic the extra-cellular reductive conditions. GSH is a reducing agent metabolized by the cells and present in the extra-cellular compartment with a concentration of 10  $\mu\text{M}$ ;<sup>[19]</sup> being the disulfide bond energy of approximately 60 kcal/mol, it is very labile to thiols and reducing agents, such as glutathione.

While several studies have been focusing on the reduction-triggered degradation of different systems at high GSH level, to mimic the intracellular concentration of 2-10 mM, GSH degradation in extracellular conditions is rarely mentioned before.<sup>[20]</sup> Such observation raised interesting questions regarding the possibility of obtaining a cell-responsive degradable hydrogel for ESD application.

Finally, our results showed that dPAA hydrogel could deliver active molecules during the hydrogel degradation phase, potentially assisting the healing of the tissue after the ESD procedure.

## **5.2 Design and synthesis of an injectable biodegradable nanocomposite**

### *5.2.1 Study design*

In this paragraph we give a brief overview of the different steps composing the present study. A degradable nanocomposite hydrogel, dPAA, was synthesized and characterized. It is composed of a polyamidoamines-based network with embedded breakable silica hollow nanocapsules, BNCs.

Both the BNCs and the polymeric backbone of the scaffold contain disulfide linkers that could be cleaved in presence of glutathione (GSH). The nanocomposite could be completely degraded even at a very low concentration of GSH (i.e. 10  $\mu\text{M}$ ), which was chosen to mimic the extracellular environment. Degradation and release kinetics of model protein cytochrome, loaded into the particles, were evaluated.

Next, we tested the cell-mediated degradation of dPAA in the presence of adult Human Dermal Fibroblasts (HDFa) proliferating onto the scaffolds. The assay demonstrated the achievement of cell-controlled degradation of the material; complete dissolution of the scaffold was observed after 96 hours when  $2.5 \times 10^5$  cells were seeded onto the nanocomposite.

Then, the injection of the hydrogel solution (i.e. before complete gelation) was attained through a 23-gauge needle and the formation of the hydrogel was evaluated *ex vivo*. This allowed us to observe a fast gelation (< 10 minutes), probably due to the increase of temperature and the interactions between the dPAA and the collagen present in the submucosal layer, where the injection was performed. Moreover, the dPAA was able to provide a stable and long-lasting mucosal elevation when tried as SFC.

Finally, the dPAA was tested as SFC for ESD procedures *in vivo*, on a porcine stomach.

The formation of the hydrogel and SFC *in vivo* was observed after 3 minutes and allowed the surgeon to perform the ESD procedure with a single injection. The adherence of part of the dPAA to the muscularis layer not only protected it during the procedure but also potentially offers several advantages in the phase following the surgery. The cell-mediated degradation of the nanocomposite indeed has shown to lead to the release of the active component loaded into the particles. This behavior could be exploited to release antibiotics or active factors to assist the healing of the wounded tissue and finally to achieve a complete clearance of the hydrogel from the body. Experiments are ongoing to test the *in vivo* degradation of the material.

### 5.2.2 Synthesis of breakable nanocapsules

Recently, our group has proposed the synthesis of innovative redox-responsive breakable hybrid organosilica nanocapsules.<sup>[21]</sup> This platform is composed of a silica shell able to encapsulate functional proteins in their active folding and it is engineered to degrade upon contact with a reducing agent, such as GSH present in the biological environment with a complete release of the loading.

Thus, we decided to exploit these BNCs to construct nanocomposite hydrogels able to release active molecules during the degradation of the material.

Cytochrome C (Cyt-C) was chosen as model cargo, since its strong absorption in the visible region allowed us to investigate the release kinetics during the hydrogel degradation.

The synthesis of the BNCs, in order to prevent denaturation of the loaded active molecule, was performed following the reported reverse nano-emulsion procedure. In particular, the silica precursor, tetraethyl orthosilicate (TEOS) was added to bis[3-(triethoxysilyl)propyl]disulfide in a ratio 7:3 TEOS:bispropyldisulfide derivative, in order to introduce the redox-sensitive moiety (Figure 5.2a). Well-defined and monodispersed spherical nanocapsules with a diameter of around  $60 \pm 10$  nm were obtained (Figure 5.2b).

Then, the obtained pristine BNCs were functionalized with 3-aminopropyltriethoxysilane, to be able to covalently link the BNCs to the polymeric hydrogel network (Figure 5.2b). A scheme of the synthesis and functionalization, as well as the SEM of the pristine and functionalized BNCs and of the degradation via GSH is displayed in Figure 5.2.

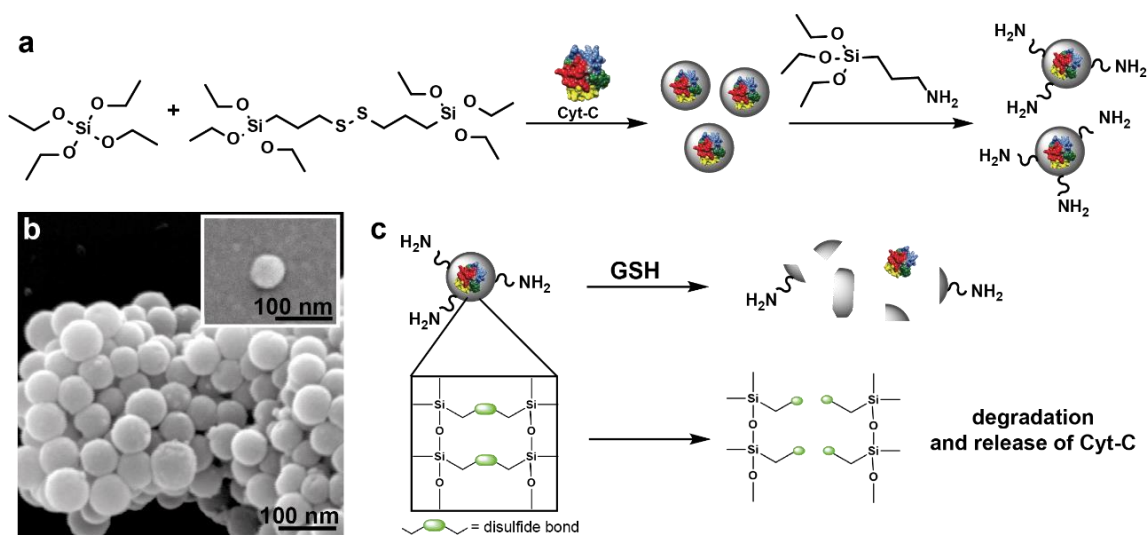


Figure 5.2 Scheme of the synthesis and functionalization of BNCs containing disulfide moiety in the framework and loaded with Cyt-C inside the silica capsule (a); SEM image of the monodispersed functionalized BNCs, in the insert SEM picture of a naked nanoparticle (b); scheme of degradation after GSH exposure and release of Cyt-C (c).

The surface functionalization was confirmed by the shift from negative to positive values of the  $\zeta$ -potential, from -10.5 mV of the pristine nanocapsules to + 2.2 mV.

Then, the functionalized BNCs (1 mg/ml) were used to synthesize the dPAA nanocomposite hydrogel through surface-grafting of the aminated BNCs to the polyamidoamine backbone of the scaffold.

### 5.2.3 Synthesis of the nanocomposite hydrogel, dPAA

Our goal when designing the network of the dPAA was to achieve a degradation that could be triggered by cells proliferating onto the material, without the need of any additional stimulus. Thus, we incorporated a disulfide cross-linker in the polymeric network of the hydrogel, i.e. cystamine. Disulfide bonds are susceptible of thiol exchange in the presence of reducing agents, such as glutathione (GSH), which is a cell metabolite.

We hypothesized that the reducing microenvironment given by the presence of GSH in the extracellular environment could trigger the cleavage of the disulfide bonds, therefore providing the dissolution of the scaffold.

Disulfide-modified polyamidoamines-based hydrogels containing BNCs were synthesized following the previously reported method with some modifications.<sup>[17]</sup> In particular, amino groups on BNCs were reacted with the unsaturated moiety of N,N'-methylene bisacrylamide, MBA (Figure 5.3a).

Briefly, a mixture of MBA, and N,N-dimethylethylenediamine, DMEN, was stirred in a BNCs water dispersion (1 mg/ml) at room temperature in presence of cystamine. A transparent liquid was obtained after 30 minutes, and then it was left in static conditions to complete the gelation process in 2 days. Figure 5.3a,b show a schematic representation of the synthesis and structure of the nanocomposite network.

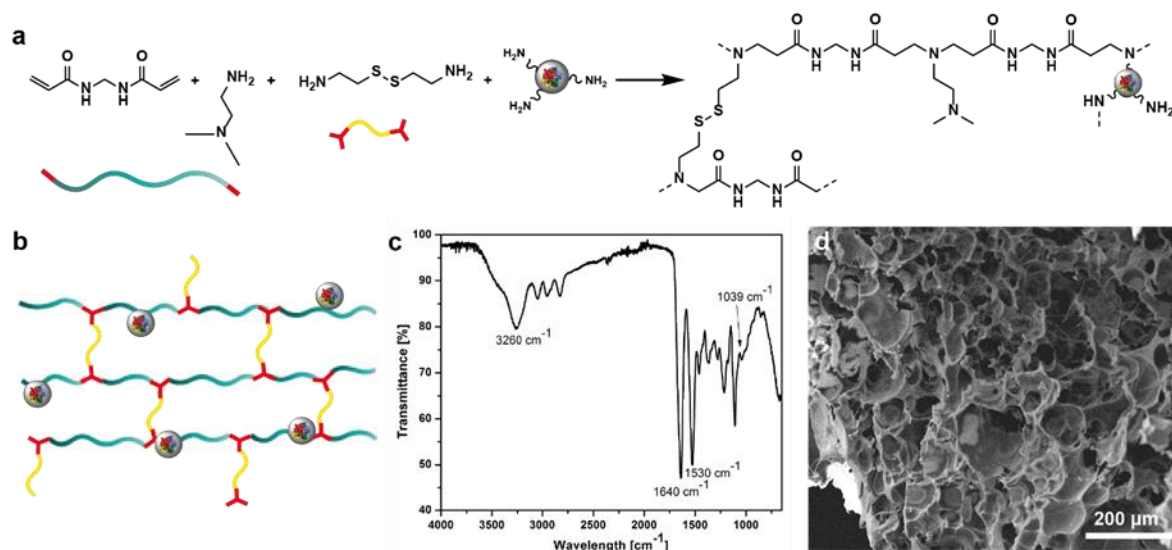


Figure 5.3 Synthesis of dPAA, embedding BNCs (a); scheme of the network (b); FTIR trace of dPAA (c); SEM showing the porosity of the nanocomposite (d).

The synthesis afforded transparent hydrogels formed in water at room temperature using a catalyst-free Michael-type addition. Gelation was confirmed by the absence of gravitational flow when the test tubes containing the hydrogels were inverted, through the so called “inverted test tube method”.

The formation of a cross-linked network was further confirmed by Fourier transformed infrared spectroscopy (FTIR), showed in Figure 5.3c. In particular, peaks at 1640 and 1530  $\text{cm}^{-1}$  are typical for the absorption of the amides carbonyl (st and  $\nu$  of C=O), while the 3260  $\text{cm}^{-1}$  band is attributed to the N-H stretching (st  $\text{NH}_2$ ). Furthermore, the absorption band at 1039  $\text{cm}^{-1}$ , which was ascribed to the vibration of C-S-S-C bond, confirmed of the successful incorporation of the disulfide cross-linker in the polymeric network. Since the samples were lyophilized to allow a correct peak determination, the presence of adsorbed water cannot be seen from FTIR spectrum, apart from a weak residual shoulder at 3430  $\text{cm}^{-1}$ , which is related to the OH angular deformation of water.

The morphological analysis of the obtained hydrogel scaffolds was assessed via scanning electron microscopy (SEM) of the lyophilized scaffolds. SEM showed a highly porous structure, with pores diameter in the range of 40 to 100  $\mu\text{m}$ , as can be seen in Figure 5.3d.

#### 5.2.4 Degradation in presence of GSH

For ESD application, hydrogels should maintain the required mucosal elevation for the whole time of the procedure (i.e. 30 min to 1 hour), and then degrade into fragments, in order to have a complete clearance from the body.

The nanocomposite presented in this work is degradable upon exposure to GSH, via the incorporation of cystamine cross-links throughout the polymeric network and in the BNCs framework. The potential degradation mechanism of the network is shown in Figure 5.4.

The degradation kinetics of the dPAA was examined by measuring swelling ratio variations as function of time in the presence of a low concentrated GSH solution (i.e. 10  $\mu\text{M}$  GSH solution in PBS), mimicking the extracellular environment. Hydrogels, incubated in PBS in the absence of GSH were used as control.

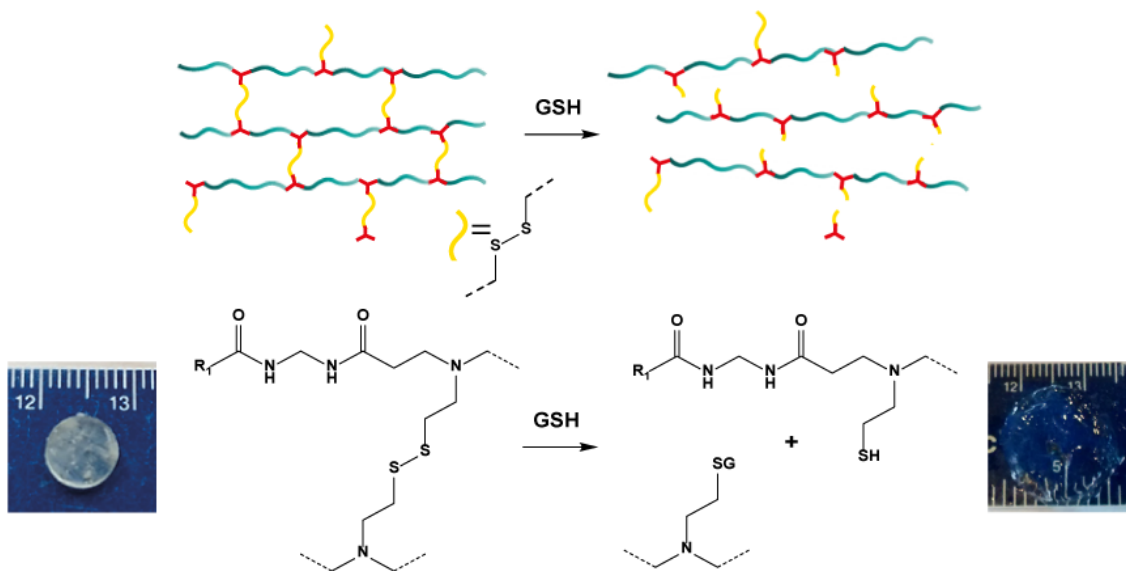


Figure 5.4 Mechanism of network degradation upon exposure to GSH, schematic representation and pictures of the hydrogel network before and during degradation. The yellow lines represent the disulfide units; the degradation of the hydrogel scaffold occurs at the disulfide cleavage site by thiol-disulfide exchange.

The swelling ratio curve of dPAA showed two different phases: an initial phase where clear increase in swelling was observed, followed by a rapid downward phase (Figure 5.5). The imbibing of the solvent into the hydrogel caused the initial increasing phase. This was then quickly outweighed by the cleavage of the disulfide bonds, leading to the complete degradation of the hydrogel.

A clear point of reverse gelation, defined as the point where there are less than 2 cross-links per polymer chain and the branched polymer chains dissolve,<sup>[22]</sup> was identified after 24 hours. As disulfide bonds are cleaved, mass loss increases with time until there is no longer a sufficient number of cross-links to maintain the 3D network. Finally, the equilibrium swelling value was found equal to zero after 3 days, due to complete disintegration of the hydrogel network.



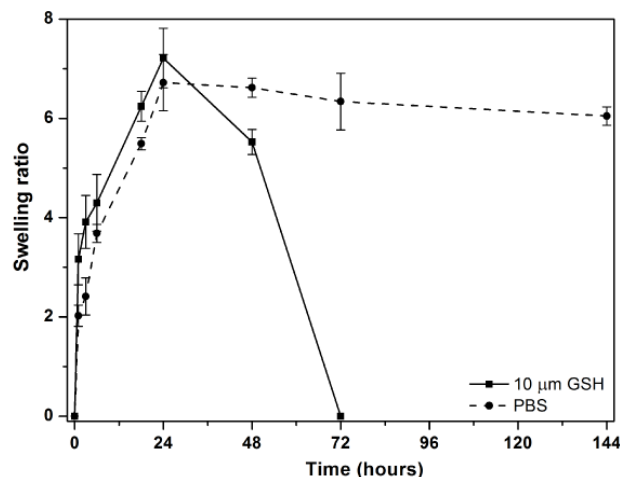


Figure 5.5 Swelling ratio of dPAA nanocomposite hydrogels incubated with 10  $\mu$ M GSH solution (solid line) and in PBS (dashed line), showing the degradation of dPAA nanocomposite hydrogel in presence of GSH.

The dPAA equilibrated in PBS showed instead a first phase of swelling followed by a plateau that was reached after 24 hours, demonstrating that the nanocomposite is stable in absence of reducing agent. The swelling was followed for 6 days.

### 5.2.5 Tunability of the degradation kinetic

To evaluate the effect of the disulfide cross-linker density on the degradation kinetics of the hydrogel nanocomposite, other two samples were synthesized. These scaffolds had the same composition of the dPAA, except for the amount of cystamine. In particular, they contained a lower and a higher amount of cystamine, 10-wt% and 40-wt%, compared to the dPAA hydrogel, which had 20 wt%.

In this way, we sought to establish a range of degradation profiles and times that could be achieved in response to GSH reducing microenvironments and that could be controlled by adjusting the molar ratio of the disulfide bond.

The degradation kinetics were evaluated by immersing the samples in the reducing solution of GSH, 10  $\mu$ M, and by measuring the swelling ratio after precise time intervals, as already described in paragraph 5.2.4.

The degradation profiles of the three samples are reported in Figure 5.6.



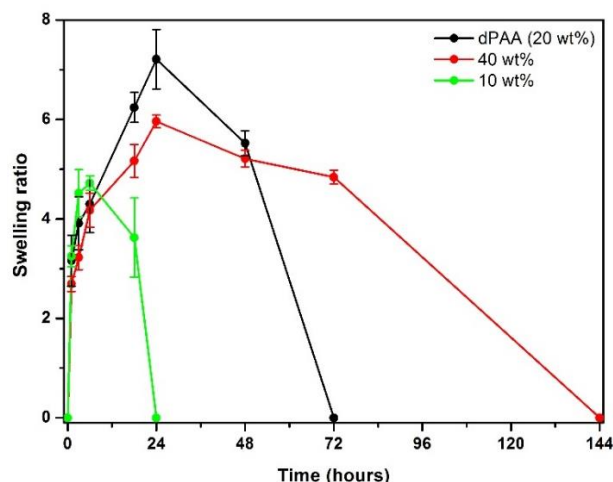


Figure 5.6 Swelling ratio of the nanocomposite hydrogels containing different cystamine amounts, incubated with 10  $\mu$ M GSH solution, showing the degradation of the network over time. Hydrogel containing 10 wt% of cystamine is displayed in green, the one with 40 wt% is in red; dPAA was added as a reference.

The degradation time was found to be proportional to the amount of disulfide cross-linker; in particular a decrease was observed with the scaffold containing 10 wt% of cystamine, which completely degraded after 24 hours. Instead the sample cross-linked with an higher amount of cystamine (40 wt%) displayed a longer degradation profile, terminating after 6 days with the complete disintegration of the network.

The possibility of tuning the degradation kinetic of the nanocomposite scaffold developed by changing the ratio of the disulfide linker, show its potential for applications where a precise control of the breakability over time is required.

### 5.2.6 Release of the model protein

As mentioned in the previous sections, the degradable hydrogel was decorated with breakable nanocapsules able to degrade with the same mechanism of the hydrogel, through the reduction of the disulfide bonds, and able to release their content, as already reported previously by our group.<sup>[21]</sup>

The fragmentation of the BNCs in presence of the reducing GSH after 72 hours, was further confirmed by scanning transmission electron microscope (STEM), as shown in Figure 5.7.

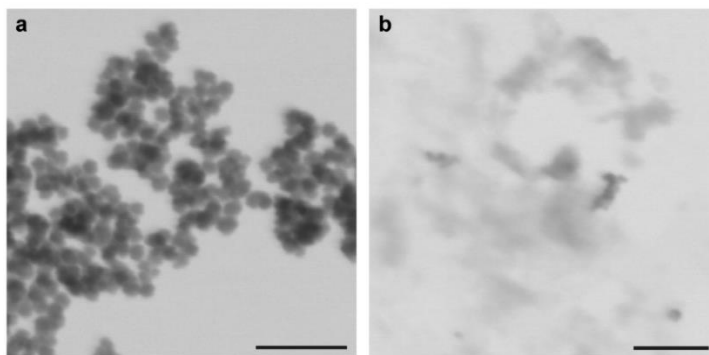


Figure 5.7 STEM images of the same particles before (a) and after (b) treatment with the reducing agent solution; scale bar is 250 nm.

Cytochrome-C, Cyt-C, was used as a model protein to study the release kinetics thanks to its strong absorption in the visible region, due to the presence of the eme group.

The BNCs were thus embedded into the dPAA and the Cyt-C released from the nanocomposite was investigated, by incubating the scaffold in the 10  $\mu$ M solution of GSH in PBS.

The cumulative release of Cyt-C from the dPAA is reported in Figure 5.8 and shows a slow release in the first 6 hours, followed by an increase of detected Cyt-C. The release of Cyt-C from the scaffold is highly augmented by the degradation of the hydrogel structure, which can be seen from the shape of the curve between 24 and 72 hours, showing a steep growth in absorption. The overall amount of protein release from the scaffold was estimated to be 67% of the initial loading, on bases of what previously reported for the BNCs system.<sup>[21]</sup>

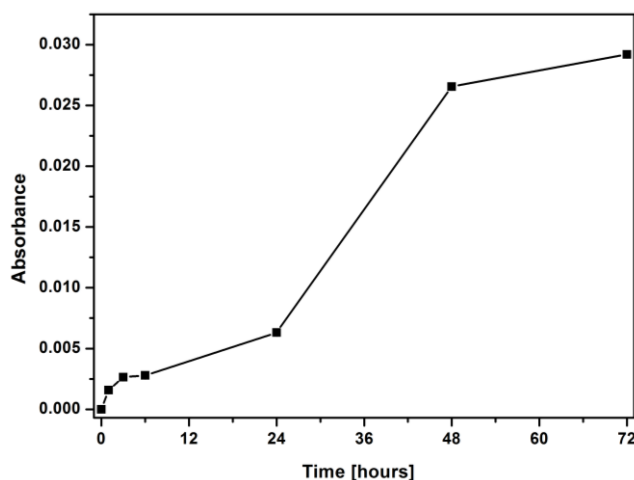


Figure 5.8 Cyt-C cumulative release from the BNCs embedded into the dPAA analyzed over 72 hours.

Overall, the incorporation of cleavable groups, both in the embedded nanoparticles and into the hydrogel network, which can degrade in response to endogenous stimuli, offers an attractive strategy for *in vivo* procedures, such as ESD. The system can be completely cleared from the body and release molecules of choice during the degradation process, such as a drug to assist the healing of the wound or *in situ* chemotherapy. The versatility of the synthesis allows the tailor-made nanocomposite hydrogel preparation in response to the needs of individual patients.

### 5.3 In vitro and ex vivo analyses

#### 5.3.1 Cell-mediated degradation

Since the degradation of dPAA and the release of the model protein could be efficiently achieved at low GSH concentration, such as the extracellular one, we tested the degradation of the scaffold in the presence of cells. In particular, Human Dermal Fibroblast (HDFa) were chosen for this study because fibroblasts residing within the extracellular matrix in the body are critical for matrix synthesis and repair. Upon injury or wound formation, these cells migrate to the wound site to repair the damaged tissue.<sup>[23]</sup> Thus, to simulate the cell-mediated degrading conditions *in vivo*, we selected HDFa.

The dPAA hydrogels for this test were synthesized in a 8 mm diameter and ~1 mm height disc shape and.  $2.5 \times 10^5$  HDFa were seeded onto the hydrogels and cultured in the corresponding growth medium; acellular hydrogels incubated in growth medium were used as control.

AlamarBlue assay indicated that the majority of the encapsulated cells were viable and proliferating onto the scaffold (Figure 5.9a) up to 4 days. This is consistent to what has been observed for similar polyamidoamines-based scaffolds in the previous chapters and it confirmed that dPAA containing disulfide moieties supported cell encapsulation and viability. Figure 5.9 displays as well an image of the 3D proliferation of the cells stained in red (Vibrant DiD stain) for better visualization, indicating that they permeate in the depth of the scaffold. A 3-channel visualization of the surface of the dPAA is reported in Figure 5.9c and is indicative of the growth of the cells onto the scaffold.

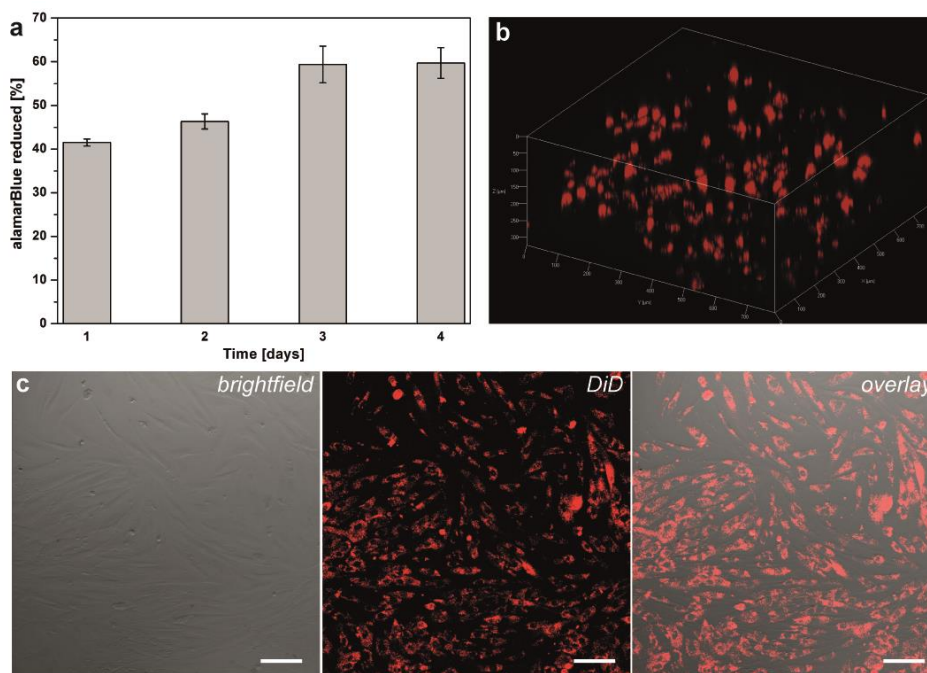


Figure 5.9 Viability of HDFa onto the degradable nanocomposite measured with alamarBlue assay (a). The plot displays the percentage of reduced alamarBlue, which is proportional to the cell metabolic activity of the cells, as function of time. The result shows an increase in metabolic activity, thus indicates the proliferation of cells onto the scaffold. Proliferation of the cells in 3D (b); 3-channel visualization of the HDFa (c), scale bar is 100  $\mu\text{m}$ . Cells in (b) and (c) were stained with Vybrant DiD (red) to facilitate the imaging.

As hypothesized, the hydrogel underwent degradation responding to cell-secreted GSH, in the absence of any external stimulus. In addition, many cell surface molecules contain thiol groups and thus could contribute to the cleavage of the disulfide bonds of the network.

The scaffold resulted largely reduced in size and weight after 72 hours and the complete degradation was achieved after 96 hours (Figure 5.10a,b), demonstrating a good agreement with the GSH degradation tests (see paragraph 5.2.4).

It was observed that the degradation process resulted into a gradual movement of the cells from the nanocomposite to the bottom of the well containing the scaffold (Figure 5.10c). The viability of HDFa measured after the degradation of the scaffold showed that 87 % of the cells were viable, thus confirming that the degradation products were non-toxic. Previous studies on linear polyamidoamines systems have shown that the degradation products were completely non-cytotoxic, since the degradation produced oligomers.<sup>[24]</sup>

The acellular hydrogels used as control displayed minimal degradation during the course of the studies (Figure 5.10a, dashed line). This small degradation (17 %) is probably due to the presence of fetal bovine serum in the culture medium, which contains various proteins and amino acids with thiol groups.

The results obtained confirmed that the dPAA hydrogels were prone to HDFa-mediated degradation through thiol reductive exchange, therefore showing potential for *in vivo* applications requiring degradation of the scaffold.

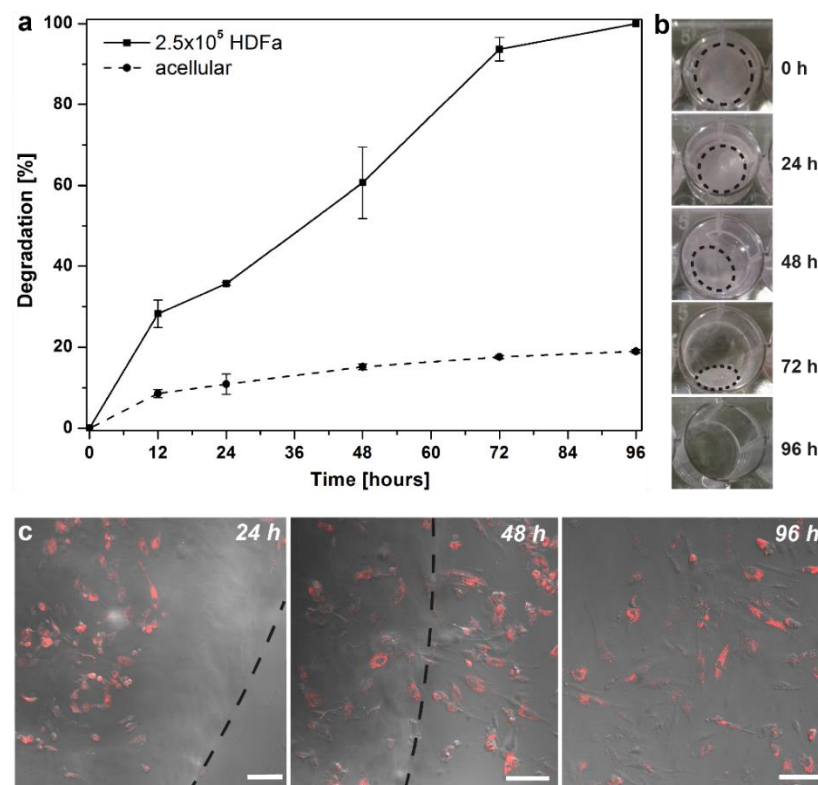


Figure 5.10 HDFa-mediated degradation as function of time of dPAA hydrogels, solid line, containing  $2.5 \times 10^5$  cells and control (acellular dPAA), dashed line (a); macroscopic pictures showing the cell-mediated degradation of the dPAA (b). Overlay images (i.e. brightfield and DiD channel) of the HDFa growing onto the scaffold (24 h) and gradually transferring to the bottom well plastic as the dPAA gets degraded (48 and 96 h); scale bar is 100  $\mu\text{m}$ .

### 5.3.2 dPAA injectability and formation of SFC

Since the ESD procedure requires the injection of a SFC solution underneath the mucosa, we first optimized the synthetic procedure of the hydrogel to obtain a material that could be delivered *in vivo* via injection, and then rapidly gel inside the body.

Polyamidoamine-based hydrogels have the great advantage of allowing network formation under physiological conditions. This approach has been already investigated in the past years for various injectable hydrogel preparations.<sup>[25]</sup> This mechanism has been shown to be applicable to a wide range of commercially available precursors, forming polymer networks with minimal structural deficiencies within a surgically relevant timeframe, while avoiding the production of free radicals.<sup>[26]</sup>

Thus, taking advantage of the catalyst-free water-based reaction through which we could obtain the hydrogels, and having observed a time window of several hours between the beginning of the polymerization and the complete gelation, we decided to test the obtained scaffold for the injection procedure.

When the polyaddition reaction between MBA and DMEN was carried out using the biodegradable cystamine cross-linker, we could observe the formation of a clear solution after 30 minutes, indicating that the reagents were completely dissolved and have started the polyaddition reaction.

The ability of this hydrogel solution to flow through a disposable 23-gauge catheter injection needle was then examined. The dPAA solution was able to flow under hand pressure and the maximum needle injection pressure was found to be comparable to saline solution (Figure 5.11a). Then, we observed that this viscous hydrogel solution reacted at room temperature in static conditions to form a self-standing hydrogel after 48h.

Better results were obtained by raising the temperature to 37 °C, when we observed the formation of a self-standing hydrogel in 18 hours.

However, knowing that intestinal submucosa is rich in type I collagen and that this presents amino and hydroxyl groups as side groups, we postulated the possible formation of hydrogen bonds that could lead to a faster gelation kinetic *in vivo*.

We therefore tested this hypothesis by injected the dPAA solution *ex vivo* in the submucosa of a porcine stomach. The injection was performed on the tissue at 37 °C and the gelation, with formation of a SFC, was immediately observed (Figure 5.11b). There was no leaching of the

solution away from the injected site, and the tissue was cut opened, revealing the formation of the dPAA after 8-10 min post injection *ex vivo* (Figure 5.11c).

The nanocomposite hydrogel was found completely adhered to the submucosal layer and it had to be removed with scissors and tweezers. Moreover, it was confirmed that there had not been diffusion of the solution into the surrounding tissues.

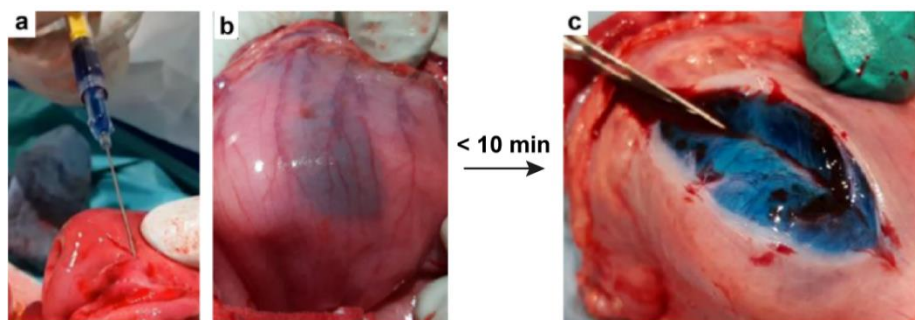


Figure 5.11 Injection of the dPAA solution stained with Methylene Blue via a surgical 23-gauge needle (a); formation of a mucosal elevation (b); gelation occurred in less than 10 minutes, achieving a solid and elastic hydrogel, adhered to the tissue (c).

The investigation of injectability and gelation time was then performed *in vivo*. The dPAA showed a gelation time of approximately 3 minutes when injected in the submucosal layer in a living pig.

It is undeniable that the physiological conditions of temperature (37 °C) and pH (7.4), contribute to the faster gelation than what observed *in vitro*, as already reported for similar systems.<sup>[27]</sup> However, tests done *in vitro* at 37 °C and pH 7.4 did not give the same results, suggesting the contribution of additional factors.

We believe that the intermolecular interaction between the hydroxyl and amino groups of the collagen side chains with amide groups of dPAA lead to the formation of hydrogen bonds that further cross-link the polymer network.

Moreover, the formation of mechanical entanglements between the collagen fibers and the dPAA backbone could also contribute to the formation of an interpenetrated hydrogel network, favoring the faster formation of a stable and elastic hydrogel *in situ*. This behavior was observed via SEM of the explanted tissues, which showed interactions between the hydrogel scaffold and collagen fibers (Figure 5.12a).



*In vivo* images of the dPAA formed in situ (Figure 5.12b) and stained with Methylene Blue also displayed fibrous formation within the hydrogel matrix (Figure 5.12c). However, a deep investigation is currently ongoing to explain this behavior.

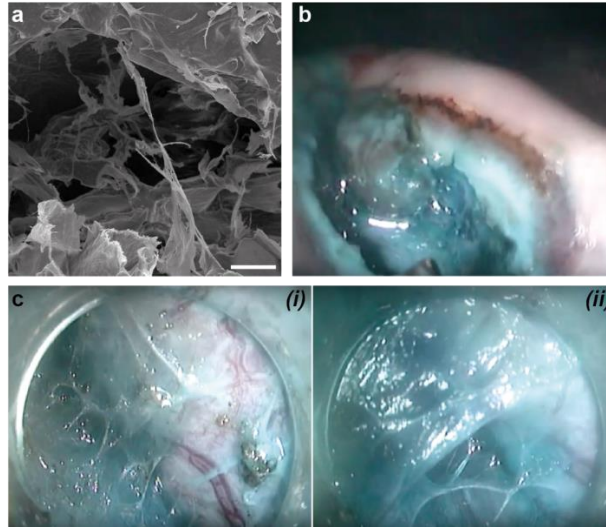


Figure 5.12 SEM image of the explanted tissue and hydrogel, showing collagen fibers within the hydrogel matrix (a), scale bar is 100  $\mu\text{m}$ ; endoscopy images of the dPAA stained with Methylene Blue formed *in vivo* (b) and close up (c) showing with fibrous formation within the hydrogel matrix.

In ESD procedures the ability of mucosal lifting and its maintenance are essential to avoid perforation and safely complete the *en bloc* resection of the lesion.

Thus, we next examined the formation and lasting of a SFC *ex vivo* by the dPAA and a NS. In particular, fresh resected porcine stomachs were used and 2 ml of NS or dPAA solution were injected. Protrusions appeared at the injection site and the height changes in submucosal elevation were recorded after 10 seconds, 10 minutes and 1 hour, to cover the whole time of the ESD procedure, which is approximately 40 minutes (Figure 5.13).

Although both the examined solution and the hydrogel led to the mucosal elevation right after the injection, the dPAA nanocomposite displayed higher mucosal lifting, 8.3 mm vs 6.7 mm, for the dPAA and the NS respectively, with the same amount of solution injected. This showed that already part of the NS solution was absorbed by the surrounding tissues after 10 seconds.



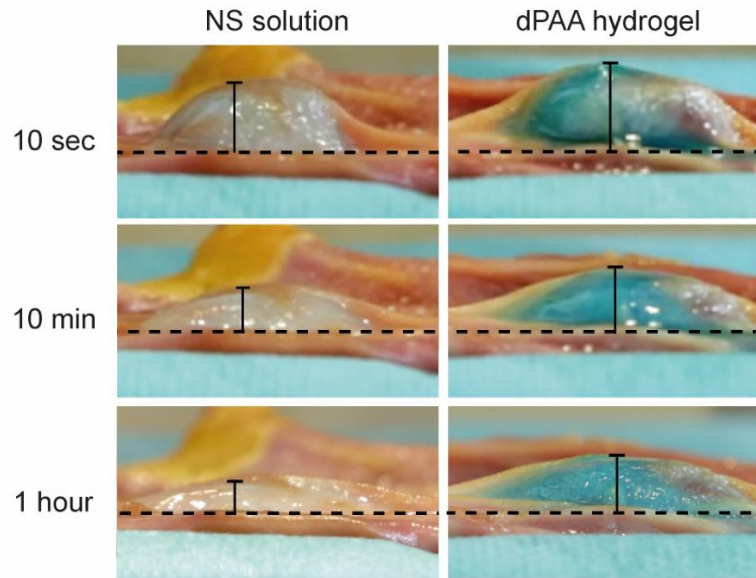


Figure 5.13 Change in mucosal elevation as a function of time after the injection of NS or dPAA into a resected porcine stomach. Methylene blue was mixed as color agent. Height values (black bar) obtained for NS were 6.7 mm, 4.2 mm and 2.9 mm after 10 sec, 10 min and 1 h respectively; for dPAA were 8.3 mm, 6.4 mm, 5.8 mm after 10 sec, 10 min and 1 h respectively.

After the injection of the hydrogel solution, the formation of a solid SFC was detected, which showed only a slight change in size over 1 hour, i.e. from 8.3 mm to 5.8 mm. No significant change in shape or consistency of mucosal lifting was observed. This behavior was due to the formation of the dPAA hydrogel under the submucosa.

In contrast, the elevation created with NS gradually collapsed, showing a reduction of 37% in size after 10 minutes and of more than half after 1 hour (i.e. height from 6.7 mm to 2.9 mm). In short, we could confirm the higher performance of the dPAA nanocomposite in the formation of a higher and longer lasting mucosal elevation.

#### 5.4 *In vivo* ESD procedure

ESD was performed by the surgeon Pietro Riva at IRCAD, Strasbourg

Seen the promising results obtained in the *in vitro* experiments, we performed a feasibility study to evaluate the *in vivo* efficacy of dPAA in a living pig. We first set appropriate lesion

sizes of approx. 3 cm in diameter in the porcine stomach and then 8-10 ml of the hydrogel solution were injected in the submucosa.

The ESD procedure was performed in triplicate in different areas of the same porcine stomach; NS solution was used as control.

In Figure 5.14a is reported the endoscopic view of the stomach at time 0 before the injection of the hydrogel solution. It shows the set of an appropriate lesion of approx. 3 cm in diameter. We observed that in all the cases the injected dPAA solutions in the submucosa led to the gelation of the material in 3 minutes, which thus formed a clear and stable mucosal elevation (Figure 5.14b,c).

A comparison with the normal saline solution generally used, showed initially no significant difference compared to the SFC formed by dPAA. However, the elevation of the SFC formed by NS had obviously reduced after 15 min, due to quick diffusion of the NS at the target site and absorption of the liquid by the tissue, thus it was necessary to repeated the injections to keep the lifted submucosa and be able to finish the surgery.

In contrast, the mucosal lifting obtained with dPAA allowed the surgeon to perform the entire ESD procedure (40 min) without requiring a second injection, therefore significantly simplifying the procedure and avoiding large injection of liquids.

The presence of the hydrogel allowed the use of the common electrocautery settings and the long-lasting conservation of the mucosal elevation created with the dPAA enabled the surgeon to smoothly accomplish the circumferential resection (Figure 5.14d).

No significant complications or perforation occurred during the procedure thanks to the reliable and long-lasting mucosal lifting achieved with the dPAA.

Then, the lesion was dissected *en bloc* without any sign of mucosal or muscularis damage, confirming that the dPAA hydrogel formed *in situ* was able to “dissect” the submucosal layer (Figure 5.14e). Intact mucosal specimens were conveniently achieved via the performed ESD procedures. This is essential, as a definite resection provides accurate histological assessment and thus, can reduce the risk of neoplastic recurrence.

We could observe that part of the hydrogel adhered to the muscularis layer, under the resected mucosa. In this way a protecting layer of hydrogel was obtained onto the newly formed cavity (Figure 5.14f).

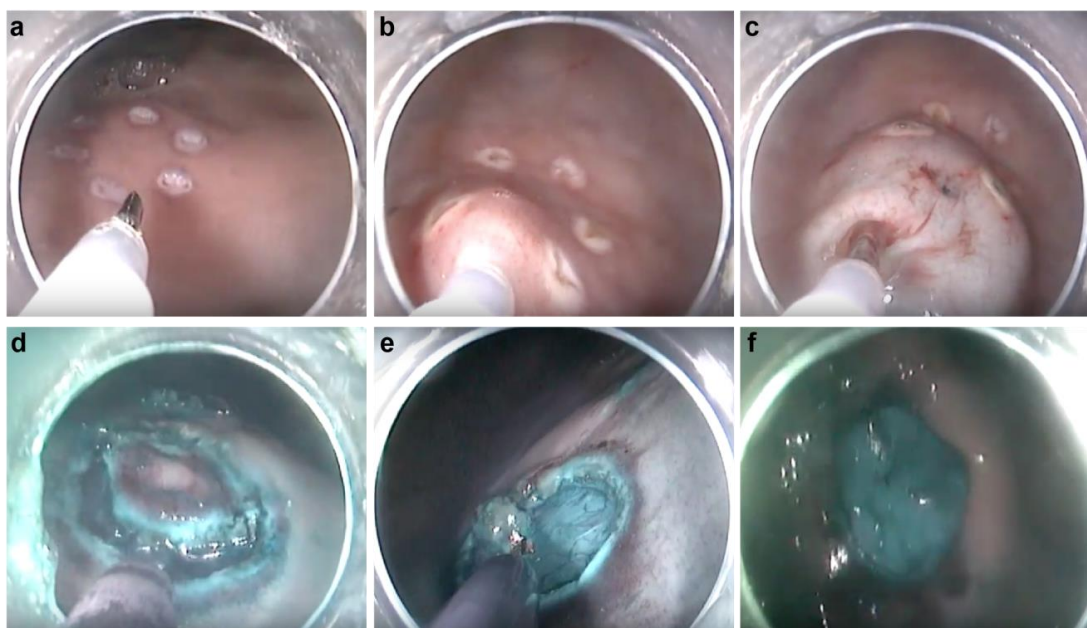


Figure 5.14 Endoscopic views of the different steps of the ESD procedure performed using the dPAA stained with Methylene Blue. Setting of the lesion, approx. 3 cm in diameter (a); injection of the dPAA solution (b); formation of the SFC after gelation of the dPAA (c); circumferential cutting (d); complete resection with protective layer of dPAA that remained adhered to the muscularis (e); wound left after ESD with layer of the dPAA (f).

The possibility of releasing an active component from the dPAA during its degradation is highly beneficial at the end of such delicate procedure. Biomolecules, such as adrenaline, proton-pump inhibitors or antibiotics could potentially be efficiently delivered to assist the cauterization of the resected tissue or the prevention of inflammations.

Moreover, the design of the nanocomposite hydrogel enhances the versatility of the system, enabling the selection of different possible releasing factors, personalized in relation to the patient's requirements.

The reported non-survival animal study was conducted to examine the formation of SFC from the dPAA *in vivo* and the feasibility of ESD procedure with the novel material.

Survival *in vivo* studies are undergoing to assess the kinetic of the degradation of the dPAA after ESD procedure, as well as the efficacy of the release.

## 5.5 Conclusions

A degradable nanocomposite hydrogel was successfully developed by embedding breakable nanocapsules into a disulfide-containing polyamidoamines-based hydrogel.

We demonstrated that the disulfide bonds of the embedded BNCs and of the network could be completely cleaved in 3 days when the hydrogel is incubated in a GSH solution mimicking the extracellular concentration (10  $\mu$ M).

Most importantly, the obtained dPAA sustained the proliferation of HDFa and underwent complete degradation in response to cell-secreted molecules from HDFa seeded onto the scaffold without any external stimulus.

The degradation of the nanocomposite allowed the release of a model protein encapsulated into the BNCs.

The obtained dPAA could be delivered to the desired tissue by facile injection through a 23-gauge needle. To prove its applicability in real models, the aqueous hydrogel solution was injected in the submucosa of a porcine stomach *in vivo*. It formed an elastic hydrogel in 3 minutes most likely due to temperature increase and interaction with collagen fibers present in the submucosal layer of the mammals.

Such an important result motivated us to employ the dPAA hydrogel as a novel submucosal injection agent in ESD.

The hydrogel formed a reliable SFC *in vivo*, enabling a long-lasting mucosal elevation, which was superior to commonly used NS. This facilitated *en bloc* resection of the lesion, which was successfully accomplished with just a single injection.

No perforation, major bleeding or tissue damage were observed during ESD. Moreover, part of the *in situ* formed hydrogel adhered tightly to the muscularis, under the resected mucosa, allowing protection of the membrane during the procedure and after it.

Our results indicated a slow degradation kinetics and parallel release of the chosen active molecule *in vitro* throughout a period of 72 hours, triggered by the proliferation of cells into the scaffold.

Thus, we reasoned that a similar behavior might be experienced *in vivo*, allowing the release of antibiotics, drugs or proteins that could assist the healing of the resected tissue during the degradation of the material, and finally the complete clearance of the scaffold.

To conclude, we have demonstrated that the novel nanocomposite is a suitable SFC agent for ESD procedures. Additionally, in a second phase it can potentially be degraded by cells proliferating onto the scaffold and release the encapsulated active component.

## 5.6 Experimental part

### 5.6.1 *Synthesis and functionalization of BNCs*

Triton X-100 (7.08 ml) and n-hexanol (7.20 ml) were dissolved in cyclohexane (30 ml). Separately, a 5 mg/mL aqueous solution (1.20 ml) of cytochrome C from equine heart, Cyt-C, was mixed with tetraethyl orthosilicate (0.16  $\mu$ l) and bis[3(triethoxysilyl)propyl]disulfide (0.24 ml). After stirring, this mixture was added to the former organic medium. Eventually, 200  $\mu$ l of 30% ammonia aqueous solution were added and the water-oil emulsion was stirred overnight at room temperature.

After that, pure acetone (80 ml) was added to the reaction mixture in order to precipitate the material and the pristine BNCs (40 mg) were recovered by means of centrifugation, washing several times with water and ethanol.

Then, the surface of the obtained BNCs was functionalized to afford amino-functionalized breakable nanocapsules. The surface functionalization was performed as follows. 40 mg of nanocapsules were suspended in ethanol (5 ml). 3-aminopropyltriethoxysilane (0.094 mmol, 22  $\mu$ l) and triethylamine (TEA, 10  $\mu$ l) were added to the suspension, which was stirred at room temperature for 18 hours.

The precipitate was then washed five times with distilled water, to afford 30 mg of surface functionalized BNCs.

### 5.6.2 *Synthesis of dPAA*

In a 5 ml round bottom flask N,N'-methylene bisacrylamide (MBA; 200 mg) and N,N-dimethylethylenediamine (70  $\mu$ l) were added to a water solution of amino-functionalized BNCs freshly sonicated (1.5 ml; 1 mg/ml). Then, cystamine (65 mg) was added to the mixture that was stirred vigorously for 30 minutes at room temperature, after which a homogeneous and clear hydrogel solution was obtained.

When the hydrogels were needed for *in vitro* experiments (i.e. GSH degradation and cellular viability and degradation), the obtained solution was transferred to glass vials (500 µl per vial) and allowed to react in static conditions at r.t. Glass vials with inner diameter of 8 mm were used as molds. The hydrogels were obtained after 48 hours.

Once obtained, the disk-shaped hydrogels were freeze-dried and weighted. Dried hydrogels were used to study the swelling ratio at different pH and the degradation kinetics with different concentrations of GSH. This step allowed us as well to sterilized the materials for *in vitro* experiments.

Sterile and ultrafiltered water was used during hydrogel preparation for *in vivo* tests; the synthesis was carried out in closed sterile vials and protected from bacteria contamination, thus we assumed that the final product was free of bacterial contamination.

### 5.6.3 Degradation kinetic in presence of GSH

Degradation of dPAA hydrogels was examined in the presence of reduced glutathione (GSH), a disulfide reducing agents.

Briefly, the lyophilized hydrogels samples were incubated at 37 °C in 2 mL of a PBS solution with a GSH concentration of 10 µM. dPAA hydrogels were incubated in PBS alone as a control.

The degradation kinetics were then evaluated via swelling ratio (SR) measurements in time. SR were measured by a gravimetric method. In brief, lyophilized hydrogel samples were immersed in PBS at 37 °C. Then, the samples were removed from PBS at set time points (after 1h, 6h, 12h, 24h, 48 h, 72 h, 144 h), blotted free of surface water using filter paper and their swollen weights were measured on an analytical balance. The SR were then calculated as a ratio of weights of swollen hydrogel ( $W_s$ ) to dried hydrogel ( $W_d$ ), using the following equation:

$$SR = \frac{W_s - W_d}{W_d}$$

Degradation time was defined as the time where there were no longer sufficient cross-links to maintain the 3D network and the material was completely disintegrated. Experimentally, complete degradation was determined when we could observe a limpid solution, without solid residues.



#### 5.6.4 *In vitro cell culture*

Cryopreserved human dermal fibroblast, adult (HDFa) were purchased from Thermo Fisher and the culture was initiated as suggested on the protocol. HDFa were grown in Medium 106 supplemented with Low Serum Growth Supplement (Thermo Fisher). Cells were kept in 75 cm<sup>2</sup> culture flasks at 37 °C with a controlled atmosphere of 5% CO<sub>2</sub> and were grown until reaching 80 to 85% of confluence. Then, they were washed twice with PBS and treated with trypsin/EDTA solution to detach them from the flask surface. Cells were split every 2-3 days; the medium was changed every other day.

#### 5.6.5 *In vitro cell culture onto the nanocomposite hydrogels*

The hydrogel scaffolds were equilibrated by adding culture media at 37 °C. HDFa were detached from the culture flask by trypsination and approximately 2.5x10<sup>5</sup> cells were seeded onto the hydrogel scaffolds. Then, the samples were placed in the incubator (37 °C, 5% CO<sub>2</sub>) for about 30 minutes and fresh media was cautiously added on the top of the hydrogels to supply cells with nutrients. This was done to allow anchorage of the cells onto the scaffolds.

#### 5.6.6 *Cell staining and viability studies*

Cell viability was assessed using alamarBlue assay. Briefly, the alamarBlue solution was added to the culture medium (1:10 dilution) of unstained cells growing onto hydrogel scaffolds. After 3h incubation, 200 µL of the media were transferred to a 96-well plate and absorbance signals generated from the dye resazurin (dark blue) being reduced to resorufin (pink) by metabolically active cells were recorded using a VICTOR X5 Multilabel Plate Reader (Perkin Elmer).

Each sample was tested in three replicates and the results were expressed as percentage of reduced alamarBlue.

The viability of cells after complete degradation of the dPAA was measured by with a TC20™ Automated Cell Counter (Bio-Rad).

Where required (confocal fluorescence microscopy images), HDFa were stained with Vybrant DiD (Life Technologies, Thermo Fisher Scientific), following the reported protocol, prior to seeding them onto the scaffolds.



#### 5.6.7 Cell-mediated degradation of dPAA

The dPAA were freeze-dried and weighed ( $W_i$ ). Then HDFa cells were seeded onto the samples (see paragraph 5.6.5). The cell-laden samples were collected at pre-determined time points and were freeze-dried to obtain their dry weight after degradation ( $W_f$ ).

The cell-mediated degradation of the hydrogels,  $D$ , was calculated using the following equation:

$$D (\%) = \frac{W_i - W_f}{W_i} \times 100$$

Acellular hydrogels were used as degradation control.

#### 5.6.8 Evaluation of the gelation and formation of SFC *ex vivo*

Fresh porcine stomachs were used for the *ex vivo* tests. The hydrogel solution was injected into the submucosal layers of the pig stomach using a 23-gauge needle. The dose was 2 ml for each sample and the stomach was kept to a temperature of about 37 °C with a lamp to ensure simulation of *in vivo* conditions. Gelation of the dPAA samples was assessed by cutting open the tissue after the desired time. The experiment was repeated three times.

#### 5.6.9 Creating submucosal cushion and performing ESD in a living pig

The pig was fasted for 1 day before operation.

ESD procedure was performed by the surgeon Pietro Riva at IRCAD, Strasbourg.

A standard endoscope (Karl Storz, Tuttlingen, Germany) was used in the pig under general anesthesia. Both the dPAA solution and the NS used as control contained a small amount of Methylene Blue as a color agent in order to facilitate visualization of the SFC.

After setting appropriate lesions, the dPAA solution and NS were injected in the stomach submucosa through the endoscope accessory channel using a 23-gauge injection needle.

The mucosal elevation due to the injected dPAA at the target site was observed endoscopically before starting the ESD. It was compared under direct view with the elevation caused by NS during the procedure.

After injection, the ESD was performed and a circumferential mucosal incision was accomplished using a Needle knife (Olympus, Tokyo, Japan) Injection of dPAA and ESD were repeated three times.

The animal was euthanized after completion of experiments; the whole procedure was followed and recorded using a Silver Scope<sup>tm</sup> Video Gastroscope (Karl Storz, Tuttlingem, Germany).

The main outcome measures were (1) the rapid gelation of dPAA when injected into the submucosa and (2) the long-lasting SFC formed; (3) the feasibility of the dissection procedure during ESD; (3) the adhesion of dPAA to the muscularis layer and thus the increase of protection during the procedure and after it.

## 5.7 References

- [1] J. Ferlay, H. R. Shin, F. Bray, D. Forman, C. Mathers, D. M. Parkin, *Int. J. Cancer* **2010**, *127*, 2893.
- [2] a) H. H. Hartgrink, E. P. M. Jansen, N. C. T. van Grieken, C. J. H. van de Velde, *The Lancet*, *374*, 477; b) J. A. Ajani, D. J. Bentrem, S. Besh, T. A. D'Amico, P. Das, C. Denlinger, M. G. Fakih, C. S. Fuchs, H. Gerdes, R. E. Glasgow, J. A. Hayman, W. L. Hofstetter, D. H. Ilson, R. N. Keswani, L. R. Kleinberg, W. M. Korn, A. C. Lockhart, K. Meredith, M. F. Mulcahy, M. B. Orringer, J. A. Posey, A. R. Sasson, W. J. Scott, V. E. Strong, T. K. Varghese, G. Warren, M. K. Washington, C. Willett, C. D. Wright, N. R. McMillian, H. Sundar, *J. Natl. Compr. Canc. Netw.* **2013**, *11*, 531; c) A. G. Zauber , S. J. Winawer , M. J. O'Brien , I. Lansdorp-Vogelaar , M. van Ballegooijen , B. F. Hankey , W. Shi , J. H. Bond , M. Schapiro , J. F. Panish , E. T. Stewart , J. D. Wayne *New Engl. J. Med.* **2012**, *366*, 687.
- [3] S. Coda, S.-Y. Lee, T. Gotoda, *Gut and Liver* **2007**, *1*, 12.
- [4] a) S. Oka, S. Tanaka, I. Kaneko, R. Mouri, M. Hirata, T. Kawamura, M. Yoshihara, K. Chayama, *Gastrointest. Endosc.* **2006**, *64*, 877; b) T. Gotoda, H. Yamamoto, M. R. Soetikno, *J. Gastroenterol.* **2006**, *41*, 929.
- [5] a) M. Fujishiro, N. Yahagi, K. Kashimura, T. Matsuura, M. Nakamura, N. Kakushima, S. Kodashima, S. Ono, K. Kobayashi, T. Hashimoto, N. Yamamichi, A. Tateishi, Y. Shimizu, M. Oka, M. Ichinose, M. Omata, *Gastrointest. Endosc.* **2005**, *62*, 933; b) K. B. Cho, W. J. Jeon, J. J. Kim, *World Journal of Gastroenterology : WJG* **2011**, *17*, 2611.
- [6] a) L. Yu, W. Xu, W. Shen, L. Cao, Y. Liu, Z. Li, J. Ding, *Acta Biomater.* **2014**, *10*, 1251; b) M. Fujishiro, N. Yahagi, K. Kashimura, Y. Mizushima, M. Oka, S. Enomoto, N. Kakushima, K. Kobayashi, T. Hashimoto, M. Iguchi, Y. Shimizu, M. Ichinose, M. Omata, *Endoscopy* **2004**, *36*, 579.
- [7] K. J. Kang, B.-H. Min, J. H. Lee, E. R. Kim, C. O. Sung, J. Y. Cho, S. W. Seo, J. J. Kim, *Dig. Dis. Sci.* **2013**, *58*, 1491.
- [8] R. T. Tran, M. Palmer, S.-J. Tang, T. L. Abell, J. Yang, *Gastrointest. Endosc.* **2012**, *75*, 1092.
- [9] A. O. Ferreira, J. Moleiro, J. Torres, M. Dinis-Ribeiro, *Endoscopy International Open* **2016**, *4*, E1.

- [10] a) T. Uraoka, T. Fujii, Y. Saito, T. Sumiyoshi, F. Emura, P. Bhandari, T. Matsuda, K.-I. Fu, D. Saito, *Gastrointest. Endosc.* **2005**, *61*, 736; b) M. Fujishiro, N. Kakushima, S. Kodashima, K. Kashimura, T. Matsuura, Y. Muraki, A. Tateishi, M. Omata, *Digestive Endoscopy* **2007**, *19*, 26.
- [11] A. B. Feitoza, C. J. Gostout, L. J. Burgart, A. Burkert, L. J. Herman, E. Rajan, *Gastrointest. Endosc.* **2003**, *57*, 41.
- [12] N. Yoshida, Y. Naito, M. Kugai, K. Inoue, K. Uchiyama, T. Takagi, T. Ishikawa, O. Handa, H. Konishi, N. Wakabayashi, N. Yagi, S. Kokura, Y. Morimoto, K. Kanemasa, A. Yanagisawa, T. Yoshikawa, *J. Gastroenterol. Hepatol.* **2011**, *26*, 286.
- [13] Y. Matsui, M. Inomata, K. Izumi, K. Sonoda, N. Shiraishi, S. Kitano, *Gastrointest. Endosc.* **2004**, *60*, 539.
- [14] T. Hayashi, T. Matsuyama, K. Hanada, K. Nakanishi, M. Uenoyama, M. Fujita, M. Ishihara, M. Kikuchi, T. Ikeda, H. Tajiri, *Journal of Biomedical Materials Research Part B: Applied Biomaterials* **2004**, *71B*, 367.
- [15] I. Kumano, M. Ishihara, S. Nakamura, S. Kishimoto, M. Fujita, H. Hattori, T. Horio, Y. Tanaka, K. Hase, T. Maehara, *Gastrointest. Endosc.* **2012**, *75*, 841.
- [16] J. L. Ifkovits, J. A. Burdick, *Tissue Eng.* **2007**, *13*, 2369.
- [17] F. Fiorini, E. A. Prasetyanto, F. Taraballi, L. Pandolfi, F. Monroy, I. López-Montero, E. Tasciotti, L. De Cola, *Small* **2016**, *12*, 4881.
- [18] L. Maggini, I. Cabrera, A. Ruiz-Carretero, E. A. Prasetyanto, E. Robinet, L. De Cola, *Nanoscale* **2016**, *8*, 7240.
- [19] S. Mura, J. Nicolas, P. Couvreur, *Nat Mater* **2013**, *12*, 991.
- [20] a) F. Yang, J. Wang, G. Peng, S. Fu, S. Zhang, C. Liu, *J. Mater. Sci. Mater. Med.* **2012**, *23*, 697; b) M. Kar, Y.-R. Vernon Shih, D. O. Velez, P. Cabrales, S. Varghese, *Biomaterials* **2016**, *77*, 186.
- [21] E. A. Prasetyanto, A. Bertucci, D. Septiadi, R. Corradini, P. Castro-Hartmann, L. De Cola, *Angew. Chem. Int. Ed.* **2016**, *55*, 3323.
- [22] a) G. D. Nicodemus, S. J. Bryant, *Tissue Engineering. Part B, Reviews* **2008**, *14*, 149; b) H. Henning Winter, in *Encyclopedia of Polymer Science and Technology*, John Wiley & Sons, Inc., **2002**.
- [23] M. E. Smithmyer, L. A. Sawicki, A. M. Kloxin, *Biomaterials Science* **2014**, *2*, 634.
- [24] P. Ferruti, S. Bianchi, E. Ranucci, F. Chiellini, V. Caruso, *Macromol. Biosci.* **2005**, 613.
- [25] M. P. Lutolf, J. A. Hubbell, *Biomacromolecules* **2003**, *4*, 713.
- [26] C. D. Pritchard, T. M. O'Shea, D. J. Siegwart, E. Calo, D. G. Anderson, F. M. Reynolds, J. A. Thomas, J. R. Slotkin, E. J. Woodard, R. Langer, *Biomaterials* **2011**, *32*, 587.
- [27] M. K. Nguyen, D. K. Park, D. S. Lee, *Biomacromolecules* **2009**, *10*, 728.

## **6. Instrumental techniques**

### **Abstract**

An overview of the main techniques used in this thesis work is given in this chapter.

The general features and basic principles are described for each of them, while the experimental details and conditions regarding particular measurements performed are reported in the experimental section of the related chapter.

Commonly used characterization and experimental techniques, such as infrared spectroscopy and NMR, are not included in the discussion.

## 6.1 Scanning electron microscopy (SEM)

Scanning electron microscopy (SEM) is a method for high-resolution imaging of surfaces; it uses electrons for imaging the samples.

Since their introduction in the early 1950's, scanning electron microscopes have enabled the development of new areas of study in the medical and physical science fields.<sup>[1]</sup>

SEM scan a sample with a focused high-energy electron beam, to generate a range of signals at the surface of solid specimens.

The signals produced by the electron-sample interactions give information on the samples' external morphology and chemical composition.

Generally, data are collected over a selected area of the surface of the sample, and a 2-dimensional image is delivered. It displays the intensity of the emitted signal as a brightness scale, thus showing spatial variations in the sample with respect to the interaction with the electron beam. By synchronizing the position in the image scan to that of the scan of the incident electron beam, the image represents the morphology of the sample surface area.

Areas ranging from approximately 1 cm to few microns in width can be imaged in a scanning mode using conventional SEM techniques, having magnification up to more than 500000x and resolution of nanometers.

SEM instruments are also capable of performing analyses of selected point on the sample, for example when qualitatively or semi-quantitatively data are required to determine the chemical composition of the surface (EDX mode).

The advantages of SEM over light microscopy include much higher magnification and greater depth of field, up to 100 times than that of light microscopy.

From the point of view of the fundamental principles of SEM, this microscope works by generating a beam of incident electrons in an electron column, which is placed above the sample chamber. The electrons are generally produced by a thermal emission source or by a field emission cathode.

Thermal emission sources are based on a thin conductive wire, usually made of tungsten, which is heated to temperatures where the energy of the weakest bounded electrons exceeds the work function of the material, thus allowing for the electron emission. Field emission sources instead

use electric field applied between a cathode and an anode in a way that the work function of the cathode dramatically decreases and electron emission is possible even at room temperature. In any case, an anode is placed directly under the source to provide electrons acceleration towards the base of the column. The energy of the incident electrons can be then modulated between 100 eV and 30 keV, depending on the evaluation objectives.

The electrons are focused into a defined electron beam by means of several electromagnetic lenses in the SEM column. Scanning coils near the end of the column direct and position the focused beam onto the sample surface, which causes a repulsive electric field and a condensation of the electrons, thus focusing them on the column aperture.

The beam is then divergent and must be refocused on the sample, which is done by focusing lenses located just above the specimen (Figure 6.1).

Upon interaction of the electron beam with the sample, incident electrons cause electrons to be emitted from the sample due to elastic and inelastic scattering events within the sample's surface and near-surface material.

Several signals can be thus recorded, including backscattered electrons; secondary electrons, which are used to produce the typical SEM image; diffracted backscattered electrons, which can be used to gain information on the crystal structures and orientations of minerals and X-ray photons that are used for elemental analysis.

Backscattered electrons are high-energy electrons ejected by an elastic collision of an incident electron. The energy of backscattered electrons is comparable to that of the incident electrons. Secondary electrons are lower-energy electrons resulting from inelastic scattering and can be formed by collisions with the nucleus where substantial energy loss occurs or by the ejection of loosely bound electrons from the sample atoms. The energy of secondary electrons is typically 50 eV or less. Together with the backscattered electrons, they are commonly used for imaging samples. Due to their very low energy, only secondary electrons near the surface can leave the sample and produce the output signal.

The volume in which secondary electrons are produced is relatively small, which leads to a high axial resolution (a few nm).

The final image is thus a map of the secondary electron density, depending on the properties of the sample.

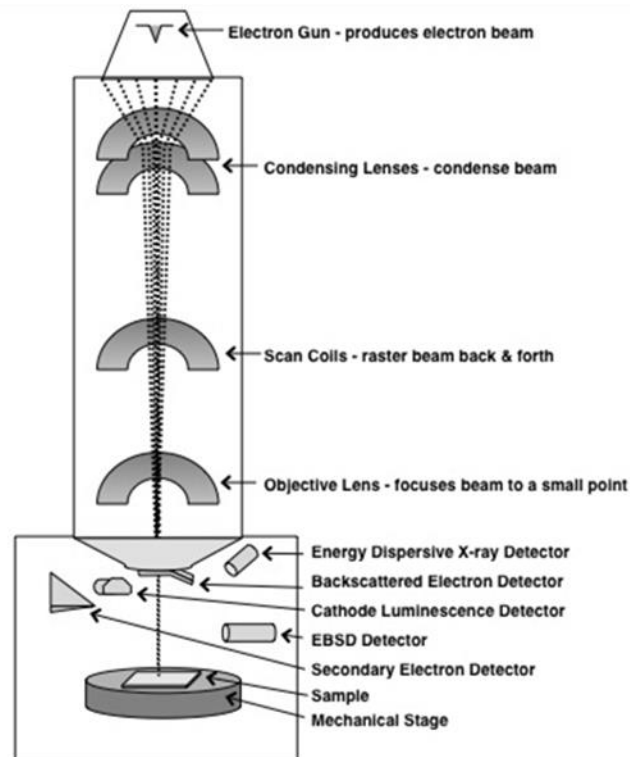


Figure 6.1 Schematic representation of SEM setup; adapted from [www.colgate.edu/academics/departments-and-programs/geology/facilities](http://www.colgate.edu/academics/departments-and-programs/geology/facilities)

X-ray generation is instead produced when the excited electrons of specific orbitals return to lower energy states, yielding X photons that are of a fixed wavelength related to the difference in electronic energy levels for a given element. Thus, characteristic X-rays are produced for each element, allowing for a chemical composition mapping of the sample surface.<sup>[2]</sup>

## 6.2 Confocal laser scanning microscopy (CLSM)

Confocal laser scanning microscopy (CLSM) is a powerful technique which combines high-resolution optical imaging with depth selectivity, thus allowing optical sectioning. This means that it allows the imaging of visual sections of tiny structures within the sample that would be difficult to physically section, and then construct 3D structures from the obtained images.



The principle of CLSM was developed by Marvin Minsky in 1953, but it took other thirty years before it was fully developed to incorporate a laser scanning process. It became a standard technique toward the end of the 1980s.

It offers many advantages over conventional optical epifluorescence microscopy, including the ability to control depth of field, elimination or reduction of background information away from the focal plane, and the capability to collect serial optical sections from thick sample.

The key to the confocal strategy is the use of spatial filtering techniques to eliminate out-of-focus light.

The principles of this type of microscopy are schematically presented in Figure 6.2.

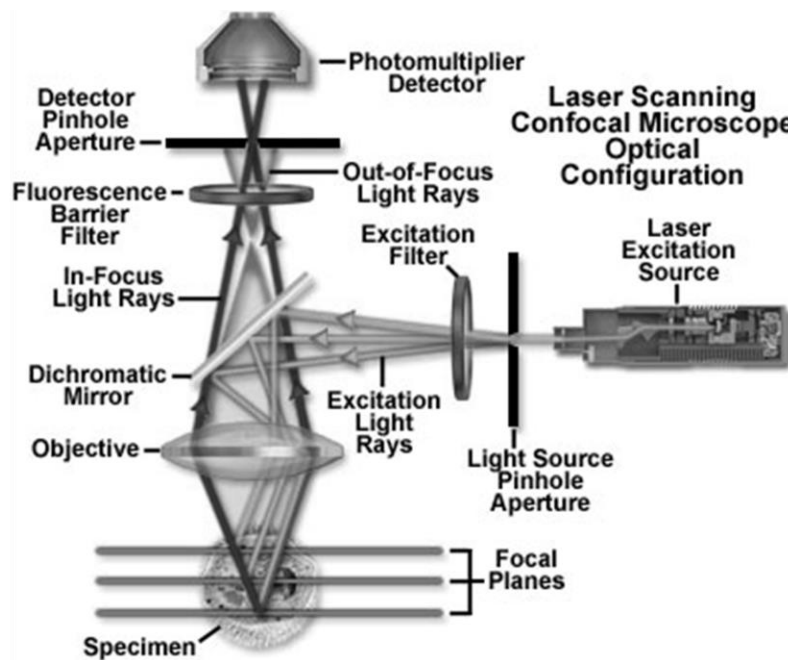


Figure 6.2 Schematic picture showing the principles of CLSM. Adapted from [www.olympusmicro.com/](http://www.olympusmicro.com/)

The CLSM is based on conventional optical microscopy but instead of a lamp, a laser beam is focused onto the sample.

Coherent light emitted by the laser system (excitation source) passes through an excitation pinhole aperture that is placed in a conjugate plane (confocal) with a scanning point on the specimen and a second pinhole aperture located in front of the detector.

The intensity of the laser light is adjusted by neutral density filters and brought to a set of scanning mirrors that can move them very precisely and quickly. One mirror tilts the beam in the X direction, the other in the Y direction. Together, they tilt the beam in a raster fashion. The beam is then brought to the back focal plane of the objective lens which focuses it onto the sample. Secondary fluorescence emitted from points on the sample (in the same focal plane) pass back through the dichromatic mirror and are focused as a confocal point at the detector pinhole aperture. This light travels backwards through the same path that the laser travels. The effect of the scanning mirrors on this light is to produce a spot of light that is not scanning, but standing still.

The amount of fluorescence emission that occurs at points above and below the objective focal plane is not confocal with the pinhole. Since only a small fraction of the out-of-focus fluorescence emission is delivered through the pinhole aperture, most of this extraneous light is not detected by the photomultiplier and does not contribute to the resulting image. The dichromatic mirror, barrier filter, and excitation filter perform similar functions to the analog components in an epifluorescence microscope.

Refocusing the objective in a confocal microscope, shifts the excitation and emission points on a specimen to a new plane that becomes confocal with the pinhole apertures of the light source and detector. Moreover, the information can be also collected from different focal planes (z-axis) by raising or lowering the microscope stage or objective lens. Slices imaged in succession in “z-stack” mode can be processed to create a 3D image.

In traditional fluorescence microscopy, the entire sample is exposed to intense illumination from the source lamp, and the resulting image of secondary fluorescence emission is generally projected onto the surface of an electronic array detector. In contrast, the mechanism of image formation in a confocal microscope is essentially different.

The CLSM consists of multiple laser excitation sources, a scan head with optical and electronic components, electronic detectors (usually photomultipliers), and a computer for acquisition, processing, analysis, and display of images. These properties actually allow the user to record 3D-images using different combinations of excitation and emission wavelengths as long as the emission spectra of the diverse species do not completely overlap, which is a key tool when analyzing bio-samples that require the use of multiple labels.<sup>[3]</sup>

### 6.3 Dynamic light scattering (DLS)

Dynamic light scattering (DLS), sometimes referred to as photon correlation spectroscopy, is a non-invasive, widespread technique for measuring the size and size distribution of molecules and particles in dispersion, typically in the submicron region.

Particles suspended in a solution are in Brownian motion due to random collisions with molecules from the liquid.

Because of this motion, particles are diffused through the solution, with the diffusion coefficient,  $D$ , being inversely proportional to the particles size, according to the Stokes-Einstein equation:

$$D = \frac{k_B T}{3\pi\eta_0 d}$$

Where  $D$  is the diffusion coefficient;  $k_B$  is Boltzmann's constant;  $T$  is absolute temperature;  $\eta_0$  is the viscosity and  $d$  is the hydrodynamic diameter.

From this equation it is clear that  $D$  will be relatively small for large particles, thus the particles will move slowly; while  $D$  will be larger for smaller particles and the particles will move more rapidly.

Therefore it is possible to compute the sphere size distribution and give a description of the particle's motion in the medium, by observing the motion and determining the diffusion coefficient of particles in liquid media.

Shining a monochromatic light beam, usually a laser, onto the particles solution causes the light to scatter.

The scattered light that is observed comes from a collection of scattering elements, so that the observed intensity of the scattered light at any instant is a result of the interference of light scattered by each element. Hence, it depends on the relative positions of the elements.

With the particles being in motion, the relative positions of particles changes in time, producing fluctuations of the scattered light intensity. These fluctuations are random due to the fact that particles are in Brownian motion. The intensity fluctuates faster for smaller particles and slower for bigger particles (Figure 6.3).

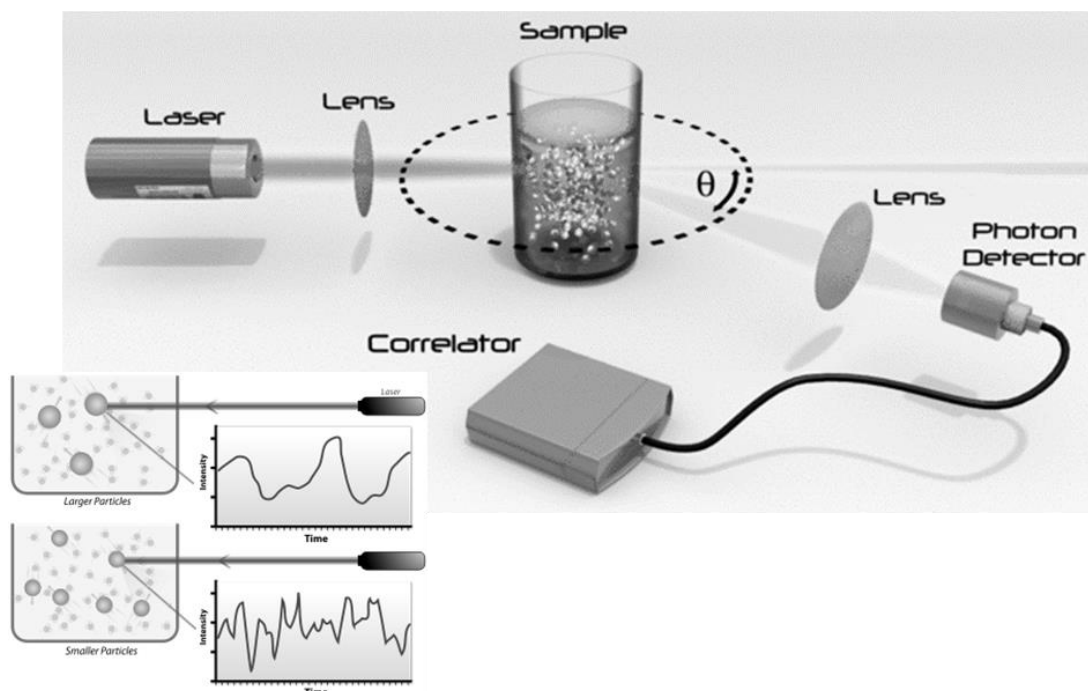


Figure 6.3 Scheme of the setup of the DLS and representation of the random intensity fluctuations of the scattered light, obtained from two dispersions of particles of different size. Adapted from [www.lsinstruments.ch/technology/dynamic\\_light\\_scattering\\_dls/](http://www.lsinstruments.ch/technology/dynamic_light_scattering_dls/)

The fluctuations of the scattered light are analyzed using the autocorrelation function (ACF), which has a decay which depends on delay time.

For small particles with rapid motion and rapid intensity fluctuations, the autocorrelation function is a rapidly decaying exponential function with a large decay constant, while for large particles the exponential decays more slowly with a smaller decay constant. The ACF is then used to calculate the diffusion coefficient and therefore the size of the particles.

The particle size is displayed as a statistical distribution of scattering intensity, volume or number of particles.

The fundamental size distribution generated by DLS is the intensity distribution, which is weighted according to the scattering intensity of each particle and directly measured by the instrument. The intensity distribution is the general and most common way to show DLS data. The volume and the number distributions are subsequently calculated from the intensity distribution by using Mie theory.

The volume distribution describes the relative proportion of multiple components in the sample, based on their volume rather than based on their scattering (intensity). However it is

based on the assumption that the sample is composed by spherical homogeneous particles and that there is no error in the intensity distribution.

The number distribution is calculated by assigning a size value to each particle inspected. This method builds a distribution where each particle has equal weighting once the final distribution is calculated.

Generally, volume and number distributions, derived from the intensity distribution, are best used for comparative purposes.

## **6.4 Zeta potential**

Zeta potential is a parameter characterizing electrochemical equilibrium on interfaces. It is a measure of the magnitude of the electrostatic or charge repulsion/attraction between particles. Particles dispersed in a suspension usually carry an electrical charge, because their surface contains chemical groups that can ionize or because it can adsorb ions of the opposite charge. The charge on the surface of each particle is counterbalanced by ions of opposite sign forming an ionized layer which surrounds the surface of the particles in solution.

The concentration of the counter ions is higher in the area adjacent to the particle's surface, while decreases gradually with distance from the particle. Equal number of positive and negative ions exist in the area far from the particle's surface, thus the overall suspension is neutral. This ions distribution is called "diffuse electrical double layer".

It is formed of two main layers, the layer of counter-ions strongly attracted around the surface of the particle, called "Stern layer", and the co-ions farther away from the particle, which form the "diffuse layer", where the number of cationic and anionic charges are evenly balanced (Figure 6.4).

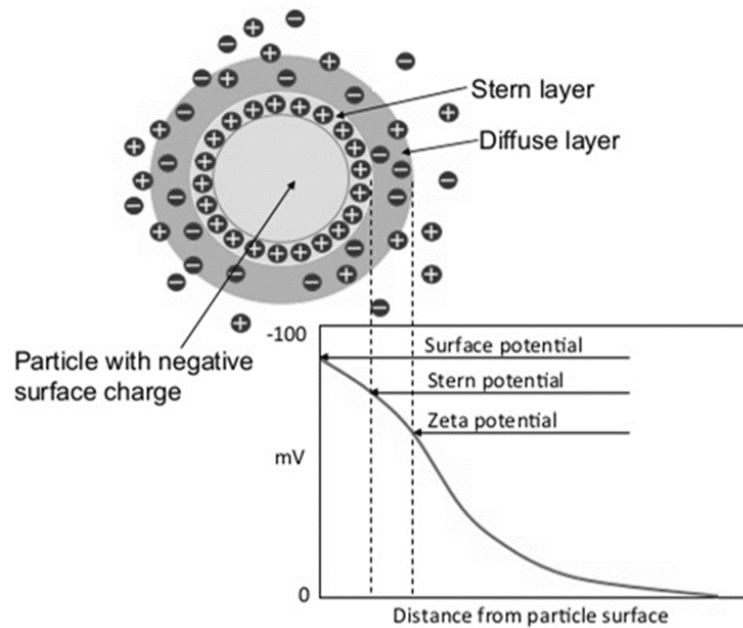


Figure 6.4 Layers surrounding a particle dispersion in liquid media; adapted from Abd Karim Alias, “*Emulsion stability*”, **2013**, ed. University Sains Malaysia

The particles in a dispersion undergo Brownian motion, moving together with the Stern layer and a part of diffuse layer. The interface between the non-moving and moving ions is called “slipping plane”, which is thus associated with the tangential motion of the ions relative to the surface.

The electric potential corresponding to the slipping plane versus a point far away from the particle is the "Zeta potential" ( $\zeta$ ). It is measured in mV and it reflects what one particle “sees” as it approaches another particle.

If the repulsion between two particles is large enough, they will be stabilized by electrostatic repulsion, and the value of  $\zeta$  potential will be high. On the contrary, a low  $\zeta$  potential increases the possibility of particles colliding.

The most effective method to measure the particles charge is to apply an electric field to the suspension and to measure how fast the particles move towards the opposite electrode. The velocity of the moving particles is proportional to their surface charge, therefore the  $\zeta$  value can be determined by measuring the speed of the particles in the applied electric field.

Electrophoretic light scattering is the method normally used to determine the speed of the particles. It is based on the detection of scattered light coming from a dispersion of particles irradiated by a laser light.

Because the shift between the frequency of the scattered light and that of the incident light is proportional to the speed of the moving particles, the electrophoretic mobility of the particles can be measured from this frequency shift. Such technique is based on the Doppler effect, therefore this method is also called “Laser Doppler Method”.

The frequency shift  $\nu_D$  is related to the particles mobility,  $U$  by the equation:

$$\nu_D = \frac{Uq}{2\pi} \cos \frac{\vartheta}{2} = \frac{Un}{\lambda} \sin \vartheta$$

where  $q$  is the scattering vector ( $q=4\pi n \sin(\theta/2)/\lambda$ );  $\lambda$  is the wavelength;  $n$  is the refractive index of the medium, and  $\vartheta$  is the scattering angle.

The zeta potential measurement is then performed in a glass cell resembling the electrophoresis scheme; thus, it is worth noticing that the movement of the particles is directed by the electro-osmotic flow occurring in the measure cell, and the typical parabolic profile of the final flow, which is the sum of the electro-osmotic one and the particle true mobility, is expected and taken as a good indicator of reliability of the measurement.<sup>[4]</sup>

## 6.5 Fluorescence spectroscopy

Fluorescence spectroscopy is a technique used for analyzing luminescent signals emitted from a sample. Through the recording of the emission and excitation of the sample, it allows to gain information on the intensity of photons emitted from a sample after it has absorbed photons.

The emission spectrum in particular, is the wavelength distribution of the emission measured at a single constant excitation wavelength, while the excitation spectrum is the dependence of the emission intensity in the scanned excitation wavelength window, measured at a single emission wavelength.



These spectra are recorded on spectrofluorimeters composed by an excitation source (in this thesis a 450 W xenon arc lamp), a dual grating monochromator and a reference detector (Figure 6.5). Emission of the sample is collected at 90° to the incident light, then it goes through a second monochromator, to finally reach the detector, which is normally equipped with a photomultiplier tube for the amplification of the incoming signal.

The spectra are corrected for the source intensity (lamp and excitation grating) and for the detector response and emission grating by standard correction curves.<sup>[5]</sup>

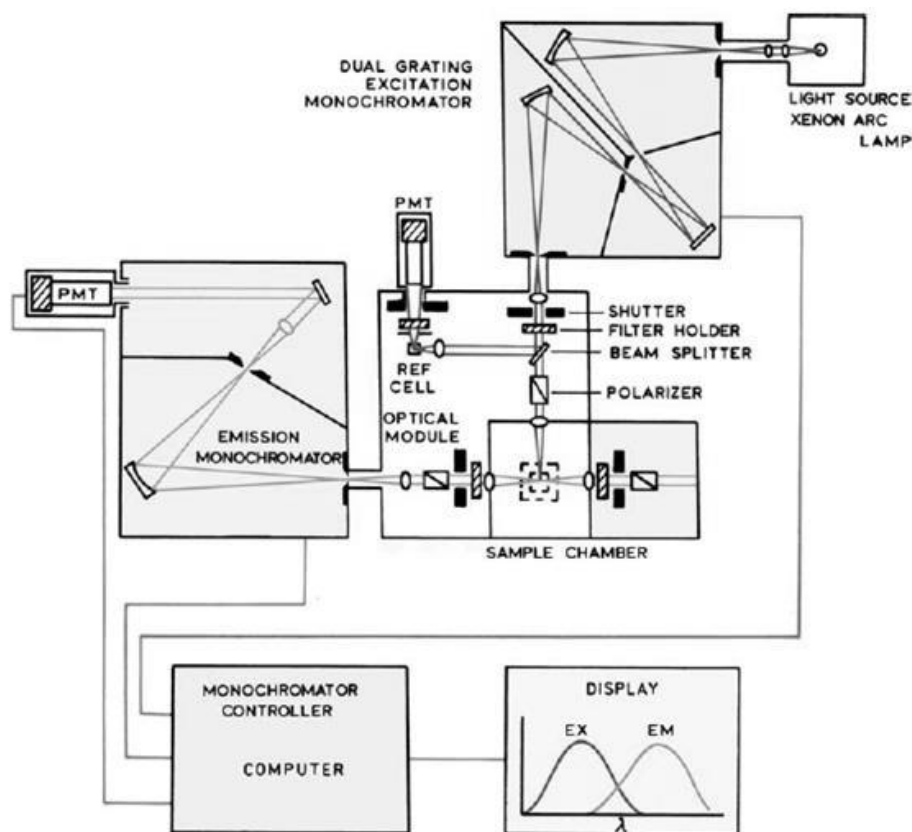


Figure 6.5 Schematic representation of a typical spectrofluorimeter setup; adapted from [www.scienceteen.com](http://www.scienceteen.com)

## 6.6 Luminescence quantum yield

The photoluminescence quantum yield (PLQY) of a sample is the ratio of photons absorbed to photons emitted through fluorescence. Thus, PLQY gives the probability of the excited state

of the sample to be deactivated by fluorescence rather than by another, non-radiative mechanism.

Absolute PLQY can be measured by using an integrating sphere. This is an instrument that collects all the emitted photons with a calibrated photodiode and relate them to the absorbed ones.

It is made of a hollow spherical cavity, internally coated with reflective material able to reflect the incident light on any point on this surface and distribute them equally to all other points, to minimize the effects of the original direction of light.

In a general setup (Figure 6.6), the light from a xenon lamp is monochomatized at a selected wavelength and brought to the sphere through an optical fiber. The light reaches the sample, which is placed inside the sphere, and the light that it emits is collected to a detector.

The reference measure is done in the same setup conditions.

The quantum yield of the sample is corrected for the reference, to give the absolute PLQY.

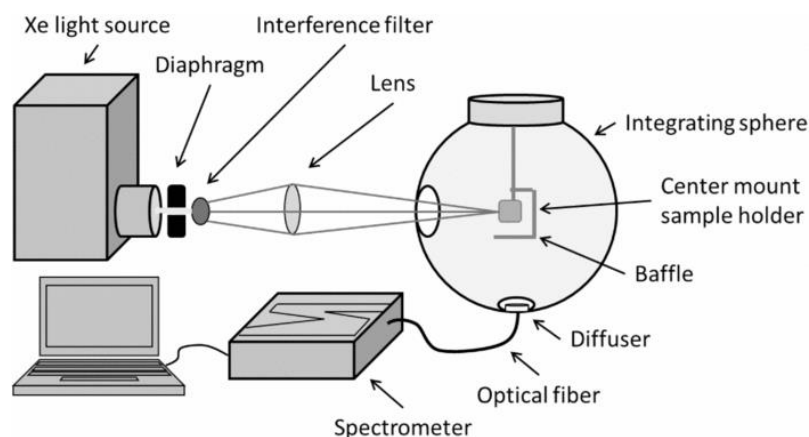


Figure 6.6 Schematic integrating sphere setup.

## 6.7 Lifetime measurements

The excited state lifetime is a measure of the time a fluorophore spends in the excited state before returning to the ground state by emitting a photon; it can range from picoseconds to hundreds of nanoseconds.

It is measured using a spectrofluorimeter equipped with a pulsed excitation source, which is typically a flash lamp or a laser, and a time-correlated single-photon counting module (TCSPC). Each pulse of excitation generates an electrical signal, which represents the START input of the TAC (time-to-amplitude converter). The photons emitted from the excited sample are translated to an electrical signal from the detector, which represents the STOP signal for the TAC. The final voltage measured by the TAC is proportional to the time between the START and the STOP signals, and is recorded as a histogram of number of photons emitted in time.

The final decay obtained in this way can be fitted to give values of excited state lifetime and the relative contribution of each component in case of multi-exponential decays.

## 6.8 References

- [1] J. J. Bozzola, in *eLS*, John Wiley & Sons, Ltd, **2001**.
- [2] a) <http://www.mee-inc.com/hamm/scanning-electron-microscopy-sem/>;  
b) [http://www.zeiss.com/microscopy/en\\_de/products/scanning-electron-microscopes.html](http://www.zeiss.com/microscopy/en_de/products/scanning-electron-microscopes.html).
- [3] <http://bitesizebio.com/19958/what-is-confocal-laser-scanning-microscopy/>.
- [4] a) J. Lyklema, in *Fundamentals of Interface and Colloid Science, Vol. Volume 2*, Academic Press, **1995**; b) A. V. Delgado, F. González-Caballero, R. J. Hunter, L. K. Koopal, J. Lyklema, in *Pure Appl. Chem.*, Vol. 77, **2009**, pp. 1753.
- [5] J. R. Lakowicz, *Principles of fluorescence spectroscopy*, Springer, New York, **2006**.



# Curriculum Vitae



## Personal information

*Name* Federica Fiorini  
*Date of Birth* 29 March 1988  
*Nationality* Italian  
*Address* 46 blvd de la Victoire, 67000 Strasbourg, France  
Via Ceradini 5, 20129 Milano, Italy  
*Phone* +39 3343486638  
*E-mail* ffiorini@unistra.fr, fiorini.fede@gmail.com

## Education

November 2012 – September 2016

PhD student in Chemical Sciences (Ecole Doctorale des Sciences Chimiques), Laboratoire de Chimie et des Biomatériaux Supramoléculaires, Institut de Science et d'Ingénierie Supramoléculaires - Université de Strasbourg (France)

Supervisor: Prof. Luisa De Cola

September 2014 – March 2015

Visiting Graduate Research Fellow, Department of Nanomedicine, Houston Methodist Research Institute, Houston, TX (USA)

Supervisor: Dr. Ennio Tasciotti

December 2010 - September 2012

Master of Science in Chemical Sciences, Department of Chemistry, Università degli Studi di Milano (Italy); Final mark: 110 cum laude

Supervisors: Prof. Giuseppe Di Silvestro and Prof. Maurizio Benaglia

October 2007 - December 2010

Bachelor of Science in Chemistry, Department of Organic and Industrial Chemistry, Università degli Studi di Milano (Italy)

## Scientific publications

- F. Fiorini, E. A. Prasetyanto, F. Taraballi, L. Pandolfi, F. Monroy, I. Lopez-Montero, E. Tasciotti, L. De Cola, "Nanocomposite Hydrogels as Platform for Cells Growth, Proliferation and Chemotaxis", *Small*, **2016**, 12, 4881
- A. Colombo, F. Fiorini, D. Septiadi, F. Nisic, A. Valore, D. Roberto, C. Dragonetti, M. Mauro, L. De Cola, "Neutral N<sup>+</sup>C<sup>-</sup>N terdentate luminescent Pt(II) complexes: synthesis, photophysical properties and bio-imaging application", *Dalton Transaction*, **2015**, 44, 8478
- F. Fiorini, G. Alonci, P. Riva, S. Perretta, L. De Cola, "Biodegradable hydrogels for submucosal fluid cushion", manuscript in preparation
- F. Fiorini, E. Longhi, L. De Cola, "Visualizing 3D cell proliferation in a novel hybrid emission switchable hydrogel", manuscript in preparation
- V. Giglio, F. Fiorini, L. Maggini, L. De Cola, "Mesoporous Silica Nanodiscs: a Powerful Tool for Intracellular and Extracellular Drug Delivery", to be submitted
- V. Rizzi, F. Fiorini, G. Lamanna, E. A. Prasetyanto, P. Fini, L. De Cola, P. Cosma, "A Green Approach: Polyamidoamine-based hydrogel potential for Direct Blue and Direct Red removal from wastewater", manuscript in preparation

## International conferences presentations

- F. Fiorini, E. A. Prasetyanto, F. Taraballi, L. Pandolfi, F. Monroy, I. Lopez-Montero E. Tasciotti, L. De Cola, Nanocomposite hydrogels as Platforms for cells Growth, Proliferation and Chemotaxis, Forum BioChem 2016 - Meeting Academia-Industry, June 2016 (Illkirch, FR); *poster presentation*
- F. Fiorini, E. A. Prasetyanto, F. Taraballi, L. Pandolfi, F. Monroy, I. Lopez-Montero, E. Tasciotti, Chemotaxis and Bioactivity in a New Class of Nanocomposite Hydrogel Systems, 4th Sino-French Symposium on Polymers and Soft Matter, October 2015 (Strasbourg, FR); *oral presentation*
- F. Fiorini, L. De Cola, Mesoporous Silica Nanocomposite Hydrogel: a novel platform for tissue engineering applications, B.E.S.T. Innovation Symposium, August 2015 (Strasbourg, FR); *oral presentation*
- F. Fiorini, E. A. Prasetyanto, F. Taraballi, L. Pandolfi, E. Tasciotti, L. De Cola, Mesoporous Silica Nanocomposite Hydrogels: a novel platform for sustained release of small molecules, E-MRS, May 2015 (Lille, FR); *oral presentation*

- F. Fiorini, E. A. Prasetyanto, L. De Cola, Hydrogels as 3D scaffolds to study cell-material interaction, 5th International BioNanoMed 2014 Congress, March 2014 (Krems, Austria); *poster presentation*
- F. Fiorini, E. A. Prasetyanto, L. De Cola, Hybrid hydrogels as 3D scaffolds to study cell-material interaction, 48th EuChem Conference on Stereochemistry, May 2013 (Brunnen, CH); *poster presentation*

## **Awards**

- “Best Poster Prize” awarded from Labex Medalis at the Forum BioChem 2016 - Meeting Academia-Industry
- "Best Design/Prototype" at the B.E.S.T. Innovation Course 2015 organized by IRCAD/IHU and supported by Stanford Biodesign
- "Young Scientist Award" from European Materials Research Society (E-MRS), in recognition of an outstanding contribution to the E-MRS 2015 Spring Meeting, Symposium X, "Nanomedicine advancing from bench-to-bedside: the role of materials"
- "Naturalia & Biologia 2014" subvention for the participation to an international scientific conference

## Acknowledgements

I wish to thank Prof. Luisa De Cola for the opportunity she gave me to carry on the PhD in her amazing group and under her supervision. I also would like to thank her for the many things I could learn from her, the fruitful discussions and advices, not to mention for the very interesting and challenging projects that she gave me the possibility to work on.

I am very thankful to Dr. Ennio Tasciotti for hosting me at the Houston Methodist Research Institute in Texas and allowing me to carry on part of my research projects in his laboratories.

I would like to thank all the collaborators for the precious work. In particular Dr. Francesca Taraballi and Laura Pandolfi from Houston Methodist Research Institute; Prof. Francisco Monroy and Dr. Ivan Lopez-Montero from Universidad Complutense de Madrid; Prof. Silvana Perretta and Pietro Riva from IRCAD/IHU in Strasbourg.

I would also like to acknowledge Dr. Valentina Giglio and Dr. Vito Rizzi for the interesting work done together.

I kindly acknowledge Professors Gianluca Farinola, Alessandro Mordini, Peter Seeberger and Fouzia Boulmedais for accepting to be part of my thesis commission.

Finally, I wish to dearly thank my mom and dad, my brother, Pietro and all of my friends for their tireless support throughout these years.

Last but not least, I would like to thank all my colleagues (and friends) for the many ways in which they helped me during my work and my time in Strasbourg.

I thank ERC grant "Magic", Université de Strasbourg and Houston Methodist Research Institute for financial support





# Soft hybrid materials for cell growth and proliferation

## Résumé

Le travail de recherche présenté dans cette thèse consiste en la conception et les études *in vitro* / *in vivo* d'échafauds d'hydrogel pour la prolifération et migration cellulaires en trois dimensions (3D). Dans ce contexte, des hydrogels à base de polyamidoamines avec des propriétés physicochimiques intéressantes et une biocompatibilité élevée ont été développés pour différentes applications biomédicales.

En particulier, un hydrogel avec des sondes fluorescentes d'iridium(III) incorporés de manière covalente, a été conçue comme plate-forme 3D de culture cellulaire, pour la visualisation directe des cellules vivantes en temps réel, et a démontré être un puissant outil de bioimagerie pour les investigations de cellules *in vitro*.

En outre, un hydrogel nanocomposite, capable d'induire *in vitro* la chimiotaxie des cellules souches par la libération d'une chimiokine, a été développé. Sa biocompatibilité et une faible réponse inflammatoire ont été testés *in vivo*, ce qui a confirmé le potentiel du matériaux en tant qu'implant pour l'ingénierie tissulaire artificielle.

Enfin, un hydrogel nanocomposite injectable et biodégradable a été réalisé comme un nouvel agent pour la dissection sous-muqueuse endoscopique (ESD), qui est une procédure clinique appliquée pour les lésions néoplasiques digestives au stade précoce. L'hydrogel, formé *in situ* après l'injection, a permis une ESD rapide et sûr, et pourrait être dégradé par les cellules proliférantes sur l'échafaud, avec le relargage d'un composant actif encapsulé.

Mots-clés: hydrogel; biocompatibilité; bioimagerie; nanocomposites; implant *in vivo*; applications cliniques

## Résumé en anglais

The research work presented in this thesis focuses on the design and *in vitro/in vivo* investigation of hydrogel scaffolds for three-dimensional (3D) cell proliferation and migration.

In such a context, polyamidoamines-based hydrogels with interesting physicochemical properties and high biocompatibility have been developed for different biomedical applications.

In particular, a hydrogel with covalently incorporated iridium(III) fluorescent probes, has been conceived as a 3D cell culture platform for the direct visualization of living cells in real-time, demonstrating to be a powerful bioimaging tool for *in vitro* cells investigation.

Moreover, a nanocomposite hydrogel, able to induce *in vitro* chemotaxis of stem cells via the release of a chemokine, was developed. Its biocompatibility and low inflammatory response were tested *in vivo*, confirming the potential of the material as an artificial tissue engineering implant.

Finally, an injectable biodegradable nanocomposite hydrogel was realized as a novel agent for endoscopic submucosal dissection (ESD), which is a clinical procedure applied for early stage neoplastic lesions. The hydrogel, formed *in situ* after the injection, allowed a fast and safe ESD, and could be degraded by cells proliferating onto the scaffold, with the release of an encapsulated active component.

Keywords: hydrogel; biocompatibility; bioimaging; nanocomposites; in vivo implant; clinical applications